Development Length Criteria for Plain and Ransome Bars

A Thesis

Submitted to the College of Graduate and Postdoctoral Studies

In Partial Fulfillment of the Requirements

For the Degree of Master of Science

In the Department of Civil, Geological, and Environmental Engineering

University of Saskatchewan

Saskatoon, SK

By:

Umesh Poudyal

PERMISSION TO USE

In presenting this thesis in partial fulfilment of the requirements for a Postgraduate degree from the University of Saskatchewan, I agree that the Libraries of the University may make it freely available for inspection. I further agree that permission for copying of this thesis in any manner, in whole or in part, for scholarly purposes may be granted by the professor or professors who supervised my thesis work or, in their absence, by the Head of the Department or the Dean of the College in which my thesis work was done. It is understood that any copying or publication or use of this thesis or parts thereof for financial gain shall not be allowed without any written permission. It is also understood that due recognition shall be given to me and to the University of Saskatchewan in any scholarly use which may be made of any material in my thesis.

Requests for permission to copy or make other use of material in this thesis in whole or part should be addressed to:

Head of the Department of Civil, Geological, and Environmental Engineering

University of Saskatchewan

Engineering Building

57 Campus Drive

Saskatoon, Saskatchewan S7N 5A9

Or

Dean of College of Graduate and Postdoctoral Studies

University of Saskatchewan

116 Thorvaldsen Building, 110 Science Place

Saskatoon, Saskatchewan S7N 5C9

ABSTRACT

Historical bars such as plain and Ransome bars were used in reinforced concrete structures until about the mid-1950s in the U.S and Canada. Bond provisions for plain and Ransome bars are not included in the current edition of Canadian and American codes. Twenty-two splice specimens reinforced with either plain, Ransome, or deformed bars were therefore tested monotonically under four-point loading as a part of a multi-year experimental investigation to develop bond provisions for plain and Ransome bars. The reinforcement was cast either in the bottom or top position. Load versus deflection behaviour, cracking patterns, and maximum load attained by all specimens are presented. Moment curvature analysis was performed for the specimens to calculate the tensile resistance of the reinforcement at the maximum load level.

Reliability-based provisions for splice and development length were proposed for plain bars from a test database of splice specimens. A comparison of the proposed development length required for plain bars as compared to deformed bars, calculated in accordance with CSA A23.3, suggests that plain bars require fifty percent more development length than deformed bars when cast in the bottom position. However, when reinforcement is cast in the top position, the required development length for plain square and plain round bars is two and three times that for modern deformed bars, respectively.

Similarly, reliability-based provisions for splice length were proposed for Ransome bars. A comparison of the proposed splice length of Ransome bars and that calculated for deformed bars in accordance with CSA A23.3 suggests that the bond capacity of Ransome bars closely matches to that of deformed bars when bars are cast in the bottom position. However, the required splice length for Ransome bars is around 25% more than that for modern deformed bars when cast in the top position.

CO-AUTHORSHIP

All of the experimental work presented in this thesis was conducted by Umesh Poudyal and reviewed by Dr. L.R Feldman. The results of a select number of specimens reinforced with plain bars presented in the experimental program were published in the proceedings of the 2017 CSCE Annual General Conference in Vancouver, Canada. A manuscript summarizing the findings of thesis related to plain bars was submitted to the ACI Structural Journal on July 10, 2017, with a revised version of the manuscript submitted on November 9, 2017. A second manuscript, summarizing the findings related to Ransome bars, was submitted to the ACI Structural Journal on September 19, 2017.

ACKNOWLEDGEMENTS

The author would like to specially thank his supervisor, Dr. Lisa R. Feldman, for her continuous guidance, mentorships and suggestions. The author would also like to acknowledge the guidance of his advisory committee members: Dr. Leon Wegner, and Dr. Mohamed Boulfiza.

The author would also like to thank Brennan Pokoyoway and Dale Pavier, Structures Laboratory technicians, for their immense support in the execution of experimental program. Assistance of fellow graduate students and undergraduate research assistants in specimen preparation and testing is also highly appreciated.

Scholarship support from the University of Saskatchewan is gratefully acknowledged. Donation of concrete by Lafarge Holcim for research project is also acknowledged.

Finally, the author would like to thank his family and friends for their support and encouragement throughout the duration of his M.Sc. program.

TABLE OF CONTENTS

CHAPTER 3

EXPERIMENTAL PROGRAM

CHAPTER 4

ANALYSIS OF RESULTS AND DEVELOPMENT LENGTH CRITERIA FOR PLAIN BARS

CHAPTER 5

ANALYSIS OF RESULTS AND SPLICE LENGTH CRITERIA FOR RANSOME BARS

APPENDICES

LIST OF TABLES

LIST OF FIGURES

LIST OF SYMBOLS

a	Shear span
d_b	Nominal bar diameter for round bars or nominal side face dimension for square and Ransome bars
$d_{b,EQ}$	Nominal bar diameter for round bars or equivalent round diameter for square and Ransome bars
E_c	Modulus of elasticity of the concrete
f_c	Compressive stress corresponding to strain in the concrete at any given location along the height of the cross-section
f'_c	Concrete compressive strength
f_u	Concrete cube strength
f_r	Modulus of rupture of concrete
f_{s1}	Tensile stress at a first point along a reinforcing bar
f_{s2}	Tensile stress at a second point along a reinforcing bar
f_y	Nominal yield strength of the spliced longitudinal bars
f_{yd}	Dynamic yield strength of the spliced longitudinal bars
f_{ys}	Static yield strength of the spliced longitudinal bars
I_{cr}	Cracked moment of inertia
I_e	Effective moment of inertia
I_g	Gross moment of inertia
jd	Lever arm
k_1	Bar location factor
k_2	Bar size factor

l	Length of a longitudinal bar
L	Centre-to-centre span length
L_d	Development length
L_s	Lap splice length
M	Bending Moment
M_a	Moment due to applied load
M_{cr}	Cracking moment
$\sum p$	Perimeter of all longitudinal reinforcing bars in a section
P_{max}	Maximum applied load
R_y	Maximum height of profile of the longitudinal reinforcement
T	Tensile resistance of the spliced longitudinal reinforcement at the maximum load level
u	Bond stress
u_{avg}	Average bond stress
V	Shear force
x	Distance from the centre-line of a beam support to a given section along the specimen length
y_t	Distance from the centroidal axis of the gross section, neglecting reinforcement, to the extreme tension fibre
Δf_s	Change in tensile stress
Δx	Distance between two points in a section
Δ_x	Deflection at a section located at a distance of *x* from the support
$\dot{\varepsilon}$	Strain rate
ε_c	Concrete strain corresponding to f_c

ε_0	Concrete strain corresponding to maximum compressive stress of concrete
ψ	Top cast factor
●	Symbol denoting plain round longitudinal reinforcement in a given specimen mark number
■	Symbol denoting plain square longitudinal reinforcement in a given specimen mark number
◆	Symbol denoting Ransome longitudinal reinforcement in a given specimen mark number
◙	Symbol denoting deformed longitudinal reinforcement in a given specimen mark number
↓	Symbol denoting that the longitudinal reinforcement in a given specimen was cast in the bottom position
↑	Symbol denoting that the longitudinal reinforcement in a given specimen was cast in top position

CHAPTER 1
INTRODUCTION

1.1 Background

Reinforced concrete is a common structural material in construction in most countries including the U.S.A and Canada and has been used in construction since the late 19th century (Loov, 1991). In the early 1900s, different shapes of bars were patented to use as the reinforcement. Figure 1.1 shows some of the different shapes of deformed steel bars that were available (Abrams, 1913). Plain (i.e. smooth) bars were used as reinforcement until the mid-1950s in the United States and Canada, and until the mid-1960s in Europe. Due to a shortage of deformed bars resulting from industrial unrest, plain bars re-emerged in U.K in the mid 1970s (Feldman and Cairns, 2017). Ransome bars (i.e. square twisted bars) were also used as reinforcement until the mid-1950s in the United States and Canada. Although plain and Ransome bars are no longer used as reinforcement, many historical structures are reinforced with these bars. These structures are now in the need of re-assessment and rehabilitation. As current Canadian and American codes do not have any bond provisions for plain or Ransome bars, it is essential to develop the reliability-based bond provisions for the assessment of historical structures.

The bond behaviour of plain bars is different than that of deformed bars. Plain bars cannot transfer bond forces through mechanical interlock as they do not have deformations. Hence, the bond capacity of plain bars is believed to be less than that of deformed bars. On the other hand, the bond behaviour of Ransome bars is hypothesized to be somewhat similar to that of modern deformed bars. Ransome bars transfer bond forces through their twisted configuration and, as a result, the bond capacity of Ransome bars is expected to be similar to that of deformed bars and greater than that of plain bars.

Research related to plain bars ceased once deformed bars became the norm in construction. Bond provisions for plain bars in historical editions of U.S and Canadian concrete codes were based upon limited investigations using test specimens that are now known to produce inaccurate results (ACI Committee 408, 2003). The current bond provisions for modern deformed bars are based upon test results of beam-end and splice

specimens which replicate the actual stress state in the concrete surrounding the reinforcement in flexural members. It is therefore important that new provisions for plain and Ransome bars be developed based upon experimental data of test specimens similar to those used for deformed bars. Hassan and Feldman (2012), and Sekulovic MacLean and Feldman (2014) have developed the test database using splice specimens reinforced with plain bars. Similarly, Knight and Feldman (2013) conducted a preliminary investigation for Ransome bars. This investigation extends the previous studies with additional splice specimens to develop the reliability-based bond provisions for both plain and Ransome bars in terms of splice and development length.

1.2 Objectives

The primary objective of the current investigation is to develop reliability-based bond provisions in terms of splice and development length for plain and Ransome bars for assessing historical structures. The sub-objectives of the current investigations are:

i. To compare the cracking pattern and load deflection behaviour of splice specimens reinforced with plain and Ransome bars to that of similar specimens reinforced with deformed bars.
ii. To observe the failure mechanism of splice specimens reinforced with plain bars with splices longer than that required to cause yielding of the reinforcement.
iii. To determine the top cast factors for plain and Ransome bars based upon the tensile resistance of the reinforcement at the maximum load level.
iv. To use a 5% fractile value to incorporate adequate structural safety.
v. To compare the proposed splice and development length for plain and Ransome bars with existing splice and development length equations for modern deformed bars in accordance with CSA A23.3.

1.3 Scope and Methodology

Eight splice specimens reinforced with plain bars, twelve splice specimens reinforced with Ransome bars, and two splice specimens reinforced with deformed bars were tested monotonically under a four-point loading system in the current investigation. The

reinforcement in the specimens was cast either in bottom or top position. The experimental program was conducted to develop reliability-based bond provisions in terms of splice or development length for plain and Ransome bars. Replicate specimens were not tested in the current investigation. The relevant parameters in this investigation were bar diameter, splice length, bar shape, and casting position for specimens reinforced with plain bars. All of these parameters, with the exception of bar shape, were also included for specimens reinforced with Ransome bars. Other relevant parameters such as concrete cover, bar spacing, and transverse reinforcement were not included in the current investigation and are potential parameters to be included in a follow-up investigation.

1.4 Thesis Outline

The outline of thesis is as follows:

Chapter 1 presents the research background, objectives, scope, and methodology of the current investigation.

Chapter 2 presents the literature review related to bond between reinforcement and concrete that includes mechanics of bond, factors affecting bond, test specimens to evaluate bond, and historical code requirements relevant to plain and Ransome bars.

Chapter 3 presents the experimental program and includes the geometry of the specimens, material properties, preparation of specimens, and testing of splice and companion specimens.

Chapter 4 presents the analysis of the results of the specimens reinforced with plain bars. Visual observations such as crack pattern and end slip of the bar, load versus deflection behaviour, moment curvature analysis, and a proposed splice and development length equation for plain bars are included in this Chapter.

Chapter 5 presents the analysis of the results of the specimens reinforced with Ransome bars. Visual observations such as crack pattern and end slip of the bar, load versus

deflection behaviour, moment curvature analysis, and a proposed splice length equation for Ransome bars are included in this Chapter.

Chapter 6 summarizes the findings and significant conclusions of the current investigation and provides recommendations for future investigations.

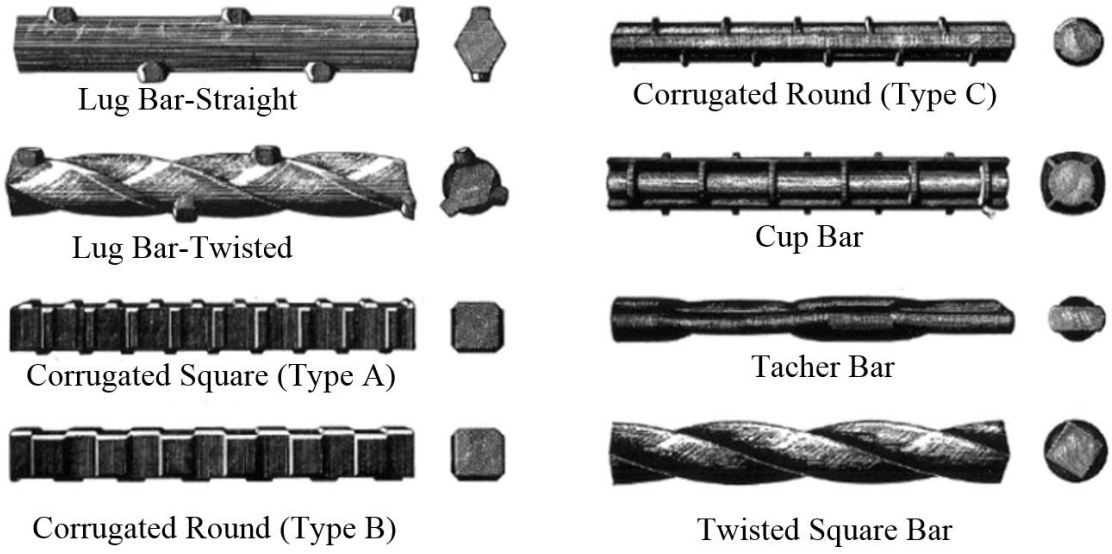

Figure 1.1: Historical Reinforcing Bar Types (Abrams 1913)

CHAPTER 2
LITERATURE REVIEW

2.1 General

This chapter presents information related to the bond behaviour between plain or Ransome bars and the surrounding concrete. Various test specimens that are used to study the bond behaviour between reinforcing bars and concrete are also discussed. In addition, significant factors that affect the bond between historical reinforcement and concrete as well as relevant past research are also discussed. Finally, the research leading to the calibration of code provisions for splice and development length such that an adequate level of structural safety is ensured is also discussed.

2.2 Bond Behaviour of Plain and Ransome Bars

Bond is necessary to transfer the force between longitudinal reinforcement and the surrounding concrete. One of the fundamental assumptions of flexural analysis is that perfect bond exists between the longitudinal reinforcing bars and the surrounding concrete. The lack of necessary bond between the longitudinal bars in a section and the surrounding concrete results in a premature failure referred to as a bond failure.

Plain bars were widely used as reinforcing bars at the beginning of the twentieth century. Both round and square plain bars were used as reinforcement in historical structural members. The bond behaviour of plain bars is different than that of modern deformed bars. Plain bars do not have lugs or other surface deformations and so do not transfer forces by bearing of these deformations against the surrounding concrete once slip initiates. Transfer of the force prior to slip of a plain bar is due to the adhesion between bars and concrete. After slip occurs, adhesion is lost and the only mechanism to transfer force is due to the frictional forces resulting from the surface roughness of the bars (Abrams, 1913). Hence, the bond capacity of plain bars is believed to be less than that of deformed bars.

Ransome bars (i.e. square twisted bars) were also widely used at the beginning of the twentieth century. Ernest L. Ransome patented these bars in 1884 (Hurd 1996). The main

objective of Ransome to twist the plain square bars was to develop a method that provides continuous bond along the length of reinforcing bars rather than relying on mechanical anchorages to transfer the forces between reinforcement and concrete as are needed for plain bars. Ransome was originally criticized for injuring the bars by twisting them. However, they were eventually accepted and used as reinforcement in concrete construction (Hurd, 1996).

The bond behaviour of Ransome bars is expected to be different from that of plain bars but hypothesized to be somewhat similar to that of modern deformed bars. Figures 2.1(a) and (b) show the bond behaviour of deformed and Ransome bars, respectively, where in each case the bar is embedded in a concrete block and subjected to tensile force, *P*. In addition to the effects of adhesion and friction, force is transferred through mechanical interlock caused by lugs, and due to the twisted configuration of the bars for deformed and Ransome bars, respectively, and so radial stresses occur in both kind of bars after slip occurs. However, for deformed bars, these stresses occur at discrete locations and at a constant angle, whereas for Ransome bars these stresses occur along the entire bar length with varying angle.

2.3 Mechanics of Bond in Reinforced Concrete

Figure 2.2 shows a simply supported beam subject to four-point loading (Figure 2.2 (a)) to illustrate the mechanics of force transfer between the concrete and the longitudinal reinforcement. The bending moment diagram due to the applied four-point loading is shown in Figure 2.2(b). Tensile stresses and strains are developed at the bottom face of the beam, and flexural cracks are developed within the midspan region of the beam once the tensile stress in the concrete exceeds the modulus of rupture (MacGregor and Bartlett, 2000). Assuming that perfect bond between concrete and reinforcement exists, a portion of the tensile force will be resisted by the concrete in regions of intact concrete between the cracks. As a result, the tensile stresses in the reinforcing steel and the concrete, respectively, at the level of the reinforcement will vary as shown in Figures 2.2 (c) and (d). A complete loss of bond between the steel reinforcement and the surrounding concrete occurs at the location of cracks. The tensile force at the crack locations can be calculated from the following equation:

$$T = \frac{M}{jd} \qquad \text{[Eq. 2.1]}$$

where M is the bending moment at the crack location, and jd is the lever arm between the tensile force in the longitudinal reinforcement and the centroid of the compressive force in the concrete. A variation in the tension force is referred to as shear flow and is calculated using Equation 2.2. The loss of bond between the reinforcing bar and the concrete causes a uniform tension force over the length of the bar and hence shear flow will be reduced to zero.

$$\frac{dT}{dx} = u \sum p \qquad \text{[Eq. 2.2]}$$

where u is the bond stress, and $\sum p$ is the perimeter of all longitudinal reinforcing bars in the section.

Figure 2.2 (e) shows the actual bond stress distribution in the beam due to the variation in the steel and concrete stresses. The bond stress depends upon the location of cracks and the tension carried by the concrete, and so predicting the actual bond stress distribution is quite complicated. However, the average bond stress between two points on a reinforcing bar can be calculated from the following equilibrium relations:

$$(f_{s2} - f_{s1})\frac{\pi {d_b}^2}{4} = u_{avg}(\pi d_b \Delta x) \qquad \text{[Eq. 2.3]}$$

where f_{s2} and f_{s1} are the tensile stress at two points on a reinforcing bar that are located at a distance of Δx apart with f_{s2} being greater than f_{s1}, and d_b is the diameter of reinforcing bar. Taking f_{s2}-f_{s1} as Δf_s (i.e. difference in tensile stress between two points) gives

$$u_{avg} = \frac{\Delta f_s d_b}{4\Delta x} \qquad \text{[Eq. 2.4]}$$

2.4 Factors Affecting Bond

The major factors that affect the bond strength between historical reinforcing bars and concrete are described in this section.

Concrete Cover

Feldman and Bartlett (2005) observed that the maximum average bond stress measured for plain steel bars is independent of concrete cover. These bars lack mechanical interlock with the surrounding concrete thus the likelihood of splitting failure is reduced. However, other researchers (Edward and Yannopoulos 1979, and Cairns 2004), have observed that bond stress is affected by the concrete cover for plain bars. The effect of concrete cover on the bond stress of Ransome bars has yet to be studied.

Development Length

Hassan and Feldman (2012) and Sekulovic MacLean and Feldman (2013) reported that there is a linear and proportional relationship between the normalized maximum applied load as a function of development length and bar diameter for plain bars. This finding differs from the linear but not proportional relationship reported in the case of deformed bars (ACI Committee 318, 2014). The reason is that for deformed bars, once slip initiates, any deformation of the bar in the development length will create mechanical interlock (Barnes et al., 2003). The expression for development length in current American and Canadian codes is, however, simplified from the fitted equation of test results. The relationship is yet to be developed for Ransome bars.

Bar Size

For a given splice length, larger bars require large forces to cause bond failure for the same degree of confinement (ACI Committee 408, 2003). However, the bond force at failure increases more slowly than the bar area due to the fact that yield force increases proportionally to the bar diameter raised to the second power whereas bond strength increases linearly with the bar diameter. A longer embedment length is therefore required for a larger bar to fully develop.

Bar Surface Condition

The surface roughness of a reinforcing bar plays an important role in the bond strength, especially for the plain bars, because of the sliding friction resistance mechanism that acts between reinforcing steel and concrete. The surface roughness of the bar can be measured

as the maximum height of profile, R_y, which is established as the distance between the highest peak and the deepest valley of the bar surface (Mitutoyo, 2006). As historical plain bars have rougher surfaces than the modern plain bars, the surface roughness of modern bars can be made representative of historical bars by using sandblasting techniques (Feldman and Bartlett, 2005).

Concrete Compressive Strength

Bond strength increases with increased concrete compressive strength. Orangun et al. (1977) reported that the square root of the concrete compressive strength represents the concrete contribution on bond between deformed bars and concrete for specified values of f'_c below 55 MPa. Feldman and Bartlett (2005) also reported that the bond strength of plain bars is proportional to the square root of the concrete compressive strength. It is assumed that a similar relationship also holds true for Ransome bars.

Transverse Reinforcement

Transverse reinforcement confines spliced bars by limiting the progression of splitting cracks and thus increases the bond force required to cause failure for deformed bars (Orangun et al., 1977). However, in the case of plain bars, splitting failure is less likely to occur as there are no radial stresses along the bar length. Hence, the role of transverse reinforcement on the bond strength between plain bars and concrete might not be as significant as compared to that between deformed bars and concrete. On the other hand, the effect of transverse reinforcement on the bond strength between Ransome bars and concrete could be significant.

Bar Shape

Different shapes of plain bars such as round, square, oval etc. were available in the mid 1920s (Erlemann, 1999). The specifications for square and round deformed bars were introduced in 1947 (ASTM, 1947) with square bars then being excluded in 1950 (ASTM, 1950). Sekulovic MacLean and Feldman (2014) studied the effect of bar shape on the bond of plain bars and found that round bars are more sensitive to casting position than square bars due to the differences in shape of voids that form under the bar. Howell and

Higgins (2007) recommended that using an equivalent round diameter is reasonable when evaluating square deformed bars, which results in equal cross-sectional area of the square bar and the equivalent round bar.

Casting Position

Bar position during concrete placement has a significant impact on the bond strength between concrete and modern deformed bars, because greater settlement and accumulation of bleed water at the bar will occur with greater depth of concrete below a bar (ACI Committee 408, 2003). The bond of plain bars is even more affected by casting position than that of deformed bars because plain bars rely predominantly on adhesion between reinforcement and concrete to transfer bond forces (Chana, 1990; Sekulovic MacLean and Feldman, 2014). Preliminary research, based upon the results of a limited experimental investigation, suggests that Ransome bars appear to be more sensitive to casting position than plain square bars (Knight and Feldman, 2013).

2.5 Test Methods

Figure 2.3 shows different test specimens that have been used to study the bond behaviour between reinforcing steel and concrete (ACI Committee 408, 2003). The pullout specimen (Figure 2.3(a)) is widely used because of its simplicity and ease of fabrication. Pullout specimens are placed on a bearing block or plate with a monotonic or repeated tensile force applied to the longitudinal reinforcement. However, this is the least realistic of the four types of test specimens shown in Figure 2.3 because the stress field in the concrete within these specimens does not match that of flexural elements as would be found in construction. When the bar is placed in tension, compression will be induced in the surrounding concrete.

Figure 2.3(b) shows a beam-end specimen which can simulate the stress state of reinforced concrete members subjected to flexure (ACI Committee 408, 2003). The compressive force exerted on the concrete is located away from the reinforcing bar by placing a reaction plate at a distance approximately equal to the bonded length of the reinforcement. A small length of a bar adjacent to the loaded end of the specimen is usually left unbonded to prevent the formation of a conical failure surface. Bond stresses

measured from beam-end specimens are reasonably equivalent to those obtained from splice specimens (ACI Committee 408, 2003).

Figure 2.3(c) is a beam anchorage specimen which is typically simply supported and tested under four-point loading so that bond behaviour of the reinforcement within the shear span and constant moment regions can be studied using a single specimen. The main disadvantage of beam anchorage specimens is that the reinforcement at the end of these specimens is subjected to compression because of the reaction forces and, in turn, increase the bond strength (ACI Committee 408, 2003).

Splice specimens (Figure 2.3(d)) are generally fabricated with a lap splice in the constant moment region between the two load points. They are relatively easy to fabricate and provide a realistic stress-state in the concrete surrounding the reinforcing bars in the constant moment region. Bond stresses measured from splice specimens are reasonably equivalent to that obtained from beam-end specimens. Splice specimens and beam-end specimens have provided the bulk of the data used to establish current design provision for development length for modern deformed bars (ACI Committee 408, 2003).

2.6 Previous Splice Specimen Test Results of Plain and Ransome Bars

Bond provisions for deformed bars should not be applied to plain bars and Ransome bars due to the anticipated difference in the bond behaviour between each bar type and the surrounding concrete. Hence, test results of beam-end and/or splice specimens are required for the development of reliable bond provisions for plain and Ransome bars.

Hassan and Feldman (2012) started the database to develop the bond provisions for plain bars. This investigation studied the effects of reinforcing bar size and lap splice length on the bond of splice specimens reinforced with plain bars in the bottom cast position. The investigation concluded that splice specimens reinforced with plain steel bars have about 60% of the capacity of the similar specimens reinforced with deformed bars based on a comparison of the applied load that they were able to resist. Sekulovic MacLean and Feldman (2014) extended this work and included other parameters such as bar shape and casting position. They reported that round bars are more sensitive to casting position than

square bars and top cast factors of 0.4 and 0.6 capture the reduction in bond resistance of splice specimens reinforced with round and square bars, respectively, based on the as-test value of the maximum applied load.

Knight and Feldman (2013) performed a limited experimental investigation on the bond behaviour of Ransome bars that included six splice specimens. The parameters of the investigations were lap splice length, and casting position. They reported that the resistance of specimens reinforced with Ransome bars are close to the capacity of the similar specimens reinforced with deformed bars based on a comparison of the applied maximum load.

The calculation of the tensile resistance of reinforcement at the maximum load level is necessary to establish bond provisions in terms of lap splice and development length. However, Hassan and Feldman (2012), Sekulovic MacLean and Feldman (2014), and Knight and Feldman (2013) did not conduct the necessary analysis and so did not report these values. The investigation discussed herin, therefore, extends these previous studies with additional splice specimens to present lap splice and development length provisions for plain and Ransome bars based on calculations of the tensile resistance of the reinforcement.

2.7 Historical Code Requirements

In this section, historical code requirements relevant to the bond stress and/or development length of plain and Ransome bars are discussed.

2.7.1 Plain Bars

Abrams' (1913) comprehensive research work on the bond between steel and concrete was the main basis for the provisions for bond in the early editions of American concrete codes. Abrams' (1913) recommendation of an allowable maximum bond stress of $0.04f'_c$ was included in the 1920 edition of ACI for plain bars (ACI, 1920). Requirements for end hooks for plain bars to provide additional anchorage were included in the 1951 edition of ACI 318 and resulted in an increased allowable maximum bond stress of $0.045\ f'_c$ (ACI Committee 318, 1951). This was also the first code to recognize top cast effects with an

allowable maximum bond stress for top cast conditions set as 0.03 f'_c. After many researchers (Clark 1946, Rehm 1961 etc.) determined that deformed bars have superior bond performance, they became the norm in concrete construction. The 1963 edition of ACI was the last to include provisions for plain bars. The allowable bond stress for plain reinforcement was set as one half that of deformed bars conforming to ASTM A305 (ASTM A305, 1950) and the reduction in allowable bond stress for top bars was set as thirty percent.

The concept of development length, as will be discussed in detail in Section 2.8, was instead adopted in the 1971 edition of ACI 318 (ACI 318, 1971). The development length equation for deformed bars was based upon the allowable bond stress set in the 1963 edition of ACI 318 (ACI 318, 1963).

2.7.2 Ransome Bars

There was no mention of Ransome bars in any of the bond provisions in U.S and Canadian code editions. It is not clear whether the provisions for deformed bars were also meant for Ransome bars. The only known code to specifically provide bond provisions for Ransome bar is British Standard BS 8110-1 (BSI, 1997). The allowable bond stress for Ransome bars in this code is $0.4\sqrt{f_{uc}}$, where f_{uc} is the concrete cube strength. According to this standard, the development length of Ransome bars is 1.25 times that of modern deformed bars, provided that all other parameters are held constant.

2.8 Establishing Proposed Splice and Development Lengths for Plain and Ransome Bars

Because of the non-uniform nature of the distribution of the actual bond stress (Feldman and Bartlett, 2007), allowable average bond stress is no longer used in bond provisions in current Canadian and U.S codes. Provisions for deformed bars are now expressed in terms of splice and development length.

A splice or development length is the bonded length of a reinforcing bar required to develop its nominal yield stress (ACI 408, 2003). If the splice or development length is not sufficient to fully develop the yield stress in the reinforcing bar, the bar will pull out

before yielding, potentially leading to a premature failure of the structural member (MacGregor and Bartlett, 2000). A splice length is used to represent the bonded length of reinforcing bars that are lap spliced whereas development length is used to represent the bonded length of a reinforcing bar at any portion of the member length. In a lap splice, the force in one bar is transferred to the concrete, which then transfers it to the adjacent bar. Lap splices are frequently required for reinforcement in beams and columns as reinforcing bars are manufactured in standard lengths only.

A statistical approach is a viable method to establish bond provisions in terms of splice and development length of reinforcement because a theoretical analysis based upon structural mechanics is quite complicated. Orangun et al. (1977) used a statistical analysis of the data obtained from test results of splice specimens with and without transverse reinforcement to derive the empirical equation for the development length for modern deformed bars. The equation was adopted for use in the 1989 edition of ACI 318 (ACI 318, 1989). The resulting equation for development length included terms for: bar diameter, d_b; the specified yield strength of the reinforcing bars, f_y; the concrete compressive strength, f'_c; cover or bar spacing; and a transverse reinforcement factor. Development and splice length for deformed bars have been updated as the test database has increased (ACI Committee 408, 2003).

Current Canadian and American codes do not include any bond provisions for plain and Ransome bars. However, ACI Committee 562 has developed a code for the repair, evaluation, and rehabilitation of existing concrete structures. Although, provisions for the bond evaluation of plain and Ransome bars are not included in the current edition, they are targeted for inclusion in a future edition of this code.

Provisions expressed in terms of splice and development length for plain and Ransome bars have been established in the current investigation using a similar approach as was implemented for deformed bars to aid in the structural evaluation and rehabilitation of historical concrete structures, as will be discussed in Chapters 4 and 5. Note that a 5% fractile approach has been used in the current investigation to calibrate a proposed equation for the splice and development length of plain and Ransome bars as an

appropriate level of structural safety to account for deviations in nominal and actual material properties, construction tolerances etc. (Orangun et. al, 1977). Furthermore, the proposed code provisions are established with consideration of the worst case scenario when the lap splices are located within the region of highest flexural stresses. Actual construction practice generally dictates that lap splices be located away from the highest moment zone.

2.9 Summary

This chapter presented the background information and current research status for the bond behaviour of plain and Ransome bars. Test results of splice and beam-end specimens have provided the bulk of the data to establish the code provisions for splice and development length for deformed bars. Hence, splice specimens were used in the current investigation to develop proposed bond provisions in terms of splice length for plain and Ransome bars. Bond provisions are established based upon a statistical analysis of test data to provide adequate structural safety, as will be discussed in Chapters 4 and 5. Details of the experimental program will be discussed in the next chapter.

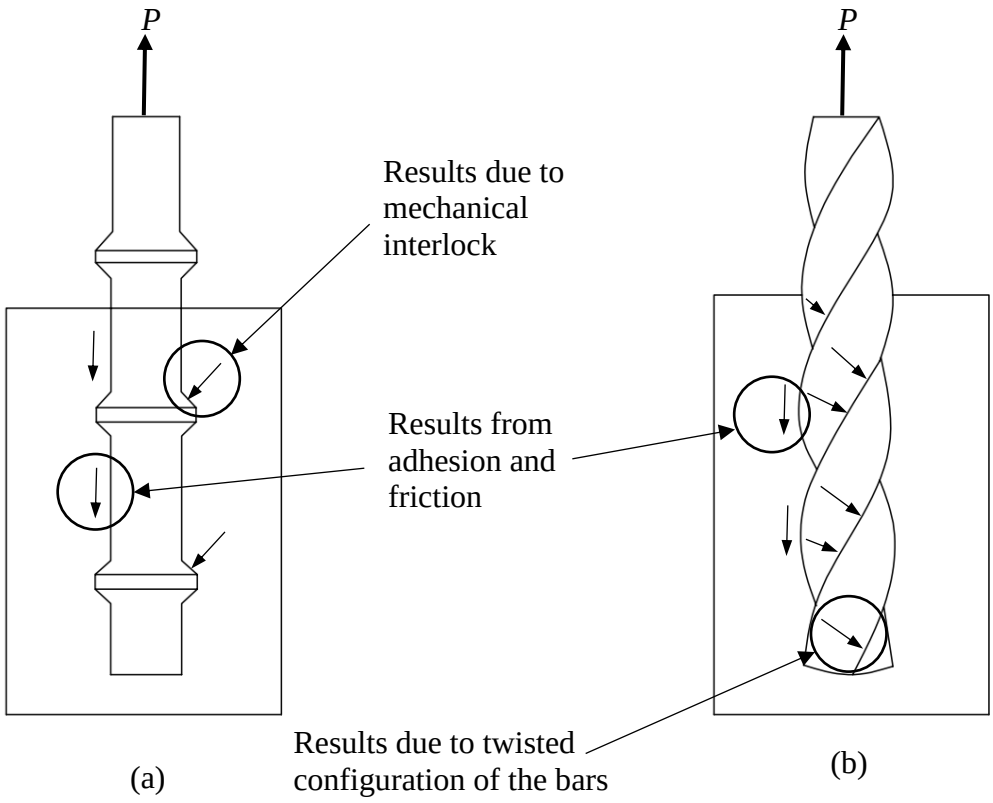

Figure 2.1: Bond Behaviour of a) Deformed Bars, and (b) Ransome Bars

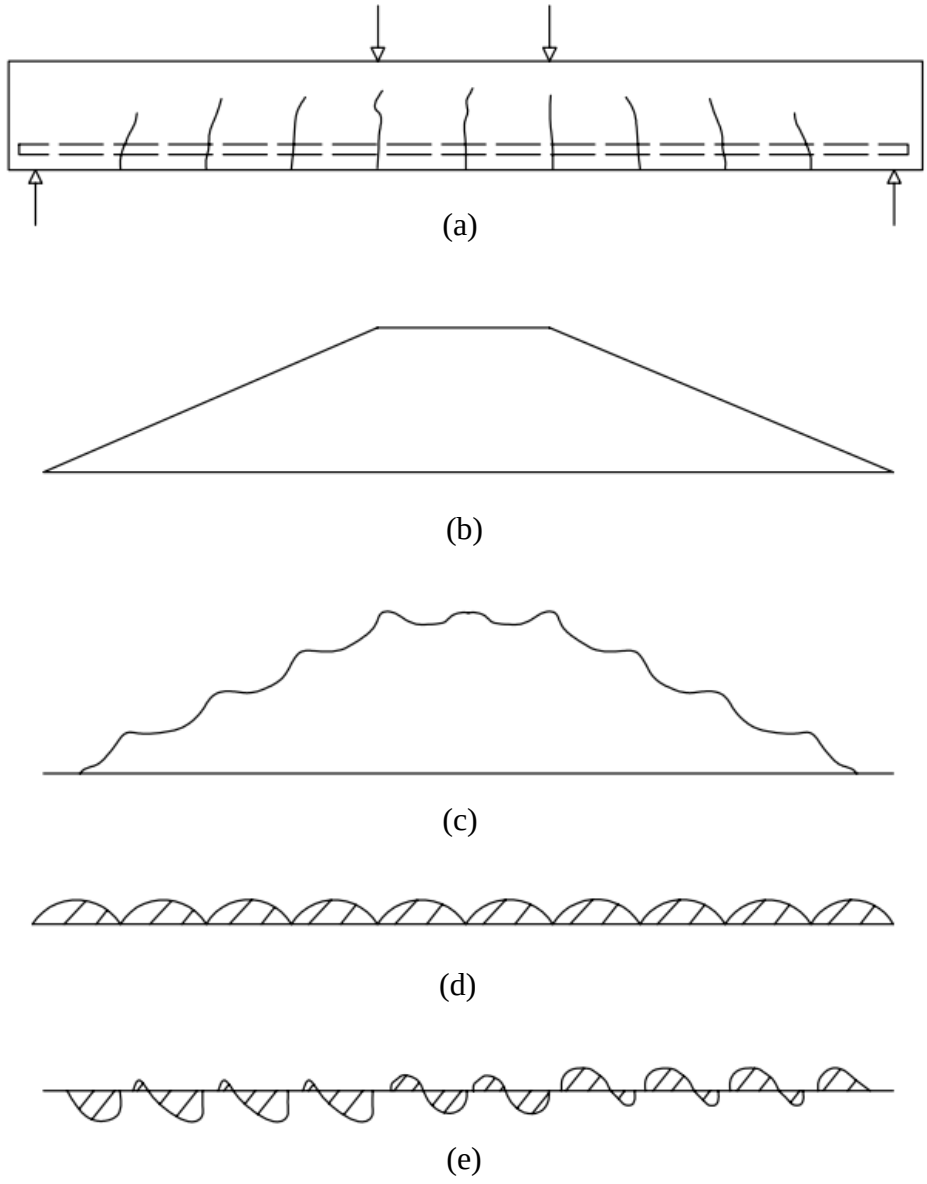

Figure 2.2: Variation of Tensile Concrete Stress, Steel Stress, and Bond Stress Along a Cracked Concrete Beam (after MacGregor and Bartlett 2000): (a) Reinforced Concrete Beam, (b) Bending Moment Diagram, (c) Variation in Steel Stress, (d) Tensile Stress in Concrete, and (e) Bond Stresses

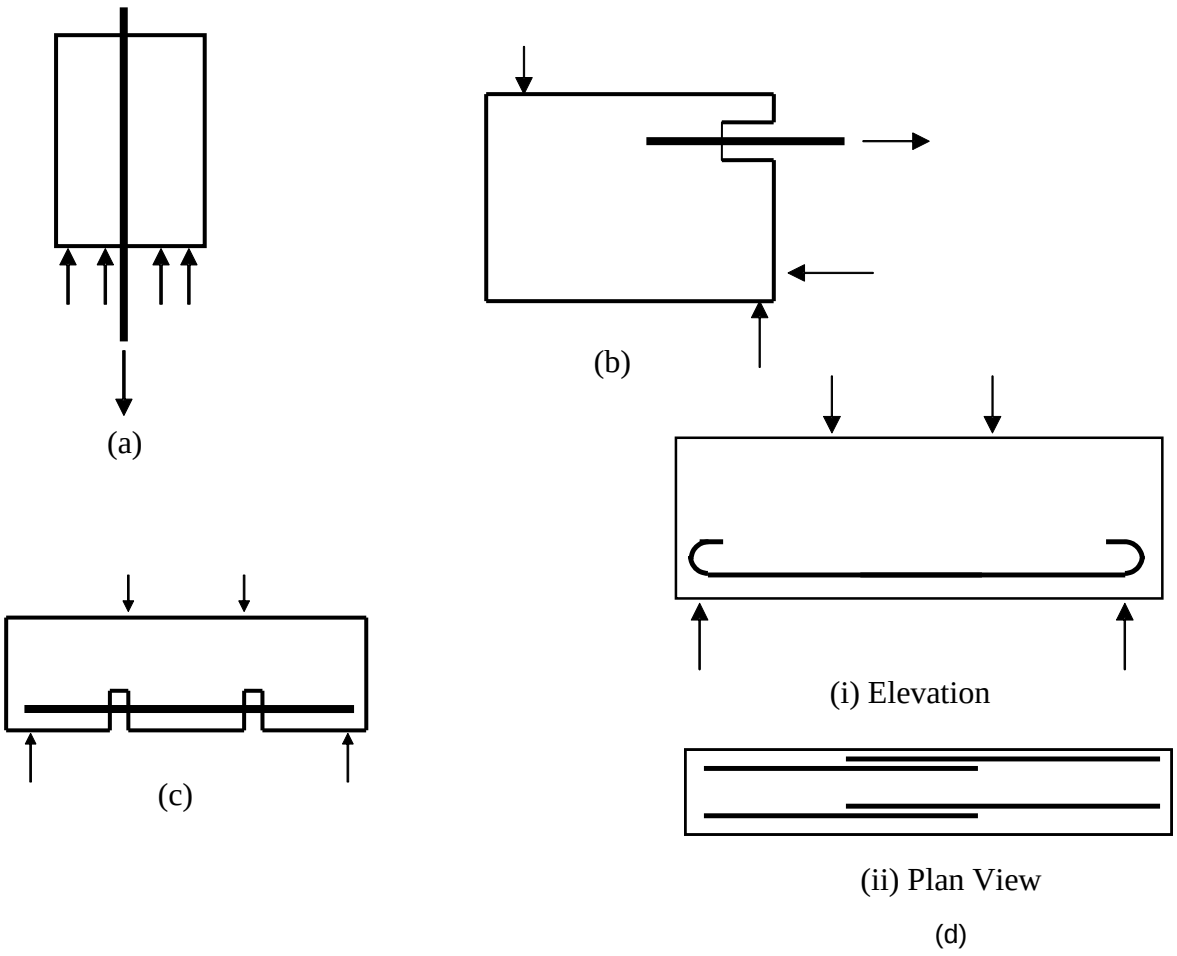

Figure 2.3: Test Specimens to Evaluate Bond: (a) Pullout Specimen; (b) Beam-End Specimen c) Beam Anchorage Specimen, and d) Splice Specimen (after ACI Committee 408, 2003)

CHAPTER 3
EXPERIMENTAL PROGRAM

3.1 General

This chapter presents the geometry of all specimens and methods for establishing their material properties. The preparation of specimens, including reinforcing cage assembly, concrete placement, and curing of specimens is also presented. Finally, the testing of specimens and companion specimens is described.

3.2 Test Parameters

This study investigates the effect of bar size, splice length, and casting position on the bond between plain or Ransome bars and concrete. Tables 3.1 and 3.2 show all previous splice specimens constructed and tested at the University of Saskatchewan reinforced with plain and Ransome bars, respectively. Previous splice specimens reinforced with plain bars as studied by Hassan and Feldman (2012) and Sekulovic MacLean and Feldman (2014) did not include any 19 mm square plain bars. Similarly, previous specimens reinforced with Ransome bars studied by Knight and Feldman (2013) were reinforced exclusively with 25 mm bars. Therefore, to establish a reliable development length equation for plain and Ransome bars, an extension of those previous investigations with additional specimens was required. Tables 3.3, 3.4 and 3.5 show the new splice specimens that were cast and tested in the current experimental program for plain, Ransome, and deformed bars, respectively. Specimens reinforced with deformed bars were also included in the current experimental program for direct comparison with the specimens that were reinforced with plain or Ransome bars.

Mark numbers have been used to effectively identify specimens in all Tables and in the text. The first number in the specimen identification represents the nominal bar size of the longitudinal reinforcement which is the nominal diameter for plain round or deformed bars, and the side face dimension for plain square or Ransome bars. The symbol following the nominal bar size represents the bar shape or type where a solid circle (●) represents plain round bars, a solid square (■) represents plain square bars, a solid

diamond (◆) represents Ransome bars, and circle inside a solid square (◙) represents deformed bars. The number following the hyphen represents the lap splice length of the longitudinal bars in mm, and the final symbol represents the position of reinforcing bar at casting where a downward arrow (↓) indicates that the specimen was cast in the bottom position, and an upward arrow (↑) indicates that the specimen was cast in the top position.

Two specimens reinforced with plain bars (19●-1010↓ and 19●-1210↓) were cast with long lap splice lengths so that these specimens would fail in flexure. All of the remaining specimens were designed to fail in bond. Except for two specimens with long splice lengths (19●-1010↓ and 19●-1210↓), lap splice lengths, L_s, varied from 21.6 to 32.1 times the bar size.

The cross-sectional area and equivalent diameter of a 32 mm square bar matches closely with that of a 35M deformed bar and it would have been ideal to compare these two bar sizes. However, the Universal Testing Machine does not have sufficient capacity to test intact 35M deformed bars to establish their stress-strain behaviour. Specimens having 20M deformed bar were therefore included to compare with specimens having 19 mm Ransome or plain bars. The percentage difference in the perimeter and cross-sectional areas of a 20M deformed bar and a 19mm Ransome or plain square bar is 14.1% and 17.3%, respectively.

Average as-measured top cover to the longitudinal reinforcement at casting for splice specimens is provided in Tables 3.1 to 3.5. Top cover for some specimens (25●-510↑, 32◆-410↑, 32◆-610↑, and 32◆-810↑) exceeds the tolerances prescribed by CAN/CSA A23.1-14 (2014) by 2 to 8 mm. Note that cover to the spliced longitudinal reinforcement was only measured for the top cast specimens and hence it is reported as not applicable for all bottom cast specimens. Top cover was not measured in the investigation conducted by Knight and Feldman (2013) and hence it is not reported in Table 3.2. Details of the measurement of top cover in current investigation are provided in Section 3.5.2.

3.3 Specimen Geometry

The geometry of the specimens constructed in this investigation was similar to that reported by Hassan and Feldman (2012), Sekulovic MacLean and Feldman (2014) and Knight and Feldman (2013). Figure 3.1(a) shows the cross-section of the specimens longitudinally reinforced with plain round or deformed bars, and Figure 3.1(b) shows the cross-section of the specimens longitudinally reinforced with plain square or Ransome bars. The width and height of the specimens were 305 mm and 410 mm, respectively. Two 10M deformed bars were used longitudinally in all specimens to complete the reinforcing cage. The bottom, side, and top covers to the longitudinal bars were nominally set to 50 mm for all specimens. The effective depth of specimens with 19 mm plain or Ransome bars, 32 mm Ransome bars, and 20M deformed bars were 350.5, 344 and 350 mm, respectively.

Figure 3.2 shows the arrangement of reinforcement and setup of the specimens at testing. Specimens having longitudinal reinforcement cast in top position were inverted before testing. Figure 3.2 (a) shows the elevation of the specimens at testing. The length of all specimens was 4.87 m, whereas the span length between the centreline of supports was 4.57 m. Shear span to depth ratios were approximately equal to 3.94 for all specimens. Transverse reinforcement was required to prevent sudden shear failure. Figure 3.2(b) shows the distribution of shear reinforcement along the length of specimens. Plain steel bars with a diameter of 12.7 mm were provided as stirrups for the specimens reinforced with plain or Ransome bars, whereas 10M deformed bars were provided for specimens reinforced with deformed bars. Note that the plain bars were used as stirrups for the specimens reinforced with Ransome bars because the inspection of a number of historical structures showed that plain stirrups were generally used in combination with longitudinal Ransome bars. The stirrups were spaced at 200 mm on center in the shear spans and 250 mm on center within the constant moment region. Two additional stirrups were also provided in the splice region to prevent prying action of the longitudinal reinforcement. These additional stirrups were placed at one-quarter of the splice region but did not exceed 150 mm from the ends of the splice. The total number of stirrups in the specimens varied depending upon the designed lap splice length of the specimens as

provided in the footnotes to Figure 3.2 (b). More shear reinforcement than necessary was provided in all specimens to avoid a shear failure.

All longitudinal bars had 180° hooks at one end of the bar adjacent to the beam supports to ensure that the bond failure would occur within the lap splice length. The geometry of the hooks for all 20M deformed bars was in accordance with CSA A23.1-14 (CSA 2014). Similarly, the geometry of all 19 mm plain or Ransome longitudinal bars and 32 mm Ransome bars was as prescribed for 20M diameter deformed bar and 35M diameter deformed bar, respectively, in accordance with CSA A23.1-14 (CSA 2014) as there is no standard available for the geometry of hooks for plain or Ransome bars in CSA A23.1-14 (CSA 2014).

3.4 Material Selection

3.4.1 Concrete

The concrete for the current experimental program was selected in such a way that the final product would reasonably represent historical concrete. The target 28-day concrete compressive strength was 20 MPa and general-purpose Portland Cement without admixtures and air entrainment was used. The mix design per m^3 of concrete consisted of: 270 kg cement, 993 kg sand, 1039 crushed coarse aggregate, and 145 L water. This mix design does not match with the specimens tested by Hassan and Feldman (2012) due to a change in material supplier partway through the multi-year investigation. Hassan and Feldman (2012)'s mix design consisted of: 250 kg cement, 110 kg crushed limestone and granite coarse aggregate blend, 1100 kg silica sand fine aggregate, and 140 L water. The effect of mix design on bond strength between the reinforcing bar and concrete is not within the scope of this investigation as bleed water measurements were not conducted. The maximum aggregate size was 20 mm and all aggregates conformed to CAN/CSA A23.1-14 (2014). A ready-mix supplier was used to deliver the concrete instead of using the mixer in the laboratory due to the large volume of concrete required for each construction phase.

3.4.2 Reinforcing Steel

In this section, general information and preparation of all principal longitudinal and transverse reinforcement is explained.

Plain Bars

The longitudinal reinforcement was hot-rolled CSA G40.21 300W (CSA G40.21, 2013). All round and square bars were procured in 6m lengths. All plain bars were cut using a band saw in the laboratory to the required lengths that allowed bending of the hooks at one end of the bars depending upon the lap splice length used for individual splice specimens. Historical steel bars have rougher surfaces in comparison to modern bars (Feldman and Bartlett, 2005). The average surface roughness of the sandblasted bars used by Feldman and Bartlett (2005) in their pullout test was 11.3μm which was the lower bound of the surface roughness of the longitudinal bars used in the Abrams' (1913) investigation. The longitudinal bars as received for this investigation were therefore sandblasted to increase the surface roughness. This was done using 220-grit aluminium oxide, a nozzle distance of 125mm, and a blast pressure of 698 kPa. Figure 3.3 shows the surface roughness tester that was used to measure the surface roughness of longitudinal bars following sandblasting. A total of around 30 to 40 roughness measurements were made on each bar using a Mitutoyo SJ-201 surface roughness tester with 0.25 mm stroke. The surface roughness of each bar, R_y, was characterized by the distance between the highest peak and deepest indention on the surface, R_y, within the stroke length (Mitutoyo, 2006). The size of bar was also measured at each location of surface roughness measurement using a slide calliper.

Ransome Bars

The pitch (i.e. the length per twist or revolution) of Ransome bars was selected to ensure that it matched with typical historical Ransome bars. This was achieved by reviewing the available literature and samples from an existing structure. The pitch of three 12.7 mm bars used to reinforce main floor slab of Peter-Mackinnon Building at University of Saskatchewan (Figure 3.4) had a pitch ranging from 1.9 to 2.35 turn per foot, whereas the 19 mm bar used as longitudinal reinforcement in a column supporting the main floor was

measured as 1 turn per foot (Knight and Feldman, 2013). Table 3.6 shows the value of pitch in terms of the number of turns per foot from historical literature. The pitch selected for the 25 mm bars previously reported by Knight and Feldman (2013) was 1 turn per foot. Eq.3.1, which was based upon pitch selected for 25 mm bars, was used to calculate the pitch for any other bar sizes in terms of turn/foot:

$$\text{Pitch} = \frac{1 \text{ turn/foot}}{\text{Bar size in inches}} \qquad \text{Eq. 3.1}$$

The resulting pitch for 19 and 32 mm Ransome bars were 4/3 turns per foot and 0.8 turns per foot, respectively. These values fall within the range as reported in the available literature. However, as there is a wide range of pitch in available literature, further study is required to evaluate the effect of pitch on bond strength between Ransome bars and concrete.

All longitudinal reinforcement was hot rolled CSA G40.21 300W (CSA G40.21, 2013) steel. All 19 mm square bars were procured from a single heat batch, whereas the 32 mm bars were procured from two different heat batches as the first order of 32 mm bars was insufficient for six specimens. The bars were sandblasted using a similar procedure as explained before. The bars were then twisted using a lathe (Figure 3.5), with a fixed tailstock and rotating headstock by RMD Engineering incorporation. Bars were sandblasted before twisting based upon a lesson learned from the Knight and Feldman's (2013) work. It was quite inconvenient for the sandblasting company to sandblast the twisted bars as that resulted in more grit use and time. Figure 3.6 shows that a short length at one end of each bar (i.e. 600 mm for 19 mm bars and 900 mm for 32 mm bars) was intentionally left untwisted to allow these segments to be ductile enough to allow the reinforcing steel supplier to provide 180° hook without fracturing the bars. Figure 3.7 shows a Ransome bar with a hook at one end.

Deformed Bars

Longitudinal reinforcement was Grade 400 20M modern deformed reinforcement conforming to CSA G30.18-09 (2014). All 20M modern deformed bars were procured from a single heat batch.

Transverse Reinforcement

Shear reinforcement was 12.7 mm diameter hot-rolled CSA G40.21 300W (CSA G40.21, 2013) plain steel bars for specimens reinforced with plain or Ransome bars. Specimens reinforced with deformed bars included Grade 400 10M modern deformed bars. All stirrups were bent in the laboratory. Figure 3.8 shows a sample plain stirrup that was bent in the laboratory. Stirrups were bent with 135° degree standard hooks in accordance with CAN/CSA A23.1-14 (2014) as prescribed for 10M deformed bars as there is no standard available for 12.7 mm diameter plain bars in CAN/CSA A23.1-14 (2014). The final average as-measured width and height of stirrups were 205±5mm and 310±5mm, respectively. The variations meet the tolerance as stipulated by CAN/CSA A23.1-14 (2014).

3.5 Specimen Preparation

This section describes the preparation of the splice specimens and associated companion specimens. The preparation of forms, reinforcement cage assembly, concrete placement, and testing of splice and companion specimens are discussed here.

3.5.1 Form Preparation

Six wooden forms with required dimensions were prepared in the laboratory as a maximum of six splice specimens were planned to be tested in each phase due to the space constraints in the laboratory. The actual length, width, and height of the forms varied between 4870±10 mm, 305±10 mm and 410±10 mm, respectively. These variations meet allowable tolerances provided in CAN/CSA A23.1-14 (2014). Whenever possible, forms were repaired and re-used for the subsequent phase. However, one form incurred irreparable damage while stripping a specimen in the second phase and so was replaced for the subsequent phase.

3.5.2 Reinforcing Cage Assembly

Figure 3.9 shows the reinforcing cage constructed for a specimen reinforced with Ransome bars. The construction of each reinforcing cage began by resting two 10M deformed bars on a table and wooden platforms that allowed for work to take place at a comfortable height. Stirrups were then placed at the required spacing in such a way that the deformed longitudinal bars sat in the top inside corners of the stirrups. The four longitudinal lap spliced bars were then placed on the bottom leg of stirrups. The spliced bars were initially tied together using tie wire and duct tape within the spliced location, all of which was removed before concreting so that the bond between reinforcing bar and concrete would not be compromised. The reinforcing cages were then secured by tying the longitudinal bars to all stirrups.

Figure 3.10 shows a cage in the forms prior to casting of concrete. Form release agent was sprayed on the wooden forms and plastic moulds for the companion cylinders on the day before concrete placement. Around 8-50 mm plastic chairs were placed on the bottom of each form to support the longitudinal bars and so maintained the desired cover of 50 mm. Plastic chairs were not placed within the splice region as it was thought that they might affect the consolidation of the concrete and hence affect the bond between the lapped reinforcing bars and the concrete. The same plastic chairs were also used to maintain side cover for the longitudinal bars, if necessary. Cages for top-cast specimens were inverted prior to placement in the forms such that the principal longitudinal reinforcement was in the top position for concrete placement. Slight adjustment of cages was done to ensure that they were placed correctly in the forms before the placement of the concrete. Top cover was measured for the top cast specimens at five locations along the specimens: at the specimen centreline, at the end of the spliced bars, and at two random locations within each shear span region. Note that the top cover for bottom cast specimens was not measured since the position of the longitudinal reinforcement in the bottom cast specimens was controlled by the use of plastic chairs. Two lifting hooks were tied into each reinforcing cage to lift the specimens using the overhead crane as available in the structural laboratory.

3.5.3 Concrete Placement

Concrete was unloaded from the ready-mix truck to the hopper. The hopper was then lifted by the overhead crane and was moved to the corresponding splice specimen. Concrete was placed in the forms, first in the splice region to have proper consolidation in this region, and then elsewhere. An electric vibrator (Figure 3.11) was used for compaction of the concrete. Excess concrete on the top surface was screeded and made smooth by trowel. Figure 3.12 shows a set of specimens after screeding. Concrete was also transferred to a wheel barrow and used to perform a slump test and to fill plastic moulds for the companion cylinders. Figure 3.13 (a) and (b) shows a slump test and casting of concrete companion cylinders, respectively.

All specimens were covered with wet burlap and plastic sheets (Figure 3.14) two hours following concrete placement. The burlap was dampened every 24 hours for seven days to moist-cure the specimens. Concrete cylinders were covered with plastic sheets and were cured for seven days. Specimens and companion cylinders were stripped out of the forms and moulds, respectively, following the seven-day initial curing period. Both splice specimens and companion specimens were then stored in the laboratory until the time of testing.

3.6 Testing of Splice Specimens

One side of each specimen was painted with white before testing to aid in the identification of cracking. Steel angles were glued to the unpainted (i.e. opposite) face of each specimen at locations where linear variable differential transformers (LVDTs) were to be used. Figure 3.15 shows the location of the LVDTs used to measure the deflection along the span of the splice specimens. The midspan LVDT had a range of 100 mm whereas all other LVDTs had a range of 50 mm.

A single material testing machine (MTS) actuator was used to test the specimens. The actuator was operated in displacement control rate at rate of 0.015 mm/s to failure. Figure 3.16 shows the test setup for the specimens. A 2.4 m long spreader beam (2C250x23) was used to transfer the load from the actuator to the specimens and to establish the four-point loading system. The total self weight of the spreader beam and other accessories

excluding self weight of the splice specimen was 2.77 kN. Figure 3.17 shows that the cracks were marked using a permanent marker for the duration of the test until specimens attained the maximum load.

3.7 Testing of Companion Specimens

In this section, compressive and tensile strength testing of companion cylinders are discussed. In addition, tensile testing of longitudinal reinforcement is also discussed.

3.7.1 Compressive Strength Testing of Companion Cylinders

Three companion cylinders, with a diameter of 100 mm and length of 200 mm, were tested in accordance with CAN/CSA A23.2-14 (2014) to determine the compressive strength of the concrete on the same day as the corresponding lap splice specimen was tested. Tests were performed using a Universal Testing Machine with a loading rate of 0.25 MPa/s. The loading rate complied with the specified rate prescribed by CAN/CSA A23.2-14 (2014). Cylinders were capped with a sulphur-based compound to level the top and bottom surfaces.

Figure 3.18 shows the set-up for the compression tests. A laser extensometer or compressometer was used to capture the axial strain in the specimens. Dial-gauge reading of the compressometer at different load levels was recorded manually to obtain axial strain when this method of measurement was used.

3.7.2 Splitting Tensile Strength Test of Companion Cylinders

Split cylinder testing was done to determine the tensile strength of the concrete. Figure 3.19 shows the setup for the splitting tensile strength tests. Tests in accordance with CAN/CSA A23.2-14 (2014) were performed using the Universal Testing Machine on the same day that the corresponding lap splice specimen was tested.

3.7.3 Tensile Testing of the Longitudinal Reinforcement

Mechanical properties of the longitudinal reinforcement were evaluated by performing tensile strength tests using the Universal Testing Machine. Three tensile test specimens of intact bar lengths were prepared and tested for the 20M deformed bars. Similarly, three

machined specimens conforming to ASTM Standard A 370 (2016) and three specimens of intact bar lengths were prepared and tested for plain bars from excess bar lengths for each heat batch of each bar size and type.

As the microstructure of Ransome bars varies with the distance from their centroid due to the cold work while twisting, intact lengths would ideally be used for the tensile testing of Ransome bars. However, intact lengths of the 32 mm Ransome bars could not be tested because the anticipated ultimate load for the specimens was greater than the capacity of Universal Testing Machine. Therefore, three tensile test specimens for 32 mm Ransome bars from each heat batch were machined and tested, whereas that for 19 and 25 mm Ransome bars were tested using intact bar lengths. Three tensile test specimens for each size of 19 and 25 mm Ransome bars were also machined and tested to confirm whether results from the two methods were reasonably similar or not. Figures 3.20 (a), (b) and (c) show the machined tensile specimens for 19, 25 and 32 mm Ransome bars, respectively. The cross-section of the tested length (i.e. machined portion) was made as close as possible to the original cross section of the bars so that the mechanical properties of tensile test specimens reasonably represent that of the actual reinforcement in the lap splice specimens.

Tensile test specimens for the 25mm Ransome bar were also prepared and tested as they had not been successfully tested by Knight and Feldman (2013). Full penetration welding was done between untwisted bar segments at the top and bottom of Ransome bar specimens prepared by Knight and Feldman (2013) to ensure that the specimens could be gripped by the testing machine. However, specimens failed at the penetration welds and the ultimate stress could not be captured. Note that welding was not necessary as the twisted portion was successfully gripped by the test machine.

Figures 3.21 (a) and (b) shows the test setup for the intact Ransome bar length and machined specimen, respectively. Strain was measured using either a laser extensometer with a gauge length of around 50 mm or strain gauges with a gauge length of 3 mm. Strain gauges were used in all tensile specimens of 32 mm Ransome bars and in one machined specimen of 25 mm Ransome bar. The laser extensometer was used in the

remaining specimens. Note that the laser extensometer had to be replaced by strain gauges as it ceased to function properly.

Details of the experimental program were discussed in this chapter. The results from the testing of splice specimens, concrete companion cylinders, and longitudinal reinforcement, as discussed in this chapter, are presented in Chapter 4.

Table 3.1: Previously Reported Specimens Reinforced with Plain Bars

Specimen ID	Splice Length as a Function of Bar Size	Measured Top Cover at Casting, mm
19●-305↓[a]	16.1d_b	N/A
19●-410↓[a]	21.6d_b	N/A
19●-510↓[a]	26.8d_b	N/A
19●-610↓[a]	32.1d_b	N/A
25●-410↓[a]	16.4.d_b	N/A
25●-510↓[a]	20.4d_b	N/A
25●-610↓[a]	24.4d_b	N/A
25●-810↓[a]	32.4d_b	N/A
25●-410↑[b]	16.4d_b	57
25●-510↑[b]	20.4d_b	65
25●-610↑[b]	24.4d_b	59
32●-410↓[a]	12.8d_b	N/A
32●-610↓[a]	19.1d_b	N/A
32●-810↓[a]	25.3d_b	N/A
32●-910↓[a]	28.4d_b	N/A
25■-410↓[b]	16.4d_b	N/A
25■-510↓[b]	20.4d_b	N/A
25■-610↓[b]	24.4d_b	N/A
25■-410↑[b]	16.4d_b	59
25■-510↑[b]	20.4d_b	53
25■-610↑[b]	24.4d_b	60
32■-410↓[b]	12.8d_b	N/A
32■-610↓[b]	19.1d_b	N/A
32■-810↓[b]	25.3d_b	N/A
32■-410↑[b]	12.8d_b	60
32■-610↑[b]	19.1d_b	61
32■-810↑[b]	25.3d_b	60

[a]Originally reported by Hassan and Feldman (2012)
[b]Originally reported by MacLean and Feldman (2014)

Table 3.2: Previously Reported Specimens Reinforced with Ransome Bars

Specimen ID	Splice Length as a Function of Bar Size	Measured Top Cover at Casting (mm)
25◆-410↓[c]	$16.4d_b$	N/A
25◆-510↓[c]	$20.4d_b$	N/A
25◆-610↓[c]	$24.4d_b$	N/A
25◆-410↑[c]	$16.4d_b$	Not Measured
25◆-510↑[c]	$20.4d_b$	Not Measured
25◆-610↑[c]	$24.4d_b$	Not Measured

[c]Originally reported by Knight and Feldman (2013)

Table 3.3: Specimens Reinforced with Plain Bars in the Current Experimental Program

Specimen ID	Splice Length as a Function of bar size	Measured Top Cover at Casting (mm)
19■-410↓	410($21.6d_b$)	N/A
19■-510↓	510($26.8d_b$)	N/A
19■-610↓	610($32.1d_b$)	N/A
19■-410↑	410($21.6d_b$)	60
19■-510↑	510($26.8d_b$)	60
19■-610↑	610($32.1d_b$)	61
19●-1010↓	1010($53.2d_b$)	N/A
19●-1210↓	1210($63.7d_b$)	N/A

Table 3.4: Specimens Reinforced with Ransome Bars in the Current Experimental Program

Specimen ID	Splice Length as a Function of Bar Size	Measured Top Cover at Casting (mm)
19◆-305↓	305($16.1d_b$)	N/A
19◆-410↓	410($21.6d_b$)	N/A
19◆-510↓	510($26.8d_b$)	N/A
19◆-305↑	410($16.1d_b$)	56
19◆-410↑	510($21.6d_b$)	58
19◆-510↑	610($26.8d_b$)	57
32◆-410↓	410($12.8d_b$)	N/A
32◆-610↓	610($19.1d_b$)	N/A
32◆-810↓	810($25.3d_b$)	N/A
32◆-410↑	410($12.8d_b$)	64
32◆-610↑	610($19.1d_b$)	64
32◆-810↑	810($25.3d_b$)	70

Table 3.5: Specimens Reinforced with Deformed Bars in the Current Experimental Program

Specimen ID	Splice Length as a Function of Bar Size	Measured Top Cover at Casting (mm)
20■-410↓	410($20.5d_b$)	N/A
20■-610↓	610($30.5d_b$)	N/A

Table 3.6: Pitch of Ransome Bars (in turns per foot)

Bar Size(in)	Pitch (Ransome 1894)	Pitch (Shuman 1907)	Pitch (Hool and Johnson 1918)
1/4	6	4	5
1/2	3	3 to 5	2
3/4	2	3/2 to 5/2	1
1	0.75	1 to 7/4	3/4
1 1/4	N/A	3/4 to 3/2	1/2

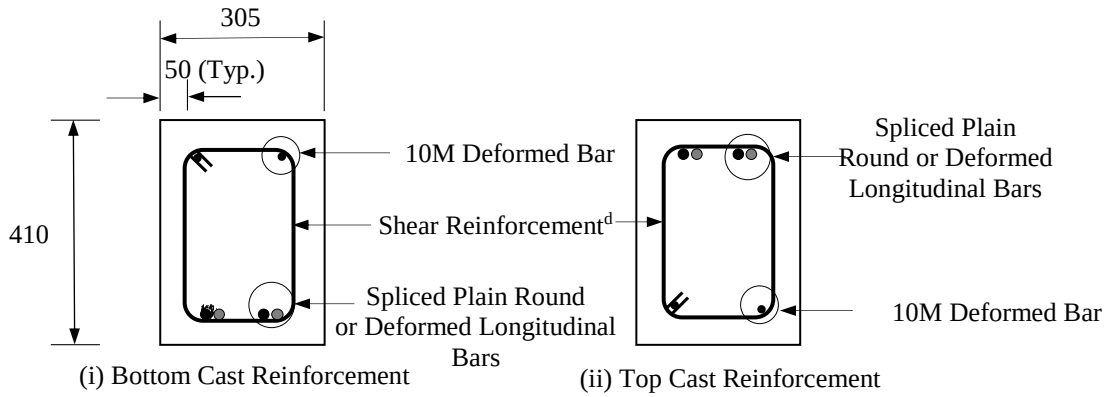

Note:
[d]12.7 mm ϕ plain round bar for specimens longitudinally reinforced with plain bars and 10M modern deformed bar for specimens longitudinally reinforced with modern deformed bar

(a)

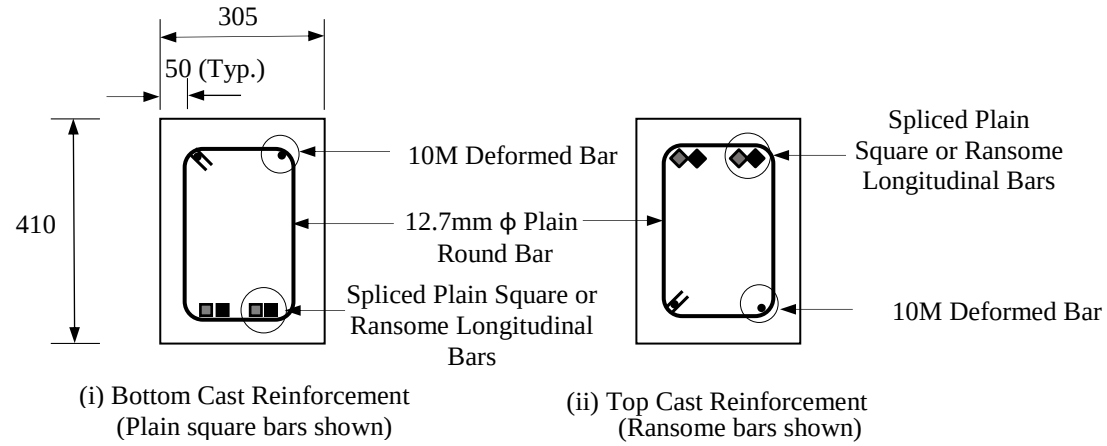

(b)

Figure 3.1 Cross-Section of Splice Specimens during Concrete Placement for (a) Plain Round or Deformed Bars and (b) Plain Square or Ransome Bars

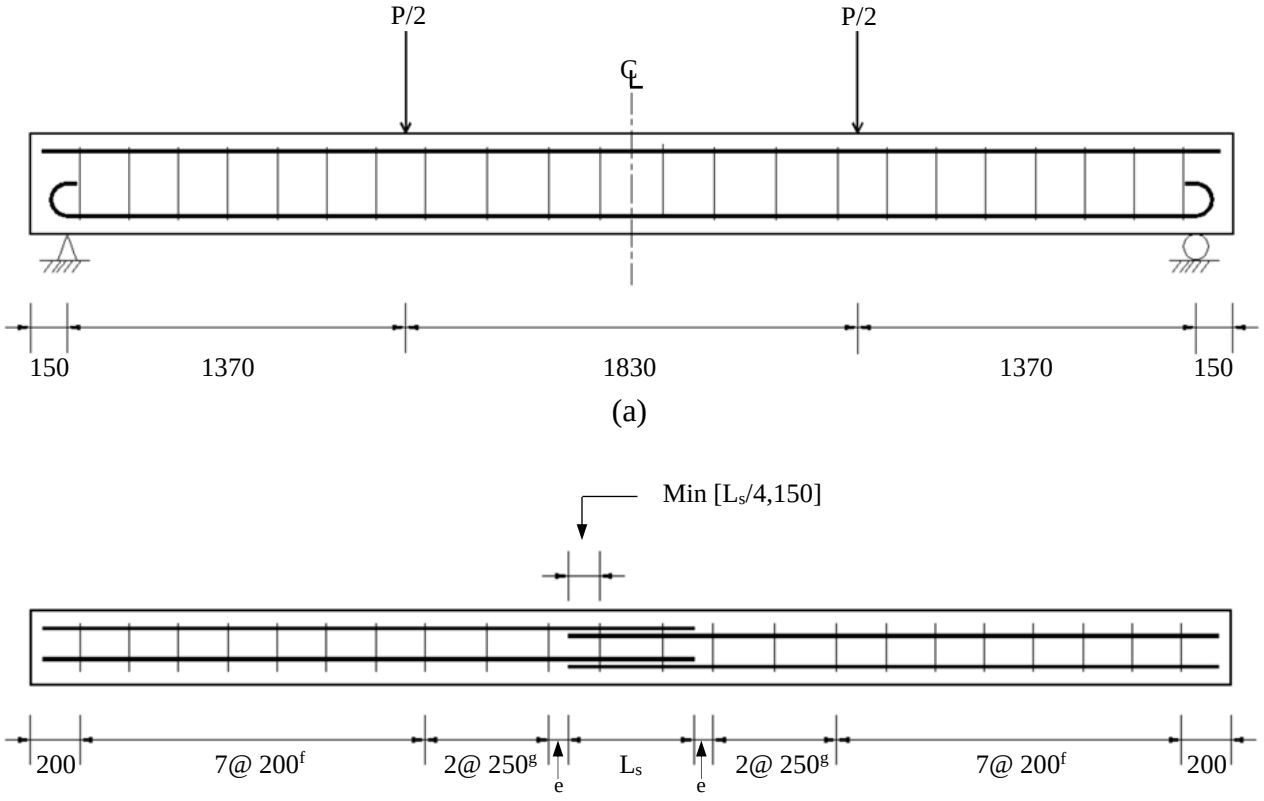

Notes:
[e]Varies with splice length
[f]7@ 200 for L_s < 1210; 8@ 200 for L_s= 1210
[g] 2 Spaces for L_s < 810; 1 space for L_s= 810 and 1010; n/a for L_s= 1210

Figure 3.2: Reinforcement Arrangement and Test Setup of the Splice Specimens: (a) Elevation, and (b) Plan View.

Figure 3.3: Surface Roughness Measurement

Figure 3.4: Ransome Bar used as a Reinforcement in the Main Floor Slab of the Peter MacKinnon Building, University of Saskatchewan

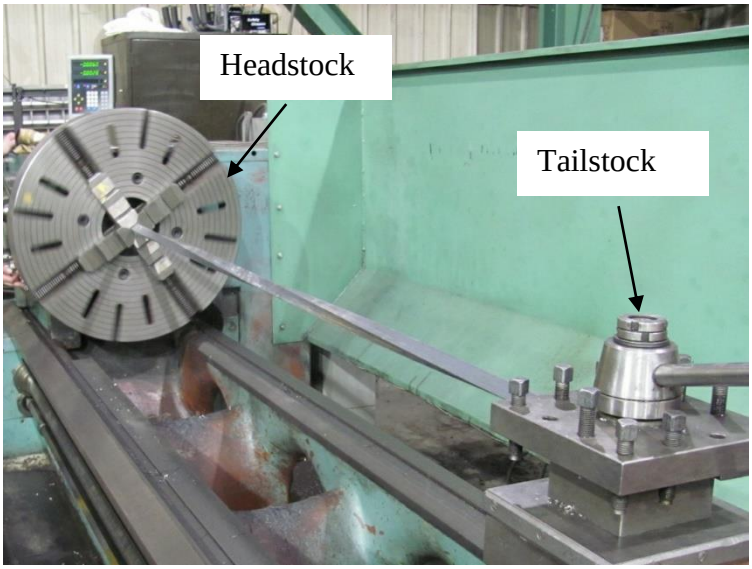

Figure 3.5: Twisting of the Ransome Bars (Photo Courtesy RMD Engineering Inc.)

Figure 3.6 Ransome Bars with Untwisted Length at One End

Figure 3.7 Ransome Bar with Hook at One End

Figure 3.8: Plain Stirrup Bent in the Laboratory

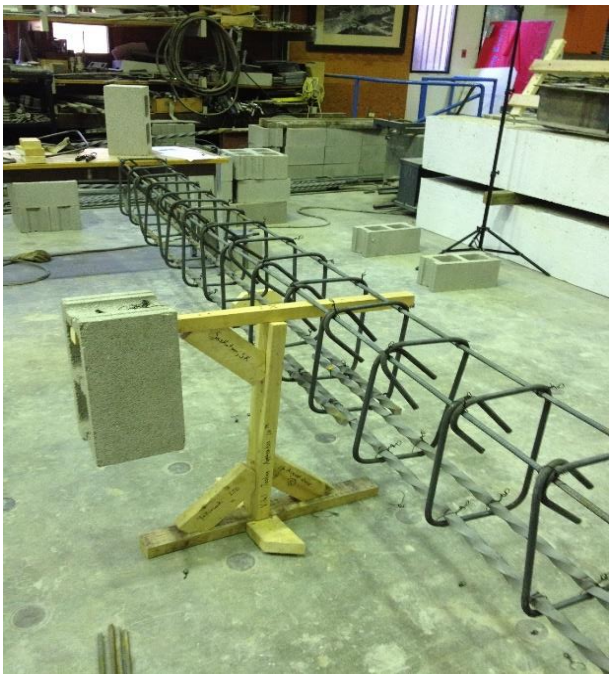

Figure 3.9: Construction of the Reinforcing Cage for Specimens Reinforced with Ransome Bars

Figure 3.10: Placement of Reinforcing Cage Prior to Casting of Concrete

Figure 3.11: Concrete Consolidation using Electric Vibrator

Figure 3.12: Concrete after Screeding Top Surface

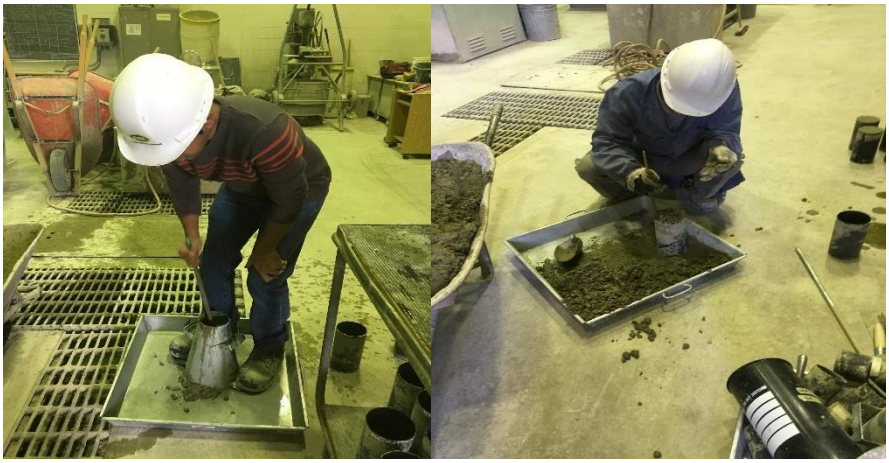

(a) (b)

Figure 3.13: Slump Testing and Casting of Concrete Companion Cylinders (a) Slump Testing and (b) Casting of Companion Cylinders

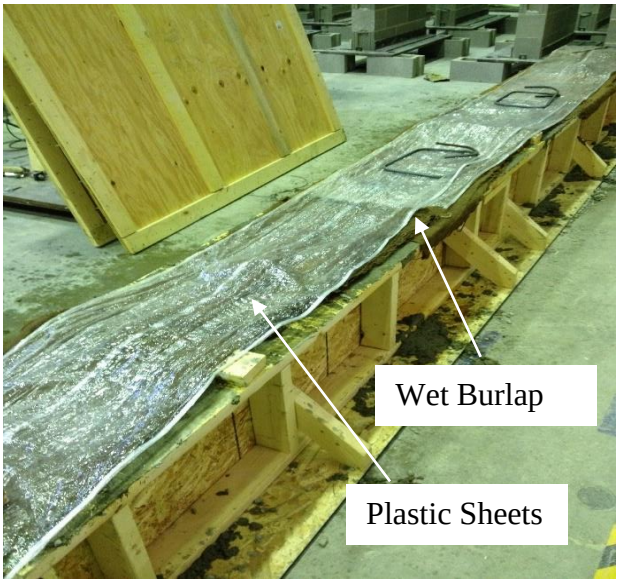

Figure 3.14: Curing of Splice Specimens

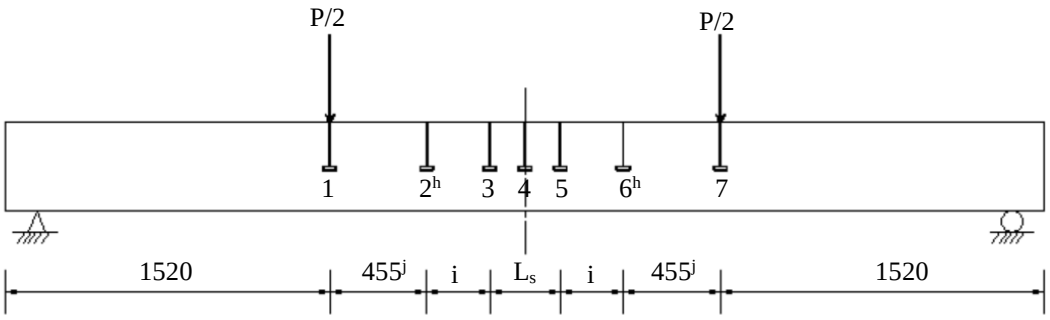

[h] LVDT No. 2 and 6 were not used for the specimens with L_s= 810, 1010 and 1210 mm.
i Varies with lap splice length provided for specimens. Indicates dimension between LVDT 3 and 1 for specimens with L_s = 810, 1010 and 1210 mm.
[j] N/A for specimens with L_s = 810, 1010 and 1210 mm.

Figure 3.15: Location of LVDTs on Specimen

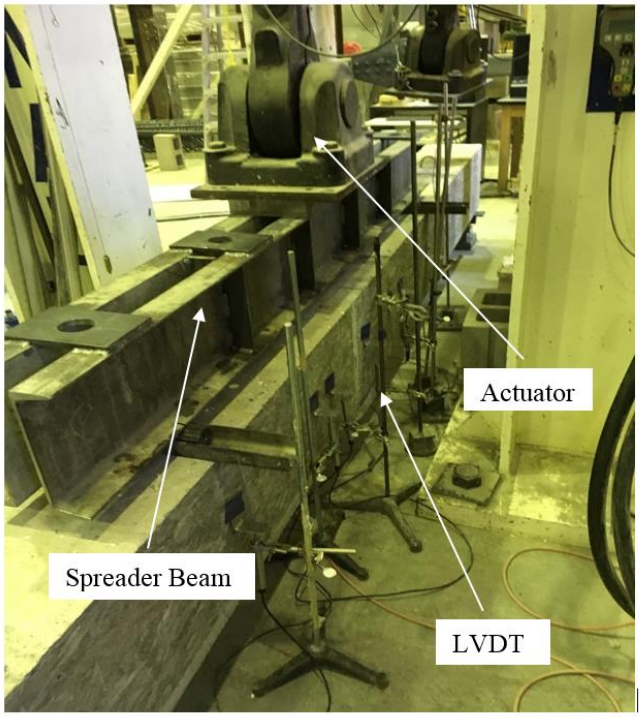

Figure 3.16: Test Setup of Splice Specimens

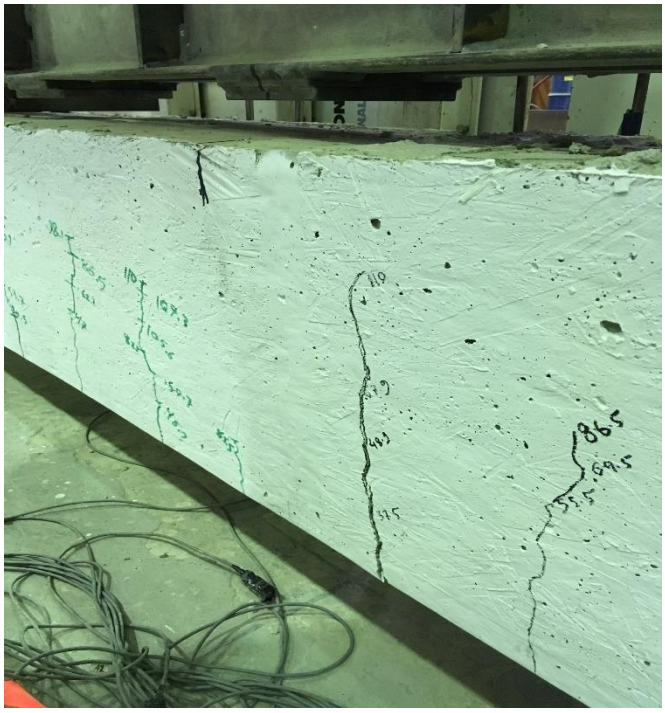

Figure 3.17: Marking of Cracks During Testing

Figure 3.18: Compressive Strength Tests of Companion Cylinders

Figure 3.19: Splitting Tensile Strength Tests of Companion Cylinders

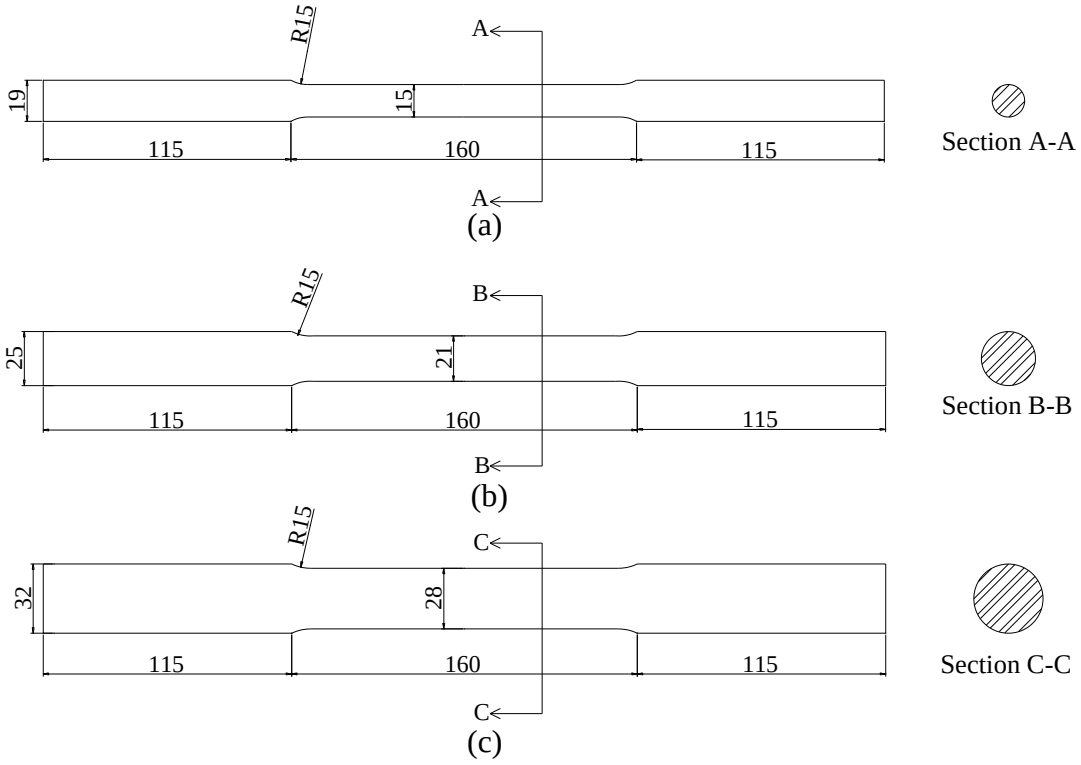

Figure 3.20: Machined Tension Test Specimens for (a) 19mm Ransome Bar, (b) 25mm Ransome Bar, and (c) 32mm Ransome Bar

Figure 3.21: Tensile Testing of Longitudinal Reinforcement (a) Intact Ransome Bar Length (b) Machined Specimen

CHAPTER 4

ANALYSIS OF RESULTS AND DEVELOPMENT LENGTH CRITERIA FOR PLAIN BARS

4.1 General

This chapter presents the as-tested material properties of the concrete and the spliced plain longitudinal reinforcement. Visual observations such as crack patterns and end slips are reported and aid in the understanding of the behaviour of specimens. Load versus midspan deflection and deflection profiles along the span length are also discussed. Recorded maximum loads are compared with predicted maximum loads to confirm whether failure of the specimens occurred before yielding of the reinforcement. Finally, a development length equation for plain bars was obtained using a regression analysis as will be discussed.

4.2 Material Properties

Table 4.1 shows the material properties as established from companion specimens testing using the methods discussed in Section 3.7 for the concrete and longitudinal reinforcing steel. Data from the specimens previously reported by Hassan and Feldman (2010) and Sekulovic and Feldman (2012) are also included.

4.2.1 Concrete

Table 4.1 shows the age of concrete at the test date, measured slump of the concrete and average concrete compressive strength (f'_c) for all specimens. Concrete slump was measured during casting of the concrete as discussed in Section 3.5.3. The average concrete compressive strength and tensile strength for all specimens was obtained from the testing of companion specimens as discussed in Section 3.7. Appendix A presents the stress-strain relationships of the concrete obtained from the concrete companion cylinder tests.

4.2.2 Reinforcing Steel

Table 4.1 shows the measured bar size as discussed in Section 3.4.2, surface roughness, static and dynamic yield stresses, ultimate stress and modulus of elasticity of the spliced

longitudinal reinforcement for all specimens. Appendix B presents the stress versus strain diagrams for all longitudinal bars tested in the current investigation. The dynamic yield strength and ultimate yield strength of longitudinal reinforcement was obtained from tensile testing of the reinforcing steel as discussed in Section 3.7.3. The static yield strength of the longitudinal reinforcement was determined in accordance with Rao et. al (1966):

$$f_{yd} - f_{ys} = 22.1 \text{ MPa} + 0.007\dot{\varepsilon} \qquad \text{[Eq.4.1]}$$

where f_{yd} represents the measured dynamic yield strength, f_{ys} represents the static yield strength, and ε̇ represents the strain rate in μmm/mm/s and is only valid for strain rates ranging from 200 to 1600 μmm/mm/s. However, Eq. 4.1 was still used for some specimens in which the strain rate exceeded the upper bound limitation as identified in Table B.1 which could result in slightly lower static yield strength values than the actual ones.

4.3 Visual Observation

This section describes the visual observations made during and after testing. Cracks were marked as testing progressed until specimens attained the maximum load. The concrete cover surrounding the longitudinal reinforcement was removed for all specimens to identify any slip of the bar.

4.3.1 Crack Patterns

All specimens exhibited similar crack patterns as the tests progressed and were similar to those specimens that were reinforced with deformed bars. Figures 4.1 and 4.2 show the crack patterns at different load levels for specimens 19■-410↓ and 19■-410↑, respectively. These specimens were chosen as representative of bottom and top cast specimens reinforced with the same bar size and shape. Crack patterns are shown at different load levels from the lowest at which cracks were visible to the attainment of the maximum load. Appendix C presents the crack patterns for the remaining specimens tested in the current experimental program.

Figures 4.1 and 4.2 show that cracks were nearly vertical (i.e. resulting from flexure) and roughly coincided with stirrups locations. It is hypothesized that cracks started to develop once the tensile stresses exceeded the tensile strength of the concrete. Most of the cracks developed within the constant moment region, as the tensile stresses developed in this region are more than those in the shear span region. Flexural cracks generally occurred at the cut ends of spliced bars due to the change in stiffness at these locations. No shear cracks developed in any specimen which indicates that a shear failure didn't govern. Top cast specimens had fewer cracks than bottom cast specimens with the same lap splice length, bar diameter, and bar type. This is due to the reduced bond capacity of specimens with bars cast in the top position in comparison to specimens with bars cast in the bottom position, as will be discussed in discussed in Section 4.8.

4.3.2 Observed End Slip of the Spliced Longitudinal Reinforcement

The concrete surrounding the spliced longitudinal reinforcement was removed after the completion of the test to identify slip of the longitudinal reinforcement. Figures 4.3 (a), (b), and (c) shows the observed end slip for specimens 19■-410↓, 19■-610↑, and 19■-610↓, respectively. Specimens 19■-410↓ and 19■-610↑ were chosen as a representative of bottom and top cast specimens reinforced with same bar size and shape, whereas specimen 19■-610↓ was chosen as a representative of the specimens in which bond failure didn't occur, as will be discussed in Sections 4.4 and 4.5. Appendix D shows photographs of the remaining specimens. Slip of the reinforcement was observed in the specimens that were designed to fail in bond except specimen 19■-610↓. This suggests that bond failure of the specimens was caused by sudden pullout of the longitudinal reinforcement. Specimen 19■-610↓ was likely to fail in flexure as no end slip was evident.

4.4 Load-Deflection Behaviour

The load versus deflection behaviour of the specimens was obtained from the recorded load and LVDT data as explained in Section 3.6. Theoretical deflection was calculated as:

$$\Delta_x(a < x < L - a) = \frac{Pa(3Lx - 3x^2 - a^2)}{12E_c I_e} \quad \text{[Eq. 4.2]}$$

where a is the shear span length, x is the distance from the centre of the support to the point of interest, L is the centre-to-centre span length, P is the applied load (total for both point loads combined) which excludes the self-weight of the specimen and spreader beam (1.77 kN) to allow for direct comparison with deflections as obtained from the LVDTs, E_c is the modulus of elasticity of concrete, and I_e is the effective moment of inertia. The effective moment of inertia was calculated in accordance with CSA A23.3 (2014) assuming I_e is constant along the length of the specimen.

$$I_e = I_{cr} + \left(I_g - I_{cr}\right)\left(\frac{M_{cr}}{M_a}\right)^3 \quad \text{[Eq. 4.3]}$$

where I_{cr} is the cracked transformed moment of inertia, I_g is the gross moment of inertia, M_{cr} is the cracking moment, and M_a is the applied moment. The cracking moment was calculated from:

$$M_{cr} = \frac{f_r I_g}{y_t} \quad \text{[Eq. 4.4]}$$

where f_r is the modulus of the rupture of concrete, and y_t is the distance from the centroidal axis of the gross section, neglecting reinforcement, to the extreme tension fibre. The modulus of rupture of concrete was calculated as:

$$f_r = 0.6\lambda\sqrt{f'_c} \quad \text{[Eq. 4.5]}$$

where λ was taken as 1 for a normal density concrete.

Figures 4.4 to 4.6 show the normalized load versus midspan deflection for specimens 19■-410↓, 19■-610↓, and 19■-410↑, respectively. Specimens 19■-410↓ and 19■-410↑ were chosen as a representative of bottom and top cast specimens reinforced with same bar size and shape, whereas specimen 19■-610↓ was chosen as a representative of the

specimens in which bond failure didn't occur. Appendix E presents the load versus midspan deflection for all remaining specimens. The theoretically predicted deflection is shown by a dashed line, whereas the actual recorded deflection is shown by a solid line. A decrease in slope was evident for all specimens after first cracking until failure of the specimen. All specimens which were designed to fail in bond showed a sudden load reduction with increase in deflection after the attainment of maximum load except specimen 19■-610↓. A small yield plateau was observed in specimen 19■-610↓ which suggests that the specimen failed after yielding of the reinforcement. This finding is consistent with the fact that no end slip was evident for this specimen as was discussed in Section 4.3.2.

Figure 4.7 shows the comparison of the load versus mid span deflection between a specimen reinforced with plain bars (i.e. 19■-410↓) and a specimen with otherwise similar geometry reinforced with deformed bars (i.e. 20◙-410↓). Note that test results related to deformed bars are provided in Appendix J. There is a similarity in the load versus mid-span deflection between these specimens. The form of the load versus midspan deflection curves are similar for both specimens and both exhibited sudden failure following attainment of the maximum load. This indicates that plain bars exhibit similar characteristics to deformed bar in terms of deflection.

Figures 4.8 and 4.9 show the deflection profile at different load levels for specimens 19■-410↓ and 19■-410↑, respectively. Markers represent the actual deflection obtained from LVDTs, whereas dashed lines represent the theoretically calculated deflection in accordance with Eq. 4.5. Appendix F presents the deflection profiles at different load levels for the remaining specimens. Actual deflections are slightly different from theoretical deflections, typically smaller in bottom cast specimens and greater in top cast specimens. The main reason for this could be due to the different stiffness in the specimen within the splice and non-splice regions. Other reasons might be due to errors from LVDT readings, and/or due to rigid body rotation of intact beam segments between cracks. Furthermore, the development of shrinkage cracks at the top surface of specimens with top cast reinforcement during casting which would eventually become a bottom surface during testing, might have decreased the stiffness of top cast specimens and

eventually affected the deflection behavior in a different way than that of the specimens with bottom cast reinforcement.

4.5 Observed and Predicted Maximum Load

Table 4.2 shows the maximum recorded loads attained by the specimens tested in current experimental program and those tested by others (Hassan and Feldman, 2012 and Sekulovic MacLean and Feldman, 2014). Table 4.2 also presents the recorded midspan deflection at the maximum applied load, theoretical curvature at maximum load, and tensile resistance in the spliced longitudinal reinforcement at the maximum load. The calculation of the theoretical curvature and tensile resistance in the spliced longitudinal reinforcement at the maximum load is discussed in Section 4.6.

All reported loads have been normalized by the square root of the concrete compressive strength to allow for direct comparison. Feldman and Bartlett (2005) have shown that the bond resistance of plain reinforcement is proportional to the square root of the concrete compressive strength. Figure 4.10 shows the comparison of observed maximum load and predicted maximum load. The predicted maximum loads were calculated in accordance with CAN/CSA-A23.3 (CSA 2014) code provisions where stress in the longitudinal reinforcement was set equal to the static yield strength, $f_{ys,}$ calculated from the as-measured dynamic yield strength, and partial material resistance factors were set equal to unity. The weight of the spreader beam (1.77 kN) and self weight of the specimen (2.94 kN/m) were subtracted when calculating the predicted maximum load to allow for the direct comparison with the recorded maximum load. As discussed in Section 3.2, two specimens (19●-1010↓ and 19●-1210↓) were intentionally cast with splice lengths longer than that which would cause yielding of the reinforcement. Figure 4.10 shows that these specimens failed at loads above the yield loads predicted using the flexural resistance procedures provided in CSA A23.3 (2014) with resistance factors set equal to unity. Figure 4.10 also shows that specimens 19●-610↓, 19■-510↓, and 19■-610↓ failed at loads above the maximum predicted loads. These specimens were considered as outliers as they failed above yield point and were not included in the subsequent regression analysis as will be discussed in Section 4.9. Specimen 32●-810↓ was identified as a physical outlier as the specimen required unloading and loading twice prior to failure.

Large plastic deformations were evident between the load cycles (Hassan and Feldman, 2012). This specimen was also excluded from further analysis.

4.6 Tensile Resistance in the Spliced Longitudinal Reinforcement

The calculation of the tensile resistance in the lap spliced reinforcing bars at the maximum load level is discussed herein. A moment curvature analysis, which is required to calculate tensile resistance in the spliced longitudinal reinforcement, is also discussed in this section.

4.6.1 Moment Curvature Analysis

A moment curvature analysis was performed to calculate the tensile resistance of the lap spliced reinforcement at the maximum load level as direct measurement was not possible without compromising the bond between reinforcing bars and surrounding concrete.

The stress versus strain relationship for concrete was modelled using Hognestad's equation (Hognestad, 1951):

$$\frac{f_c}{f'_c} = \left[2\left(\frac{\varepsilon_c}{\varepsilon_0}\right) - \left(\frac{\varepsilon_c}{\varepsilon_0}\right)^2\right] \quad \text{for } \varepsilon_c < \varepsilon_0 \qquad \text{[Eq.4.6]}$$

$$\frac{f_c}{f'_c} = \left[1 - \frac{0.15(\varepsilon_c - \varepsilon_0)}{0.0038 - \varepsilon_0}\right] \quad \text{for } \varepsilon_c > \varepsilon_0 \qquad \text{[Eq.4.7]}$$

where f_c is the compressive stress in the concrete at any given location along the height of cross-section, ε_c is the concrete strain corresponding to f_c, and ε_0 is the strain corresponding to the maximum compressive stress of the concrete:

$$\varepsilon_0 = \frac{2f'_c}{E_c} \qquad \text{[Eq.4.8]}$$

where E_c is the modulus of elasticity of the concrete.

The stress versus strain relationship for the reinforcement was modelled theoretically using the tensile properties of the longitudinal reinforcement shown in Table 4.1. The theoretically derived stress versus strain curve of the reinforcement comprised three segments. The first segment was a linear segment to represent the elastic region. The next segment was the horizontal line which represented the yield plateau. The last segment was the best fit cubic equation which represented the strain hardening region of the reinforcement.

The moment versus curvature relationship for the uncracked section was established by using simple flexural formula in which the resisting moment was set equal to the product of the curvature and the flexural rigidity of the gross section. For the cracked section, an iterative procedure was applied in which the compressive stress block was divided into 100 segments of equal depth. The calculation of the error associated with the selection of 100 segments is presented in Appendix H and it was determined that error was negligible. The magnitude of the stress in each segment was assumed to be equal to the magnitude of the stress at midheight of the segment. Figure 4.11 shows the model used to establish the moment curvature relationship for the cracked section. A linear strain profile as shown in Figure 4.11 (a) was assumed to calculate the strain in the reinforcing steel and at the centre of each of the compression segments. The compressive stress corresponding to the strain in the given segment was calculated using Equations 4.6 and 4.7. The compressive stress was then multiplied by the cross-sectional area of the segment to calculate the compressive force in each segment. The total compressive force in the cross-section was then calculated by summing the compressive forces in all of the segments (Figure 4.11 (c)). Similarly, the tensile stress in the spliced longitudinal reinforcement corresponding to the tensile strain at the centroid of reinforcing bars was calculated (Figure 4.11 (a) and (b)). The total tensile force in the reinforcement was then calculated by multiplying the cross-sectional area of the reinforcement with the tensile stress in the reinforcement. The neutral axis depth for the cross-section was then determined at a given curvature using an iterative procedure in such a way that the compressive force in the concrete and tensile force in the reinforcement were within 0.5% of each other. Finally, the resisting moment was calculated by multiplying the tensile force in the reinforcement by the lever arm. The

lever arm was calculated by subtracting the neutral axis depth from the effective depth and adding the centroid of the compressive force measured from the neutral axis location. Note that the resisting moment could also be calculated by multiplying the compressive force in the concrete above the neutral axis with the same lever arm. The detailed comparison of two methods is provided in Appendix I. The former method was selected as it yielded lower tensile resistance which would ultimately lead to longer, and so more conservative, lap splice length.

Figure 4.12 shows the theoretical moment versus curvature diagram for specimen 19●-510↓ and the diagram is similar to that obtained for a typical flexural member with deformed bars (MacGregor and Bartlett, 2000). There are four segments in the diagram. The first segment, which is almost vertical, represents the uncracked moment versus curvature behaviour of the specimen. The linearly increasing segment that follows has a reduced slope and represents the cracked moment curvature behaviour of the specimen before yielding of the reinforcement. The third segment, which is nearly horizontal, represents the moment versus curvature behaviour of the specimen after yielding of the reinforcement but before strain hardening. The final segment represents the moment curvature behaviour of the specimen when the reinforcement enters the strain hardening region. Appendix G presents the theoretical moment versus curvature diagrams for all remaining specimens. The moment at the maximum load was calculated using statics. The curvature corresponding to the maximum moment was then determined graphically from the moment versus curvature diagram. The tensile resistance of the reinforcement at the maximum load was calculated from the curvature as explained in the previous paragraph. Table 4.2 shows the tensile resistance of the reinforcement at maximum load level for each specimen. Note that the tensile resistance for all specimens was calculated based upon a nominally set cover of 50 mm to the spliced longitudinal reinforcement as presented in Section 3.3, although cover in specimen 25●-510↑, measured as discussed in Section 3.5.2 and as mentioned in Table 3.1, slightly exceeded the tolerances prescribed by CAN/CSA A23.1-14 (CSA 2014). It is also important to note that the tensile resistance of the reinforcement is reported for the total of the two lap spliced bars in each specimen.

4.7 Lap Splice Specimens with Long Lap Splice Lengths

Bischoff and Johnson (2008) reported that beams reinforced with plain bars failed suddenly after yielding of the reinforcement. The possible reason why the beams exhibited brittle failure could be due to the lack of bond between the reinforcement and concrete resulting from Poisson's effect reducing the cross-section of the bars after yielding of the reinforcement. However, Darwin (2017) found that flexural members reinforced with plain bars exhibited a ductile failure after yielding of the reinforcement. The proposed equation for the development length for plain bars can be established in a similar way to that used for deformed bars (Orangun et. al, 1977), if a ductile failure can be confirmed in specimens reinforced with plain bars. Two specimens (19●-1010↓ and 19●-1210↓) were therefore cast with longer lap splice length which would cause reinforcement to yield. Figure 4.13 shows the normalized applied load versus midspan deflection for these specimens where a long yield plateau was observed in both specimens. This indicates that the ductile mode of failure is evident for plain bars, similar to the case for deformed bars, provided that there is sufficient lap splice or development length. The surface roughness of the reinforcement might have played a vital role to provide the bond between reinforcement and concrete after yielding of the reinforcement and hence resulted in long yield plateau (Feldman, 2006). Hence, a proposed code equation for lap splice or development length for plain bars can be calibrated in a similar way to that used for deformed bars.

4.8 Effect of Casting Position

Figure 4.14 shows the ratio of the normalized tensile resistance at the maximum load level for specimens with top cast bars to that for specimens with bottom cast bars. Specimens with top cast bars had a lower tensile resistance in the reinforcement at the maximum load level. The average ratio of the normalized tensile resistance of specimens reinforced with plain bars in the top position to that in bottom position was 0.57. Current American (ACI Committee 318, 2014) and Canadian (CSA, 2014) codes require that development length for modern deformed bars be increased by 30% for reinforced members cast the in top position and hence it appeared that top cast effect for plain bars is more severe than that for deformed bars imposed by American and Canadian code

provisions. Furthermore, Chana (1990) also concluded that bond of plain bars is more affected by casting position than that of deformed bars. This is justified because plain bars do not have any ribs and so results in a complete loss of contact between these bars and concrete due to the voids that result as concrete is subjected to shrinkage. In contrast, deformed bars have ribs whose height may exceed that of resulting voids. Minimal contact with concrete will likely be maintained for these bars (Feldman, 2006).

Figure 4.14 shows that the average ratios of the normalized tensile resistance for specimens reinforced with plain round bars and plain square bars in the top position to that for specimens reinforced with respective bars in bottom position are 0.4 and 0.64, respectively. This shows that round bars are more sensitive to casting position than square bars and is due to the difference in the shape of the void under the two bar shapes as indicated in Figure 4.15 (Sekulovic MacLean and Feldman, 2012). For round bars, void forms under the bottom half of the bar perimeter whereas for square bars, void forms under the bottom face of the bar and affects a smaller portion of the perimeter than for round bars (Sekulovic MacLean and Feldman, 2012).

4.9 Predictive Equation for the Tensile Resistance of Reinforcement at the Maximum Load

A regression analysis of the 29 specimens was performed and resulted in the following predictive equation for the normalized tensile resistance, T, of the longitudinal reinforcement at the maximum load level expressed in kN/√MPa. Note that square and round bars with the same size have different cross-sectional areas. Howell and Higgins (2007) showed that for deformed bars, it is reasonable to calculate equivalent diameter for square bars that results in the same cross-sectional area of actual square bar and equivalent round bar. The same approach has been adopted here. The resulting equation is:

$$\frac{T}{\sqrt{f'_c}} = 0.00316 L_s d_{b,EQ} \psi \leq \frac{A_s f_y}{\sqrt{f'_c}} \qquad \text{[Eq. 4.9]}$$

where L_s is lap splice length in mm; $d_{b,EQ}$ is the nominal bar diameter for round bars or the equivalent round diameter of the square bars in mm; and ψ is a top cast factor as

established from Section 4.6 which is equal to 1.0 for both round and square bars cast in the bottom position, 0.40 for round bars cast in top position, and 0.64 for square bars cast in the top position. The root mean square error for Eq. 4.9 is $7.82\text{kN}/\sqrt{\text{MPa}}$. The average ratio of the experimental tensile resistance to the predicted tensile resistance for 19 mm, 25 mm, and 32 mm bars were 1.26, 1.12, and 0.95 respectively. This shows that there is a decreasing trend in the experimentally determined tensile resistance as bar size increases. Therefore, a further regression analysis was performed with the introduction of a bar size factor, ω. To be consistent with the development length equation included in the current CSA code, the bar size factor was chosen in a similar manner as per the case for deformed bars. The resulting regression equation is as follows:

$$\frac{T}{\sqrt{f'_c}} = 0.00311 L_s d_{b,EQ} \psi\omega \leq \frac{A_s f_y}{\sqrt{f'_c}} \qquad \text{[Eq. 4.10]}$$

where ω is 1.25 for 19 mm bars or smaller, and 1.0 for 25 mm bars or larger. The root mean square error for Eq.4.10 is $7.34\text{kN}/\sqrt{\text{MPa}}$. Figure 4.16 shows the fit of Eq.4.10 with the experimental tensile resistance data, with Figure 4.16 (a) showing all data for specimens longitudinally reinforced with round bars, and Figure 4.16 (b) showing all data for specimens longitudinally reinforced with square bars. The average ratio of the experimental tensile resistance to the predicted tensile resistance for 19 mm, 25 mm and 32 mm bars after the introduction of bar size factor were 1.03, 1.14, and 0.96, respectively. Note that ACI Committee 408 (ACI 408, 2003) does not recommend the use of the bar size factor in the provisions for development and splice length of deformed bars used in ACI 318-2014 (ACI 318, 2004), as there is no support in the use of bar size factor from the analysis of ACI Committee 408 database of the test results. It is also important to note that the confinement term included in the development length equation included in ACI 318-2014 (ACI 318, 2014) is the smaller of the distance from the nearest concrete surface to the longitudinal reinforcing bar, and one half of the centre-to-centre distance between longitudinal bars which varies with bar size. However, as clear concrete cover was kept constant in all specimens in the current investigation, it cannot be established whether bar size, confinement, or a combination of bar size and confinement influences the tensile resistance. Therefore, the use of the bar size factor is warranted

until such time as the test database can be extended to evaluate the effects of confinement.

4.10 Lap Splice and Development Length Equation for Plain Bars

Equation 4.10 predicts the average normalized tension resistance and is not suitable for design purposes. To ensure an adequate level of safety accounting for deviations in material properties, dimensional errors, and uncertainties involved in calculations (Orangun, 1975), a 5% fractile approach has been used iteratively and the predictive equation is modified in such a way that 95% or more of the experimental tensile resistance of the specimens exceeds the predicted tension resistance. The resulting equation is:

$$\frac{T}{\sqrt{f'_c}} = 0.00236 L_s d_{b,EQ} \psi\omega \leq \frac{A_s f_y}{\sqrt{f'_c}} \qquad \text{[Eq. 4.11]}$$

Figure 4.17 shows the predicted tensile resistance in accordance with Eq. 4.11 versus experimental tensile resistance. The proportional line is also shown which represents the theoretical case in which the predicted normalized tensile resistance is equal to the experimental normalized tensile resistance. More than 95% of the test data are above the proportional line which indicates that predictive equation can be used for design purpose as it accounts for enough structural safety.

The required lap splice length for plain bars is obtained from Eq.4.11 by setting $T=A_s f_y$, $k_1=1/\psi$, and $k_2= 1/\omega$ and by solving to get L_s resulting in the following equation:

$$L_s = 0.666 k_1 k_2 \frac{f_y}{\sqrt{f'_c}} d_{b,EQ} \qquad \text{[Eq. 4.12]}$$

where k_1 is the bar location factor which is equal to 1.0 for both round and square bars cast in the bottom position, 2.5 for round bars cast in the top position, and 1.6 for square bars cast in the top position; and k_2 is the bar size factor which is 0.8 for bar size of 19 mm or smaller, and 1.0 for bar size of 25 mm or larger. Note that as the unit of predictive tensile resistance is kN and was predicted for two spliced bars, T was substituted as $2\pi d_{b,EQ}^2 f_y/4000$ in Eq. 4.11 for the compatibility of units. It is also important to note that unit of f_y and f'_c should be used in MPa in Eq. 4.12.

Eq. 4.12, as used for the calculation of the required splice length, was based upon the measured modulus of elasticity of the longitudinal reinforcement. The modulus of elasticity of longitudinal reinforcement associated with some specimens is quite different from nominal modulus of elasticity of 200 GPa. Eq. 4.12 was therefore reassessed taking into account of the nominal modulus of elasticity (200 GPa) of longitudinal reinforcement in all specimens. It was confirmed that Eq. 4.12 is identical for both cases and hence confirms that the calculated splice length is insensitive to the range of values of modulus of elasticity as reported in this investigation.

Orangun et. al (1975) proved that the similar equation can be used for determining development length and lap splice length for deformed bars. As the cracking pattern, ductility behaviour and deflection of specimens reinforced with plain bars are similar to those reinforced with deformed bars, and the top cast effect is significant for both bar shapes, Eq. 4.12 can be used to calculate development length for plain bars.

4.11 Comparison to Development Length Equation for Deformed Bars in Accordance with CSA A23.3-14

Table 4.3 shows the comparison of the proposed development length equation for plain bars (Eq. 4.12) and the existing development length equation for deformed bars in the current CSA code with following conditions:

i) Bars are uncoated and normal density concrete is assumed.
ii) Minimum stirrups within development length are provided.
iii) The nominal yield strength of reinforcement is 300 MPa and the specified compressive strength of concrete is 20MPa.
iv) Calculations for the development length of square deformed bars were made by substituting d_b with the equivalent bar diameter.
vi) The nominal bar size was taken and was rounded off to two significant digits for the calculation of development length for both plain and deformed bars.

Table 4.3 shows that the ratio of the development length for plain bars to deformed bars ranged from 1.48 to 2.85. For the bottom cast condition, the ratio is consistently 1.48, whereas for the top cast condition the ratio varies depending upon shape of bars (1.88 for

square bars, and 2.76 for round bars). This is due to the difference in top cast factors used in the calculations for the development length of plain bars in accordance with Eq. 4.12. Figure 4.18 shows the comparison graphically.

According to historical U.S concrete codes (ACI, 1963), development length required for plain bars should be double that for deformed bars under similar conditions. Results of the current investigation suggest that this provision is somewhat conservative for the bottom cast condition; however, for the top cast condition the provision is not safe.

4.12 Summary

This chapter presented the load versus deflection behaviour and visual observations of specimens such as crack pattern and end slip of the bar. These examinations were conducted to understand the general failure behaviour of the specimens and from these examinations it was confirmed that all but one specimen designed to fail in bond did so. Evidence of ductile failure with a long yield plateau was found in the specimens with long lap splice lengths, which indicates that the ductility behaviour of specimens reinforced with plain bars is similar to that of deformed bars. Finally, the proposed code equation for the development length of plain bars obtained through analysis of 29 specimens was presented.

The behaviour and data analysis for the specimens reinforced with Ransome bars are discussed in the next chapter. Development length criteria for Ransome bars is also discussed in the next chapter.

Table 4.1: Concrete and Longitudinal Reinforcing Steel Material Properties

Specimen ID[a]	Concrete				Longitudinal Reinforcing Steel					
	Age of Concrete at Test Date (days)	Slump (mm)	Compressive Strength f'_c (MPa)	Tensile Strength f_r (MPa)	Measured Bar Size d_b (mm)	Surface Roughness R_y (µm)	Dynamic Yield Strength f_{yd} (MPa)	Static Yield Strength f_{ys} (MPa)	Ultimate Strength f_u (MPa)	Modulus of Elasticity E_s (GPa)
19●-305↓[b]	52	95[d]	17.4	n/a[f]	19.0	9.54	355	326	520	203
19●-410↓[b]	52		17.4	n/a[f]		9.67				
19●-510↓[b]	49		18.7	n/a[f]		9.86				
19●-610↓[b]	55	86[d]	21.0	n/a[f]		9.44				
19●-1010↓[b]	35	120[d]	23.8	2.27		8.65	336	315	520	196
19●-1210↓[b]	45	80[e]	20.3	2.49	18.9	8.98				
25●-410↓[b]	126	110[d]	23.7	n/a[f]	25.3	8.88	346	322	534	196
25●-510↓[b]	129		24.0	n/a[f]	25.2	8.43				
25●-610↓[b]	119		22.8	n/a[f]	25.3	8.71				
25●-810↓[b]	58	86[d]	19.2	n/a[f]		9.6	346	316	504	206
25●-410↑[c]	49	147[e]	27.1	2.54		9.19	364	334	522	243
25●-510↑[c]	47	147[e]	28.0	n/a[g]		9.09				
25●-610↑[c]	36	67.5[e]	35.8	3.29	25.4	9.21				
32●-410↓[b]	50	95[d]	19.8	n/a[f]	31.7	9.92	348	318	504	204
32●-610↓[b]	50		19.8	n/a[f]		9.72				
32●-810↓[b]	38		15.8	n/a[f]		10.1				
32●-910↓[b]	36	86[d]	19.7	n/a[f]	31.8	10.0				
19■-410↓	44	80[e]	24.7	2.36	18.8	9.55	350	320	522	162
19■-510↓	50		22.8	2.53		9.55				
19■-610↓	49		22.7	2.57		9.19				
19■-410↑	30	120[e]	22.9	2.24		8.96				
19■-510↑	28		23.0	2.40		9.4				
19■-610↑	33		24.6	2.44		9.75				
25■-410↓[b]	42	147[e]	25.5	n/a[g]	25.4	8.79	381	349	544	192
25■-510↓[b]	40		25.0	2.93	25.3	8.83				
25■-610↓[b]	56		28.1	3.05		8.86				

Table 4.1 cont'd: Concrete and Longitudinal Reinforcing Steel Material Properties

Specimen ID	Concrete				Longitudinal Reinforcing Steel					
	Age of Concrete at Test Date (days)	Slump (mm)	Compressive Strength f'_c (MPa)	Tensile Strength f_r (MPa)	Measured Bar Size d_b (mm)	Surface Roughness R_y (um)	Dynamic Yield Strength f_{yd} (MPa)	Static Yield Strength f_{ys} (MPa)	Ultimate Strength f_u (MPa)	Modulus of Elasticity E_s (GPa)
25■-410↑[c]	35	67.5[e]	33.0	3.30	25.3	9.06	349	316	542	207
25■-510↑[c]	30		33.5	2.95	25.3	9.17				
25■-610↑[c]	35		33.0	3.30	25.3	9.16				
32■-410↓[c]	28	80[e]	25.5	2.34	31.6	9.36	343	312	527	196
32■-610↓[c]	28		25.5	2.34	31.7	9.24				
32■-810↓[c]	29		26.9	3.00	31.5	9.17				
32■-410↑[c]	31		27.5	2.44	31.6	9.29				
32■-610↑[c]	30		26.2	2.72	31.7	9.52				
32■-810↑[c]	30		26.2	2.72	31.7	9.34				

[a]The first number in the specimen identification represents the nominal bar size of the spliced longitudinal reinforcement which is the nominal diameter for plain round bars and side face dimension for plain square bars. The symbol following the nominal bar size represents the bar shape or type where a solid circle (●) represents plain round bars and, a solid square (■) represents plain square bars. The number following the hyphen represents the lap splice length of longitudinal bars in mm and the final symbol represents the position of reinforcing bar at casting where downward arrow (↓) indicates that specimen was cast in bottom position, and upward arrow (↑) indicates that the specimen was cast in top position.

[b]Originally reported by Hassan and Feldman (2012)

[c]Originally reported by Sekulovic MacLean and Feldman (2014)

[d]Specimens cast with concrete Mix Design 1 as discussed in Section 3.4.1

[e]Specimens cast with concrete Mix Design 2 as discussed in Section 3.4.1

[f] Not reported

[g] Error while testing as described by Sekulovic MacLean and Feldman (2014)

Table 4.2: Test Results of the Lap Splice Specimens

Specimen ID	Splice Length as a Function of Bar Size L_s/d_b	Maximum Normalized Load $P_{max}/\sqrt{f'_c}$ (kN/√MPa)	Predicted Normalized Load $P_{max}/\sqrt{f'_c}$ (kN/√MPa)	Midspan Deflection at Maximum Load (mm)	Theoretical Curvature at Maximum Load (1/m)	Tensile Resistance in the Longitudinal Reinforcement at Maximum Load, T_{max} (kN)
19●-305↓[i]	16.1	8.50	18.0	7.38	0.00362	105
19●-410↓[i]	21.6	9.14	18.0	7.80	0.00383	110
19●-510↓[i]	26.8	9.58	17.5	9.17	0.00405	117
19●-610↓[h i]	32.1	17.8	16.7	17.5	0.00977	n/a
19●-1010↓	53.2	23.6	15.3	64.1	n/a	n/a
19●-1210↓	63.7	22.0	16.4	69.4	n/a	n/a
25●-410↓[i]	16.4	16.2	28.1	12.0	0.00451	204
25●-510↓[i]	20.4	18.4	27.7	11.0	0.00509	230
25●-610↓[i]	24.4	20.6	28.5	14.0	0.00555	249
25●-810↓[i]	32.4	29.7	30.3	17.7	0.00719	325
25●-410↑[j]	16.4	6.55	28.1	1.14	0.00191	105
25●-510↑[j]	20.4	4.69	27.7	1.68	0.00153	84.5
25●-610↑[j]	24.4	7.07	25.1	3.92	0.00214	122
32●-410↓[i]	12.8	15.6	44.5	7.81	0.00298	191
32●-610↓[i]	19.1	25.1	44.3	10.6	0.00461	291
32●-810↓[i]	25.3	31.8	46.9	11.2	0.00545	330
32●-910↓[h i]	28.4	34.5	45.8	18.6	0.00561	n/a
19■-410↓	21.6	15.8	19.8	8.98	0.00672	197
19■-510↓[h]	26.8	23.1	20.5	13.2	n/a	n/a
19■-610↓[h]	32.1	24.2	20.6	13.6	n/a	n/a
19■-410↑	21.6	9.74	20.5	6.93	0.00436	128
19■-510↑	26.8	9.36	20.4	6.79	0.00423	124
19■-610↑	32.1	14.3	20.6	12.4	0.00614	180
25■-410↓[j]	16.4	16.1	38.3	9.10	0.00388	212
25■-510↓[j]	20.4	20.0	38.3	10.4	0.00472	255
25■-610↓[j]	24.4	26.8	36.6	15.4	0.00643	349

Table 4.2 Cont'd: Test Results of the Lap Splice Specimens

Specimen ID	Splice Length as a Function of Bar Size L_s/d_b	Maximum Normalized Load $P_{max}/\sqrt{f'_c}$ (kN/√MPa)	Predicted Normalized Load $P_{max}/\sqrt{f'_c}$ (kN/√MPa)	Midspan Deflection at Maximum Load (mm)	Theoretical Curvature at Maximum Load (1/m)	Tensile Resistance in the Longitudinal Reinforcement at Maximum Load, T_{max} (kN)
25■-410↑[j]	16.4	8.97	31.3	4.67	0.00289	142
25■-510↑[j]	20.4	11.2	31.1	6.15	0.00290	174
25■-610↑[j]	24.4	12.2	31.3	6.46	0.00311	186
32■-410↓[j]	12.8	17.4	50.6	4.64	0.00308	235
32■-610↓[j]	19.1	20.1	50.8	6.48	0.00350	268
32■-810↓[j]	25.3	28.3	49.5	8.52	0.00494	373
32■-410↑[j]	12.8	12.6	49.4	3.87	0.00236	183
32■-610↑[j]	19.1	14.3	50.4	5.19	0.00260	201
32■-810↑[j]	25.3	16.2	50.4	6.74	0.00290	224

[h] Specimen Identified as Outlier

[i] Originally reported by Hassan and Feldman (2012)

[j] Originally reported by Sekulovic MacLean and Feldman (2014)

Table 4.3: Comparison of the Proposed Development Length Equation for Plain Bars and Existing Development Length Equation for Deformed Bars

Bar ID[k]	$(L_d)_{plain}$ (mm)	$(L_d)_{deformed}$ (mm)	$(L_d)_{plain}/(L_d)_{deformed}$
19●↓	679	459	1.48
25●↓	1117	755	1.48
32●↓	1430	966	1.48
19●↑	1698	596	2.85
25●↑	2792	981	2.85
32●↑	3574	1256	2.85
19■↓	765	517	1.48
25■↓	1260	851	1.48
32■↓	1613	1090	1.48
19■↑	1224	672	1.82
25■↑	2016	1107	1.82
32■↑	2581	1417	1.82

[k]The first number in bar identification represents the nominal bar size which is the nominal diameter for plain round bars and side face dimension for plain square bars. The symbol following the nominal bar size represents the bar shape or type where a solid circle (●) represents plain round bars and, a solid square (■) represents plain square bars. The final symbol represents the position of reinforcing bar at casting where downward arrow (↓) indicates that the bar is located in bottom position, and upward arrow (↑) indicates that the bar is located in top position.

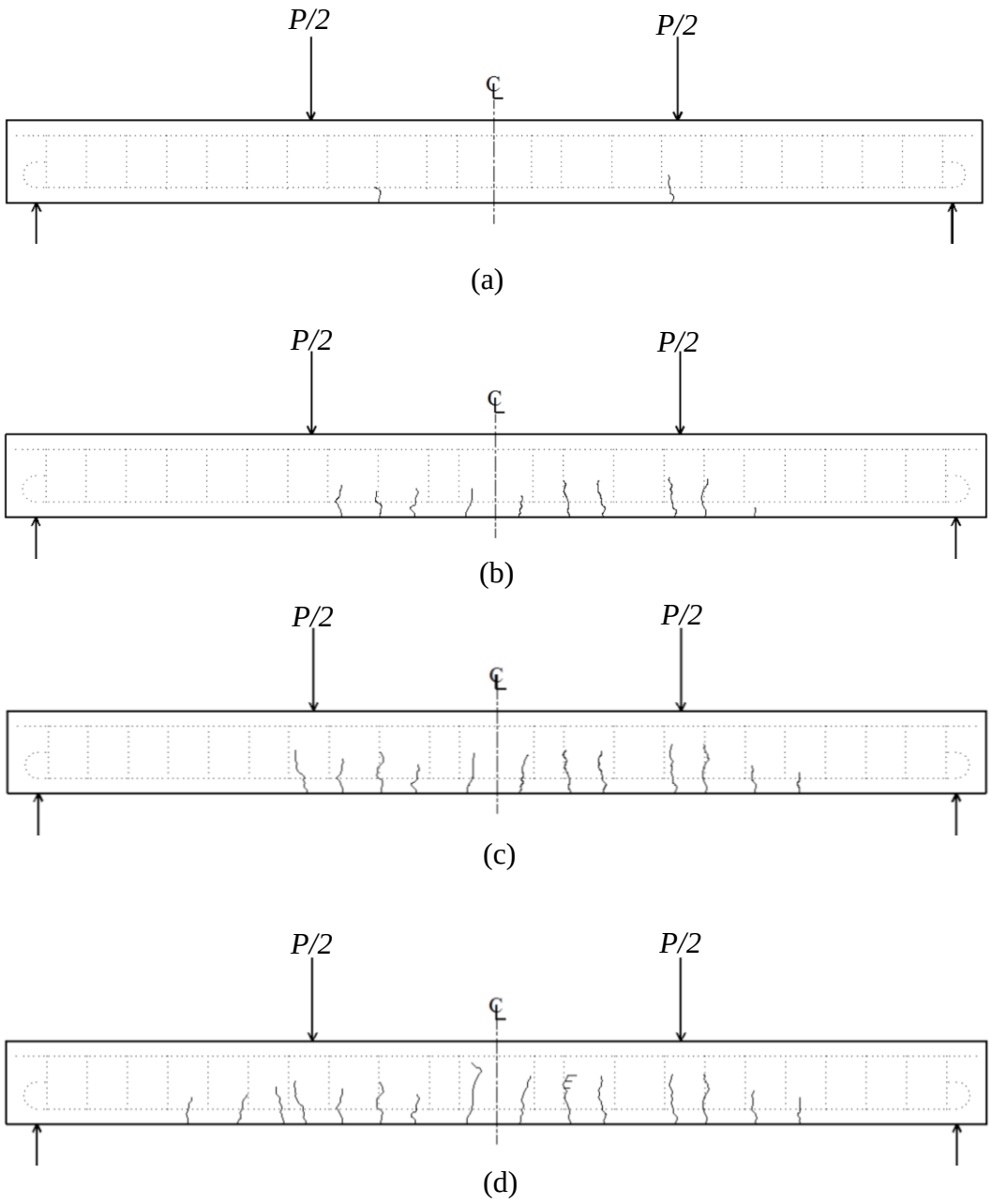

Figure 4.1: Crack Pattern for Specimen 19■-410↓ at the Following Load Levels: (a) P=0.5 P_{max}, (b) P=0.7 P_{max}, (c) P=0.9 P_{max}, and (d) P=P_{max}

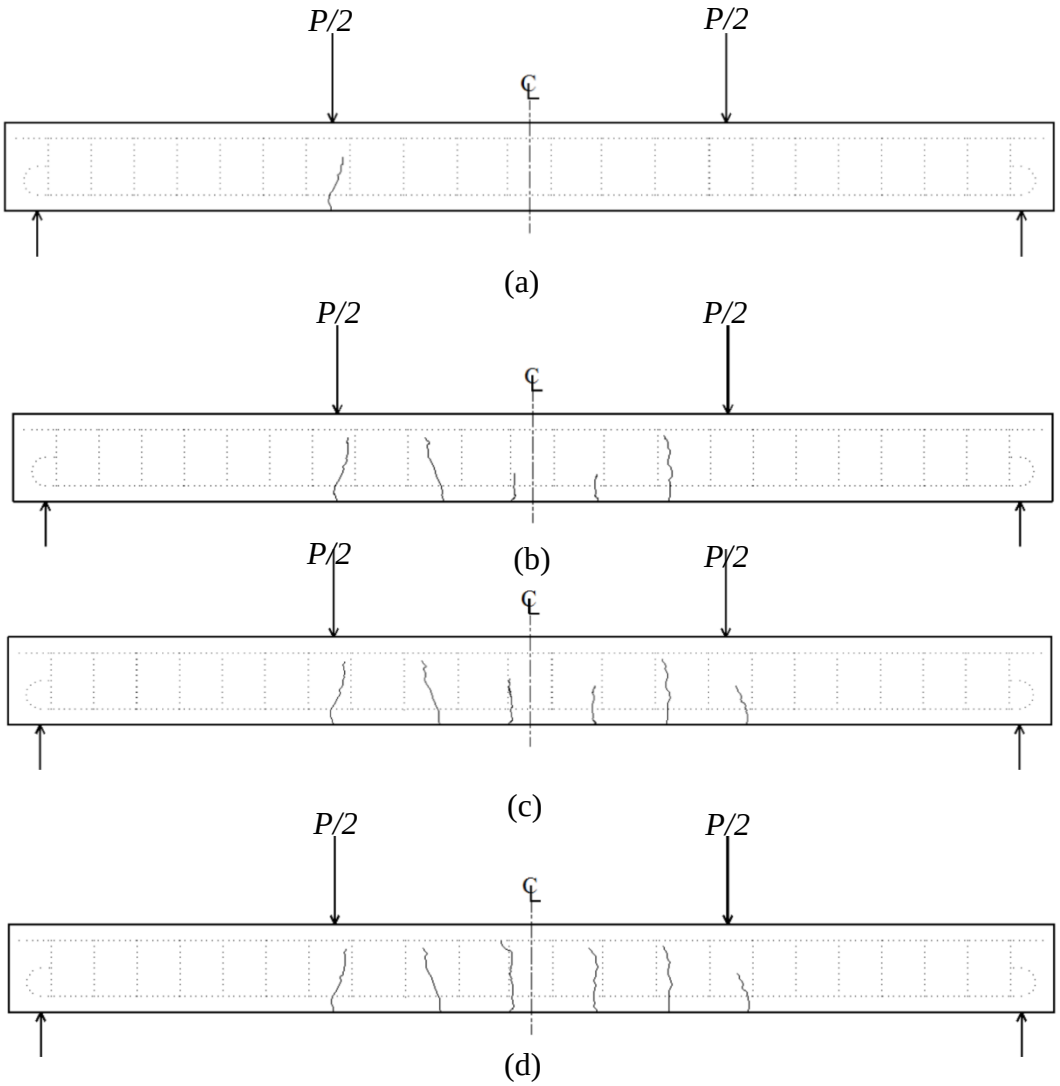

Figure 4.2: Crack Pattern for Specimen 19■-410↑ at the Following Load Levels: (a) P=0.5 P_{max}, (b) P=0.7 P_{max}, (c) P=0.9 P_{max}, and (d) P=P_{max}

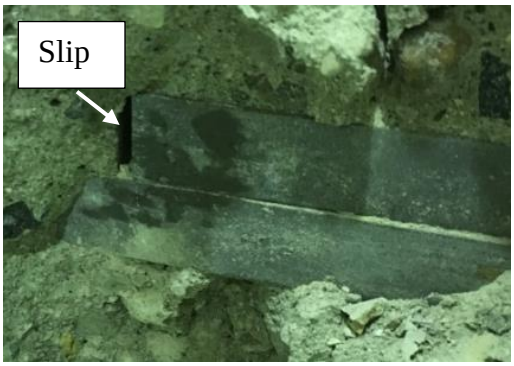

(a)

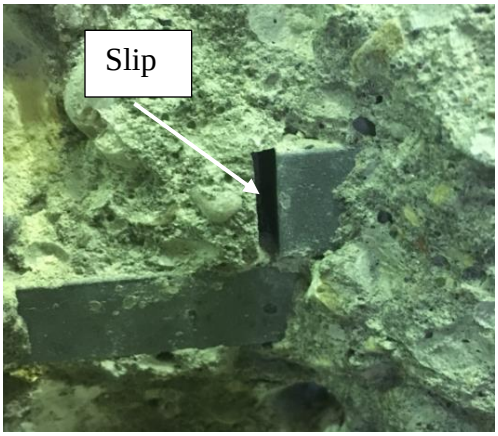

(b)

(c)

Figure 4.3: End Slip of Longitudinal Reinforcement Following Concrete Removal for Specimens (a) 19■-410↓, (b) 19■-610↑, and (c) 19■-610↓

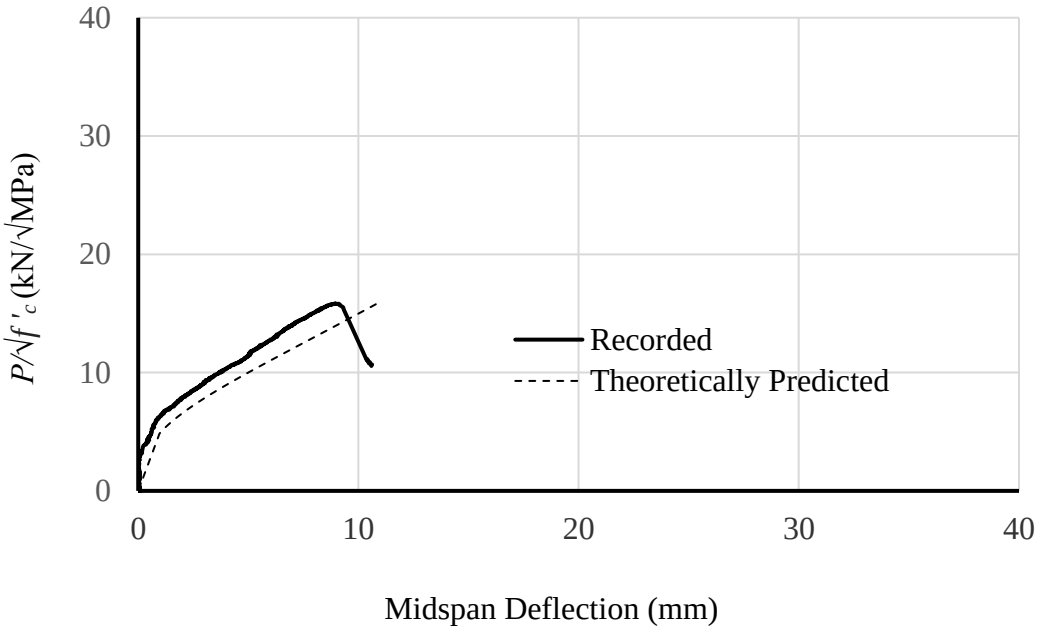

Figure 4.4: Normalized Applied Load Versus Midspan Deflection for Specimen 19■-410↓

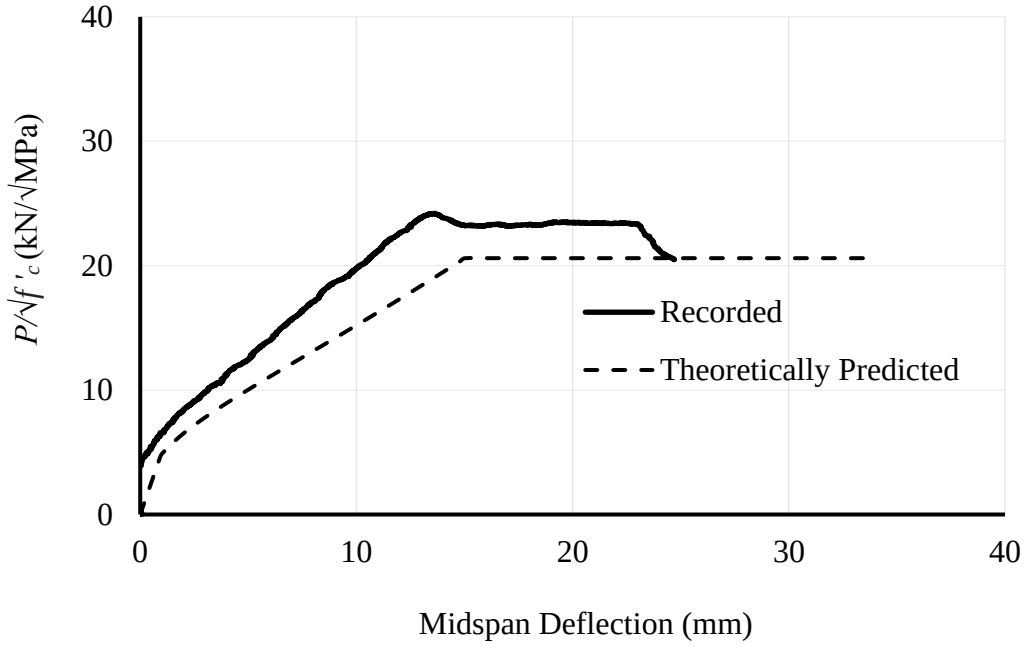

Figure 4.5: Normalized Applied Load Versus Midspan Deflection for Specimen 19■-610↓

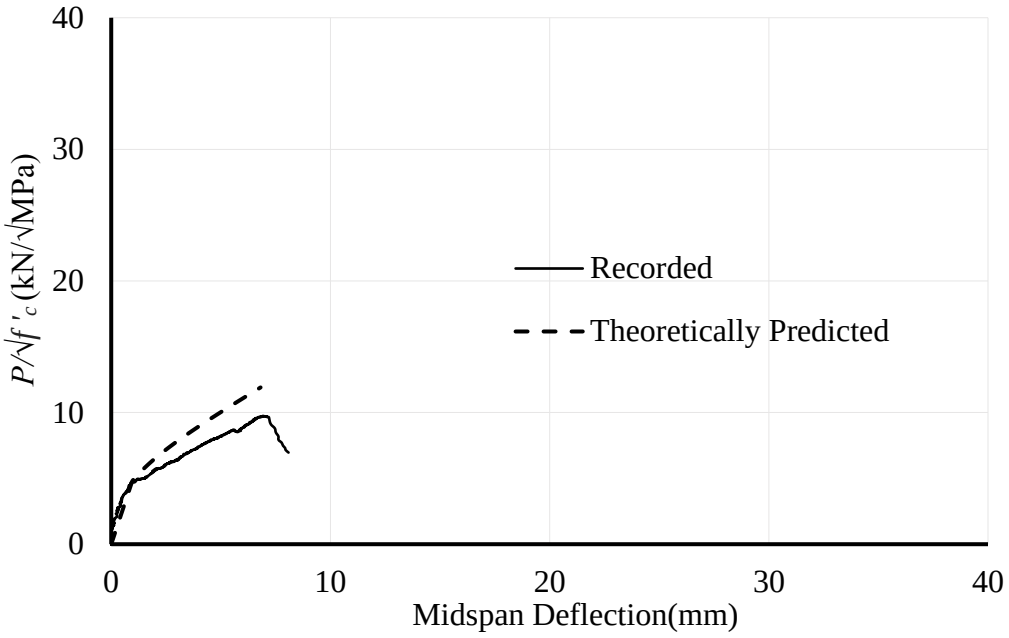

Figure 4.6: Normalized Applied Load Versus Midspan Deflection for Specimen 19■-410↑

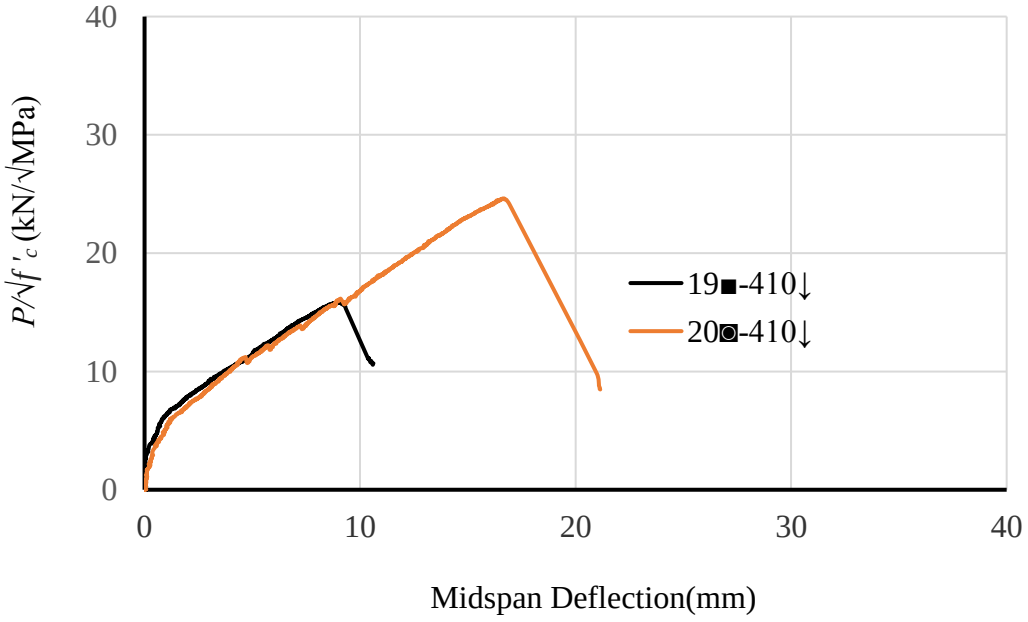

Figure 4.7: A Comparison of Normalized Applied Load Versus Midspan Deflection between Specimen 19■-410↓ and 20◙-410↓

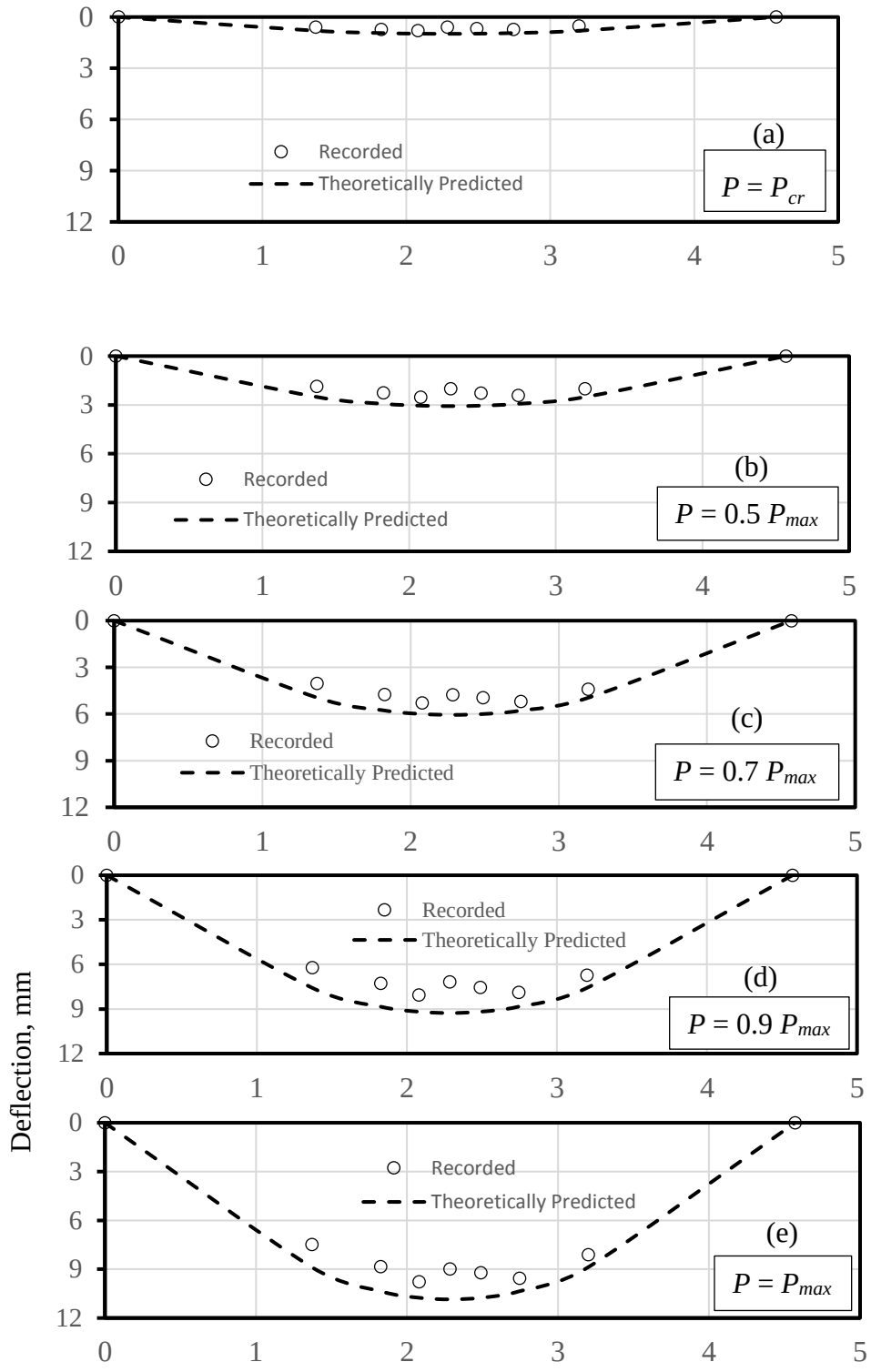

Figure 4.8: Deflection Profile at Different Load Levels for Specimen 19■-410↓: (a) $P=Pcr$, (b) P=0.5 P_{max}, (c) P= 0.7 P_{max}, (d) P= 0.9 P_{max}, and (e) $P=P_{max}$

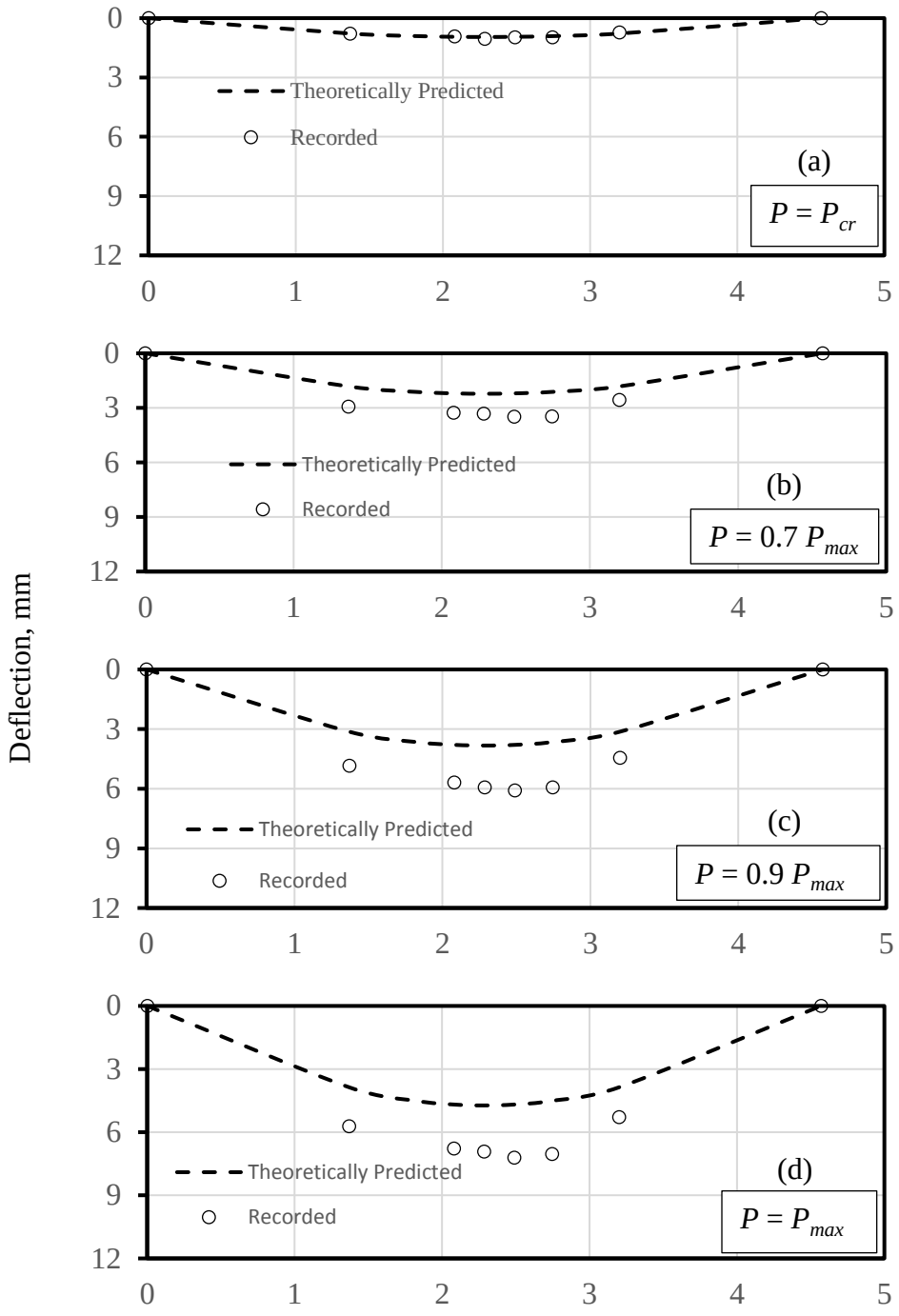

Figure 4.9: Deflection Profile at Different Load Levels for Specimen 19■-410↑: (a) $P=P_{cr}$, (b) $P=0.7\ P_{max}$, (c) $P= 0.9\ P_{max}$, and (e) $P=P_{max}$

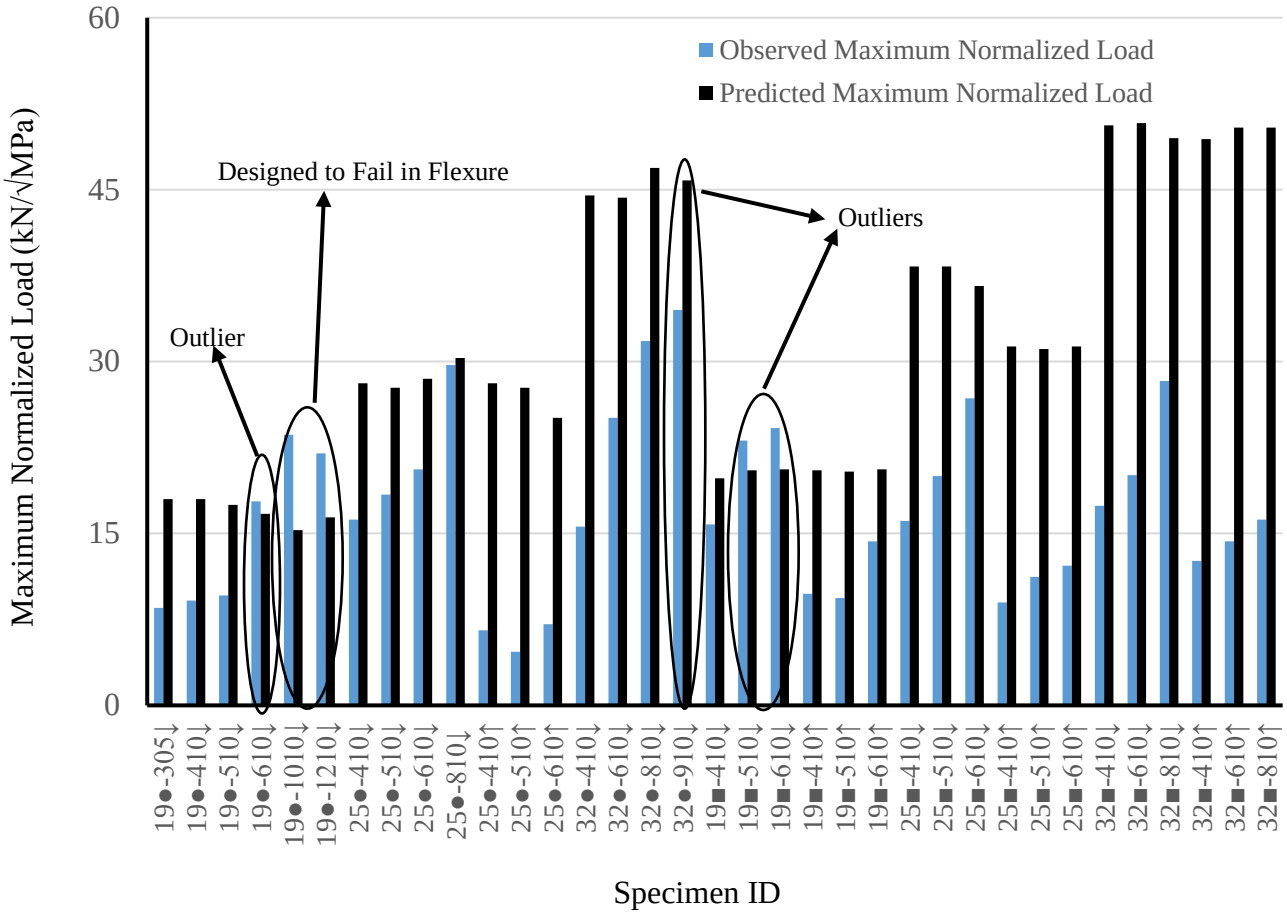

Figure 4.10 Comparison of Observed and Predicted Maximum Normalized Load for Specimens Reinforced with Plain Bars

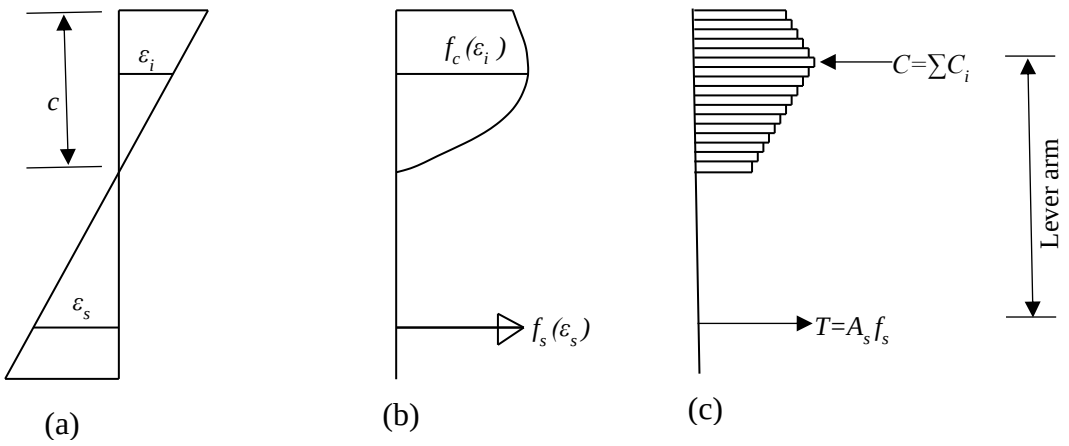

Figure 4.11: Illustration of the Moment Curvature Model (a) Strain Distribution, (b) Stress Distribution, and (c) Force Distribution on the Cross-Section of the Specimen

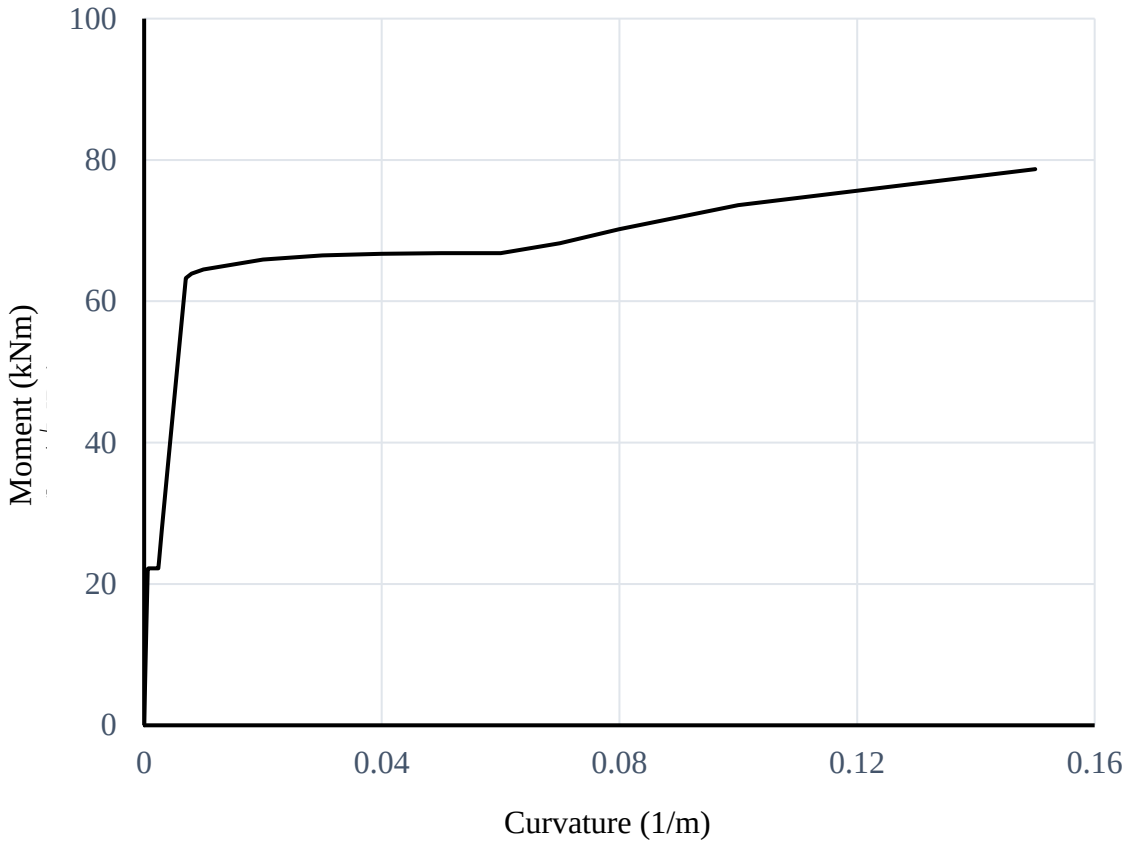

Figure 4.12: Theoretical Moment Curvature Diagram for Specimen 19●-510↓

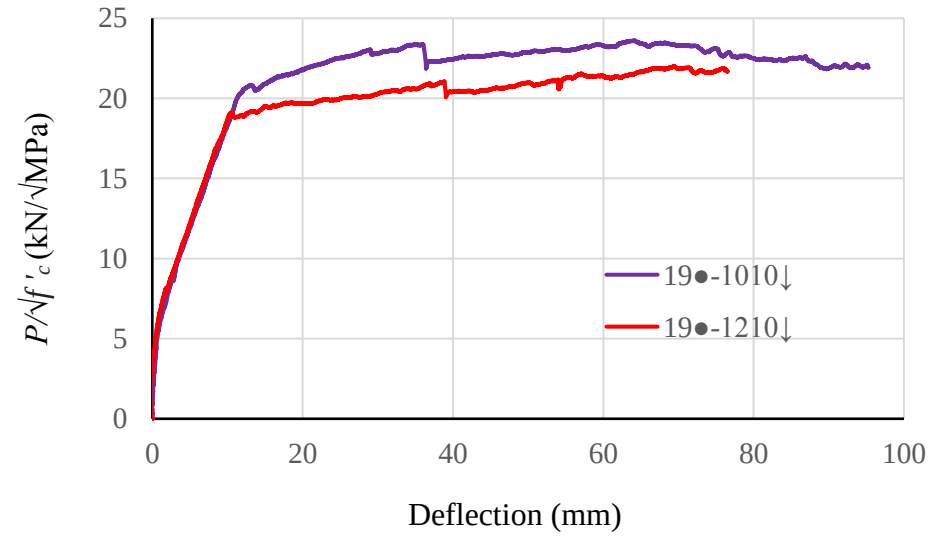

Figure 4.13: Normalized Applied Load Versus Midspan Deflection for Specimens with Long Lap Splice Lengths

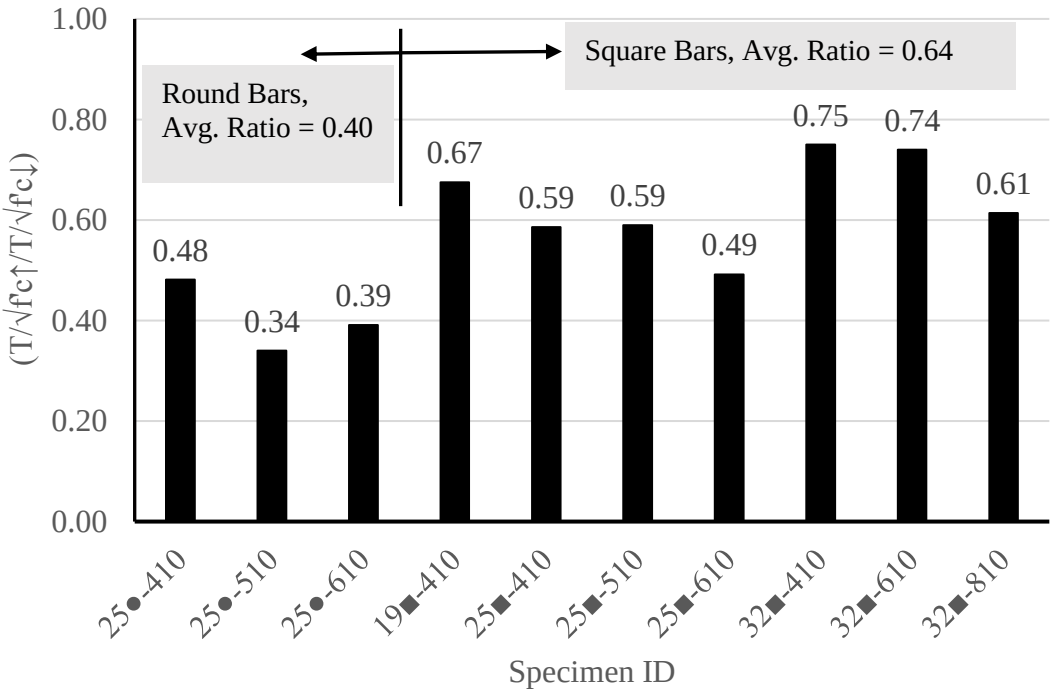

Figure 4.14: Top Cast Effect on the Normalized Tensile Resistance of the Reinforcement at the Maximum Load Level

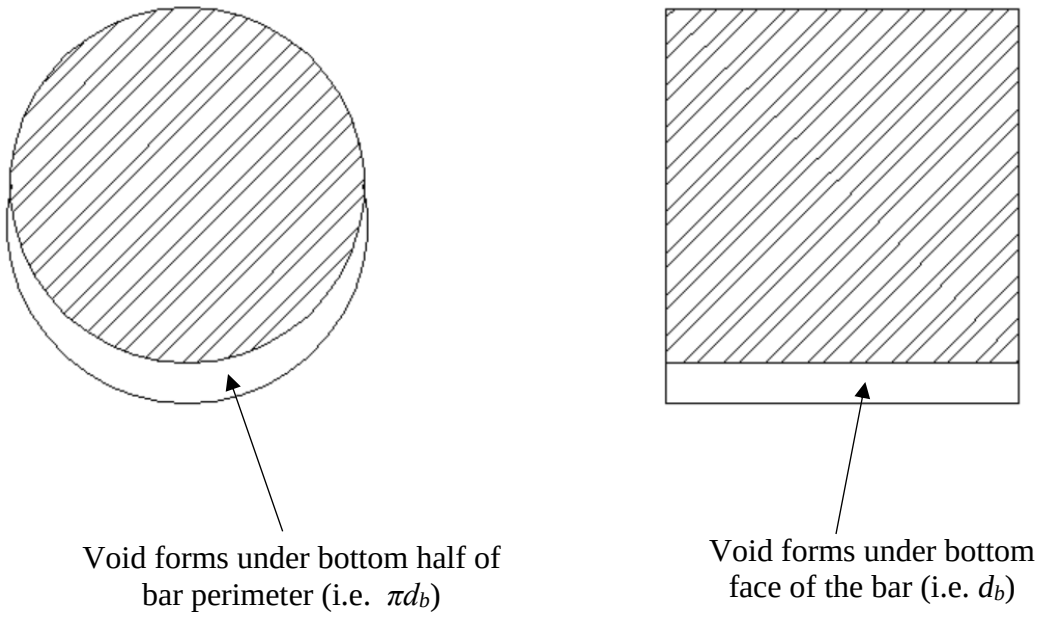

Figure 4.15: Formation of Void under Two Different Bar Shape with Same Nominal Bar Size (a) Round Bar and (b) Square Bar

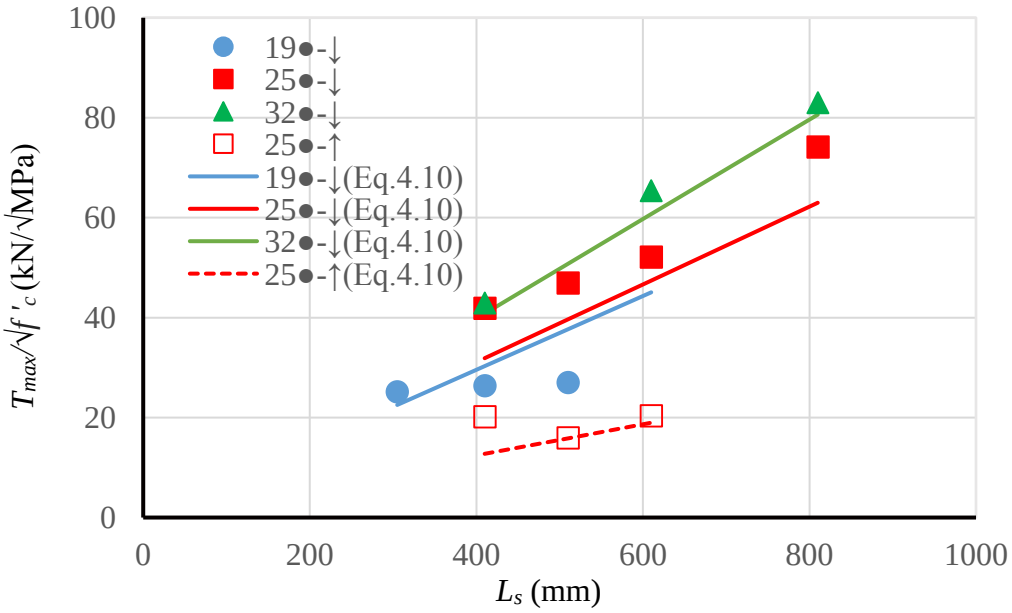

(a)

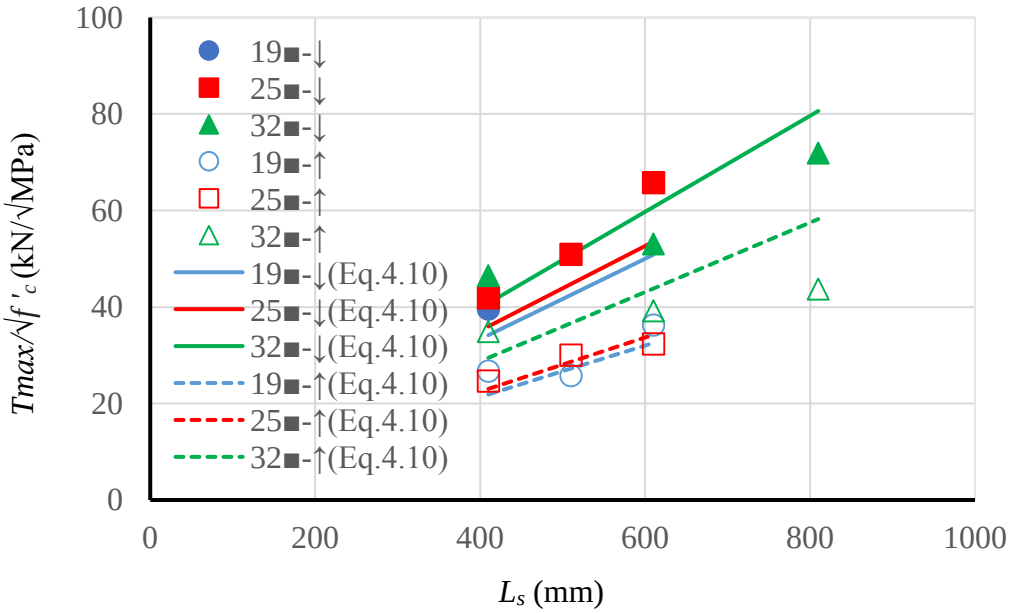

(b)

Figure 4.16: Comparison of Recorded Normalized Maximum Tensile Resistance to Those Predicted Empirically using Eq.4.10 for (a) Specimens Cast with Round Longitudinal Bars; and (b) Specimens Cast with Square Longitudinal Bars.

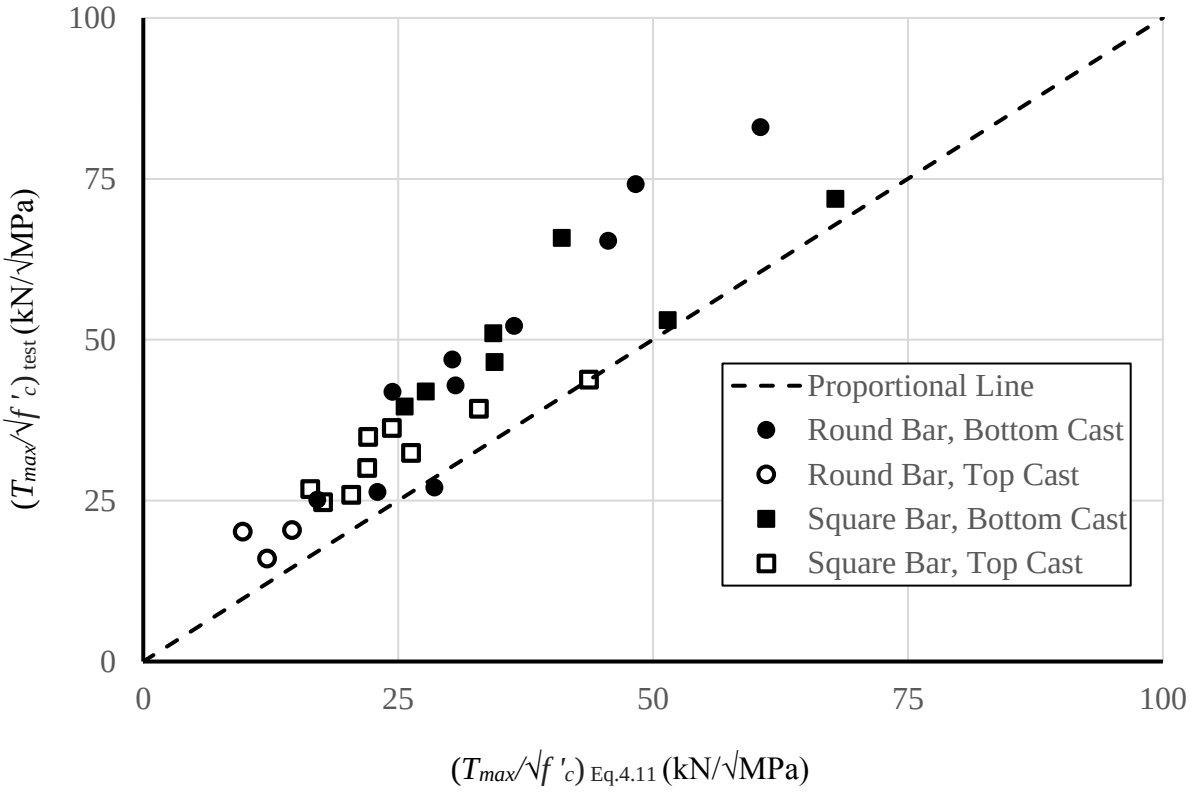

Figure 4.17: Comparison of Recorded and Predicted Normalized Maximum Tensile Resistance after 5% Fractile Approach

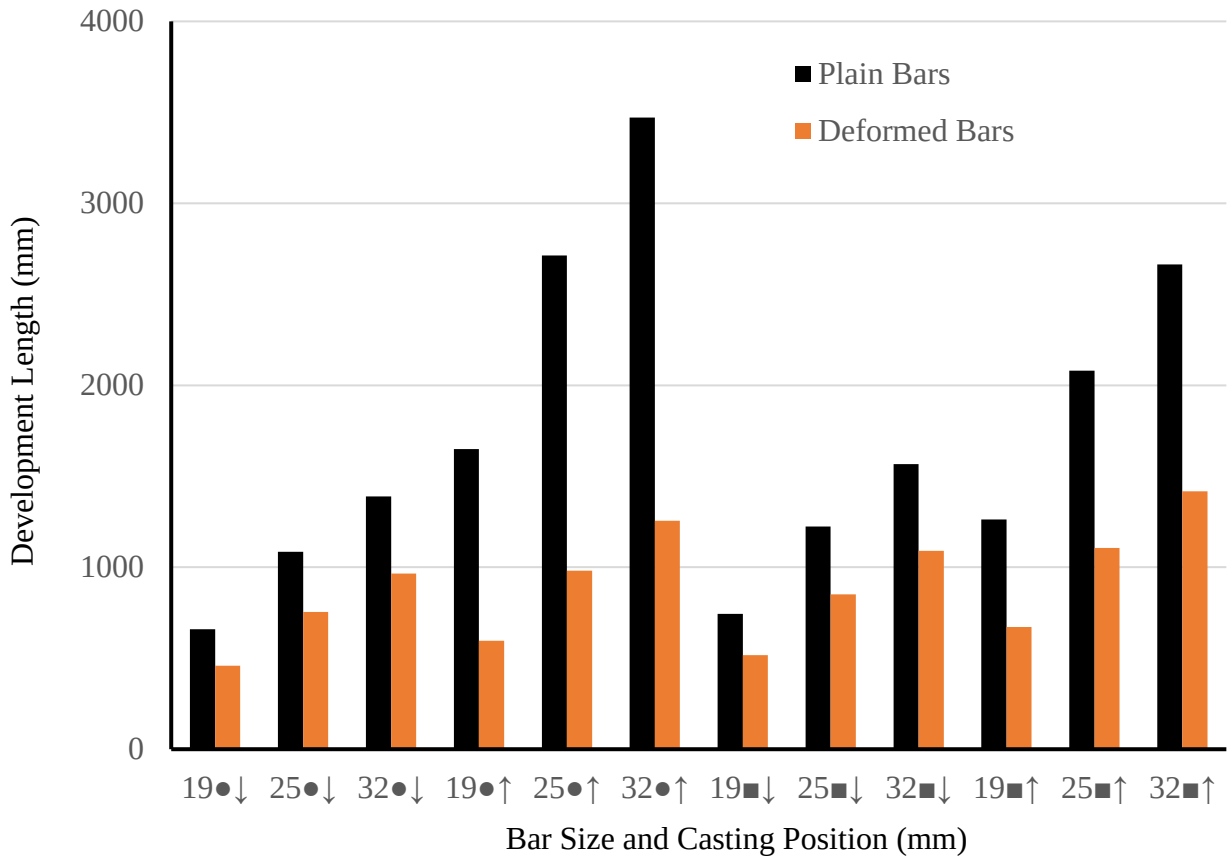

Figure 4.18 Comparison of Development Length Equation for Plain and Deformed Bars

CHAPTER 5

ANALYSIS OF RESULTS AND SPLICE LENGTH CRITERIA FOR RANSOME BARS

5.1 General

This chapter presents the as-tested material properties of the concrete and the spliced Ransome longitudinal reinforcement. Visual observations such as crack patterns and end slips are reported and aid in the understanding of the behaviour of specimens. Load versus midspan deflection and deflection profiles along the span length are also discussed. Recorded maximum loads are compared with predicted maximum loads to confirm whether failure of the specimens occurred before yielding of the reinforcement. Finally, a splice length equation for Ransome bars was obtained using a regression analysis.

5.2 Material Properties

Tables 5.1 and 5.2 show the material properties as established from tests of companion specimens using the methods discussed in Section 3.7 for the concrete and longitudinal reinforcing steel. Data from specimens previously reported by Knight and Feldman (2013) are also included.

5.2.1 Concrete

Table 5.1 shows the age of concrete at the test date, measured slump of the concrete, and average concrete compressive strength (f'_c) for all specimens. Concrete slump was measured during casting of the concrete as discussed in Section 3.5.3. The average concrete compressive strength and tensile strength for all specimens was obtained from the testing of companion specimens as discussed in Section 3.7. Appendix K presents the stress-strain relationships of the concrete obtained from the concrete companion cylinder tests.

5.2.2 Reinforcing Steel

Table 5.1 shows the measured bar size and surface roughness of longitudinal reinforcement for the specimens as discussed in Section 3.4.2. Table 5.2 shows static and dynamic yield stresses, ultimate stress, and modulus of elasticity of the spliced longitudinal reinforcement for all specimens. Appendix L presents the stress versus strain diagrams for all longitudinal bars tested in the current investigation. The dynamic yield strength and ultimate yield strength of the longitudinal reinforcement was obtained from tensile testing of the reinforcing steel as discussed in Section 3.7.3. Figure 5.1 shows the comparison of stress versus strain curve of a 25 mm plain bars and a 25 mm Ransome bars taken from the same heat batch. Unlike plain bars, the stress versus strain curve of Ransome bars does not have a definite yield plateau. Hence, the dynamic yield strength for Ransome bars was obtained using the 0.2% offset method. The static yield strength of the longitudinal reinforcement was determined in accordance with Eq. 4.1, as discussed in Section 4.2.2. Eq. 4.1 is only valid for strain rates ranging from 200 to 1600 μmm/mm/s. However, Eq. 4.1 was still used for some specimens in which the strain rate exceeded the upper bound limitation as identified in Table L.1. Figure 5.1 also shows that the ultimate strength of Ransome bar is greater than that of the corresponding plain bars; however, ultimate strain is reduced by 75% in comparison to plain bars due to the brittle nature of Ransome bars caused by the cold twisting of the bars. The reason behind the increase in the ultimate strength of Ransome bars is unknown; but is consistent with Meinheit and Felder' (2014) report of an increase in ultimate strength of 25 to 35%.

As discussed in Section 3.7.3, tests for both intact lengths and coupons for 19 and 25 mm bars were conducted for comparative purpose, whereas for 32mm bars, only coupons were tested due to the limited capacity of the testing machine. Table 5.2 shows the results of both intact bar lengths and coupons separately, wherever applicable. There is not any statistical difference in the yield and ultimate strength of Ransome bars reported from intact bar length and coupons, as coefficient of variation considering the results of both intact bar lengths and machined coupons were less than 3% for all cases as shown in Table L.1. However, the variation in modulus of elasticity is quite high but this was due to the noise in strain measurement rather than change in material properties. Therefore,

even the use of machined coupons provides reliable results for the properties of Ransome bars.

5.3 Visual Observations

This section describes the visual observations made during and after testing. Cracks were marked as testing progressed until the specimens attained their maximum load. The concrete cover surrounding longitudinal reinforcement was removed for select specimens to identify any slip of the bar.

5.3.1 Crack Patterns

All specimens exhibited similar crack patterns as the test progressed. Figure 5.2 shows the comparison of crack patterns of specimens reinforced with plain, Ransome, and deformed bars with same splice length of 410 mm and cast in bottom position for a given load of 70 kN. Note that 70 kN was chosen as it was close to the maximum attained load of the weakest specimens among the three chosen specimens so that comparison can be done at same load level. The comparison shows that crack patterns of the specimens reinforced with Ransome bars are not significantly different than for those specimens reinforced with plain and deformed bars. Figures 5.3 to 5.6 show the crack patterns at different load levels for specimens 19◆-410↓, 19◆-410↑, 32◆-410↓, and 32◆-410↑, respectively. These specimens were chosen as representative of specimens including lapped reinforcement cast in the bottom and top position with the bar sizes equal to either 19 or 32 mm. Crack patterns are shown at different load levels from the lowest at which cracks were visible to the attainment of the maximum load. Appendix M presents the crack patterns for the remaining specimens tested in the current experimental program as well as for all specimens tested by Knight and Feldman (2013).

Figures 5.3 to 5.6 show that cracks were nearly vertical (i.e. resulting from flexure) and roughly coincided with stirrups locations. Cracks started to develop once the tensile stresses exceeded the tensile strength of the concrete. Most of the cracks developed within the constant moment region, as this region is stressed more so than the shear span region. Flexural cracks generally occurred at the cut ends of the spliced bars due to the change in stiffness at these locations. No shear cracks developed in any specimen which

indicates that shear failure did not govern. Top cast specimens had fewer cracks than bottom cast specimens with the same lap splice length, diameter of bar, and bar type. This is due to the reduced bond capacity of specimens with bars cast in the top position resulting in significantly lower maximum attained load as compared to specimens with bars cast in the bottom position, as will be discussed in Section 5.8.

5.3.2 Observed End Slip of the Spliced Longitudinal Reinforcement

The concrete surrounding the spliced longitudinal reinforcement in select specimens 19◆-305↓ and 19◆-305↑ was removed after the completion of the tests. Figure 5.7 (a) and (b) show the observed end slip for specimens19◆-305↓ and 19◆-305↑, respectively. Slip of the reinforcement was observed in both specimens. This suggests that failure of the specimens was caused by sudden pullout of the longitudinal reinforcement. Observed end slip of the specimens tested by Knight and Feldman (2013) is provided in Appendix N.

5.4 Load-Deflection Behaviour

Load versus deflection behaviour of the specimens was obtained from the recorded load and LVDT data as explained in Section 4.4. Theoretical deflection was calculated in accordance with Eq. 4.2.

Figures 5.8 to 5.11 show the normalized load versus midspan deflection for specimens, 19◆-410↓, 19◆-410↑, 32◆-410↓, and 32◆-410↑, respectively. These specimens were chosen as representative of specimens including lapped reinforcement cast in the bottom and top position with bar sizes of 19 or 32 mm. Appendix O presents the load versus midspan deflection for all remaining specimens. The theoretically predicted deflection is shown by a dashed line, whereas the actual recorded deflection is shown by a solid line. A decrease in slope was evident for all specimens after first cracking until failure of the specimen. All specimens showed a sudden load reduction with increased deflection after the attainment of maximum load.

Figure 5.12 shows the comparison of the load versus mid span deflection between a specimen reinforced with Ransome bar (i.e. 19◆-410↓) and specimens with otherwise similar geometry reinforced with deformed bars (i.e. 20◙-410↓) or plain bars (i.e. 19■-

410↓). There is a similarity in the load versus mid-span deflection between these specimens. The form of the load versus mid-span deflection curves is similar for all specimens and all exhibited sudden failure following attainment of the maximum load. This indicates that Ransome bars exhibit similar characteristics to deformed bars and plain bars in terms of deflection.

Figures 5.13 to 5.16 show the deflection profile at different load levels for specimens 19◆-410↓, 19◆-410↑, 32◆-410↓, and 32◆-410↑, respectively. Markers represent the actual deflection obtained from LVDTs, whereas dashed lines represent the theoretically calculated deflection. Appendix P presents the deflection profiles at different load levels for the remaining specimens tested in current experimental program as well as all specimens tested by Knight and Feldman (2013). Actual deflections are slightly different from theoretical deflections, typically smaller in specimens with bottom cast reinforcement and greater in specimens with top cast reinforcement. The main reason for this could be due to the different stiffness in the specimen within the splice and non-splice regions. Other reasons might be due to errors from LVDT readings, and/or due to rigid body rotation of intact beam segments between cracks. Furthermore, the development of shrinkage cracks at the top surface of specimens with top cast reinforcement during casting which would eventually become a bottom surface during testing, might have decreased the stiffness of top cast specimens and eventually affected the deflection behavior in a different way than that of the specimens with bottom cast reinforcement.

5.5 Observed and Predicted Maximum Load

Table 5.3 shows the maximum recorded loads attained by the specimens tested in current experimental program and those tested by Knight and Feldman (2013). Table 5.3 also presents the recorded midspan deflection at the maximum applied load, theoretical curvature at maximum load, and tensile resistance in the spliced longitudinal reinforcement at the maximum load. The calculation of theoretical curvature and tensile resistance in the spliced longitudinal reinforcement at maximum load will be discussed in Section 5.6.

All reported loads have been normalized by the square root of the concrete compressive strength as was done for specimens reinforced with plain bars. Figure 5.17 shows the comparison of observed maximum load and predicted maximum load. The predicted maximum loads were calculated in accordance with CAN/CSA-A23.3 (CSA 2014) code provisions where stress in the longitudinal reinforcement was set equal to the as-measured static yield strength, f_{ys} calculated from the as-measured dynamic yield strength, and partial material resistance factors set equal to unity. The weight of the spreader beam (1.77 kN) and self weight of the specimen (2.94 kN/m) were subtracted when calculating the predicted maximum load to allow for the direct comparison with the recorded maximum load. Figure 5.17 shows that all specimens failed at loads below the maximum predicted yield loads which indicates that all specimens failed in bond before yielding of the reinforcement.

5.6 Tensile Resistance in the Spliced Longitudinal Reinforcement

In this section, the calculation of the tensile resistance in the lap spliced reinforcing bars at the maximum load level is discussed. A moment curvature analysis which is required to calculate tensile resistance in the spliced longitudinal reinforcement, is also discussed in this section.

5.6.1 Moment Curvature Analysis

A moment curvature analysis was performed as explained in Section 4.6.1. The only difference for the specimens reinforced with Ransome bars is the modelling of stress-strain relationship for reinforcement. Unlike plain bars, the stress versus strain curve of the reinforcement was not modelled theoretically; instead, the actual stress versus strain curve was used. The reason for this difference is that Ransome bars don't have a definite yield plateau similar to that reported for plain bars. As discussed in Section 4.6.1, the compressive stress block was divided into 100 segments of equal depth and the calculation of error associated with the selection of 100 segments is presented in Appendix R. It was determined that error was negligible.

Figure 5.18 shows the moment versus curvature diagram for specimen 19◆-510↓.The diagram is significantly different to that obtained for the typical flexural member

reinforced with deformed bars (MacGregor and Bartlett, 2000). This is due to the different stress versus strain behaviour of Ransome bars caused by the cold twisting of the bars in comparison to deformed bars. Appendix Q presents the theoretical moment curvature diagram for remaining specimens. The detailed comparison of the two different methods of establishing moment curvature relationship as discussed in Section 4.6.1, is provided in Appendix S. The tensile resistance of the reinforcement at the maximum load was calculated as explained in Section 4.6.1. Table 5.3 shows the tensile resistance of the reinforcement at maximum load level for each specimen. Note that the tensile resistance for all specimens was calculated based upon a nominal cover of 50 mm to the spliced longitudinal reinforcement as presented in Section 3.3, although cover in some specimens (32◆-410↑, 32◆-610↑, and 32◆-810↑), as shown in Table 3.4, slightly exceeded the tolerances prescribed by CAN/CSA A23.1-14 (CSA 2014). It is also important to note that the tensile resistance of the reinforcement is reported for the total of the two lap spliced bars in each specimen.

5.7 Effect of Casting Position

Figure 5.19 shows the ratio of the normalized tensile resistance at the maximum load level for specimens with top cast bars to that for specimens with bottom cast bars. Specimens with top cast bars have a lower tensile resistance in the reinforcement at the maximum load level. The average ratio of the normalized tensile resistance of specimens reinforced with Ransome bars in the top position to that in bottom position is 0.67. Current U.S (ACI Committee 318, 2014) and Canadian (CSA A23.3, 2014) codes require that development length for modern deformed bars be increased by 30% for reinforced members cast in the top position. Hence, the top cast effect of Ransome bars appeared to be more severe than that of the deformed bars based upon factors as provided in code provisions. As discussed in Section 4.8, the average ratio of the normalized tensile resistance of specimens reinforced with round and square plain bars in the top position to that in bottom position is 0.4 and 0.64, respectively. This indicates that round plain bar is more sensitive to casting position than Ransome bars. Ransome bars appeared to be slightly less sensitive to casting position than square plain bars but the difference is not statistically significant.

5.8 Predictive Equation for the Tensile Resistance of the Reinforcement at the Maximum Load

A regression analysis of the 18 specimens was performed which results in the following predictive equation for the normalized tensile resistance of the longitudinal reinforcement, $\frac{T}{\sqrt{f'_c}}$, at the maximum load level expressed in kN/√MPa.

$$\frac{T}{\sqrt{f'_c}} = 0.00407 L_s d_{b,EQ} \psi \leq \frac{A_s f_y}{\sqrt{f'_c}} \qquad \text{[Eq. 5.1]}$$

where L_s is lap splice length in mm; $d_{b,EQ}$ is the equivalent round diameter in mm as discussed in section 4.9; and ψ is a top cast factor as established in Section 5.7 which is equal to 1 for bars cast in the bottom position, and 0.67 for bars cast in the top position. The root mean square error for Eq. 5.1 is 11.5 kN/√MPa. The average ratio of experimental tensile resistance and predicted tensile resistance for 19 mm, 25 mm and 32 mm bars were 1.28, 1.17, and 0.96, respectively. This shows that there is a decreasing trend in the predictive tensile resistance as bar size increases. Therefore, a further regression analysis was performed with the introduction of bar size factor ω. To be consistent with the development length equation incurred in the current CSA code, the bar size factor was chosen in a similar manner as per the case for deformed bars. The resulting regression equation is as follows:

$$\frac{T}{\sqrt{f'_c}} = 0.00397 L_s d_{b,EQ} \psi \omega \leq \frac{A_s f_y}{\sqrt{f'_c}} \qquad \text{[Eq. 5.2]}$$

where, ω is 1.25 for 19 mm bars or smaller and 1.0 for 25 mm bars or larger. The root mean square for Eq. 5.6 is 10.5 kN/√MPa. Figure 5.20 shows the fit of Eq. 5.2 with the experimental tensile resistance data. The average ratio of the experimental tensile resistance to the predicted tensile resistance for 19, 25, and 32 mm bars after the introduction of the bar size factor were 1.05, 1.20, and 0.98, respectively. Note that ACI Committee 408 (ACI 408, 2003) does not recommend the use of the bar size factor in the provisions for development and splice length of deformed bars used in ACI318-14 (ACI 318, 2004), as there is no support in the use of bar size factor from the analysis of ACI Committee 408 database of the test results. It is also important to note that the

confinement term included in the development length equation included in ACI 318-2014 (ACI 318, 2014) is the smaller of the distance from the nearest concrete surface to the longitudinal reinforcing bar, and one half of the centre-to-centre distance between longitudinal bars which varies with bar size. However, as clear concrete cover was kept constant in all specimens in the current investigation, it cannot be established whether bar size, confinement, or a combination of bar size and confinement influences the tensile resistance. Therefore, the use of the bar size factor is warranted until such time as the test database can be extended to evaluate the effects of confinement.

5.9 Lap Splice Length Equation for Ransome Bars

Equation 5.2 predicts the average normalized tension resistance and is so not suitable for design purposes. To ensure an adequate level of safety accounting for deviations in material properties, dimensional errors, and uncertainties involved in calculations (Orangun, 1977), a 5% fractile approach has been used and the predictive equation is modified in such a way that 95% or more of the experimental tensile resistance of the specimens exceeds the predicted tension resistance. The resulting equation is

$$\frac{T}{\sqrt{f'_c}} = 0.00322 L_s d_{b,EQ} \psi\omega \leq \frac{A_s f_y}{\sqrt{f'_c}} \qquad \text{[Eq. 5.3]}$$

Figure 5.21 shows the predicted tensile resistance in accordance with Eq. 5.3 versus the experimental tensile resistance. The proportional line is also shown which represents the theoretical case in which the predicted normalized tensile resistance is equal to the experimental normalized tensile resistance.

The design lap splice length for Ransome bars is obtained from Eq.5.3 by setting $T=A_s f_y$, $k_1=1/\psi$, and $k_2=1/\omega$ and by solving to get L_s.

$$L_s = 0.487 k_1 k_2 \frac{f_y}{\sqrt{f'_c}} d_{b,EQ} \qquad \text{[Eq. 5.4]}$$

where k_1 is the bar location factor which is equal to 1.0 for bars cast in the bottom position, and 1.5 for bars cast in the top position; and k_2 is the bar size factor which is 0.8 for bar size of 19 mm or smaller, and 1 for bar size of 25 mm or larger. Note that as the unit of predictive tensile resistance is kN and was predicted for two spliced bars, T was

substituted as $2\pi d_{b,EQ}^2 f_y/4000$ in Eq. 5.3 for the compatibility of units. It is also important to note that unit of f_y and f'_c should be used in MPa in Eq. 5.4.

The equation for splice length (Eq. 5.4) was based upon measurement of the modulus of elasticity of longitudinal reinforcement. There is a notable variation in the modulus of elasticity of longitudinal reinforcement associated with splice specimens due to noise in strain measurements. The nominal modulus of elasticity of Ransome bars can be postulated to be 200 MPa, even though their stress strain diagrams are not linear before the yield point. However, as there was no effect of change in modulus of elasticity on splice length equation for plain bars, as explained in Section 4.10, it can be assumed that the variation in measured modulus of elasticity for Ransome bars as reported does not have significant impact on values of splice length as calculated using Eq. 5.4.

It is important to note that structural members reinforced with Ransome bars will not exhibit a ductile failure like the members reinforced with plain and deformed bars, as the stress versus strain curve for Ransome bars does not have definite yield plateau, as mentioned in Section 5.2.2. Hence, it is recommended that a more stringent resistance factor for reinforcing bars (i.e. less than 0.85) be used when performing a flexural analysis for the structural members reinforced with Ransome bars.

5.10 Comparison to Lap Splice Length Equation for Deformed Bars in Accordance with the CSA A23.3-14

Table 5.4 shows the comparison of the proposed splice length equation for Ransome bars (Eq. 5.4) and existing splice length equation for deformed bars in the current CSA code, with following conditions:

i) Bars are uncoated and normal density concrete is assumed.
ii) Minimum stirrups within development length are provided.
iii) The nominal yield strength of reinforcement is 300 MPa and the specified compressive strength of concrete is 20MPa.
iv) Calculations for the development length of deformed bars were made by substituting d_b with the equivalent bar diameter, $d_{b,EQ.}$

vi) The nominal bar size was rounded off to two significant digits for the calculation of development length for both Ransome and deformed bars.

Table 5.4 shows that the ratio of the splice length for Ransome bars to that for modern deformed bars ranged from 1.08 to 1.25. For the bottom cast condition, the ratio is 1.08, whereas for the top cast condition the ratio is 1.25. The difference is due to the fact that Ransome bars have a different top cast ratio than modern deformed bars. Figure 5.22 shows the comparison graphically.

5.11 Comparison to Lap Splice Length Equation for Type 1 Deformed Bars (i.e. Ransome Bars) in Accordance with the BS 8110-1:1997

British standard BS 8110:1997 (BSI, 1997) provides equations for the design bond stress for Ransome bars. The design ultimate bond stress, f_{bu}, for Ransome bars is specified as:

$$f_{bu} = \beta\sqrt{f_{cu}} \qquad \text{[Eq. 5.5]}$$

where β is a coefficient depending on a bar type and is equal to 0.4 for Ransome bars; and f_{cu} is the concrete cube strength.

Table 5.5 shows the comparison of the proposed lap splice length equation for Ransome bars (Eq. 5.4) and lap splice length equation for Type 1 deformed bars (i.e. Ransome bars) in accordance with BS 8110:1997 (BSI, 1997) with conditions similar to those mentioned in Section 5.10. The ratio of the proposed splice length and splice length in accordance with BS 8110:1997 (BSI, 1997) varied from 0.70 to 1.05. This shows that the lap splice length provisions in BS 8110-1:1997 (BSI, 1997) reasonably capture the bond behaviour of Ransome bars. Note that top cast factor used in BS 8110-1:1997 (BSI, 1997) is different than that calculated in the current investigation. The top cast factor used in BS 8110-1:1997 (BSI, 1997) is 1.4 when the minimum cover is less than twice the size of the lapped reinforcement, and 1.0 otherwise.

5.12 Summary

This chapter presented the load versus deflection behaviour and visual observations of specimens such as crack pattern and end slip of the bar. These examinations were done to understand the general failure behaviour of the specimens and from these examinations it

was confirmed that all specimens failed by the loss of bond between reinforcement and concrete. Finally, the proposed equation for the splice length of Ransome bars obtained through analysis of 18 specimens was presented.

The next chapter will present the summary and conclusions of the current investigation, followed by recommendations for future work.

Table 5.1: Material Properties

Specimen ID[a]	Age of Concrete at Test Date (days)	Slump (mm)	Compressive Strength f'_c MPa	Tensile Strength MPa	Measured Bar Size d_b (mm)	Surface Roughness R_y (um)
19◆-305↓	34	120	25.4	2.12	18.8	9.01
19◆-410↓						9.71
19◆-510↓	35	110	25.0	2.56		8.95
19◆-305↑	36		24.0	2.07		9.69
19◆-410↑	38		25.3	2.31		9.80
19◆-510↑	37		21.6	2.22		9.99
25◆-410↓[b]	65	Not Tested	20.9	Not Tested	25.0	9.22
25◆-510↓[b]	64		20.2			9.27
25◆-610↓[b]			18.2			9.65
25◆-410↑[b]	54		21.6			9.47
25◆-510↑[b]	62		19.9			9.42
25◆-610↑[b]	63		19.7			9.92
32◆-410↓	29	110	23.9	2.38	31.7	10.1
32◆-610↓	28		23.4	2.40		9.37
32◆-810↓	30	70	21.5	2.28		9.97
32◆-410↑	31		22.3	2.27		9.61
32◆-610↑						9.64
32◆-810↑	30		21.5	2.28		9.74

[a]The first number in specimen identification represents the nominal bar size (i.e. side face dimension) of the longitudinal reinforcement. The symbol that follows represents that the bar is a Ransome bar. The number following the hyphen represents the lap splice length of longitudinal bars in mm and the final symbol represents the position of reinforcing bar at casting where a downward arrow (↓) indicates that lap spliced bars were cast in bottom position, and an upward arrow (↑) indicates that the lap spliced bars were cast in top position.

[b]Originally reported by Knight and Feldman (2013)

Table 5.2: Longitudinal Reinforcing Steel Material Properties

Specimen ID	Dynamic Yield Strength f_{yd} MPa			Static Yield Strength f_{ys} MPa			Ultimate Strength f_u MPa			Modulus of Elasticity E_s GPa		
	Intact Bar Length	Machined Coupon	Average	Intact Bar Length	Machined Coupon	Average	Intact Bar Length	Machined Coupon	Average	Intact Bar Length	Machined Coupon	Average
19◆-305↓	502[e]	523[c]	508	468[e]	484[c]	472	602[e]	634[e]	618	107[e]	196[c]	129
19◆-410↓												
19◆-510↓												
19◆-305↑												
19◆-410↑												
19◆-510↑												
25◆-410↓	473[e]	477[c]	474	449[d]	448[c]	449	621[d]	627[e]	624	114[e]	208[c]	138
25◆-510↓												
25◆-610↓												
25◆-410↑												
25◆-510↑												
25◆-610↑												
32◆-410↓	n/a	485[e]	485	n/a	456[e]	456	n/a	610[e]	610	n/a	214[e]	214
32◆-610↓												
32◆-810↓												
32◆-410↑												
32◆-610↑	n/a	517[e]	517	n/a	489[e]	489	n/a	640[e]	640	n/a	248[e]	248
32◆-810↑												

[c] Reported value is the representative of 1 specimen only.
[d] Reported value is the average of 2 specimens.
[e] Reported value is the average of 3 specimens

Table 5.3: Test Results of the Lap Splice Specimens

Specimen ID	Splice Length as a Function of Bar Size L_s/d_b	Maximum Normalized Load $P_{max}/\sqrt{f'_c}$ (kN/√MPa)	Predicted Normalized Load $P_{max}/\sqrt{f'_c}$ (kN/√MPa)	Midspan Deflection at Maximum Load (mm)	Theoretical Curvature at Maximum Load (1/m)	Tensile Resistance in the Longitudinal Reinforcement at Maximum Load, T_{max} (kN)
19◆-305↓	16.1	13.0	29.1	7.55	0.00628	168
19◆-410↓	21.6	18.2	29.1	10.6	0.00930	224
19◆-510↓	26.8	22.0	29.2	12.6	0.0120	263
19◆-305↑	16.1	8.00	29.7	11.3	0.00387	112
19◆-410↑	21.6	13.5	29.1	14.5	0.00654	173
19◆-510↑	26.8	13.1	31.0	23.5	0.00645	169
25◆-410↓[f]	16.4	23.6	50.1	9.93	0.00803	267
25◆-510↓[f]	20.4	29.4	50.7	13.4	0.0101	322
25◆-610↓[f]	24.4	37.5	52.3	16.9	0.0130	386
25◆-410↑[f]	16.4	15.0	49.6	18.9	0.00518	182
25◆-510↑[f]	20.4	14.4	50.9	25.9	0.00485	170
25◆-610↑[f]	24.4	19.7	51.1	48.1	0.00651	222
32◆-410↓	12.8	23.0	70.7	6.16	0.00333	299
32◆-610↓	19.1	31.9	71.0	8.46	0.00469	400
32◆-810↓	25.3	36.2	74.3	9.99	0.00526	433
32◆-410↑	12.8	17.2	71.7	8.69	0.00245	225
32◆-610↑	19.1	23.5	75.3	9.16	0.00302	299
32◆-810↑	25.3	20.8	75.7	11.3	0.00265	265

[f]Originally reported by Knight and Feldman (2013)

Table 5.4: Comparison of Proposed Lap Splice Length Equation for Ransome Bars and Existing Lap Splice Length Equation for Deformed Bars

Bar ID[g]	$(L_s)_{Ransome}$ (mm)	$(L_s)_{deformed}$ (mm)	$(L_s)_{Ransome}/(L_s)_{deformed}$
19◆↓	559	517	1.08
25◆↓	921	851	1.08
32◆↓	1179	1090	1.08
19◆↑	839	672	1.25
25◆↑	1382	1107	1.25
32◆↑	1769	1417	1.25

[g]The first number in bar identification represents the nominal bar size. The symbol following the nominal bar size (◆) represents that the bar is Ransome. The final symbol represents the position of reinforcing bar at casting where downward arrow (↓) indicates that the bar is located in bottom position, and upward arrow (↑) indicates that the bar is located in top position

Table 5.5: Comparison of Proposed Lap Splice Length Equation for Ransome Bars and Lap Splice Length Equation for Type 1 Deformed Bars (i.e. Ransome Bars) in accordance with BS 8110-1:1997

Bar ID	$(L_s)_{Ransome}$ (mm)	$(L_s)_{Ransome,\ BS\ 8110\text{-}1}$ (mm)	$(L_s)_{Ransome}/(L_s)_{Ransome,\ BS\ 8110\text{-}1}$
19◆↓	559	803	0.70
25◆↓	921	1058	0.87
32◆↓	1179	1354	0.87
19◆↑	839	803	1.05
25◆↑	1382	1481	0.93
32◆↑	1769	1895	0.93

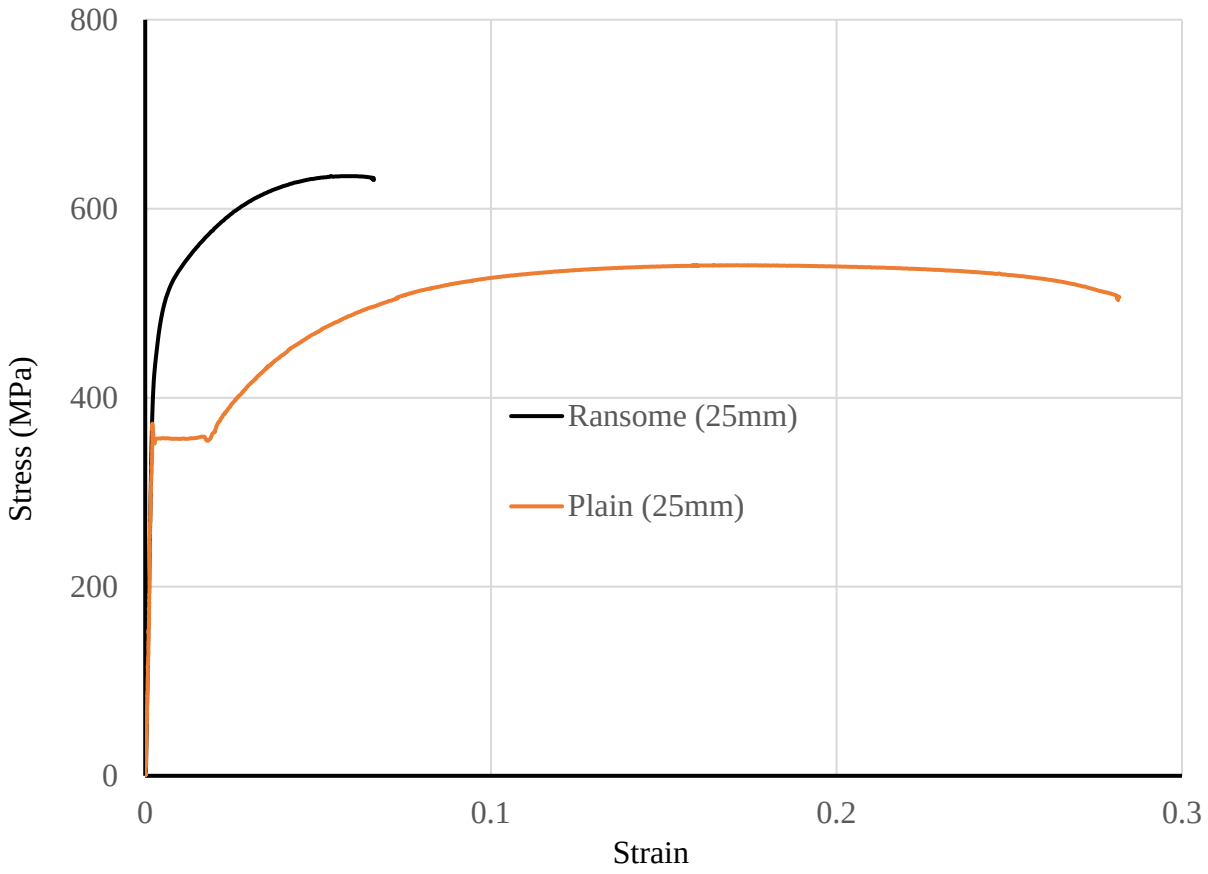

Figure 5.1: Comparison of Stress versus Strain Diagram of 25 mm Plain Bar and 25 mm Ransome Bar from the Same Heat Batch

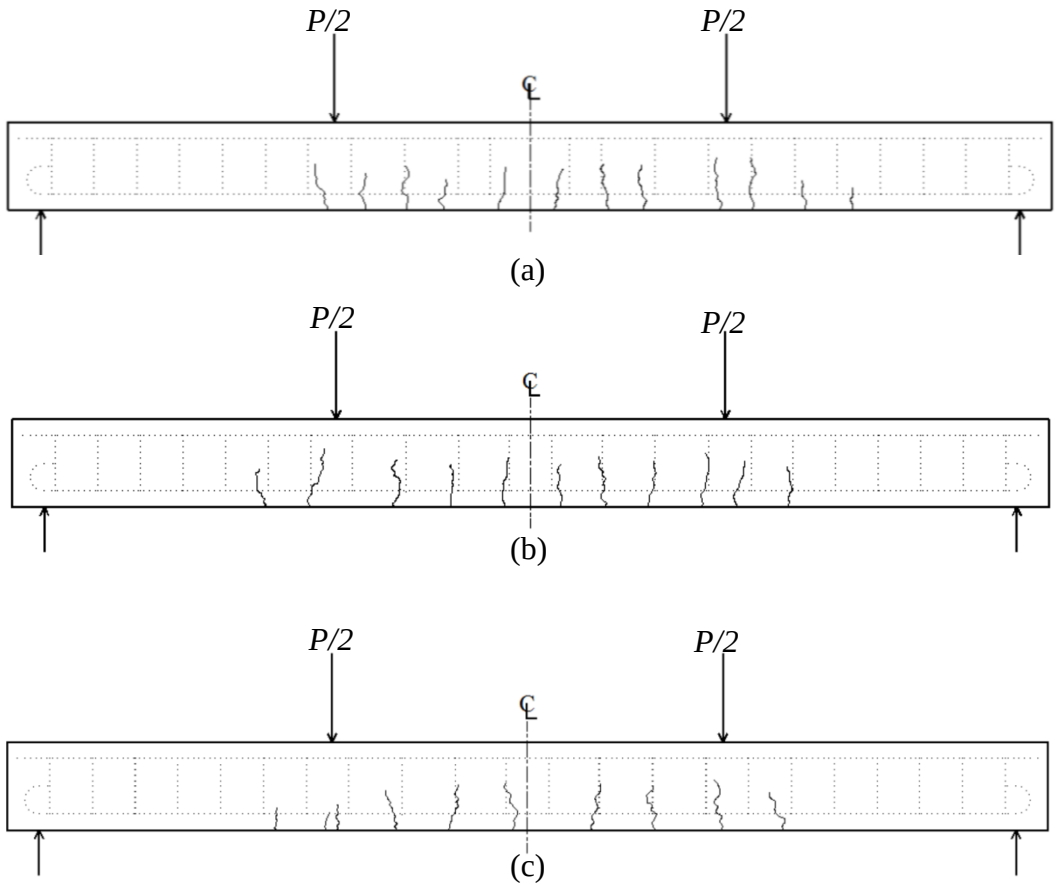

Figure 5.2: Crack Patterns at a Load Level of 70 KN for Specimens with Splice Length of 410 mm reinforced with (a) 19 mm Plain Square Bars, (b) 19 mm Ransome Bars, and (c) 20 mm Deformed Bars

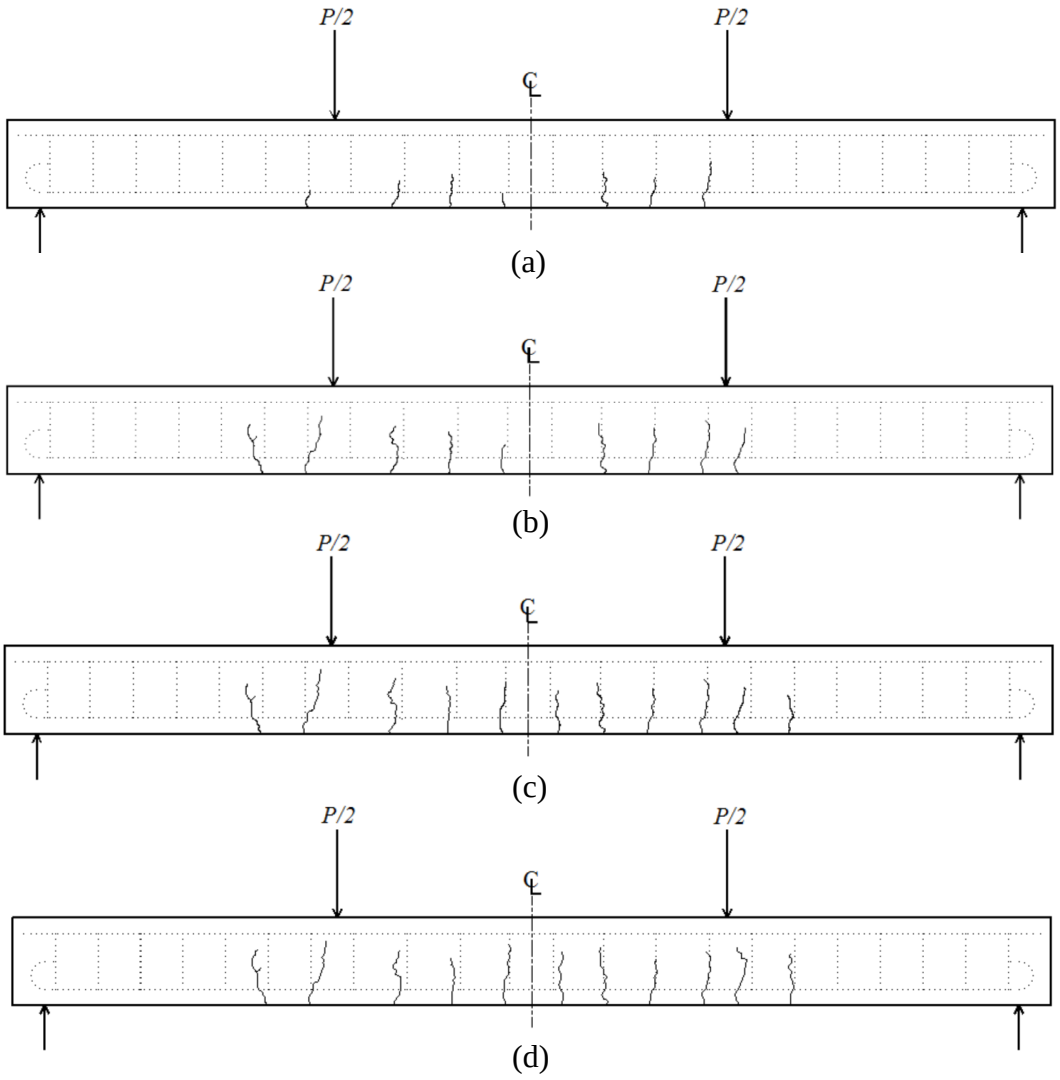

Figure 5.3: Crack Pattern for Specimen 19◆-410↓: (a) P=0.5 P_{max}, (b) P=0.7 P_{max}, (c) P=0.9 P_{max}, and (d) P=P_{max}

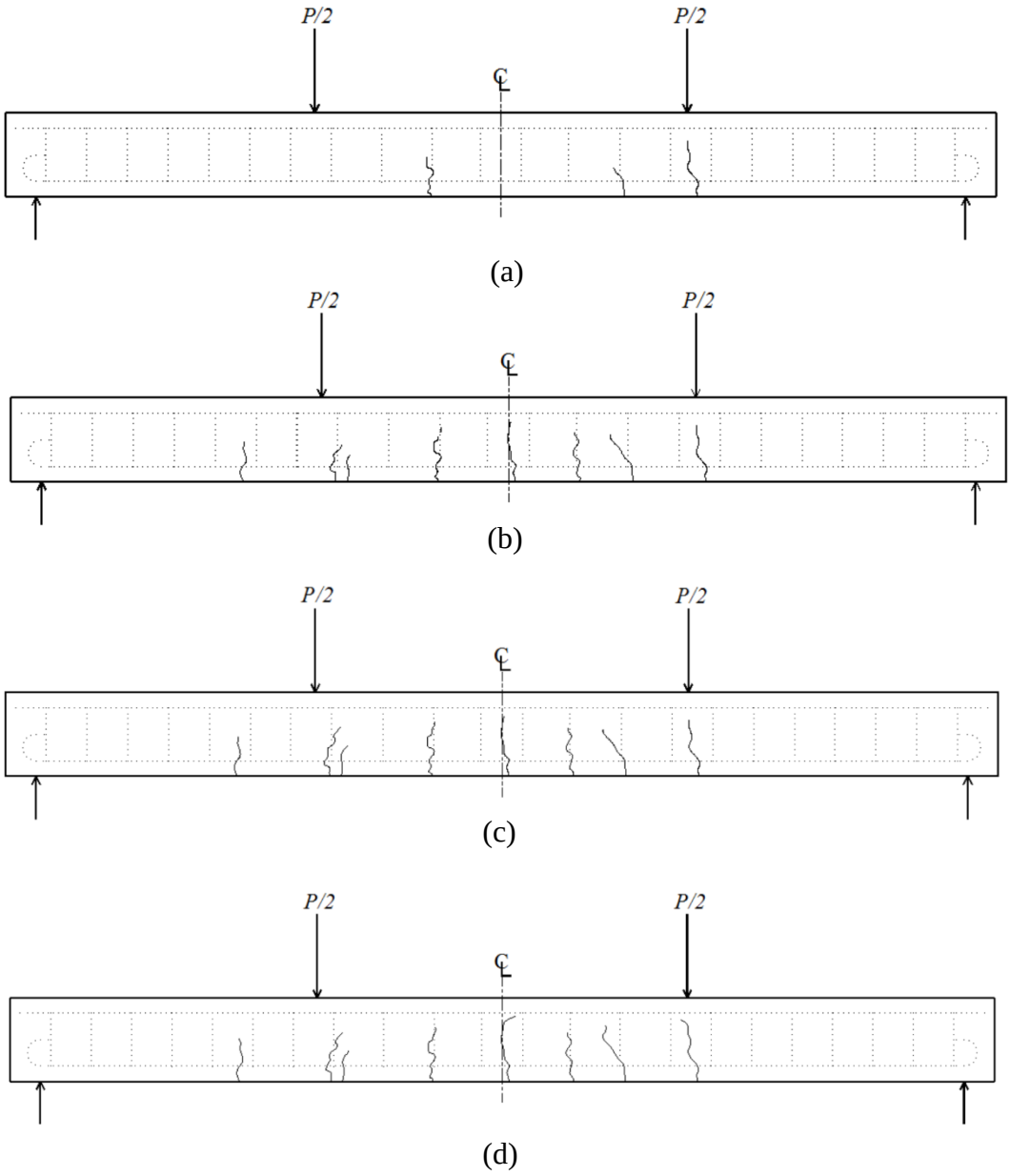

Figure 5.4: Crack Pattern for Specimen 19◆-410↑: (a) P=0.5 P_{max}, (b) P=0.7 P_{max}, (c) P=0.9 P_{max}, and (d) P=P_{max}

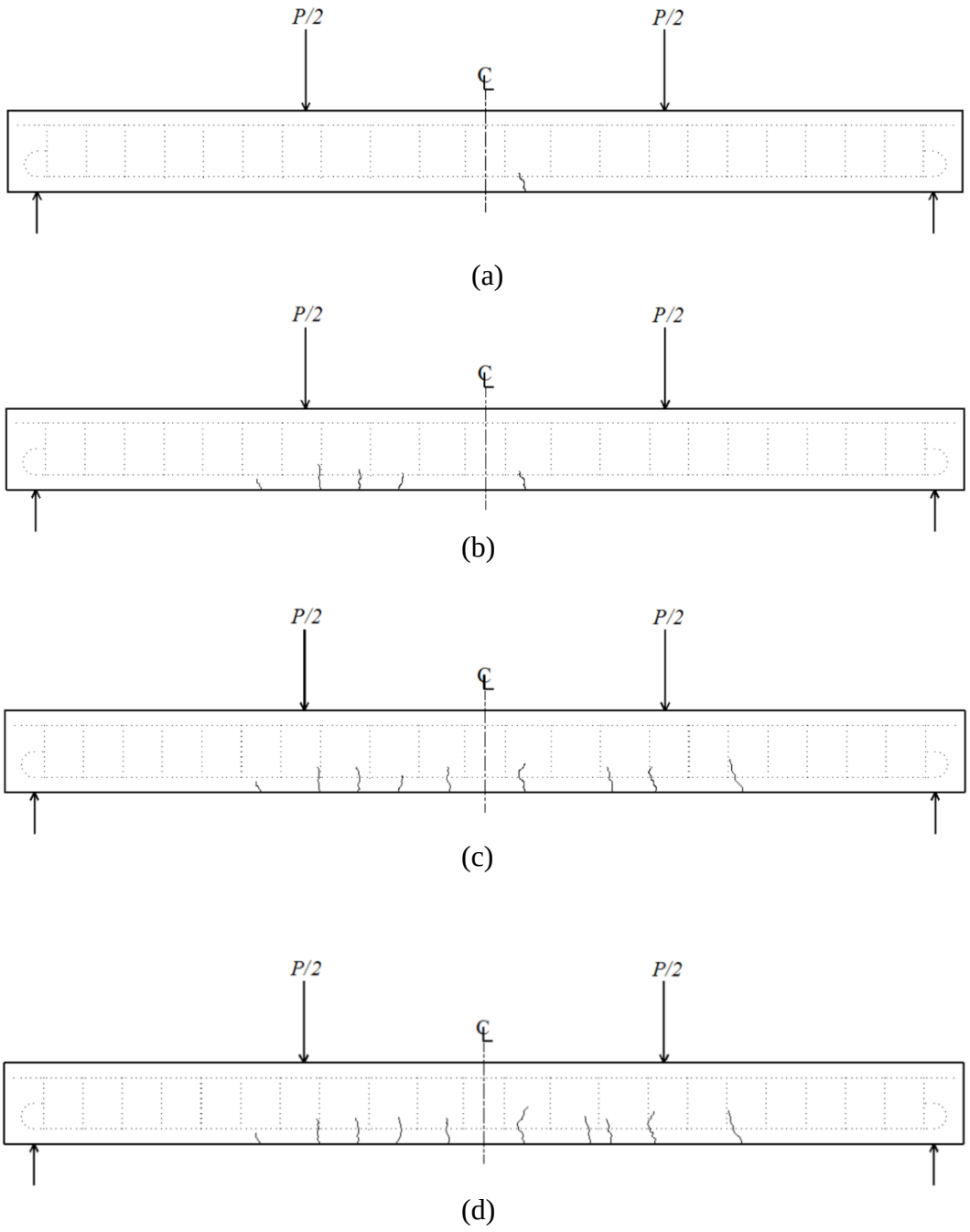

Figure 5.5: Crack Pattern for Specimen 32◆-410↓: (a) P=0.5 P_{max}, (b) P=0.7 P_{max}, (c) P=0.9 P_{max}, and (d) P=P_{max}

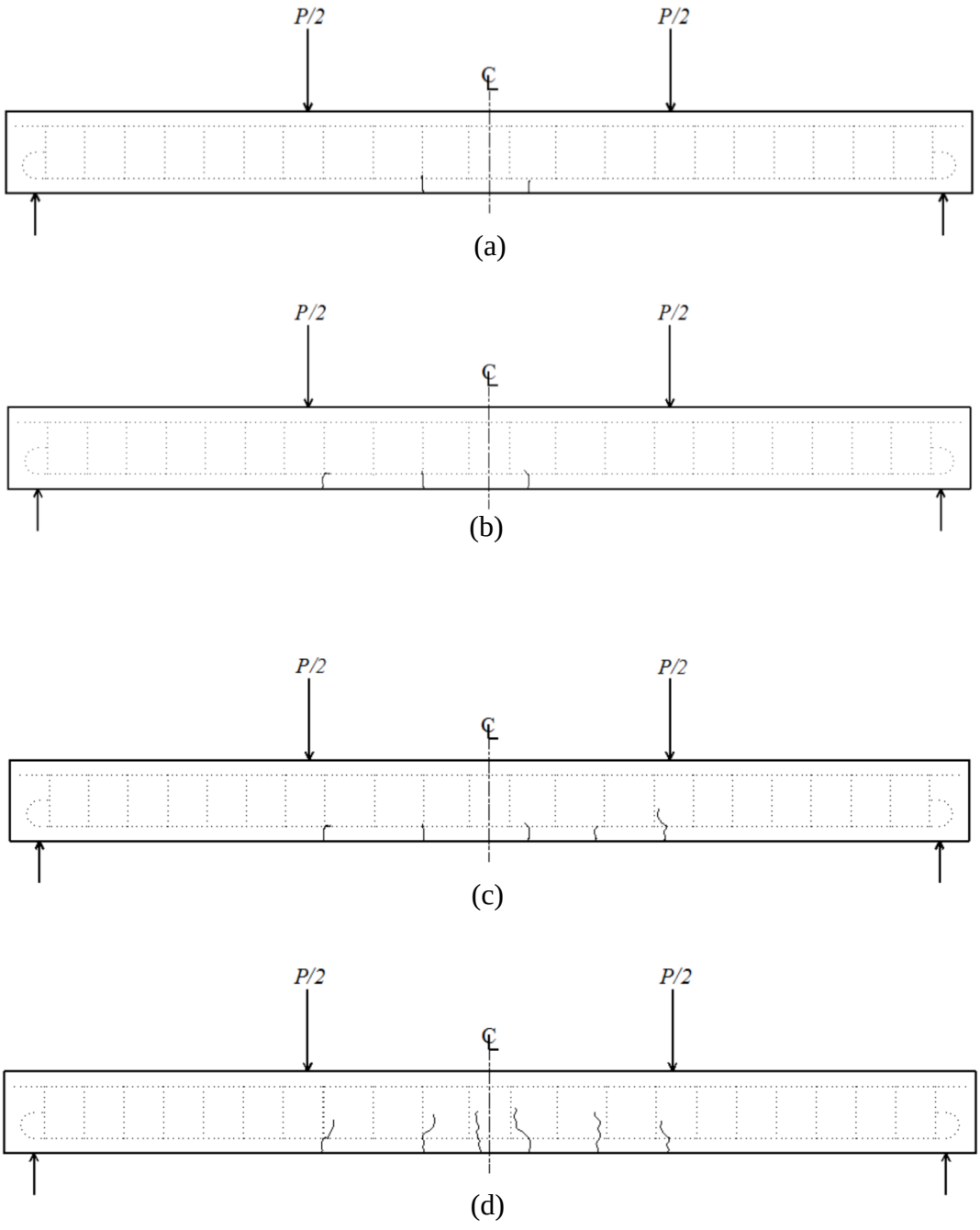

Figure 5.6: Crack Pattern for Specimen 32◆-410↑: (a) P=0.55 P_{max}, (b) P=0.75 P_{max}, (c) P=0.9 P_{max}, and (d) P=P_{max}

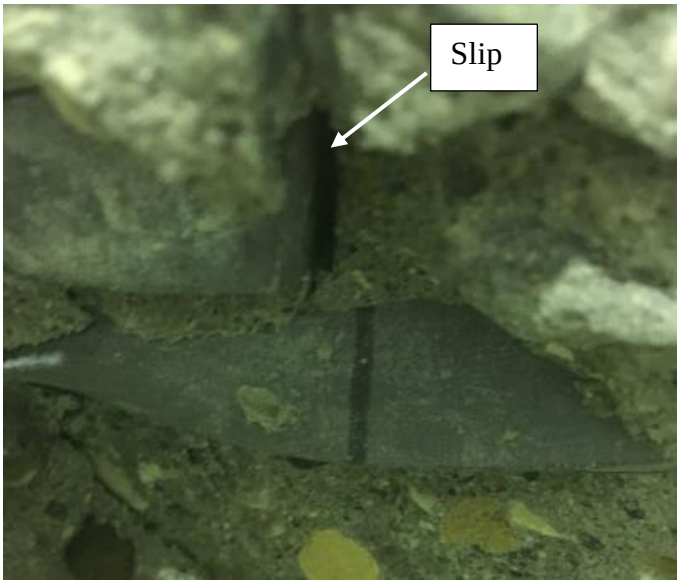

(a)

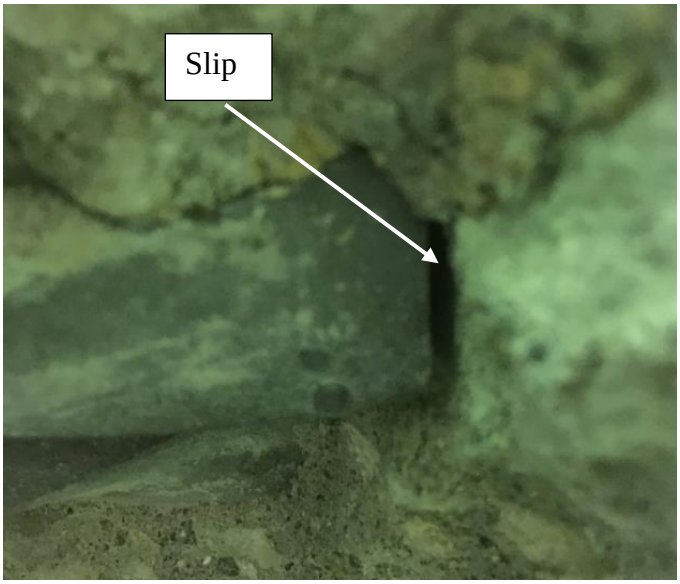

(b)

Figure 5.7: End Slip of Longitudinal Reinforcement Following Concrete Removal for Specimens (a) 19◆-305↓, and (b) 19◆-410↓

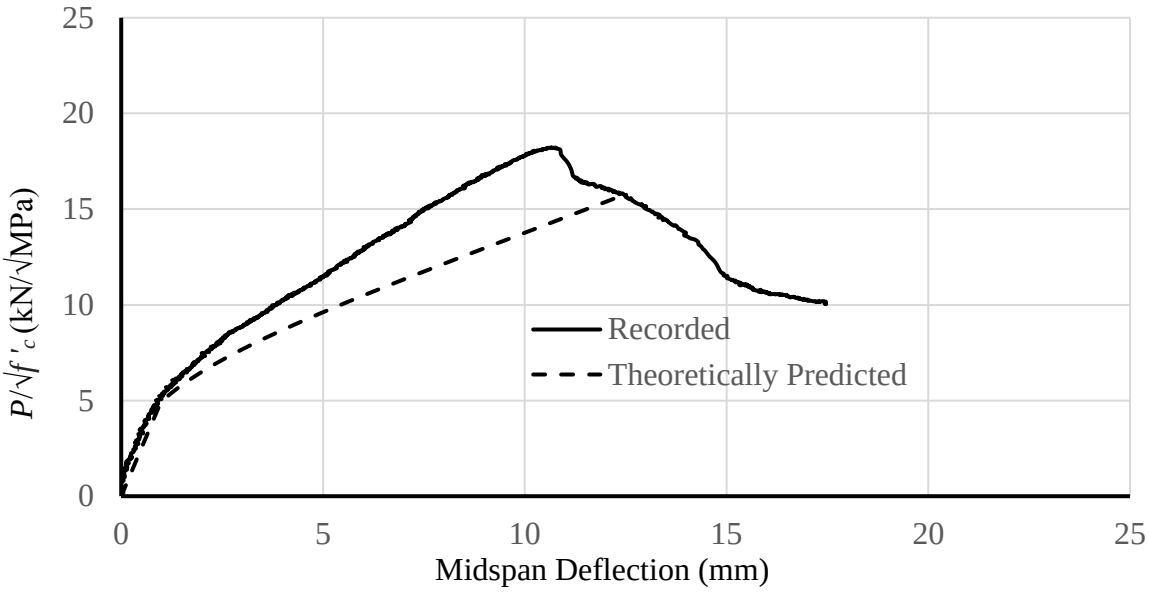

Figure 5.8: Normalized Applied Load Versus Midspan Deflection for Specimen 19◆-410↓

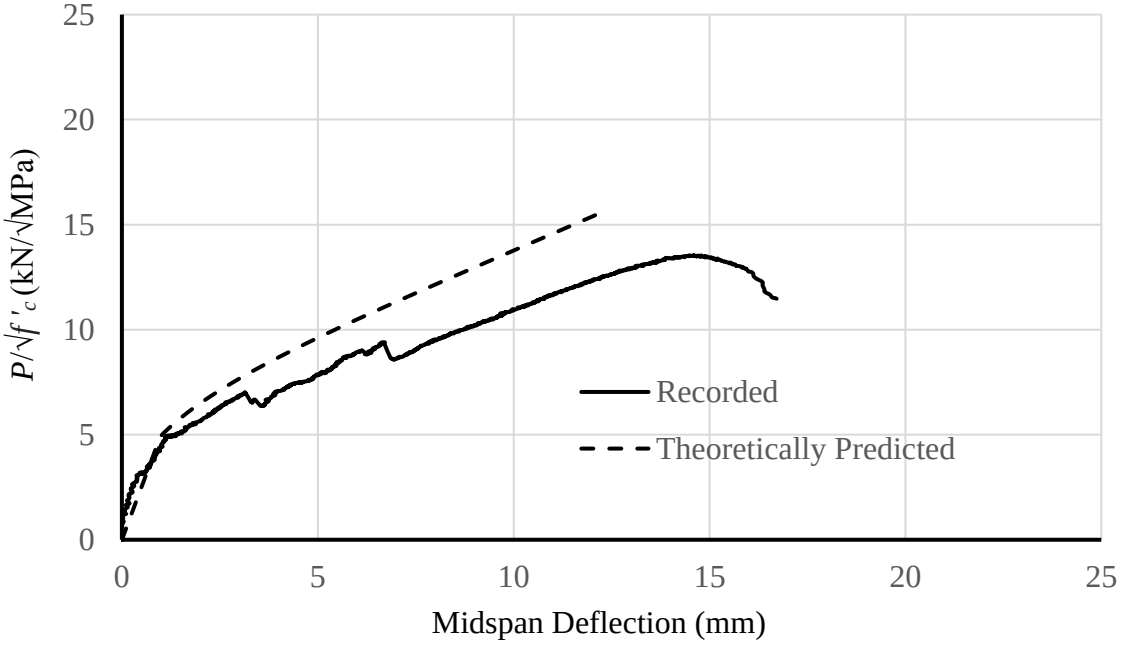

Figure 5.9: Normalized Applied Load Versus Midspan Deflection for Specimen 19◆-410↑

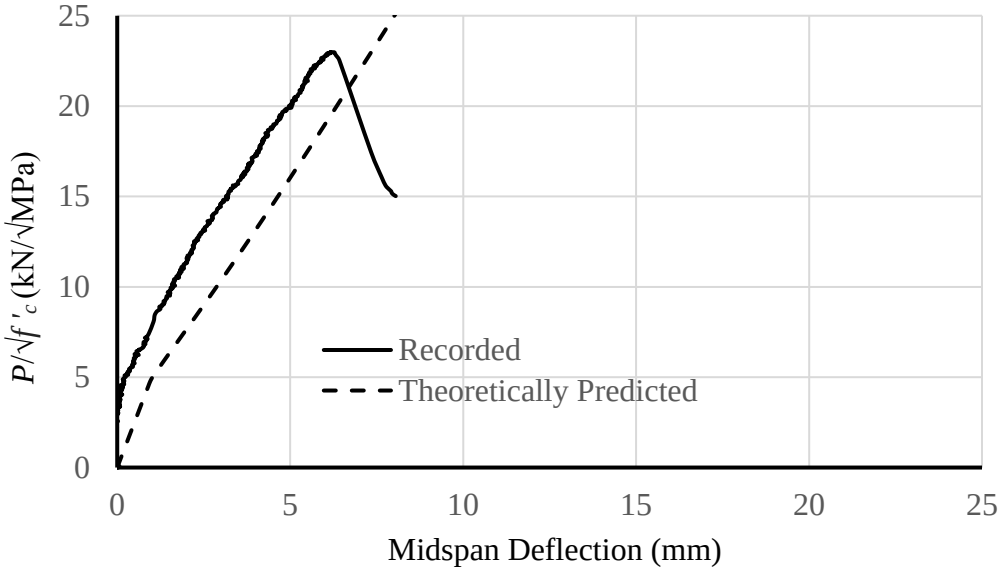

Figure 5.10: Normalized Applied Load Versus Midspan Deflection for Specimen 32◆-410↓

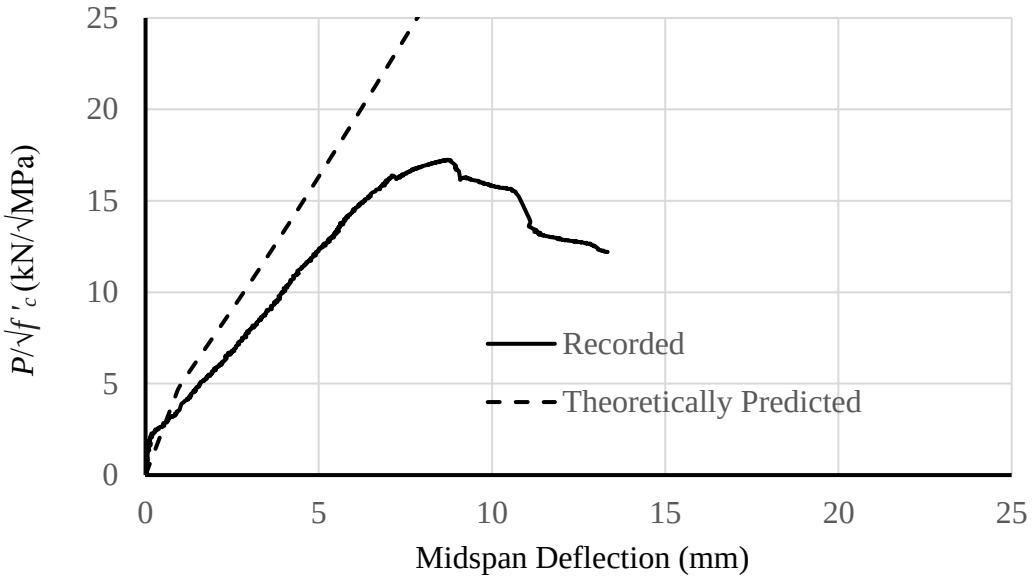

Figure 5.11: Normalized Applied Load Versus Midspan Deflection for Specimen 32◆-410↑

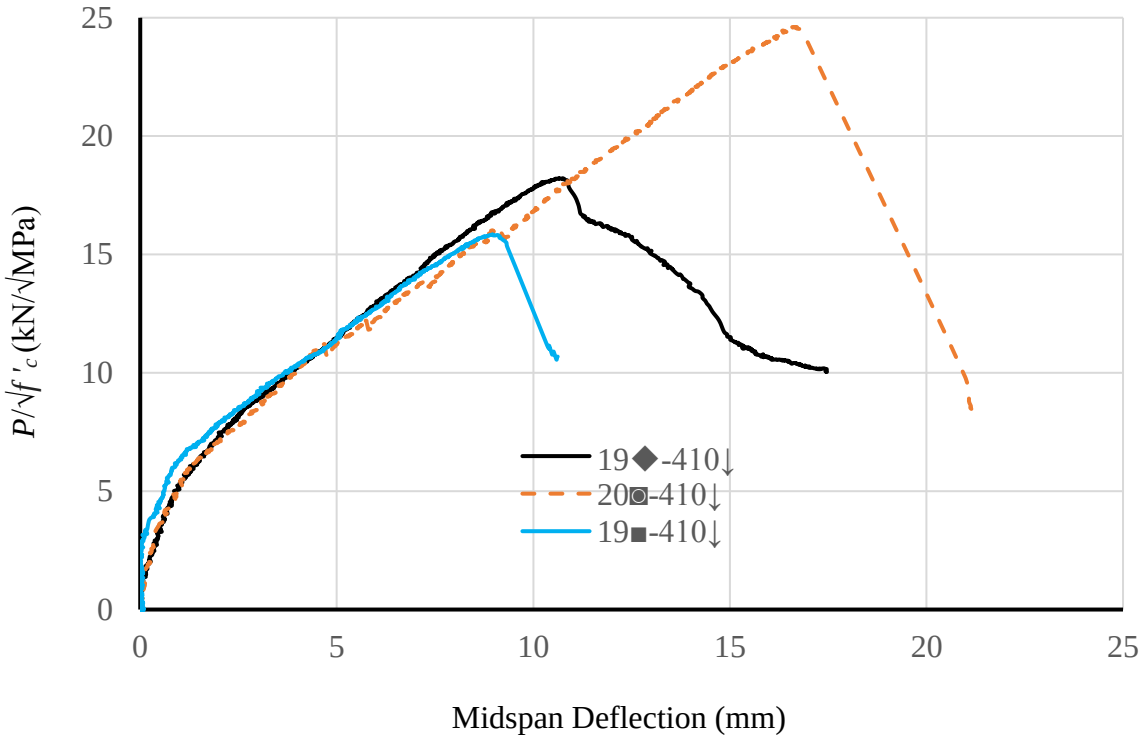

Figure 5.12: A Comparison of Normalized Applied Load Versus Midspan Deflection of Specimens 19◆-410↓, 20◙-410↓, and 19■-410↓.

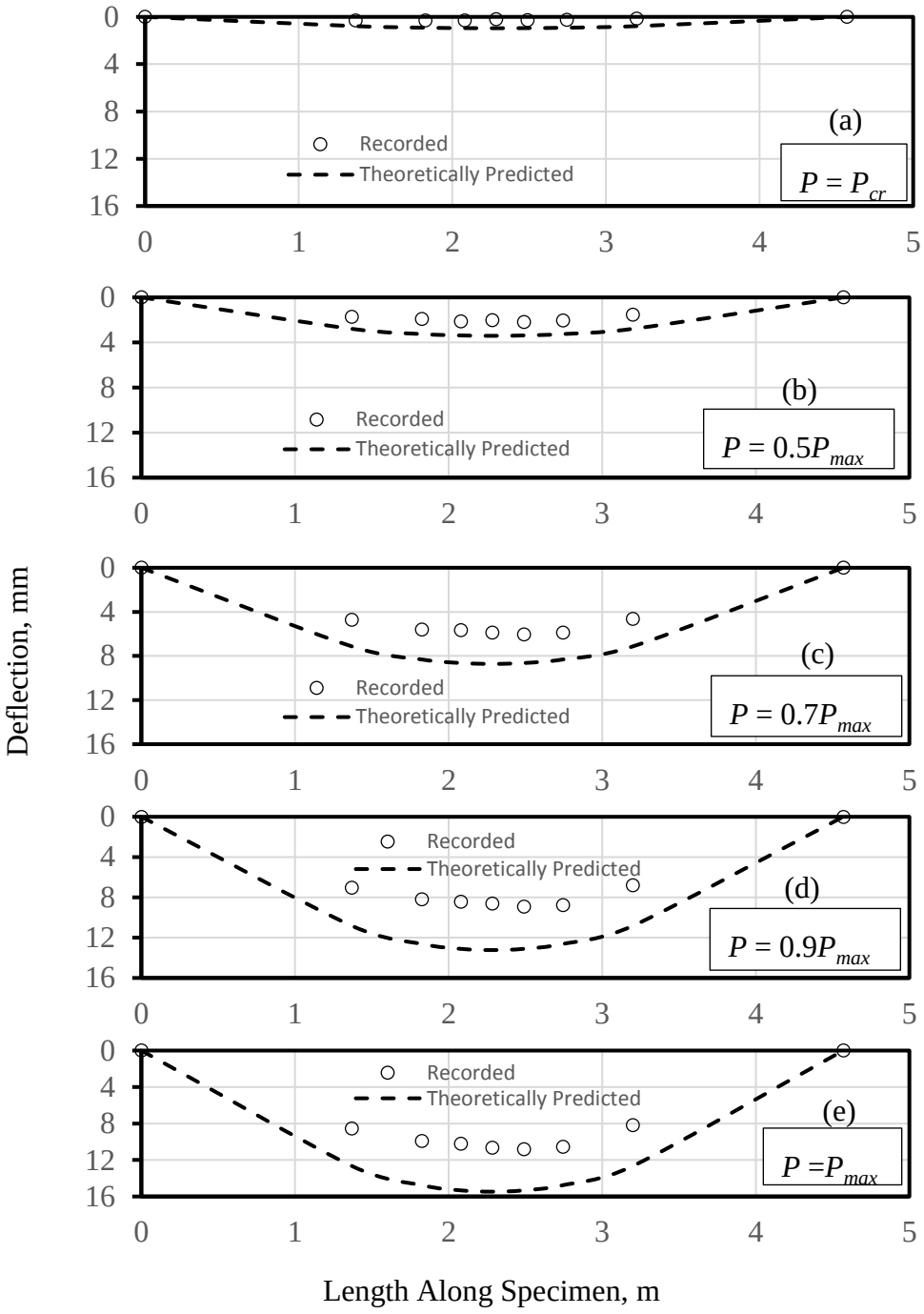

Figure 5.13: Deflection Profile at Different Load Levels for Specimen 19◆-410↓: (a) $P=P_{cr}$, (b) P=0.5 P_{max}, (c) P= 0.7 P_{max}, (d) P= 0.9 P_{max}, and (e) $P=P_{max}$

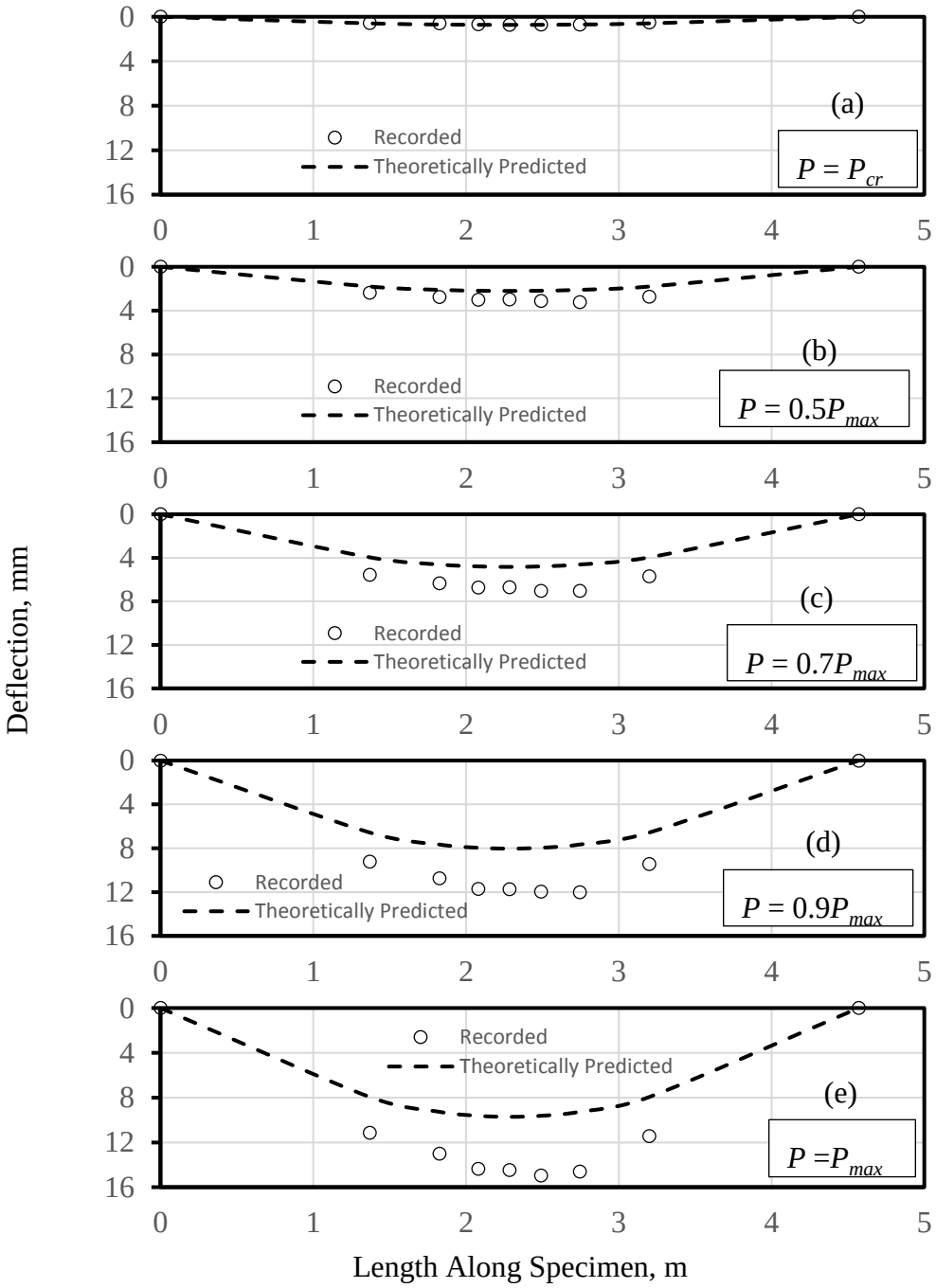

Figure 5.14: Deflection Profile at Different Load Levels for Specimen 19◆-410↑: (a) $P=P_{cr}$, (b) P=0.5 P_{max}, (c) P= 0.7 P_{max}, (d) P= 0.9 P_{max}, and (e) $P=P_{max}$

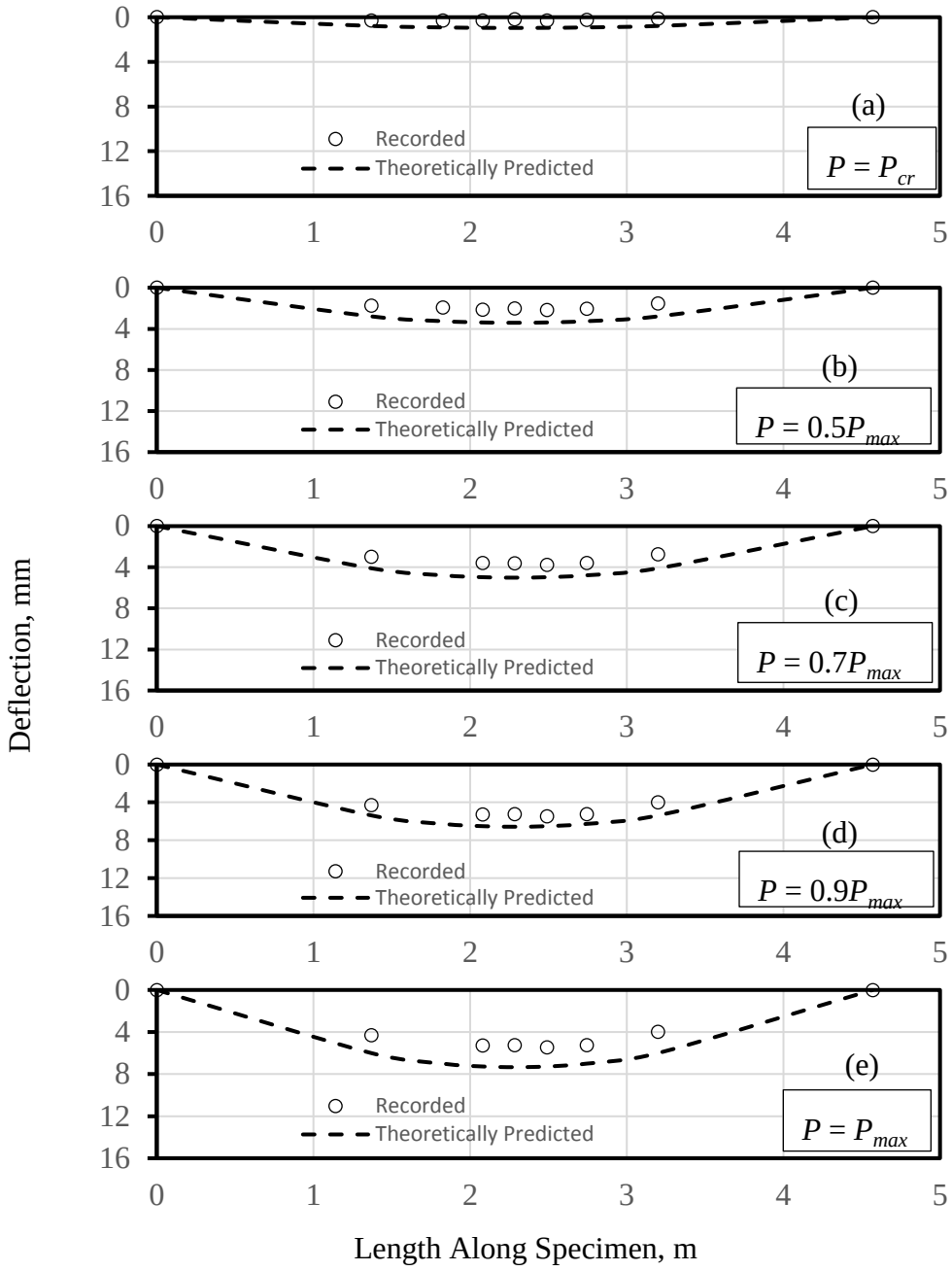

Figure 5.15: Deflection Profile at Different Load Levels for Specimen 32◆-410↓: (a) $P=P_{cr}$, (b) P=0.5 P_{max}, (c) P= 0.7 P_{max}, (d) P= 0.9 P_{max}, and (e) $P=P_{max}$

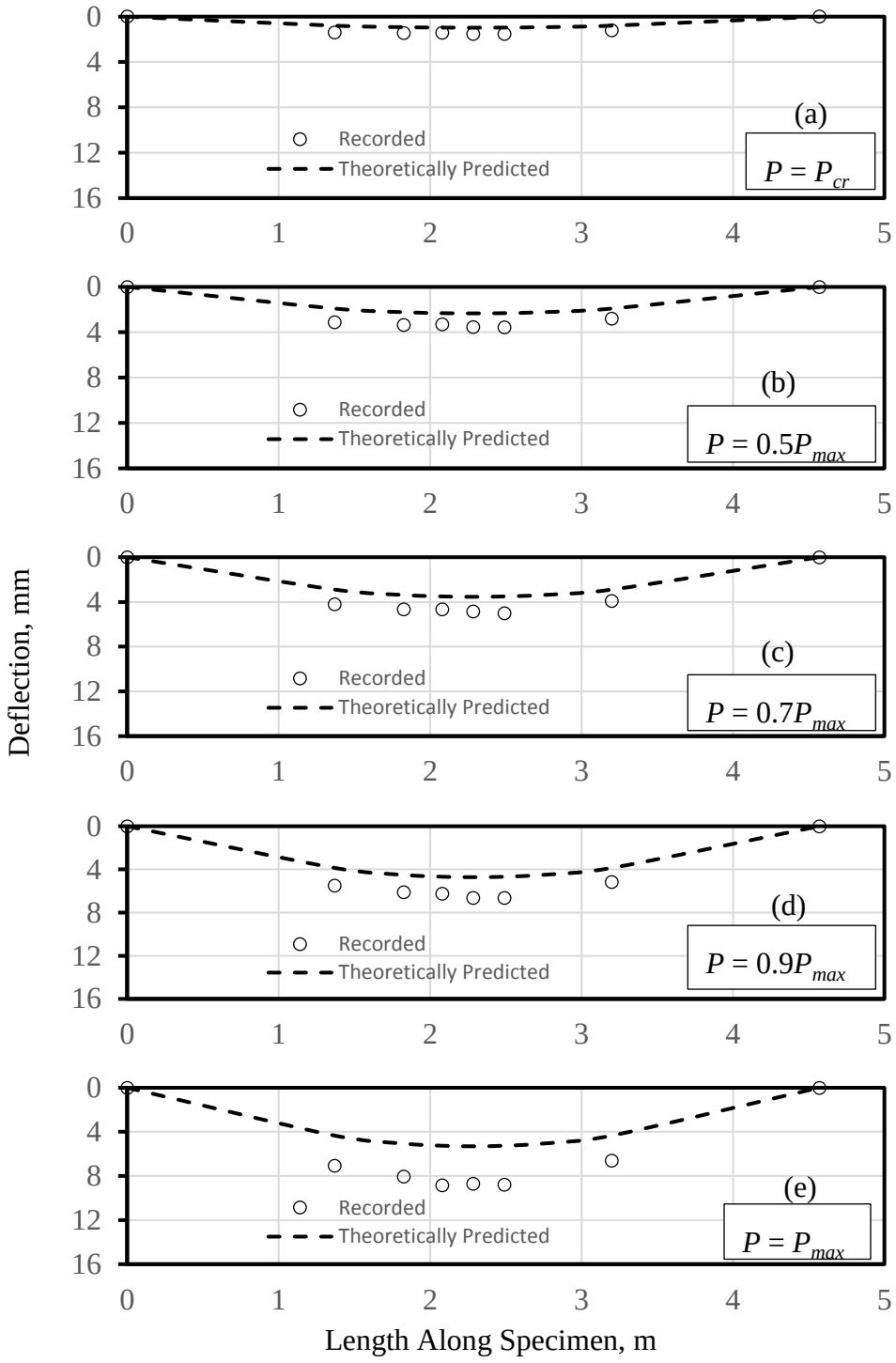

Figure 5.16: Deflection Profile at Different Load Levels for Specimen 32◆-410↑: (a) $P=P_{cr}$, (b) P=0.5 P_{max}, (c) P= 0.7 P_{max}, (d) P= 0.9 P_{max}, and (e) $P=P_{max}$

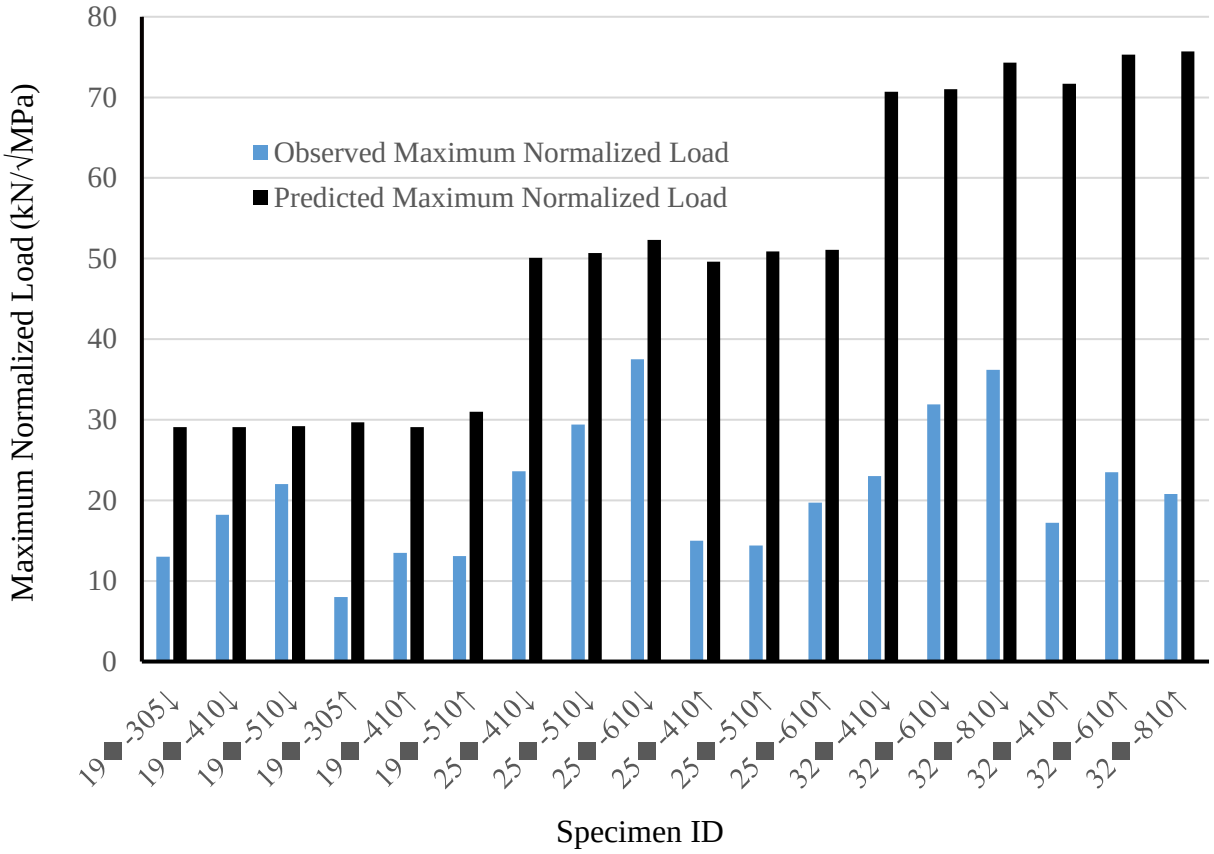

Figure 5.17:Comparison of Observed and Predicted Maximum Normalized Load for Specimens Reinforced with Ransome Bars

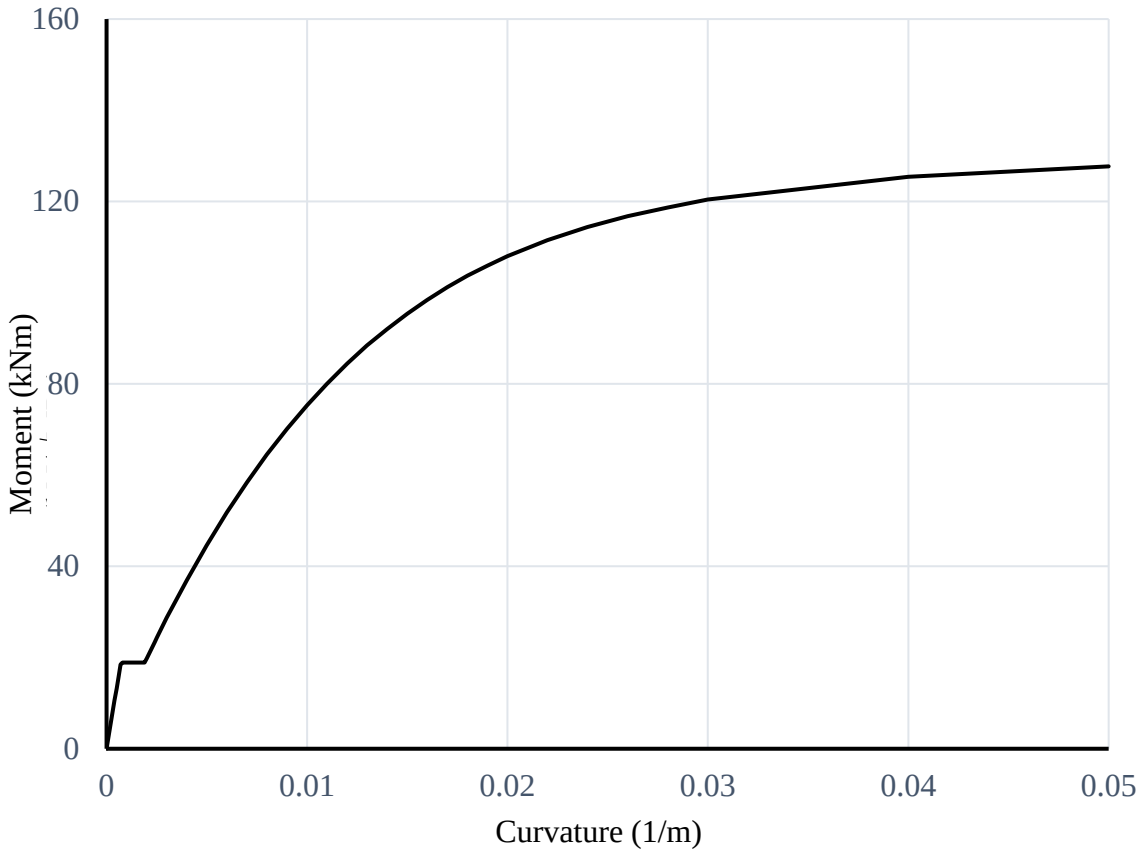

Figure 5.18: Theoretical Moment Curvature Diagram for Specimen 19◆-510↓

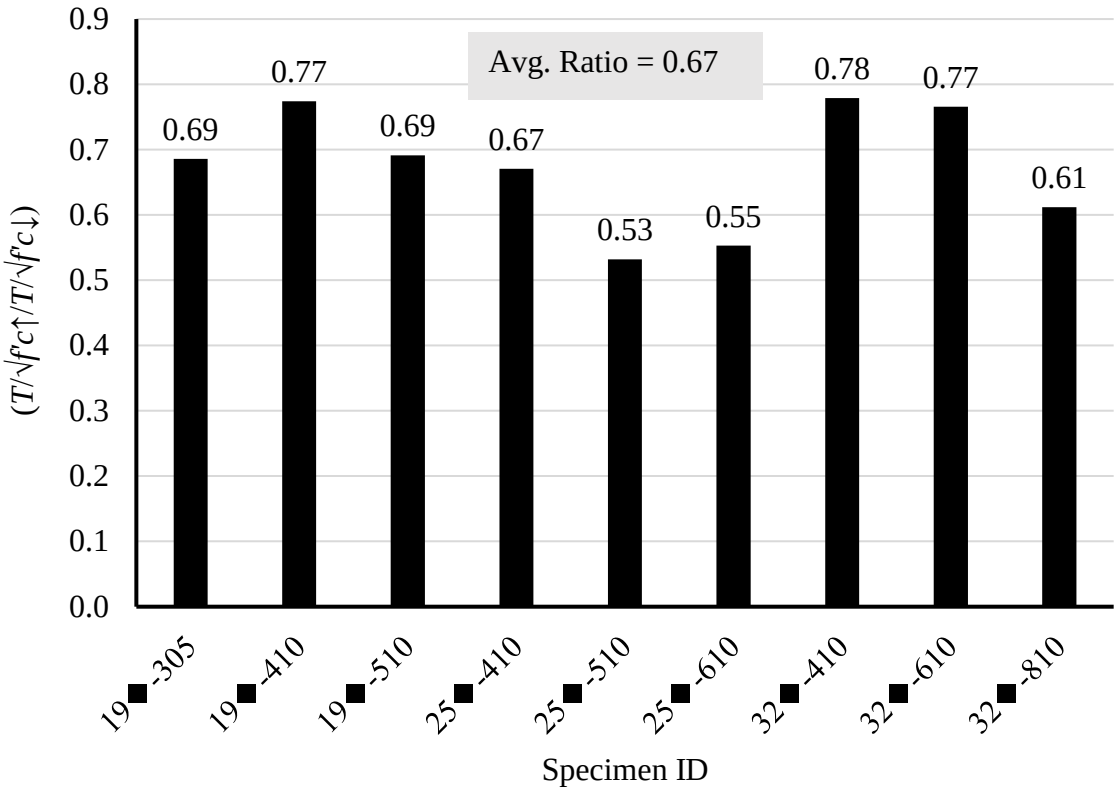

Figure 5.19: Top Cast Effect on the Normalized Tensile Resistance of the Reinforcement at the Maximum Load Level

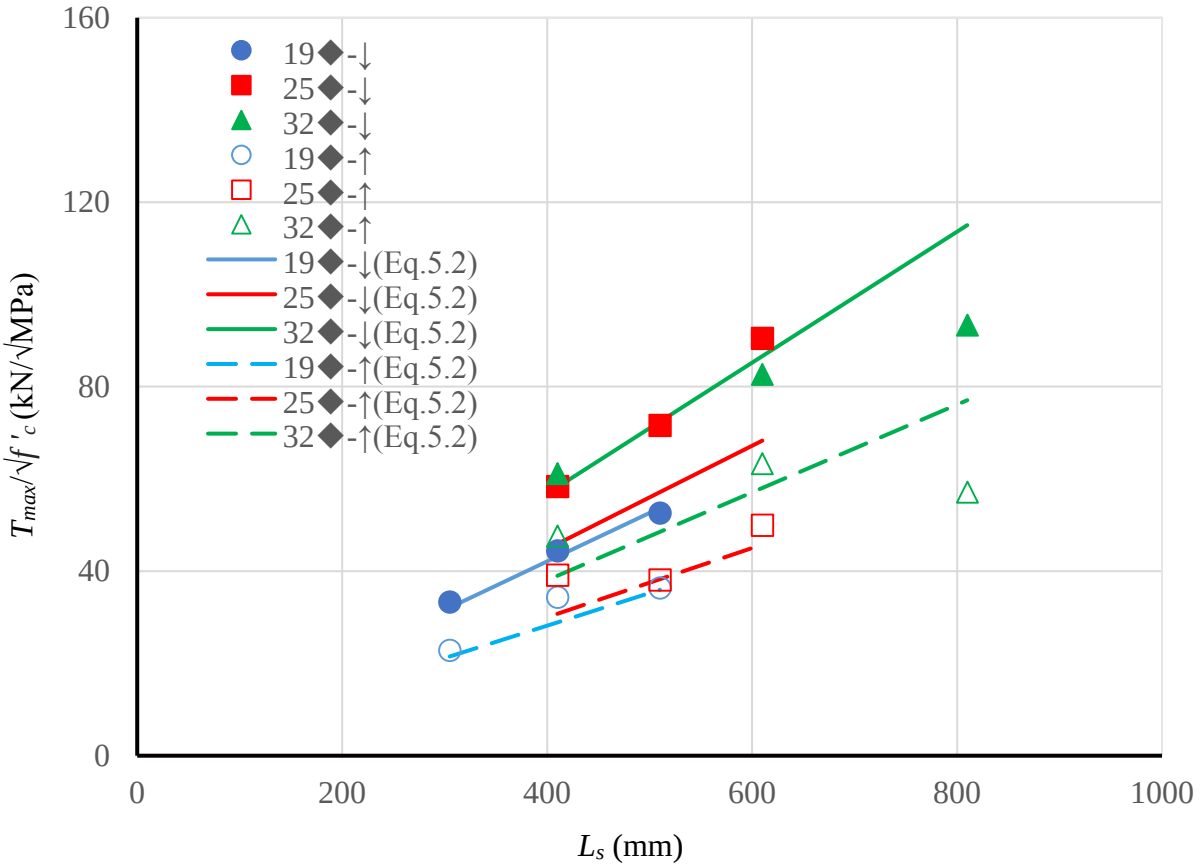

Figure 5.20: Comparison of Recorded Normalized Maximum Tensile Resistance to those Predicted Empirically using Eq. 5.2

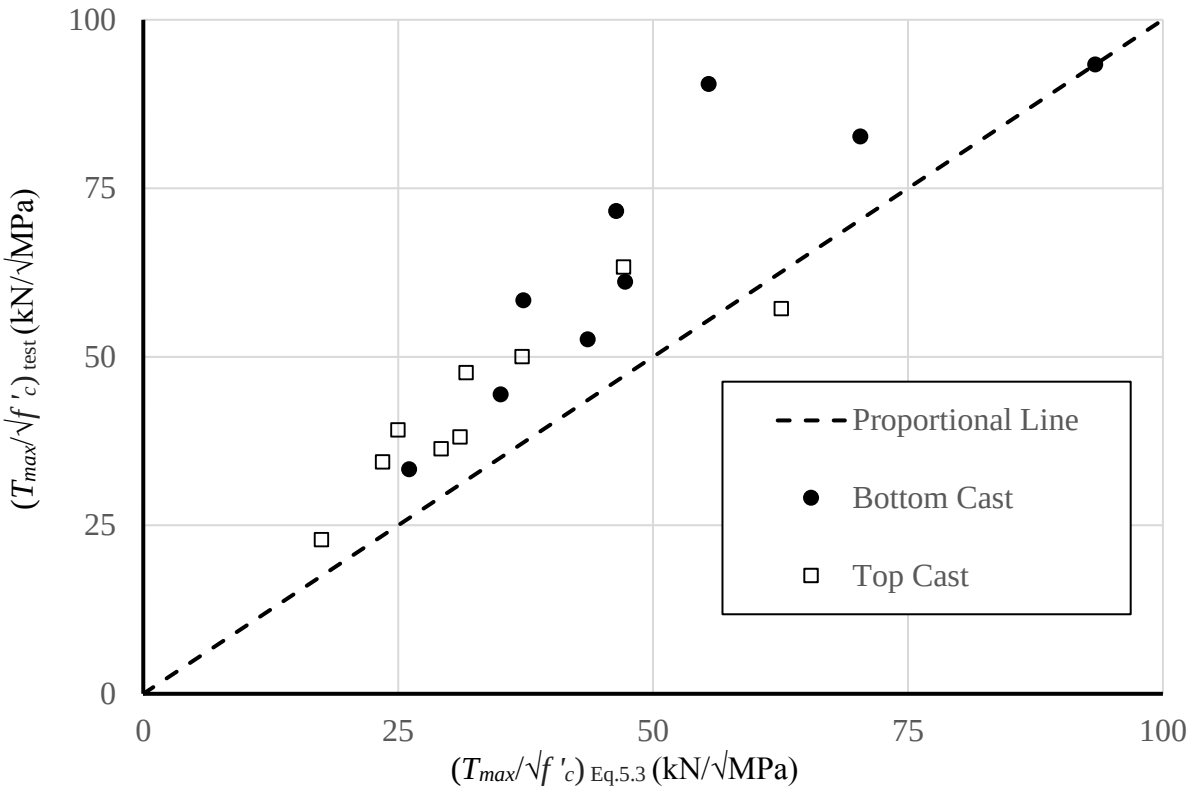

Figure 5.21: Comparison of Recorded and Predicted Normalized Maximum Tensile Resistance after 5% Fractile Approach

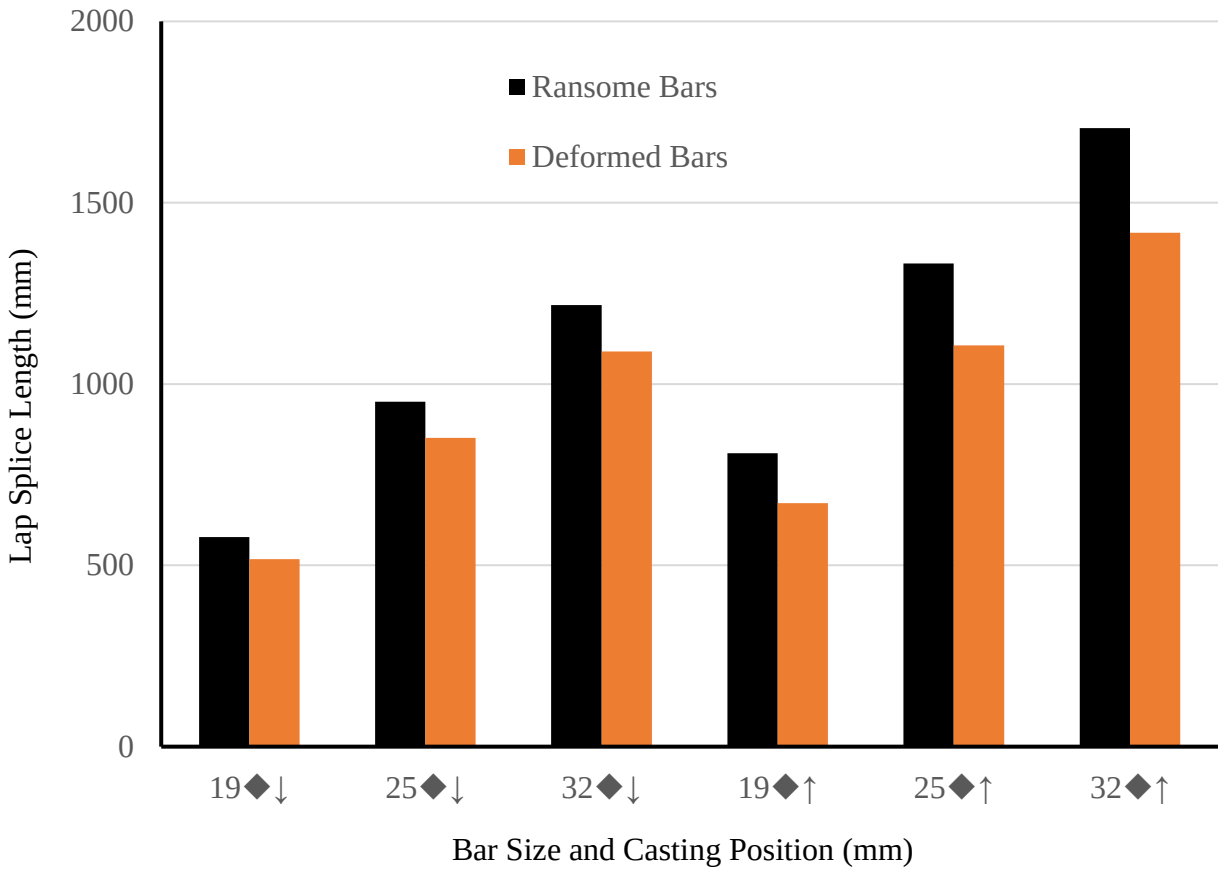

Figure 5.22: Comparison of Lap Splice Length Equation for Ransome and Deformed Bars

CHAPTER 6
CONCLUSIONS AND RECOMMENDATIONS

6.1 General

The current investigation was performed to establish splice and development length equations for plain and Ransome bars. Eight splice specimens reinforced with plain bars, two splice specimens reinforced with deformed bars, and twelve splice specimens reinforced with Ransome bars were tested monotonically under four-point loading to meet the objectives of the current investigation. Results of previous investigations (Hassan and Feldman, 2012; Sekulovic MacLean and Feldman, 2014; and Knight and Feldman, 2013) are also included in the current analysis to bolster the test database. The following sections summarize the major findings and provide recommendations for the future investigations.

6.2 Conclusions

The following conclusions are based on the results of the analysis of splice specimens reinforced with plain bars.

i. Crack patterns and load versus deflection behaviour of the specimens reinforced with plain bars are similar to those of specimens reinforced with modern deformed bars.

ii. Specimens with long lap splice lengths that were designed to fail in flexure exhibited a long yield plateau, which indicates that the ductility behaviour of specimens reinforced with plain bars is similar to that of modern deformed bars.

iii. Top cast factors of 0.4 and 0.64 capture the reduction of bond capacity of specimens reinforced with plain round bars and plain square bars, respectively, based upon the tensile resistance of the reinforcement at the maximum load level.

iv. An equation for the splice and development length of plain bars was proposed using a 5% fractile approach and is a function of bar size, equivalent bar diameter,

casting position, yield strength of the reinforcement, and concrete compressive strength. The bar size factor was chosen in a similar manner as that included in Clause 12.2.4 of CSA A23.3-14.

v. A comparison of the proposed development length of plain bars with that of deformed bars in accordance with CSA A23.3 suggests that the development length required for plain bars should be around fifty percent more than that for deformed bars for the bottom cast position. However, in the case of the top cast position, the required development length for square and round bars should be two and three times that for the deformed bars, respectively.

The following conclusions are based on the results of the analysis of the splice specimens reinforced with Ransome bars.

vi. There is no yield plateau in the stress versus strain diagram of Ransome bars due to the cold working used to produce Ransome bars. The ultimate strength of Ransome bars is greater than that of plain bars; however, the ultimate strain is reduced by 75% in comparison to plain bars due to the cold working used to fabricate the Ransome bars.

vii. Crack patterns and the load versus deflection behaviour of the specimens reinforced with Ransome bars are similar to those specimens reinforced with plain and deformed bars.

viii. A top cast factor of 0.67 captures the reduction of bond capacity for specimens reinforced with Ransome bars based upon the tensile resistance of the reinforcement at the maximum load level.

ix. An equation for the splice length of Ransome bars was proposed using a 5% fractile approach as a function of bar size, equivalent bar diameter, casting position, yield strength of the reinforcement, and concrete compressive strength.

The bar size factor was chosen in a similar manner as that included in Clause 12.2.4 of CSA A23.3-14.

x. A comparison of the proposed splice length of Ransome bars with that for modern deformed bars as provided in CSA A23.3-14 suggests that the bond capacity of Ransome bars closely matches with that of deformed bars when cast in the bottom position. However, the required splice length for Ransome bars is around 25% more than that for modern deformed bars when cast in the top position. Furthermore, the lap splice length provisions in BS 8110-1:1997 reasonably capture the bond behaviour of Ransome bars.

6.3 Recommendations for Future Work

The current investigation included proposed bond provisions for plain and Ransome bars in terms of splice length. Bond provisions for these historical bars could be updated with the addition of more specimens to database. The recommendations for future work is as follows:

i. Proposed bond provisions for plain and Ransome bars in the current investigation are based on a limited study of parameters. Other parameters such as concrete cover, spacing of bars, and transverse reinforcement can be included in future investigations.

ii. The pitch of the Ransome bars used in the current investigation was fixed for each bar size. However, a wide range of pitch is mentioned in the available literature and is expected to affect bond performance. Hence, further investigation is required to evaluate the effect of pitch on the bond strength between Ransome bars and concrete.

iii. Splices between a deformed bar and a Ransome bar or a plain bar may be required while retrofitting existing structures. Future investigation can include the study of the behaviour of splices between a deformed bar and a Ransome or a plain bar.

REFERENCES

Abrams, D.A. 1913. Tests of Bond Between Concrete and Steel. University of Illinois Bulletin No. 71, University of Illinois, Urbana, IL.

ACI. 1920. Standard Specifications No. 23: Standard Building Regulations for the Use of Reinforced Concrete. American Concrete Institute, Detroit, MI.

ACI Committee 318. 1951. Building Code Requirements for Reinforced Concrete (ACI 318-1951). American Concrete Institute, Farmington Hills, MI.

ACI Committee 318. 1963. Building Code Requirements for Reinforced Concrete (ACI 318-1963). American Concrete Institute, Farmington Hills, MI.

ACI Committee 318. 1989. Building Code Requirements for Reinforced Concrete (ACI 318-1951). American Concrete Institute, Farmington Hills, MI.

ACI Committee 318. 2014. Building Code Requirements for Structural Concrete (ACI 318-14) and Commentary (ACI 318R-14). American Concrete Institute, Farmington Hills, MI.

ACI Committee 408. 2003. Bond and Development of Straight Reinforcing Bars in Tension. American Concrete Institute, Farmington Hills, MI.

ASTM A 305. 1947. Minimum Requirements for the Deformations of Deformed Steel Bars for Concrete Reinforcement. ASTM International. West Conshohocken, PA, United States.

ASTM A 305. 1950. Minimum Requirements for the Deformations of Deformed Steel Bars

for Concrete Reinforcement. ASTM International. West Conshohocken, PA, United States.

ASTM A370. 2016. Standard Test Methods and Definitions for Mechanical Testing of Steel Products. ASTM International, West Conshohocken, PA.

BSI. 1997. BS 8110-1:1997 Structural Use of Concrete – Part 1: Code of Practice for Design and Construction. British Standards Institution, London, UK, 164 pp.

Cairns, J. 2004. Bond of Plain Round Bars. Unpublished Report, Heriot Watt University, See http://fibtg45.dii.unile.it/presentations.htm. Date Accessed October 2, 2017.

Chana, P.S. 1990. A Test Method to Establish Realistic Bond Stresses. Magazine of Concrete Research, **42** (121): 83-90.

Clark A.P 1946. Comparative Bond Efficiency of Deformed Concrete Reinforcing Bars. Journal of the American Concrete Institute, 18(4): 381- 400.

CSA. 2009. CAN/CSA G30.18-09 – Carbon Steel Bars for Concrete Reinforcement. Canadian Standards Association, Mississauga, ON, 32 pp.

CSA. 2013. CAN/CSA G40.20-13/G40.21-13 – General Requirements for Rolled or Welded Structural Quality Steel/Structural Quality Steel. Canadian Standards Association, Mississauga, ON, 120 pp.

CSA. 2014. CAN/CSA A23.1-14/A23.2-14 – Concrete Materials and Methods of Concrete Construction/Test Methods and Standard Practices for Concrete. Canadian Standards Association, Mississauga, ON, 690 pp.

CSA. 2014. CAN/CSA A23.3-14 – Design of Concrete Structures. Canadian Standards Association, Mississauga, ON, 297 pp.

Edwards A. D. and Yannopoulos P. J. 1979. Local Bond-Stress to Slip Relationships for Hot Rolled Deformed Bars and Mild Steel Plain Bars. ACI Structural Journal, **76** (3): 405-420.

Erlemann, G.G. 1999. Steel Reinforcing Bar Specifications in Old Structures. Concrete International, **21** (4): 49-50.

Feldman, L.R. 2006. Bond of Plain Steel Reinforcement in Concrete. PhD Thesis, University of Western Ontario, London, ON.

Feldman, L.R. and Bartlett, F.M. 2005. Bond Strength Variability in Pullout Specimens with Plain Reinforcement. ACI Structural Journal, **102**(6): 860-867.

Feldman, L.R. and Cairns J. 2017. Assessing Historical Provisions for Bond of Plain Bars. ACI Structural Journal, **114** (2): 463-473.

Hassan, M. 2011. Splice Tests of Plain Steel Bars in Concrete. MSc Thesis, University of Saskatchewan, Saskatoon, SK.

Hassan, M.N., and Feldman, L.R. 2012. Behaviour of Lap-Spliced Plain Steel Bars. ACI Structural Journal, **109** (2): 235-244.

Hognestad, E. 1951. A Study of Combined Bending and Axial Load in Reinforced Concrete Members. University of Illinois Engineering Experimental Station, Bulletin Series No. 399.

Hool, G., Johnson, N.C. 1918. The Concrete Engineer's Handbook. McGraw Hill, New York, NY, 885 pp.

Howell, D.A. and Higgins, C. 2007. Bond and Development of Deformed Square Reinforcing Bars. ACI Structural Journal, **104**(3): 333-343.

Hurd, M.K. 1996. Ernest L. Ransome – Concrete Designer, Contractor. Concrete International, **18** (5): 50-51.

Knight, M.R. and Feldman, L.R. 2013. Mechanical Properties and Bond Behaviour of Ransome Bars. 2013 Annual Conference of the Canadian Society for Civil Engineering, 10 pp.

Loov, R.E. 1991. Reinforced Concrete at the Turn of the Century. Concrete International, **13**(12): 67-73.

MacGregor, J.G. and Bartlett, F.M. 2000. Reinforced Concrete: Mechanisms and Design (Canadian Edition), Prentice-Hall Canada Inc., Scarborough, Ontario, Canada.

Meinheit D.F. and Felder, A.L.2014. Vintage Steel Reinforcement in Concrete Structures: A treatise on all forms of steel reinforcement employed in the design and construction of reinforced concrete of long ago, Concrete Reinforcing Steel Institute, Schaumburg, IL.

Mitutoyo. 2006. SJ-201 Surface Roughness Tester User's Manual Number 99MBB0796A. Mitutoyo Corporation, Kanagawa, Japan, 190 pp.

Orangun, C.O., Jirsa, J.O., and Breen, J.E. 1977. A Reevaluation of Test Data on Development Length and Splices. Journal of the American Concrete Institute, **74**(3): 114-122.

Ransome, E.L. 1884. United States Patent Office Letters Patent No. 516113. The National Lithographing Company, Washington, DC.

Rao, N.R.M., Lohrmann, M., and Tall, L. 1966. Effects of Strain Rate on the Yield Stress of Structural Steels. ASTM Journal of Materials, **1**(1): 241-262.

Rehm, G. 1961. Über die Grundlagen des Verbundes zwischen Stahl und Beton. Deutscher Ausschuss für Stahlbeton, 138, 59 pp.

Sekulovic MacLean M. 2013. The Effects of Casting Position and Bar Shape on the Lap Length of Plain Steel Bars in Concrete. MSc Thesis, University of Saskatchewan, Saskatoon, SK.

Sekulovic MacLean, M. and Feldman, L.R. 2014. Effects of Casting Position and Bar Shape on Bond of Plain Bars. ACI Structural Journal, **111** (2): 323-330.

Shuman, J.J. 1907. Tests of Cold Twisted Steel Rods for Concrete Reinforcement. Engineering News Record, **58**: 59-60.

Appendix A: Concrete Companion Specimens Associated with Splice Specimens Reinforced with Plain Bars

Five concrete companion cylinders were tested on same day as each associated splice specimens, as explained in Section 3.7. Three of them were tested to measure the concrete compressive strength, whereas the remaining two were tested to measure the tensile strength. Table A.1 presents the compressive strength and tensile strength of cylinders tested in the current experimental program. Figures A.1 to A.7 show the stress strain relationships for the cylinders used to measure compressive strength of concrete. These figures also show the average fit curve equation obtained by fitting a polynomial regression line with zero intercept to the average stress versus strain curve. Stress strain relationships for remaining concrete companion cylinders are provided elsewhere (Hassan, 2011 and Sekulovic MacLean, 2013).

Table A.1: Companion Concrete Cylinder Properties

Specimen ID	Concrete Cylinder ID[a]	Age at Test Date (days)	Compressive Strength f'_c(MPa)	Tensile Strength f_r(MPa)
19■-410↓	C-1-1	44	27.2	
	C-1-2		25.5	
	C-1-3		21.4	
	C-1-4			2.37
	C-1-5			2.35
Coefficient of Variation			12.1%	0.60%
19■-510↓	C-1-6	50	19.8	
	C-1-7		24.6	
	C-1-8		24.1	
	C-1-9			2.77
	C-1-10			2.30
Coefficient of Variation			11.6%	13.1%
19■-610↓	C-1-11	49	22.1	
	C-1-12		23.0	
	C-1-13		23.0	
	C-1-14			2.89
	C-1-15			2.25
Coefficient of Variation			2.29%	17.6%
19●-1210↓	C-1-16	45	15.8	
	C-1-17		22.3	
	C-1-18		22.7	
	C-1-19			2.35
	C-1-20			2.63
Coefficient of Variation			19.1%	7.95%
19■-410↑	C-2-1	30	25.8	
	C-2-2		18.4	
	C-2-3		24.6	
	C-2-4			2.05
	C-2-5			2.42
Coefficient of Variation			17.3%	11.7%
19■-510↑	C-2-6	28	22.0	
	C-2-7		20.7	
	C-2-8		26.4	
	C-2-9			2.44
	C-2-10			2.36
Coefficient of Variation			13.0%	2.36%

Table A.1 Cont'd: Companion Concrete Cylinder Properties

Specimen ID	Concrete Cylinder ID[a]	Age at Test Date (days)	Compressive Strength f'_c(MPa)	Tensile Strength f_r (MPa)
19■-610↑	C-2-11	33	24.2	
	C-2-12		26.8	
	C-2-13		22.7	
	C-2-14			2.44
	C-2-15			n/a[b]
Coefficient of Variation			8.4%	n/a
19●-1010↓	C-2-16	35	23.3	
	C-2-17		22.8	
	C-2-18		25.3	
	C-2-19			2.43
	C-2-20			2.11
Coefficient of Variation			5.56%	9.97%

[a] "C" in the concrete cylinder ID refers to concrete, the first number refers to concrete batch number and final number following the second hyphen refers to cylinder serial number.

[b] No data available due to errors in testing

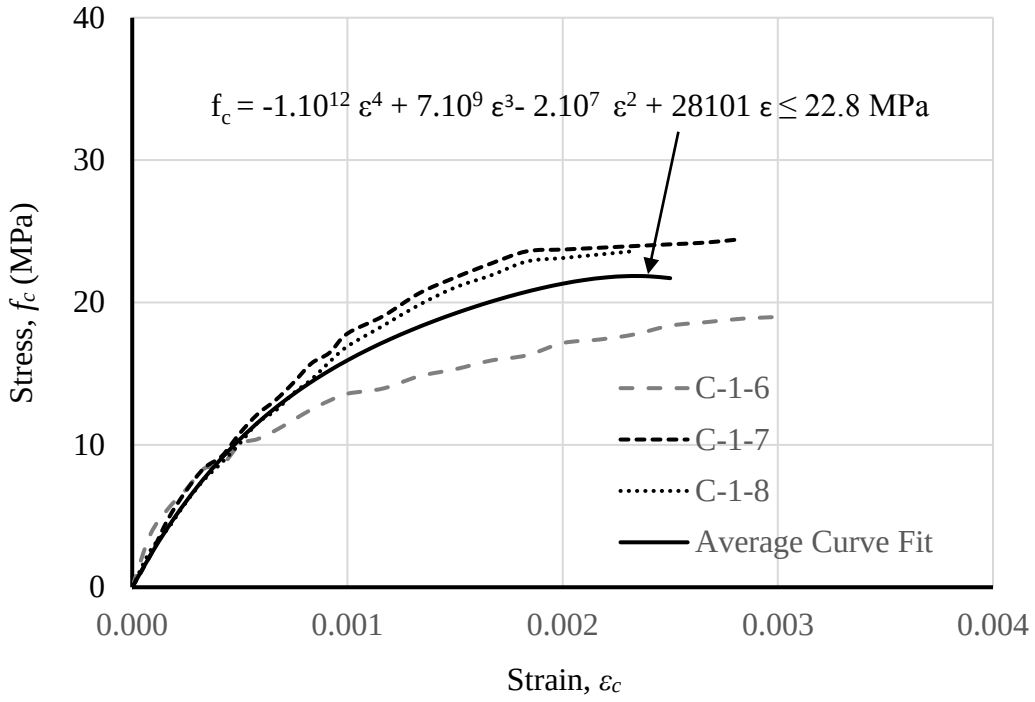

Figure A.1: Stress-Strain Relationship of Concrete Companion Specimen Associated with Specimen 19■-510↓

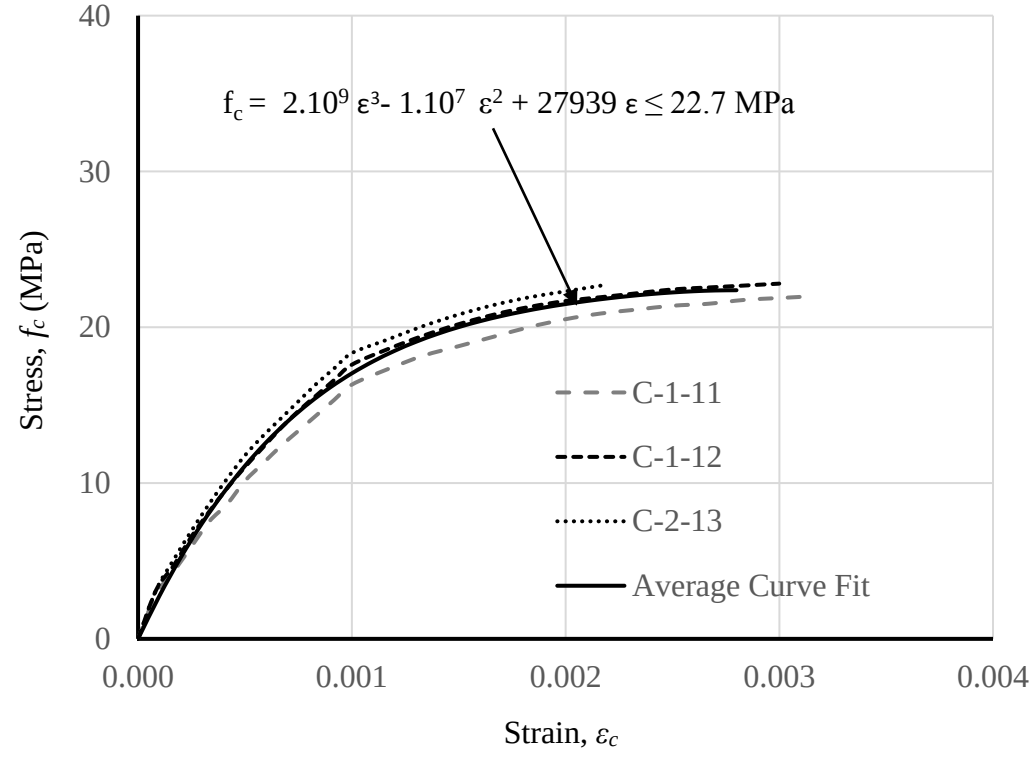

Figure A.2: Stress-Strain relationship of Concrete Companion Specimen associated with Specimen 19■-610↓

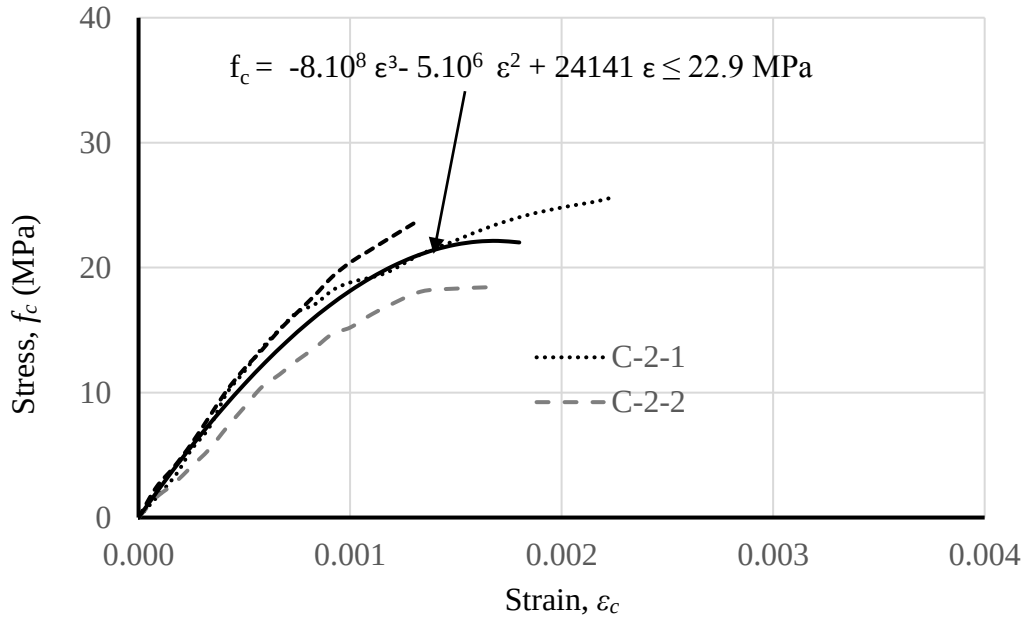

Figure A.3: Stress-Strain Relationship of Concrete Companion Specimen Associated with Specimen 19■-410↑

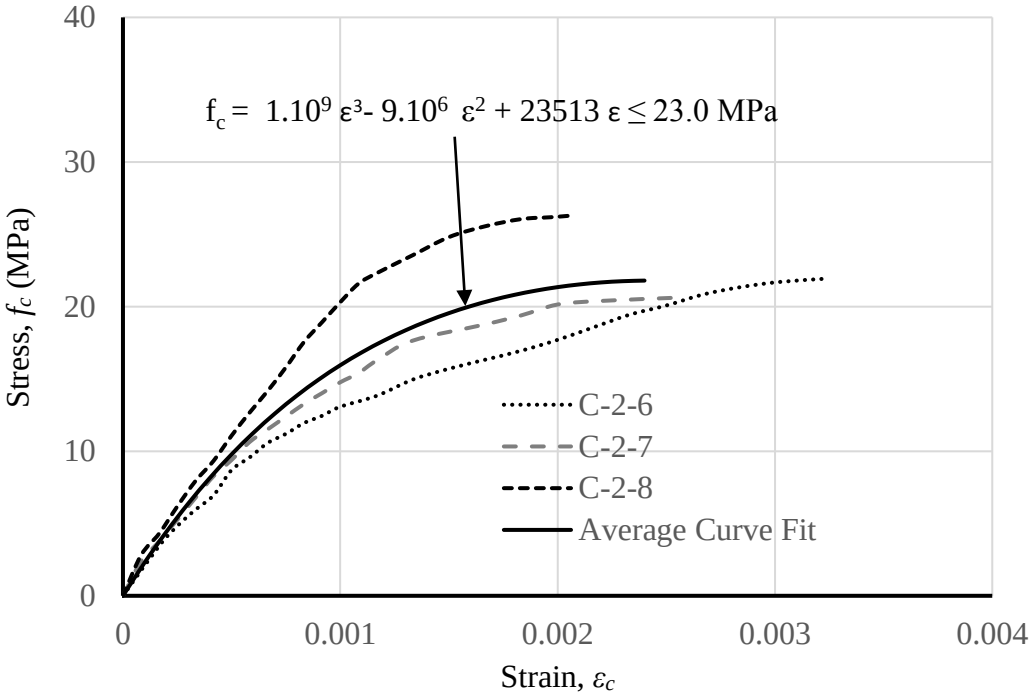

Figure A.4: Stress-Strain Relationship of Concrete Companion Specimen Associated with Specimen 19■-510↑

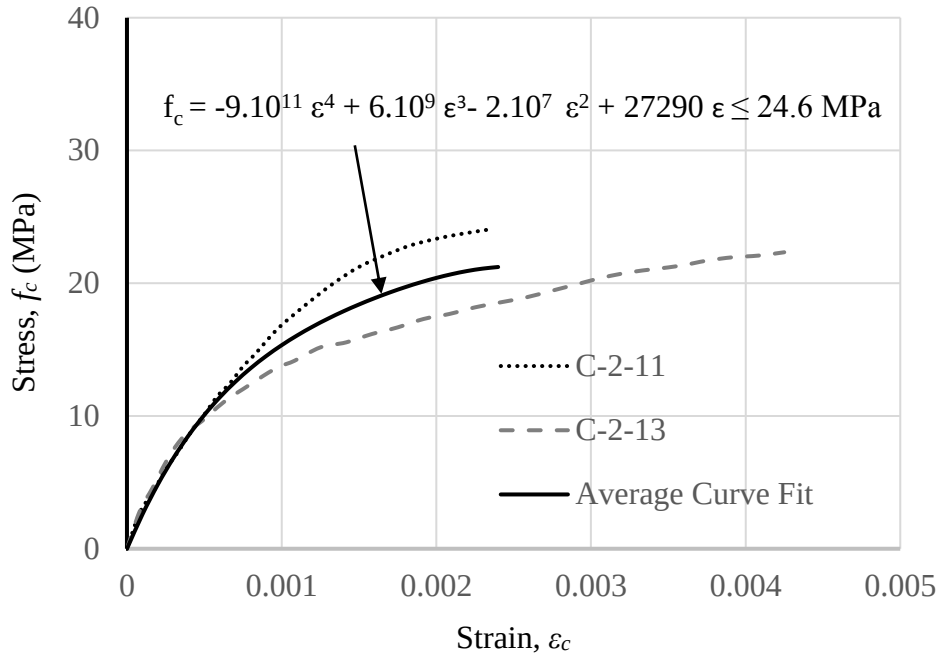

Figure A.5: Stress-Strain Relationship of Concrete Companion Specimen Associated with Specimen 19■-610↑

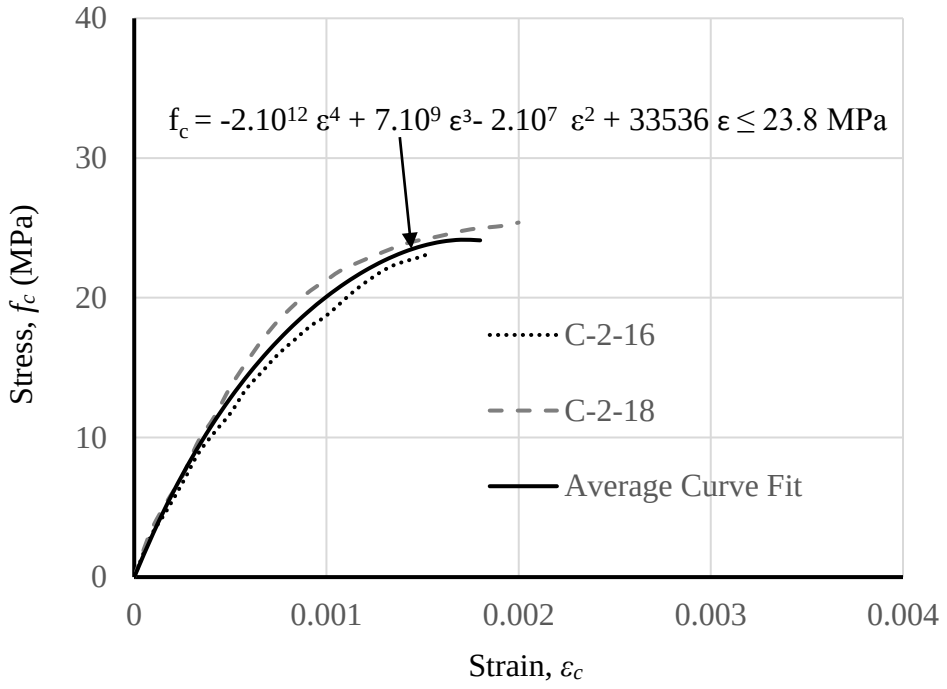

Figure A.6: Stress-Strain Relationship of Concrete Companion Specimen Associated with Specimen 19●-1010↓

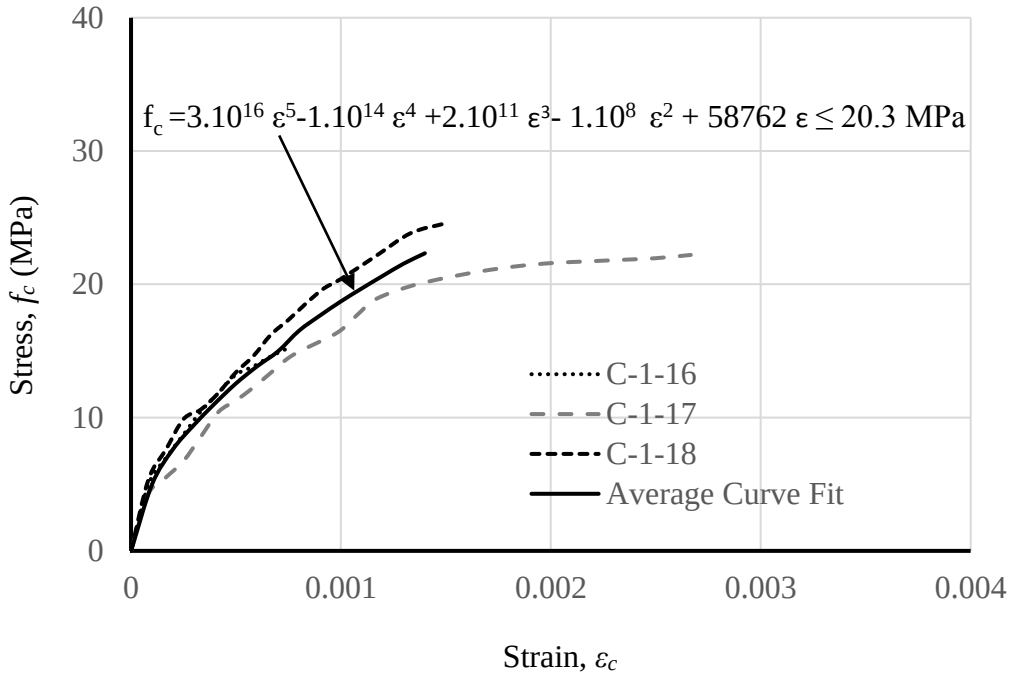

Figure A.7: Stress-Strain Relationship of Concrete Companion Specimen Associated with Specimen 19●-1210↓

Appendix B: Properties of the Plain Longitudinal Steel Bars

Six tensile specimens were tested for each heat batch and each size of the reinforcement, as explained in Section 3.7.3. Three of them were intact bar lengths and the remaining three of them were machined coupon, as explained in Section 3.7.3. Table B.1 shows the dynamic yield strength, static yield strength, and modulus of elasticity for each tensile specimen tested in the current investigation. Figures B.1 and B.2 present the stress versus strain relationships obtained from the tensile test. Stress versus strain relationships of the remaining specimens are provided elsewhere (Hassan, 2011 and Sekulovic MacLean, 2013).

Table B.1: Properties of Plain Longitudinal Reinforcement

Associated Splice Specimen ID	Steel Specimen ID[a]	Dynamic Yield Strength f_{yd}(MPa)	Static Yield Strength f_{ys}(MPa)	Modulus of Elasticity, E_s (GPa)
19■-410↓, 19■-510↓, 19■-610↓, 19■-410↑, 19■-510↑, and 19■-610↑	S19■I-1-1	342	314	210
	S19■I-1-2	345	308[c]	122
	S19■I-1-3	346	322	180
	S19■C-1-1	357	321	n/a[b]
	S19■C-1-2	352	327	n/a[b]
	S19■C-1-3	357	328	138
Coefficient of Variation		1.84%	2.41%	24.6%
19●-1010↓ and 19●-1010↓	S19●I-1-1	335	311	157
	S19●I-1-2	354	324	269
	S19●I-1-3	353	319[c]	168
	S19●C-1-1	345	308[c]	253
	S19●C-1-2	340	316	131
	S19●C-1-3	336	311	n/a[b]
Coefficient of Variation		2.41%	1.90%	31.4%

[a] The first letter in the steel specimen ID, S, refers to steel, the first number refers to the size of the longitudinal reinforcing bars, and solid circle (●) or square (■) refers to shape of longitudinal reinforcement. The letter I represents that tensile specimens were tested in intact bar lengths, whereas the letter C represents that machined coupons were tested. The second number represents the heat batch number, whereas the third number represents the replicate number within the test series.

[b] Strain response from the laser extensometer has a lot of noise

[c] Strain rate slightly exceeded upper bound limit as discussed in Section 4.2.2

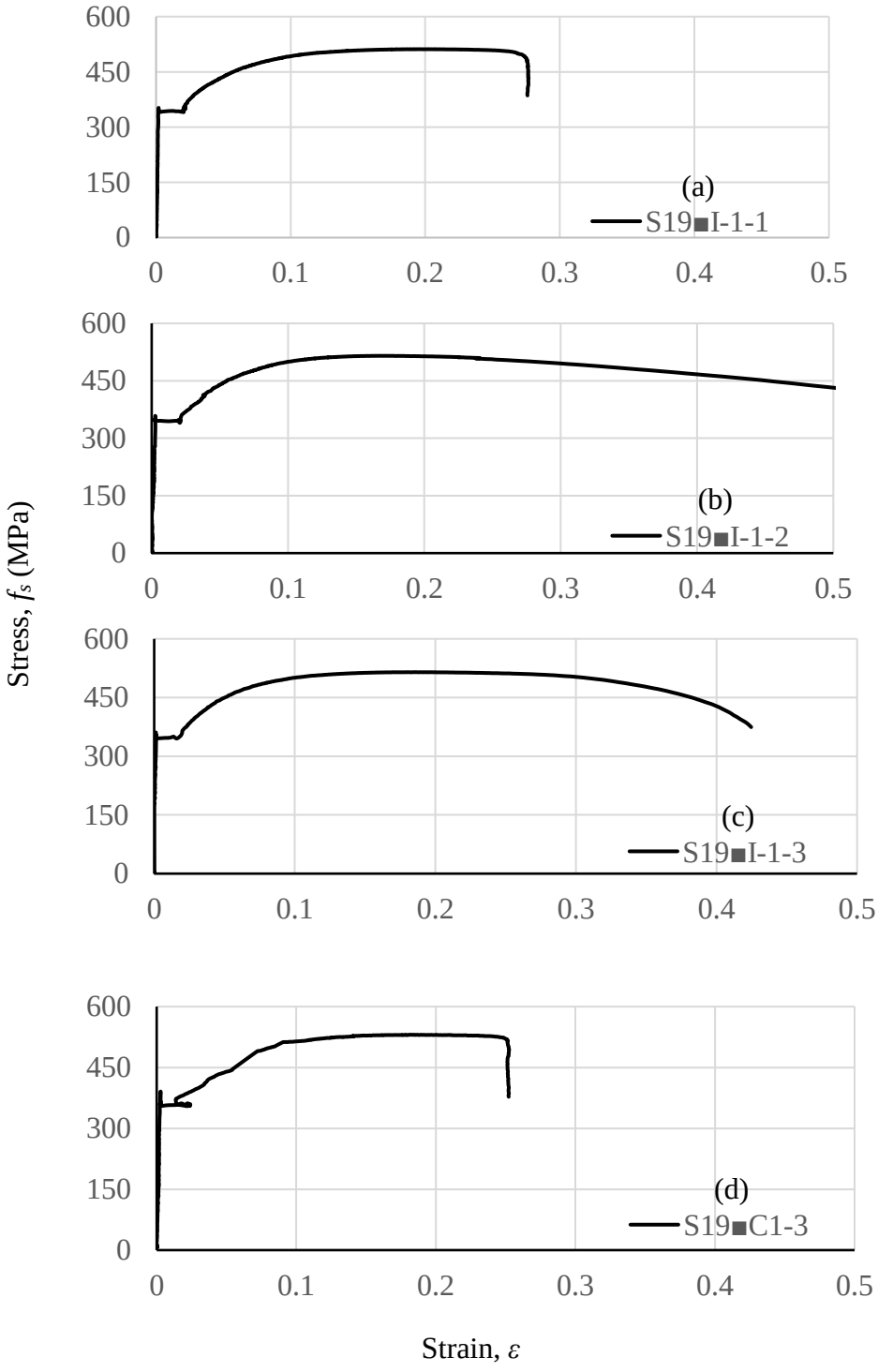

Figure B.1: Stress Versus Strain for 19mm Plain Round Bar: (a) S19■I-1-1, (b) S19■I-1-2, (c) S19■I-1-3, and (d) S19■C-1-3

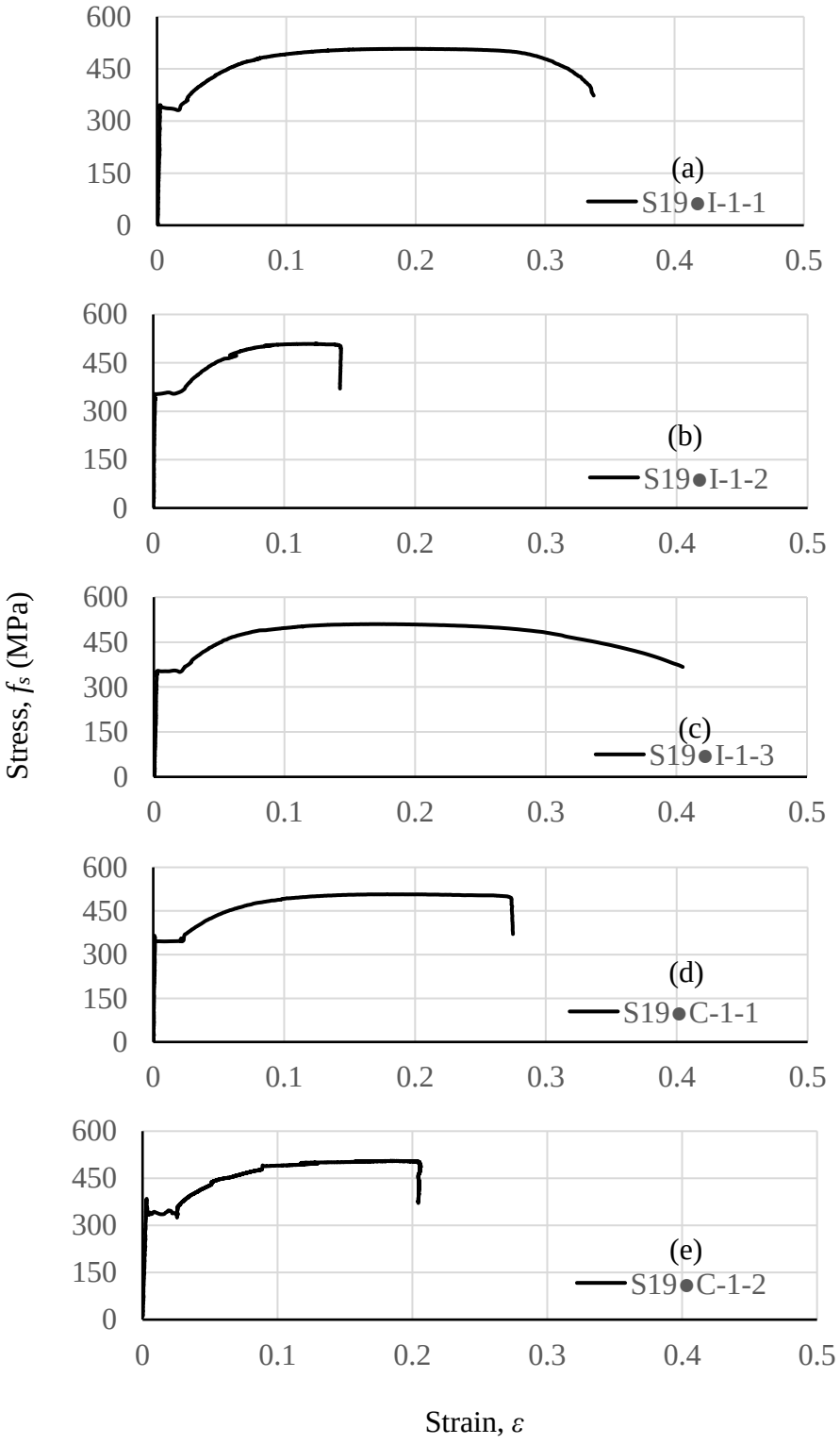

Figure B.2: Stress Versus Strain for 19mm Plain Round Bar: (a) S19●I-1-1, (b) S19●I-1-2, (c) S19●I-1-3, (d) S19●C-1-1, and (e) S19●C-1-2

Appendix C: Observed Crack Pattern of the Splice Specimens Reinforced with Plain Bars

Cracks were marked as tests of the splice specimens progressed. Figures C.1 to C.6 show the observed crack patterns of the splice specimens reinforced with plain bars during testing. Crack patterns are shown from the lowest to highest load levels in which new cracks were evident. Crack patterns of the remaining specimens are provided elsewhere (Hassan, 2011 and Sekulovic MacLean, 2013).

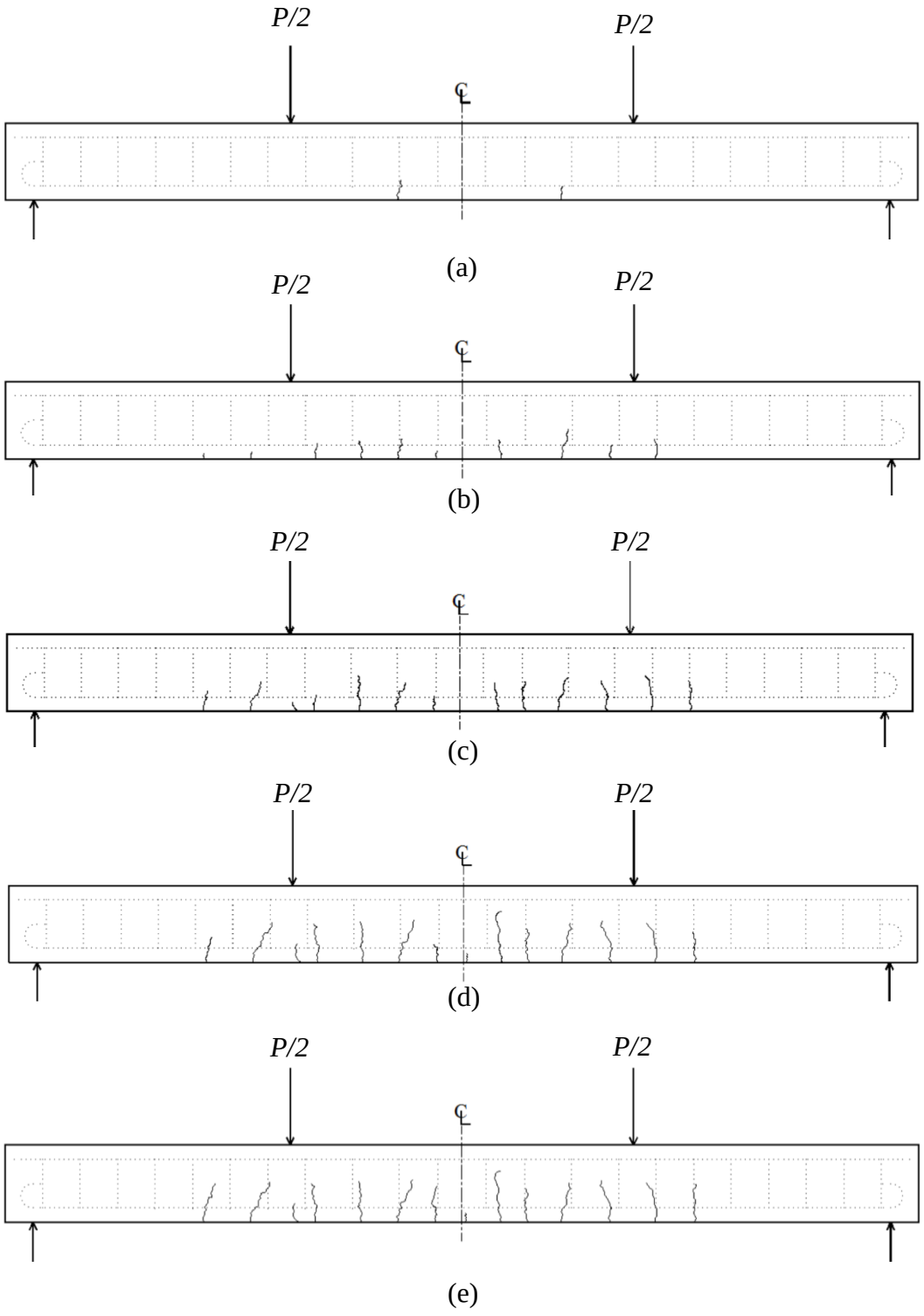

Figure C.1: Crack Pattern for Specimen 19■-510↓ at the Following Load Levels: (a) P=0.3 P_{max}, (b) P=0.5 P_{max}, (c) P=0.7 P_{max}, (d) P=0.9 P_{max}, and (d) P=P_{max}

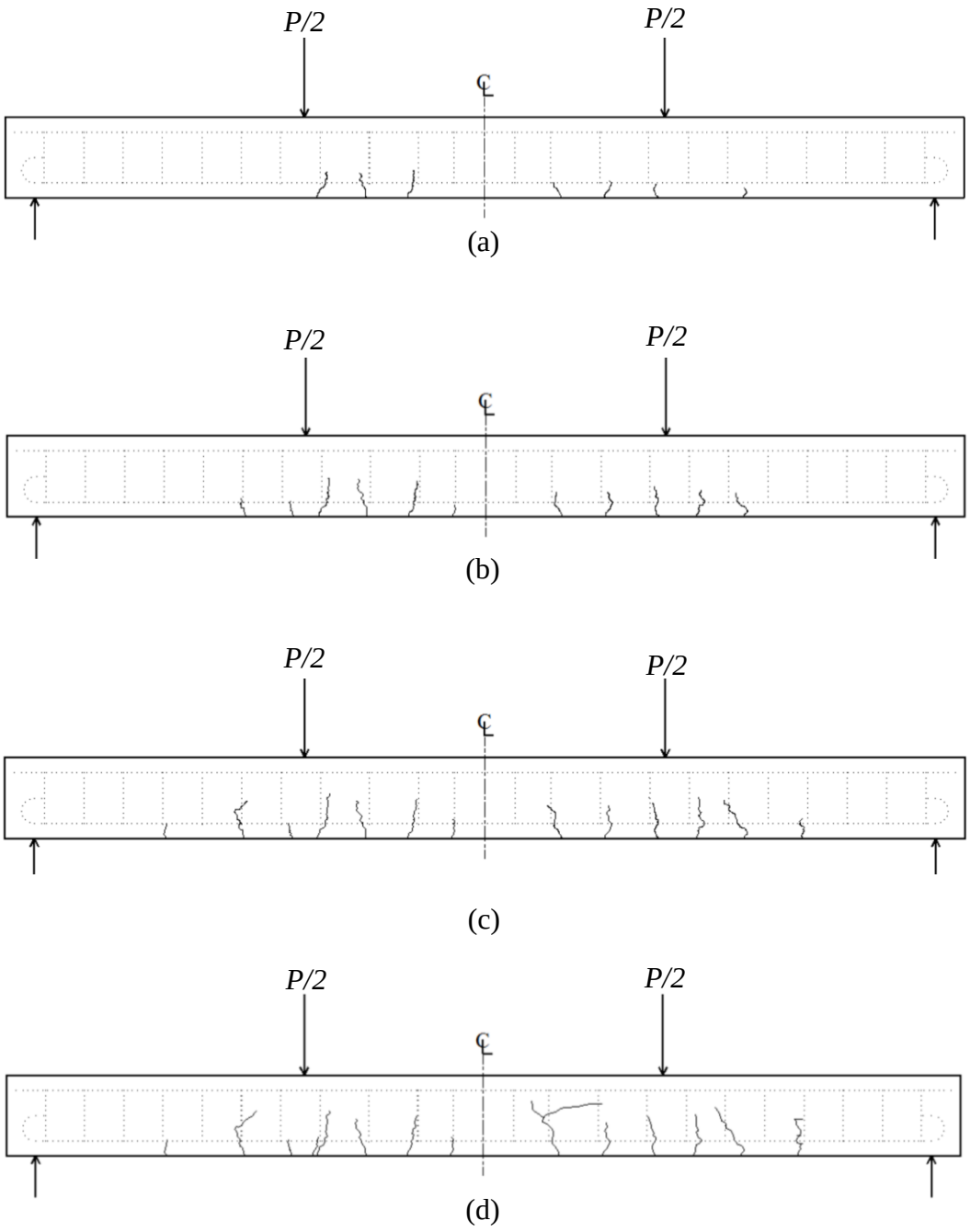

Figure C.2: Crack Pattern for Specimen 19■-610↓ at the Following Load Levels: (a) P=0.4 P_{max}, (b) P=0.6 P_{max}, (c) P=0.8 P_{max}, and (d) P=P_{max}

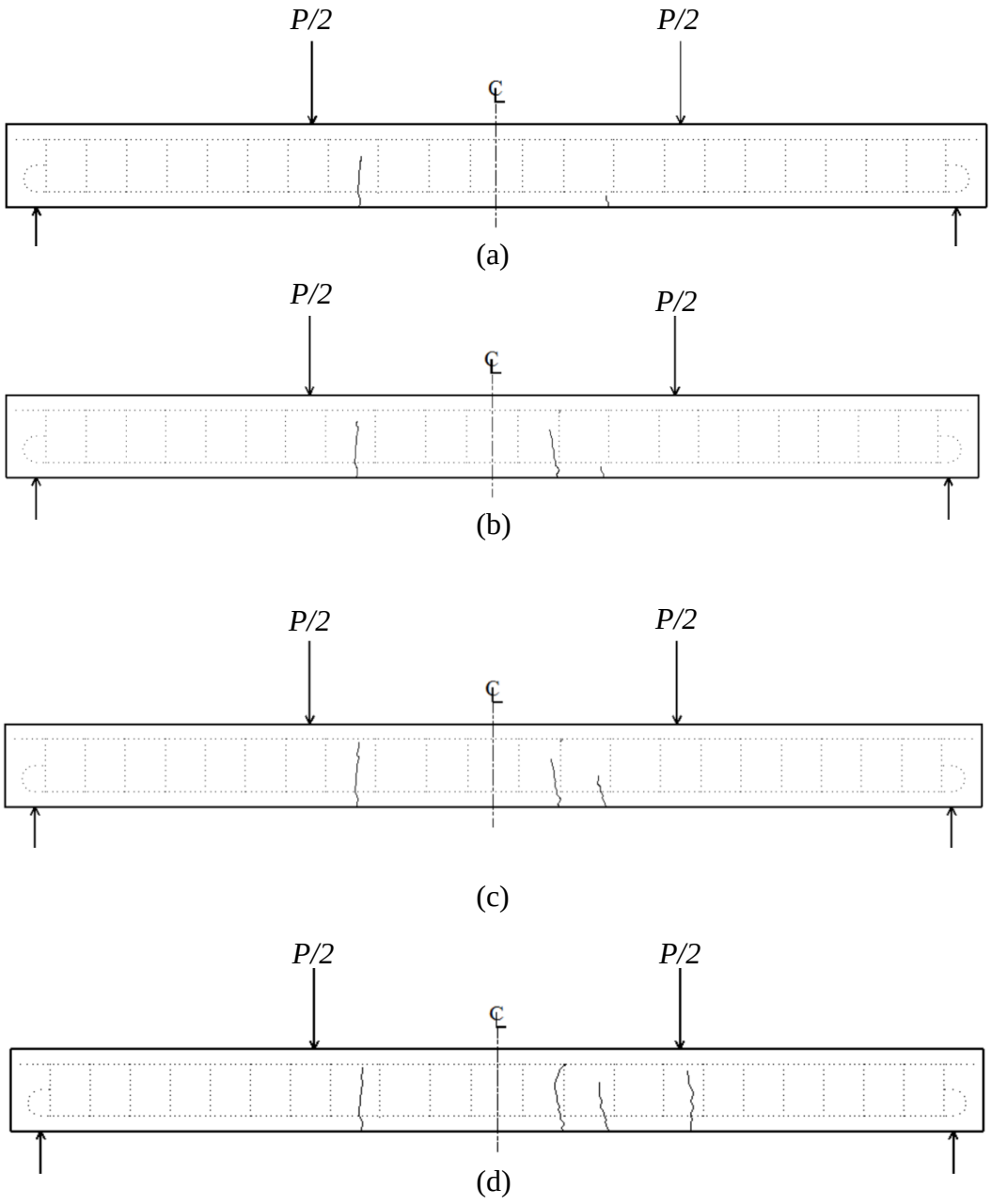

Figure C.3: Crack Pattern for Specimen 19■-510↑ at the Following Load Levels: (a) P=0.5 P_{max}, (b) P=0.7 P_{max}, (c) P=0.8 P_{max}, and (d) P=P_{max}

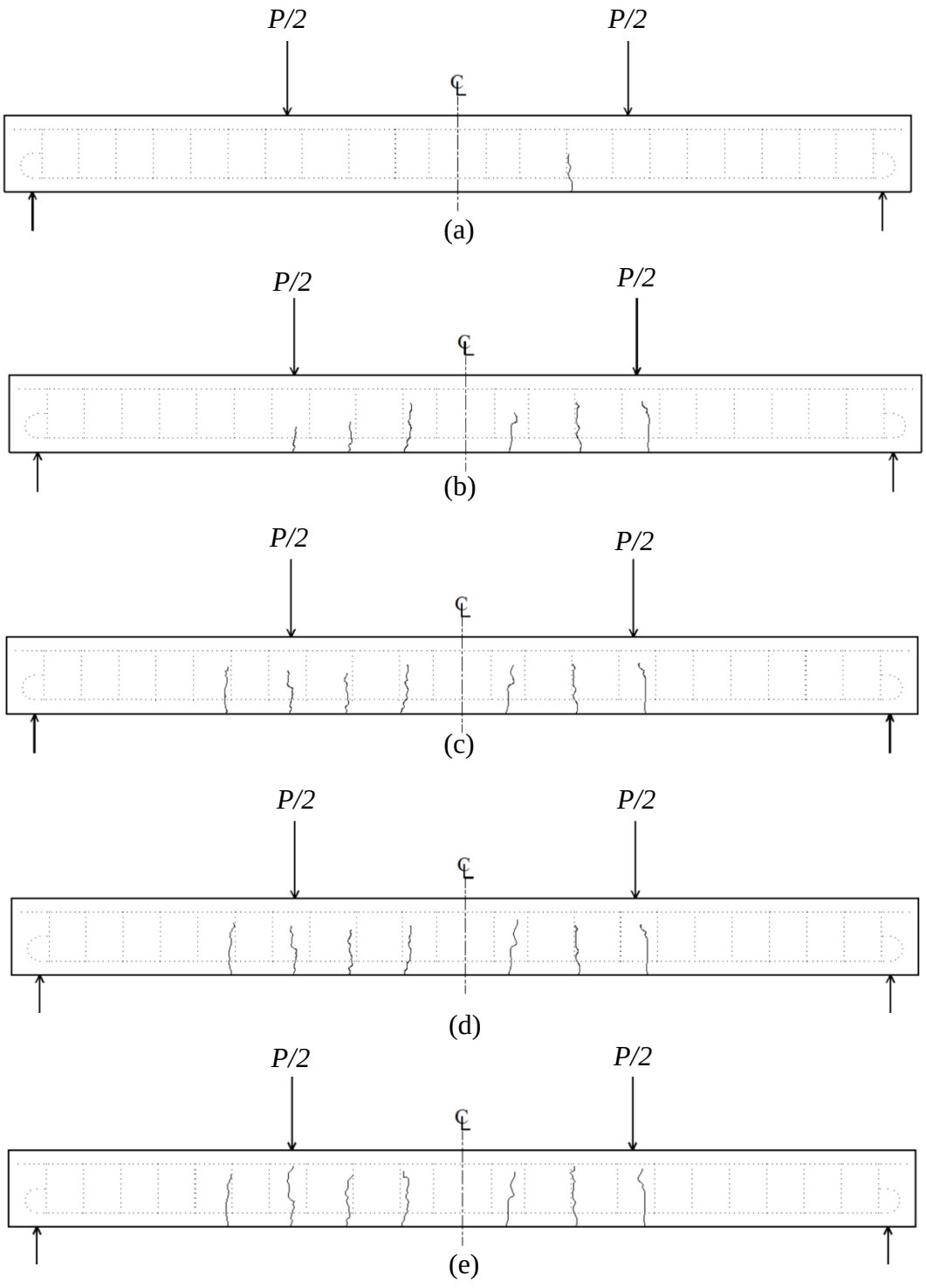

Figure C.4: Crack Pattern for Specimen 19■-610↑ at the Following Load Levels: (a) P=0.3 P_{max}, (b) P=0.5 P_{max}, (c) P=0.7 P_{max}, (d) P=0.9 P_{max}, and (e) P=P_{max}

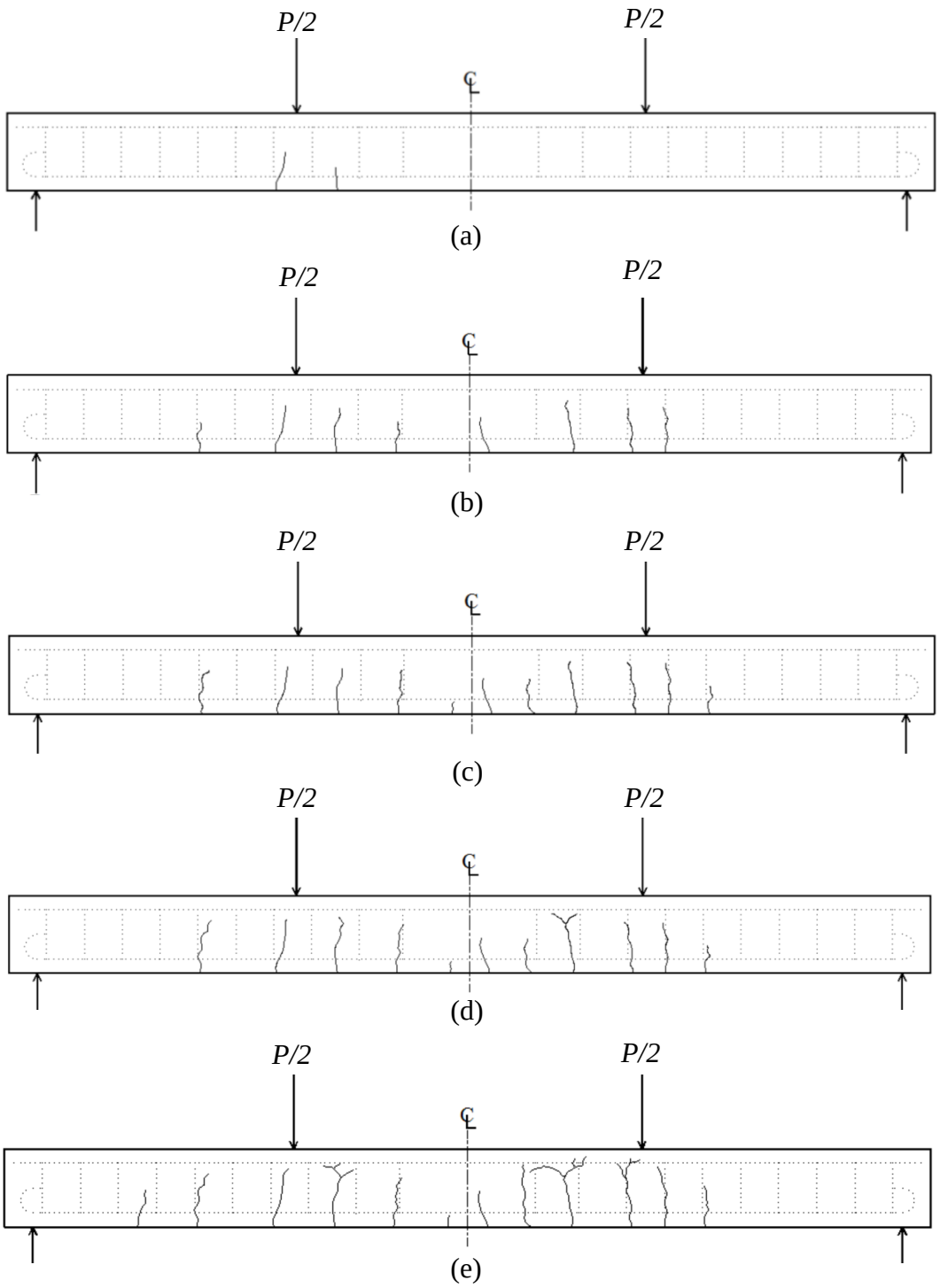

Figure C.5: Crack Pattern for Specimen 19●-1010↓ at the Following Load Levels: (a) P=0.4 P_{max}, (b) P=0.6 P_{max}, (c) P=0.8 P_{max}, (d) P=0.9 P_{max}, and (d) P=P_{max}

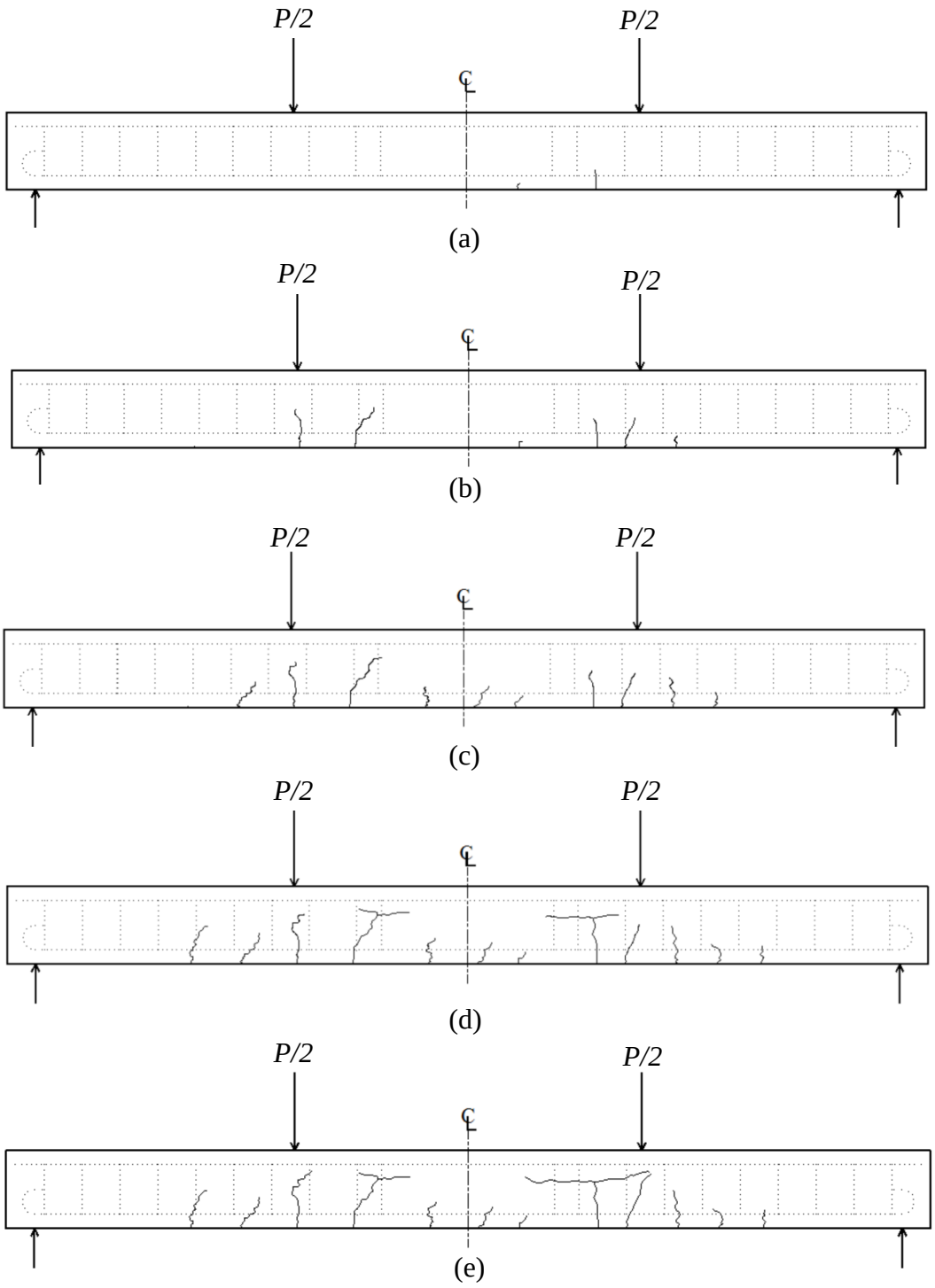

Figure C.6: Crack Pattern for Specimen 19●-1210↓: (a) P=0.3 P_{max}, (b) P=0.5 P_{max}, (c) P=0.7 P_{max}, (d) P=0.9 P_{max}, and (e) P=P_{max}

Appendix D: Observed End-Slip of the Longitudinal Reinforcement for Specimens Reinforced with Plain Bars

The concrete surrounding the spliced longitudinal reinforcement was removed after testing to observe whether there was a slip of the longitudinal reinforcement or not, as explained in Section 4.3.2. Figures D.1 to D.5 show the observed end slip of the reinforcement in the specimens. Observed end slip of the reinforcement of the remaining specimens are provided elsewhere (Hassan, 2011 and Sekulovic MacLean, 2013).

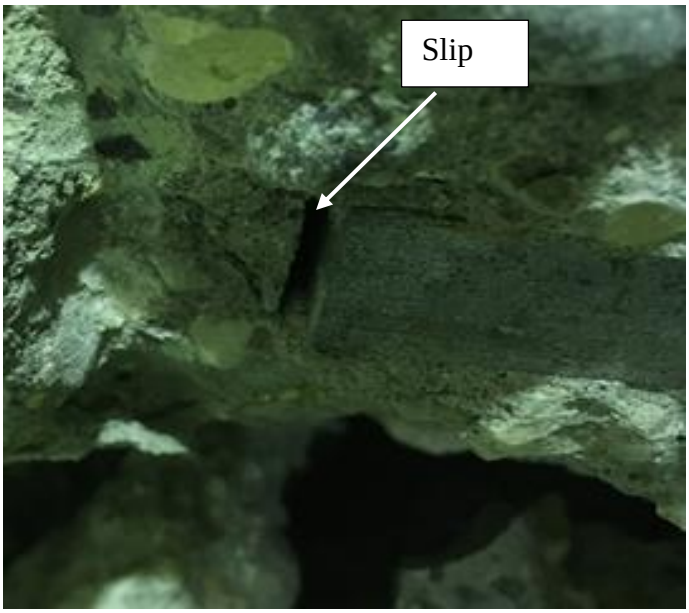

Figure D.1: End Slip of Longitudinal Reinforcement Following Concrete Removal for Specimen 19■-510↓

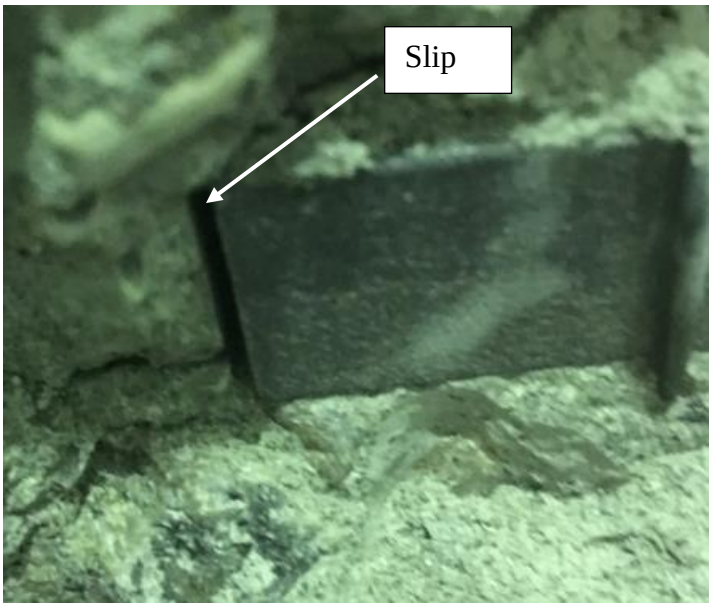

Figure D.2: End Slip of Longitudinal Reinforcement Following Concrete Removal for Specimen 19■-410↑

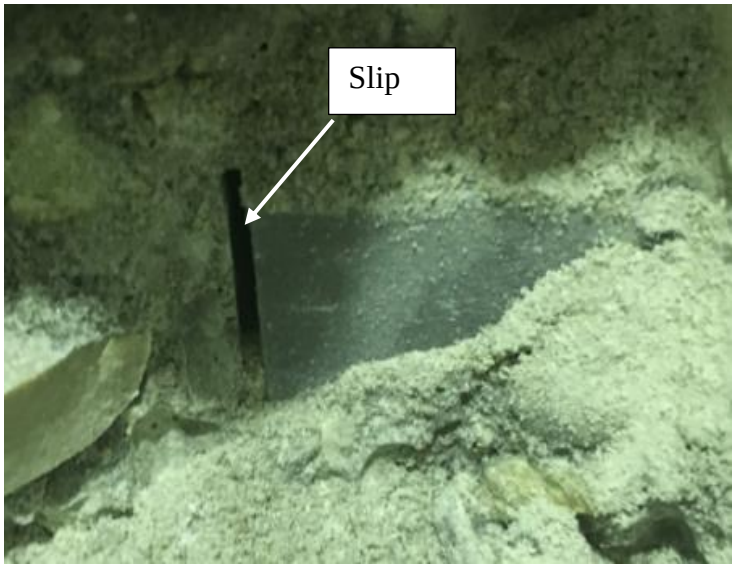

Figure D.3: End Slip of Longitudinal Reinforcement Following Concrete Removal for Specimen 19■-510↑

Figure D.4: End Slip of Longitudinal Reinforcement Following Concrete Removal for Specimen 19●-1010↓

Figure 4D.5: End Slip of Longitudinal Reinforcement Following Concrete Removal for Specimen 19●-1210↓

Appendix E: Normalized Applied Load Versus Mid Span Deflection for the Splice Specimens Reinforced with Plain Bars

Figures E.1 to E.5 show the normalized applied load versus midspan deflection for the splice specimens reinforced with plain bars. The theoretically predicted deflection is shown by a dashed line, whereas actual recorded deflection is shown by a solid line. Normalized applied load versus mid span deflection of remaining specimens is provided elsewhere in (Hassan, 2011 and Sekulovic MacLean, 2013).

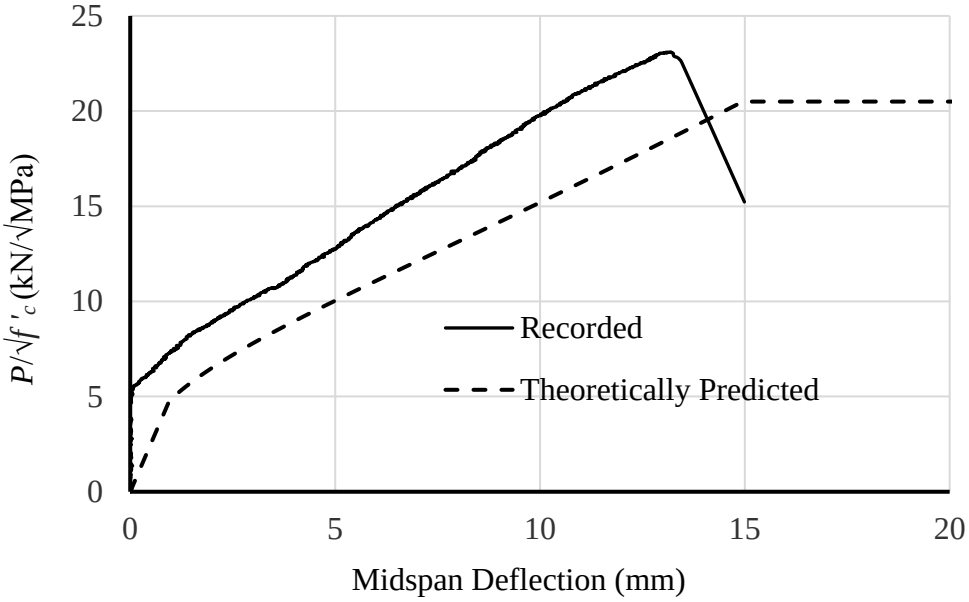

Figure E.1: Normalized Applied Load Versus Midspan Deflection for Specimen 19■-510↓

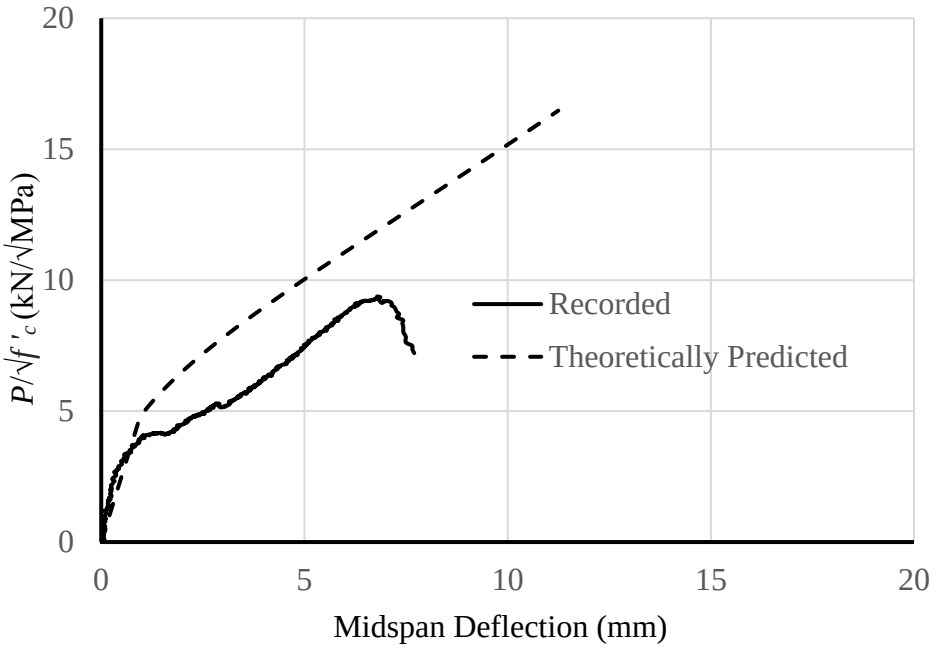

Figure E.2: Normalized Applied Load Versus Midspan Deflection for Specimen 19■-510↑

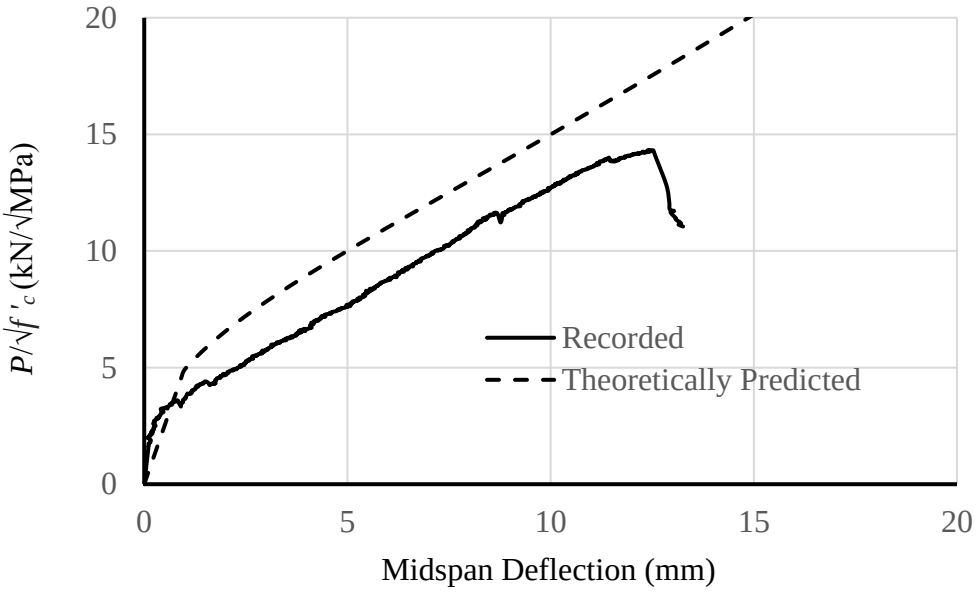

Figure E.3: Normalized Applied Load Versus Midspan Deflection for Specimen 19■-610↑

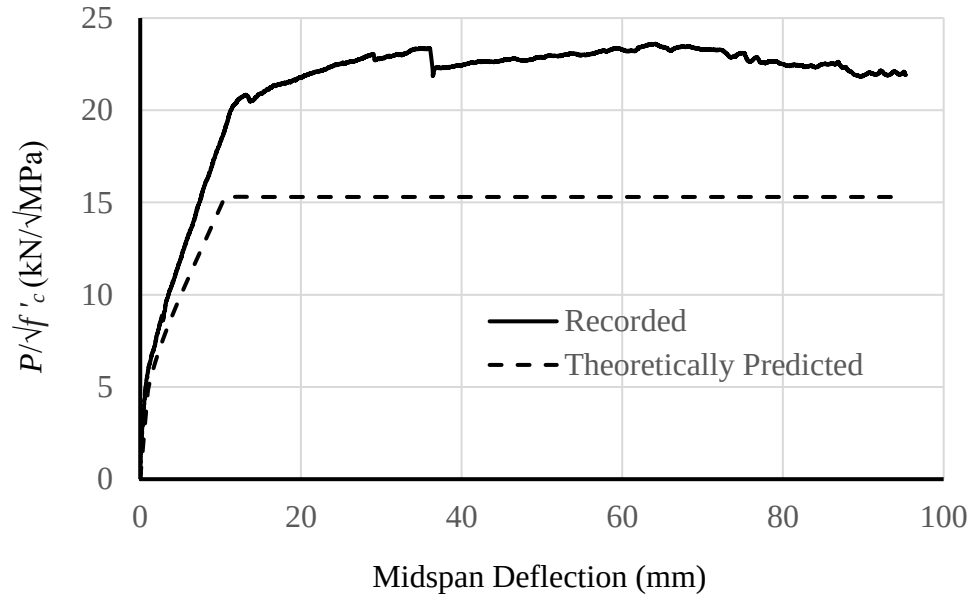

Figure E.4: Normalized Applied Load Versus Midspan Deflection for Specimen 19●-1010↓

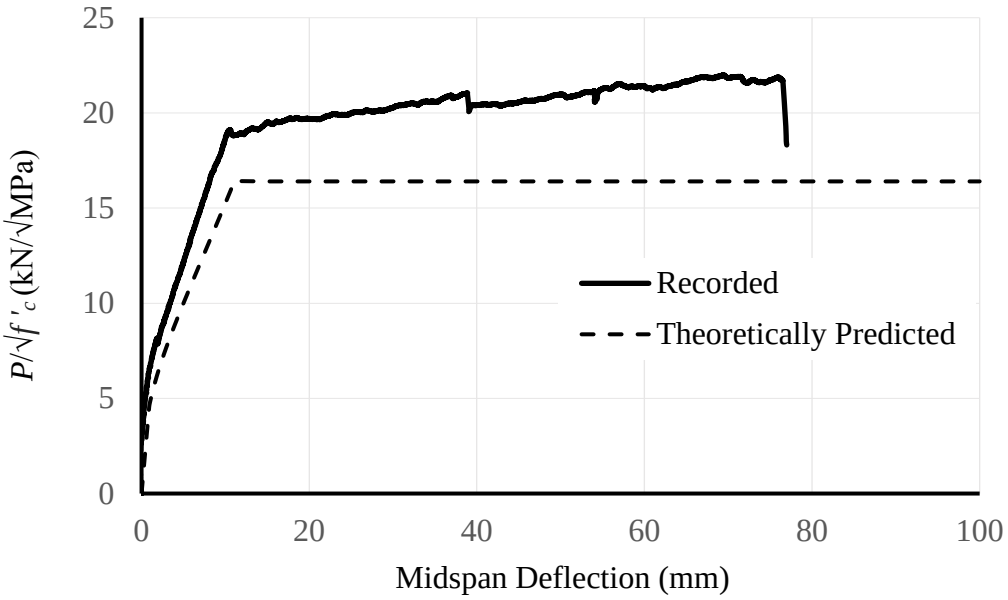

Figure E.5: Normalized Applied Load Versus Midspan Deflection for Specimen 19●-1210↓

Appendix F: Deflection Profiles of Splice Specimens Reinforced with Plain Bars

Figures F.1 to F.6 show the deflection profiles of splice specimens reinforced with plain bars at different load levels. Markers shown in the figures indicate the recorded deflection obtained from LVDTs that were located along the length of the specimens. The dashed curves represent the theoretically calculated deflection. The deflection profiles of the remaining splice specimens are provided elsewhere (Hassan, 2011 and Sekulovic MacLean, 2013).

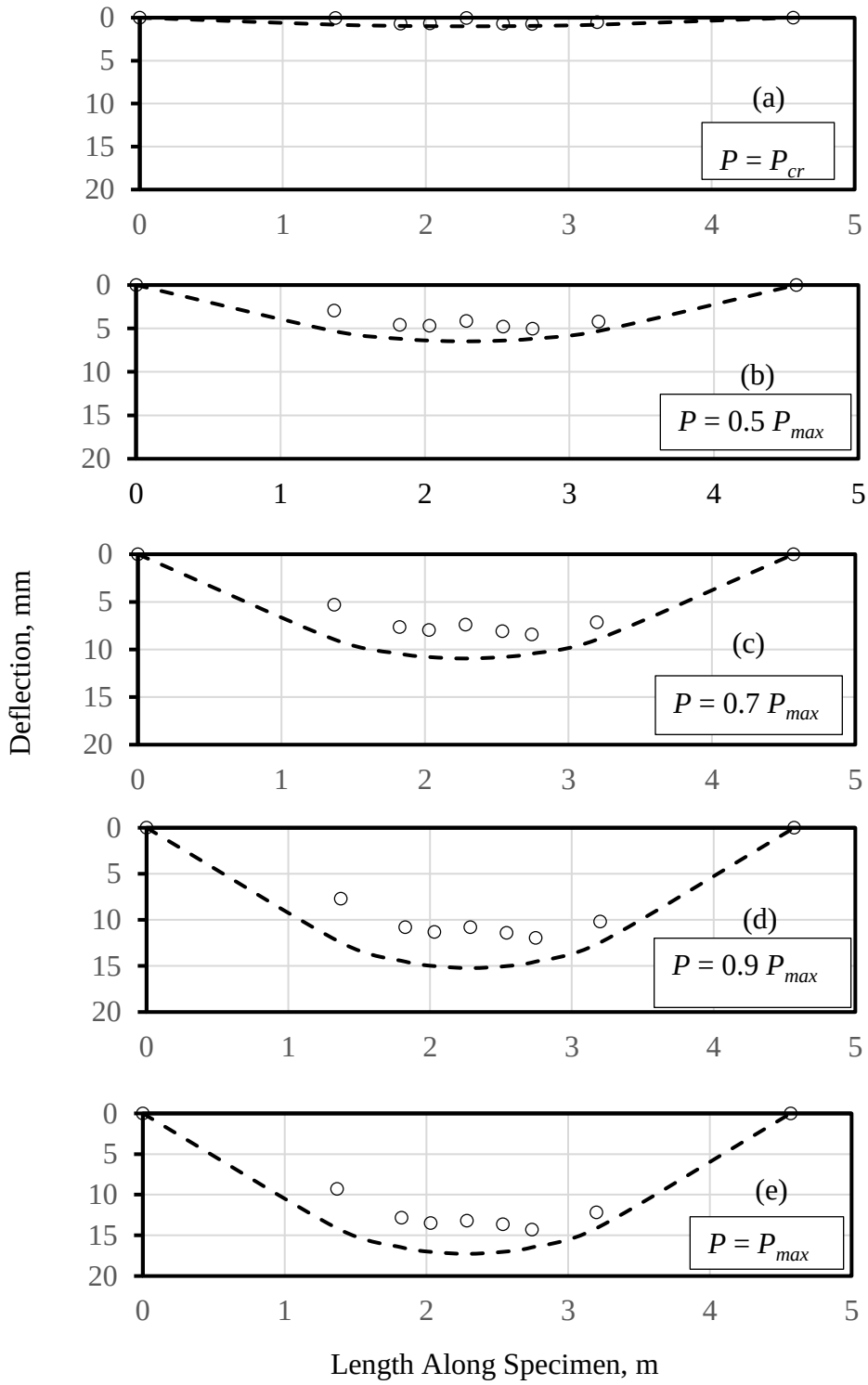

Figure F.1: Deflection Profile at Different Load Levels for Specimen 19■-510↓: (a) $P=P_{cr}$, (b) $P= 0.5\ P_{max}$, (c) $P= 0.7\ P_{max}$, (d) $P= 0.9\ P_{max}$, and (e) $P= P_{max}$

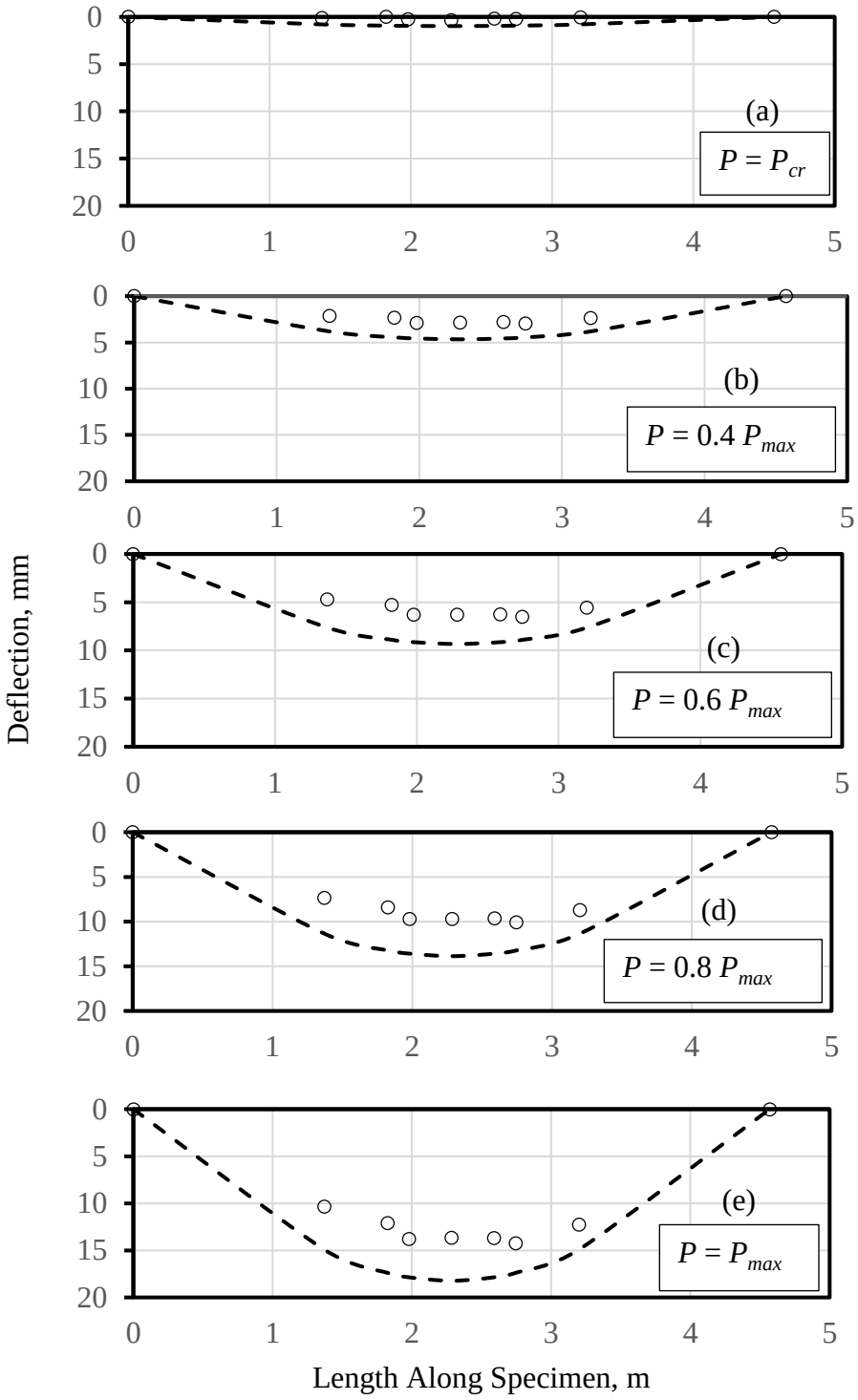

Figure F.2: Deflection Profile at Different Load Levels for Specimen 19■-610↓: (a) $P=P_{cr}$, (b) $P= 0.4\ P_{max}$, (c) $P= 0.6\ P_{max}$, (d) $P= 0.8\ P_{max}$, and (e) $P= P_{max}$

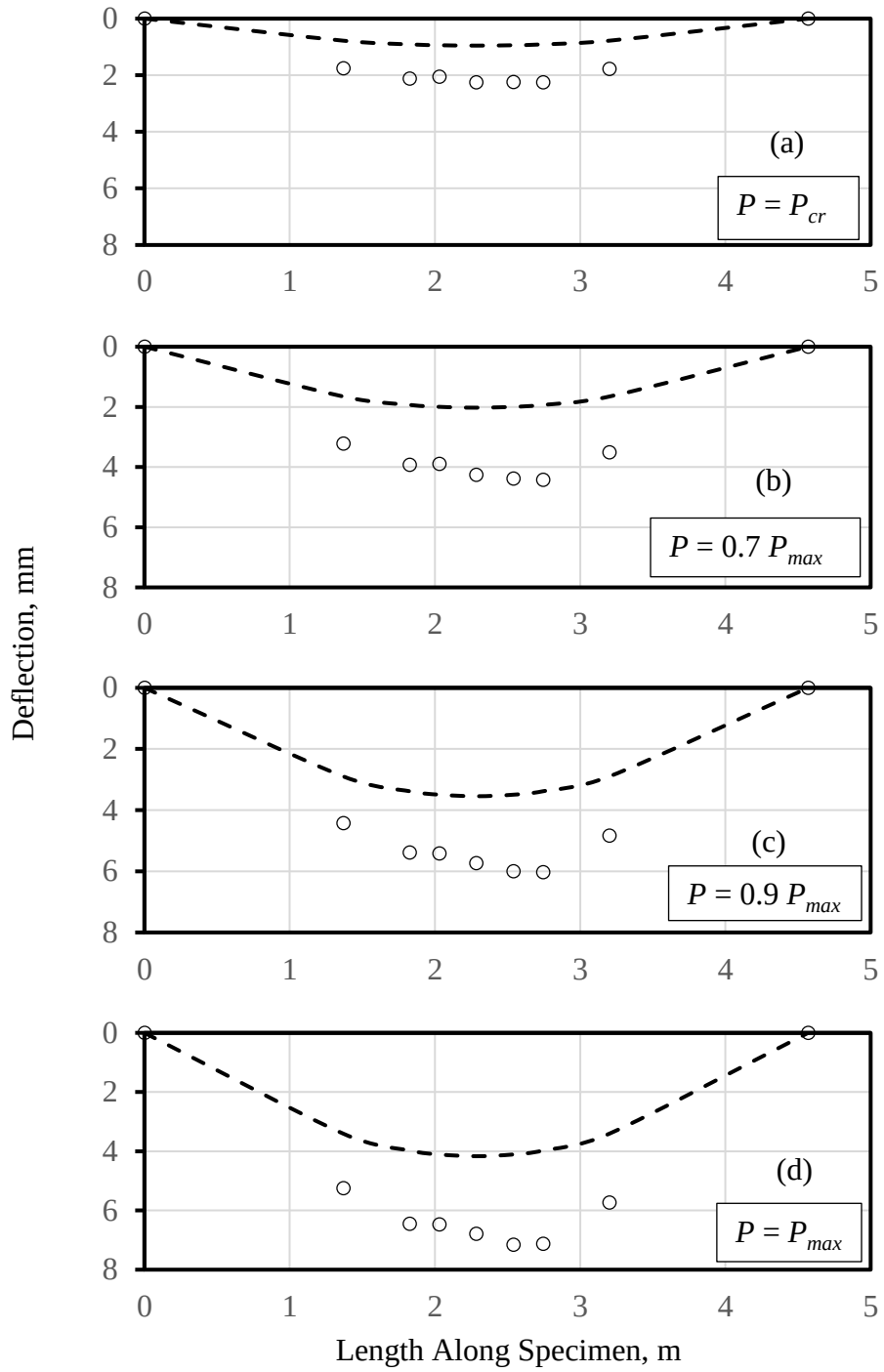

Figure F.3: Deflection Profile at Different Load Levels for Specimen 19■-510↑:(a) $P=P_{cr}$, (b) $P= 0.7\ P_{max}$, (c) $P= 0.9\ P_{max}$, and (d) $P= P_{max}$

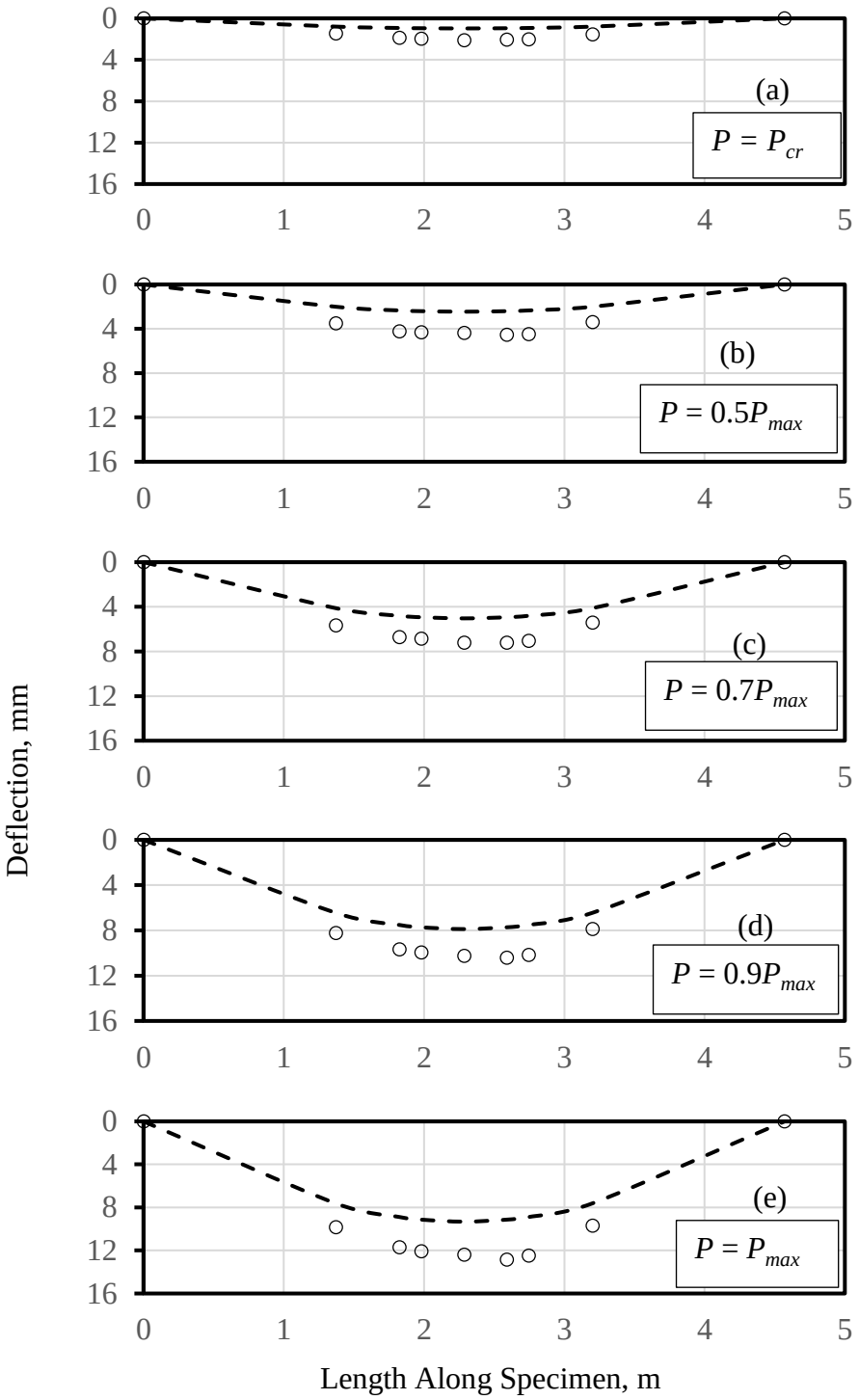

Figure F.4: Deflection Profile at Different Load Levels for Specimen 19■-610↑:(a) $P=P_{cr}$, (b) $P= 0.5\ P_{max}$, (c) $P= 0.7\ P_{max}$, (d) $P= 0.9\ P_{max}$, and (d) $P= P_{max}$

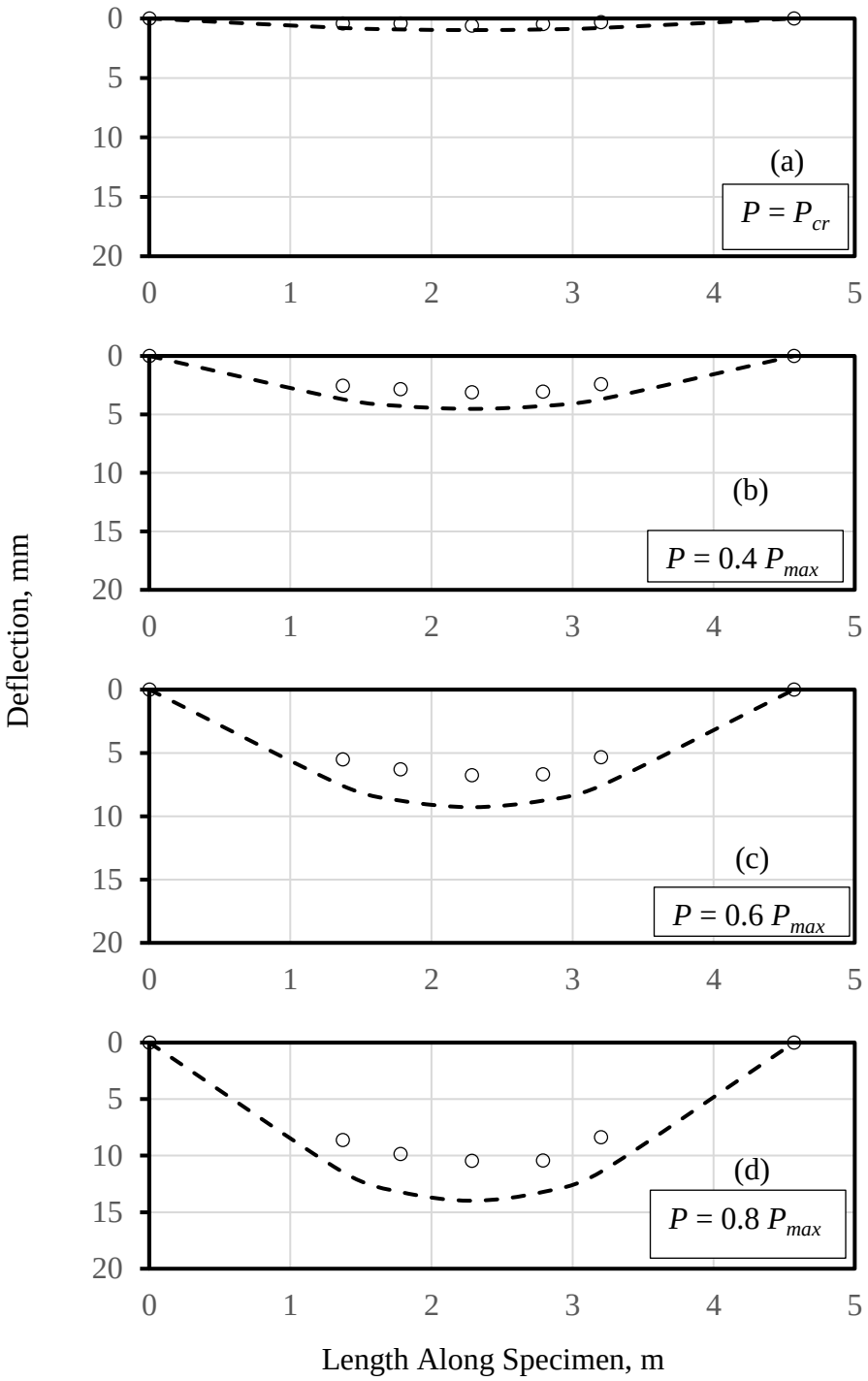

Figure F.5: Deflection Profile at Different Load Levels for Specimen 19●-1010↓:(a) $P=P_{cr}$, (b) $P= 0.4\ P_{max}$, (c) $P= 0.6\ P_{max}$, and (d) $P= 0.8\ P_{max}$

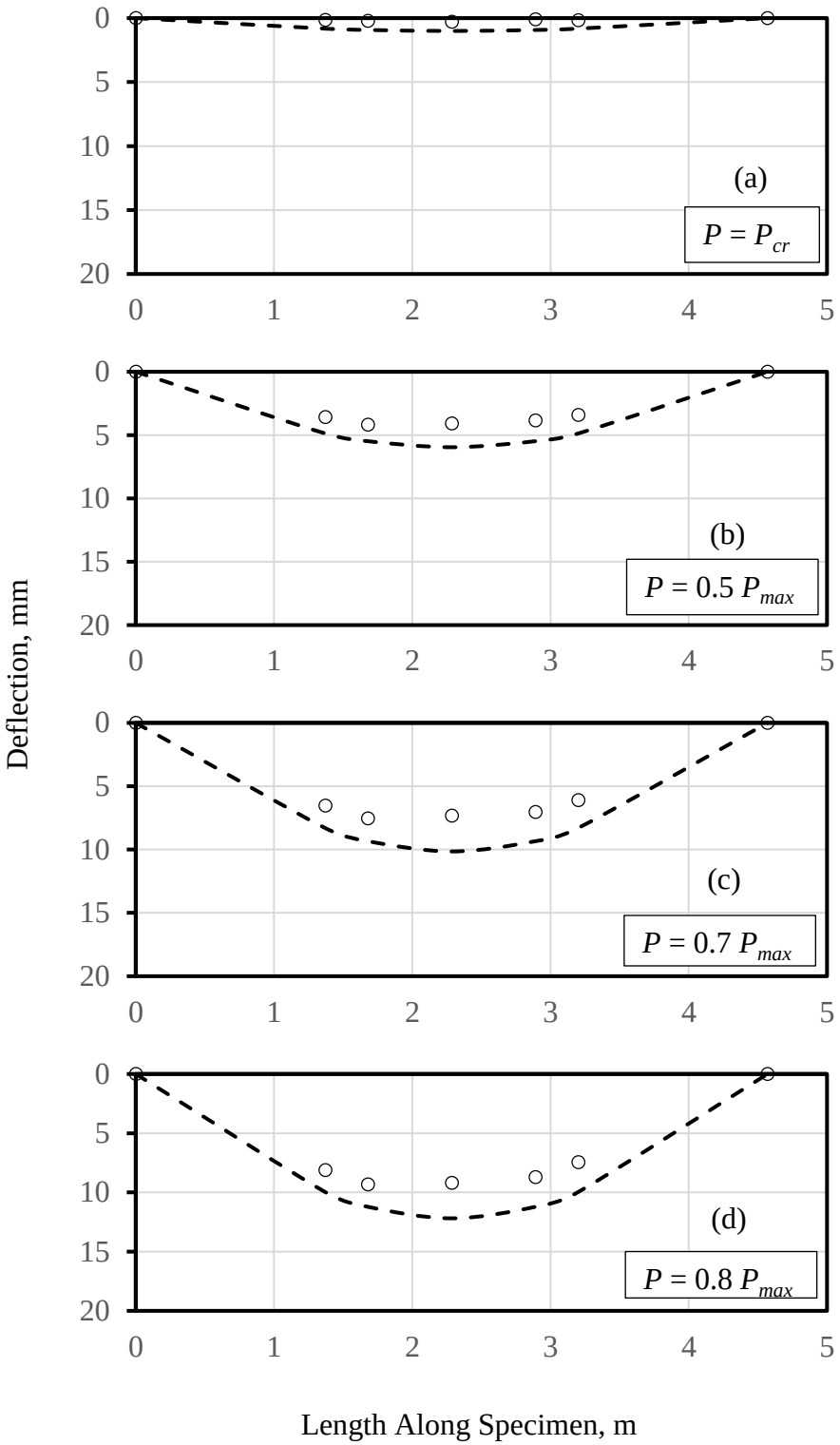

Figure F.6: Deflection Profile at Different Load Levels for Specimen 19●-1210↓:(a) $P=P_{cr}$, (b) $P= 0.4\ P_{max}$, (c) $P= 0.6\ P_{max}$, and (d) $P= 0.8\ P_{max}$

Appendix G: Moment Curvature Plots of Splice Specimens Reinforced with Plain Bars

Figures G.1 to G.24 show the theoretical moment versus curvature plots of splice specimens reinforced with plain bars. Only specimens that failed in bond before yielding of the reinforcement are included here. Strain hardening region is not shown in the diagram, as the specimens failed before reaching the strain hardening region. Specimens which have same concrete and steel properties have same moment curvature diagram (e.g. 19 ●-305↓ and 19●-410↓).

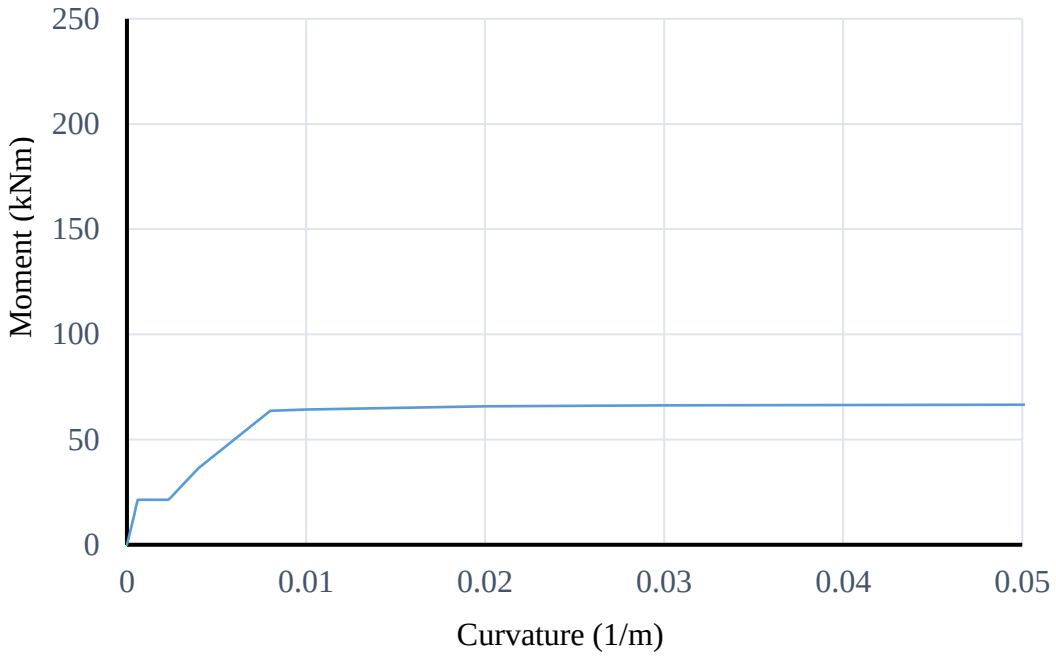

Figure G.1: Theoretical Moment Curvature Diagram for Specimen 19●-305↓ and 19●-410↓

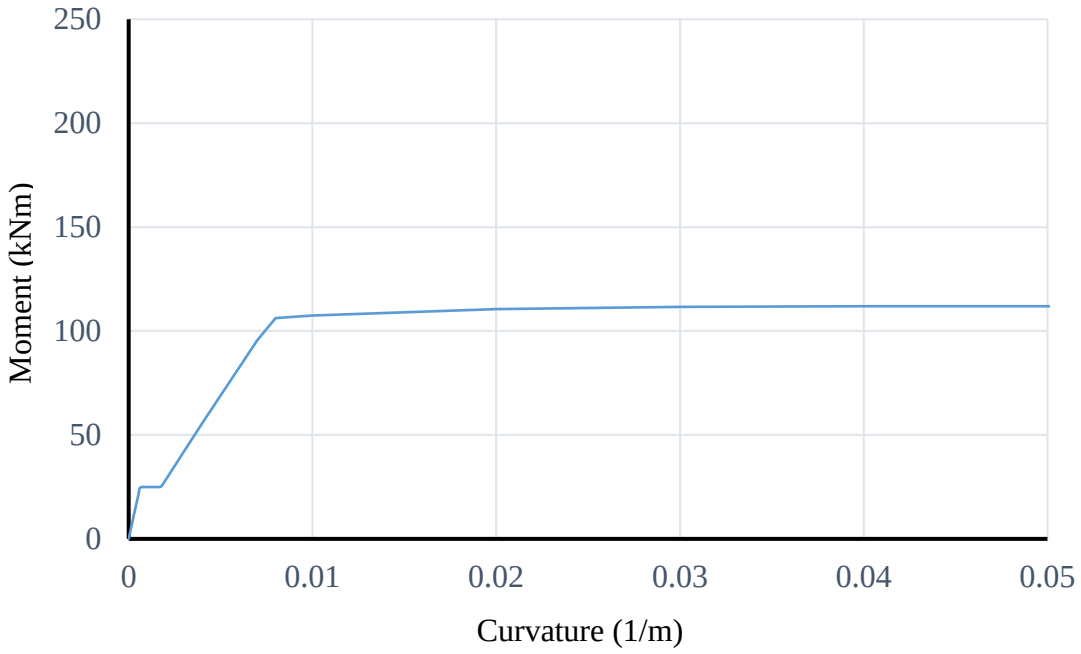

Figure G.2: Theoretical Moment Curvature Diagram for Specimen 25●-410↓

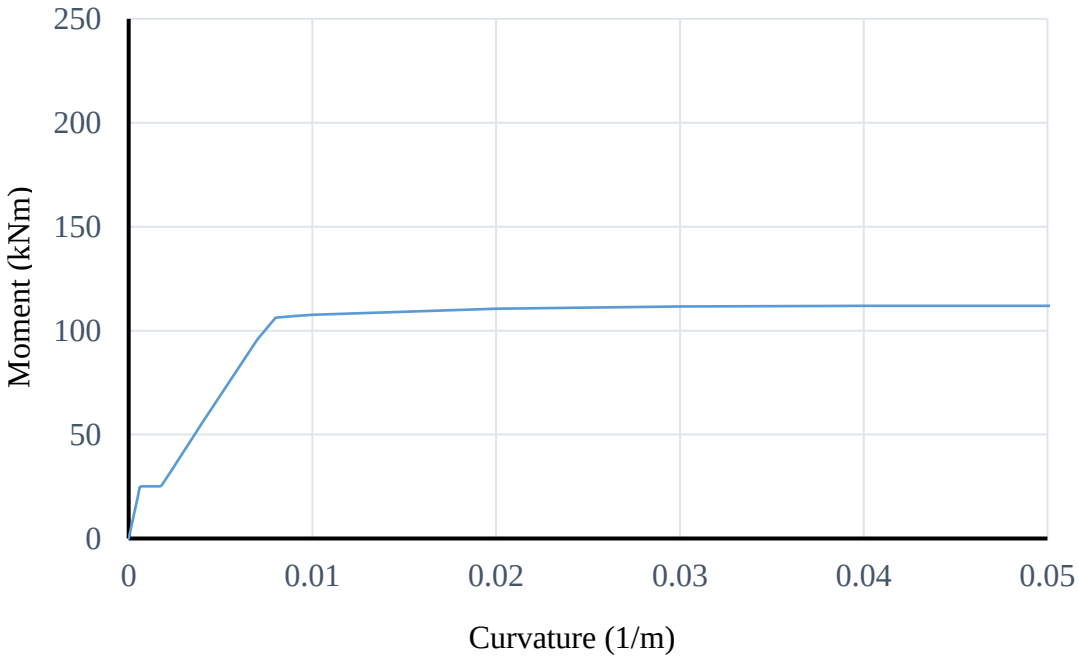

Figure G.3: Theoretical Moment Curvature Diagram for Specimen 25●-510↓

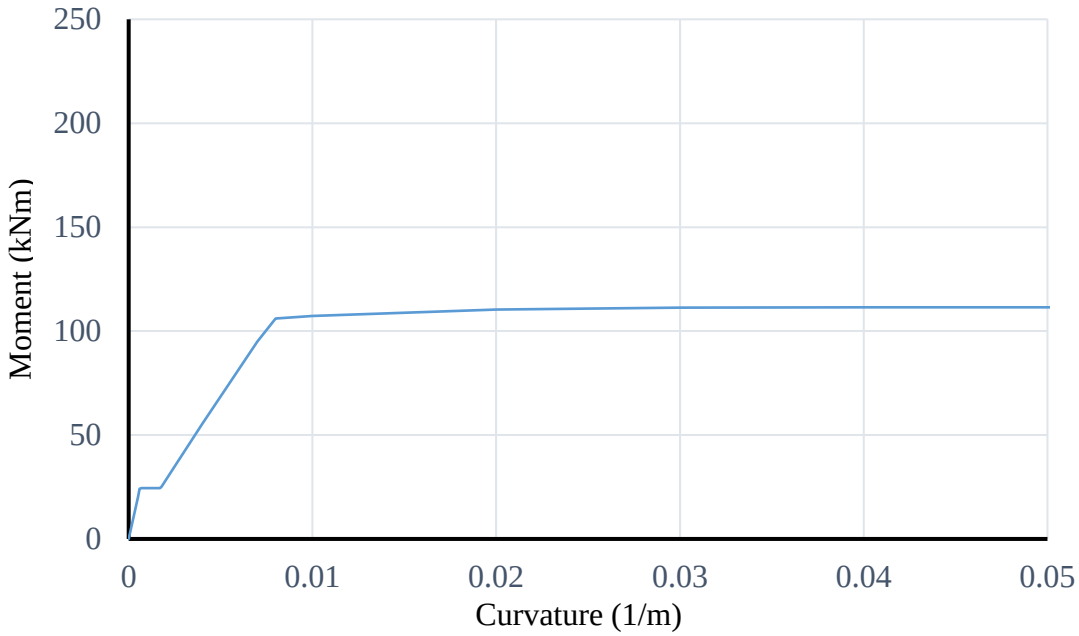

Figure G.4: Theoretical Moment Curvature Diagram for Specimen 25●-610↓

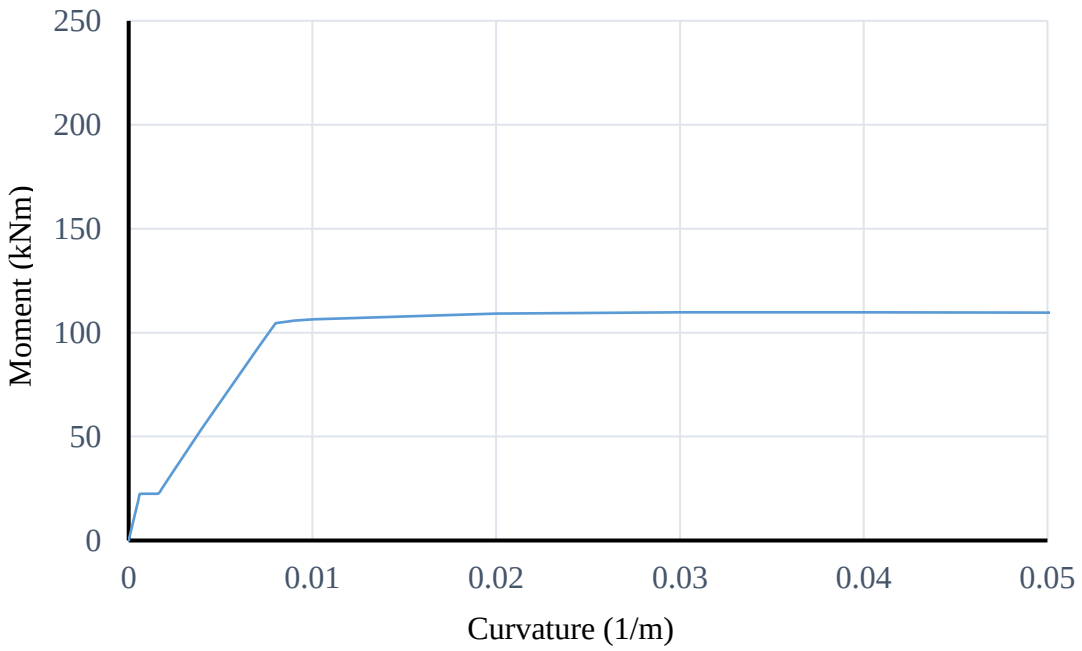

Figure G.5: Theoretical Moment Curvature Diagram for Specimen 25●-810↓

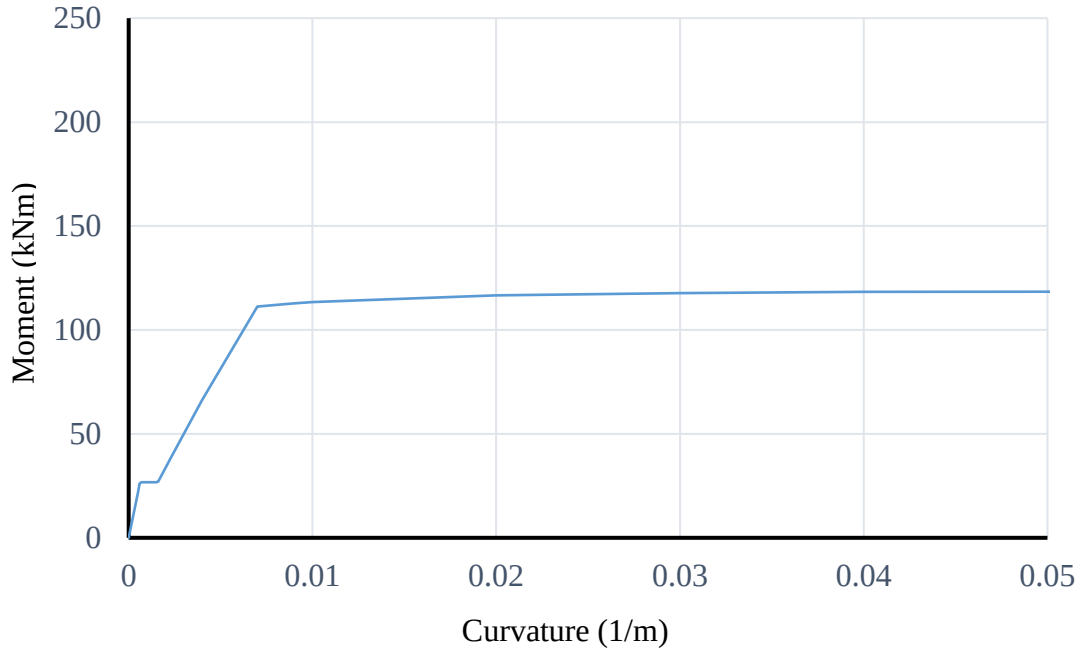

Figure G.6: Theoretical Moment Curvature Diagram for Specimen 25●-410↑

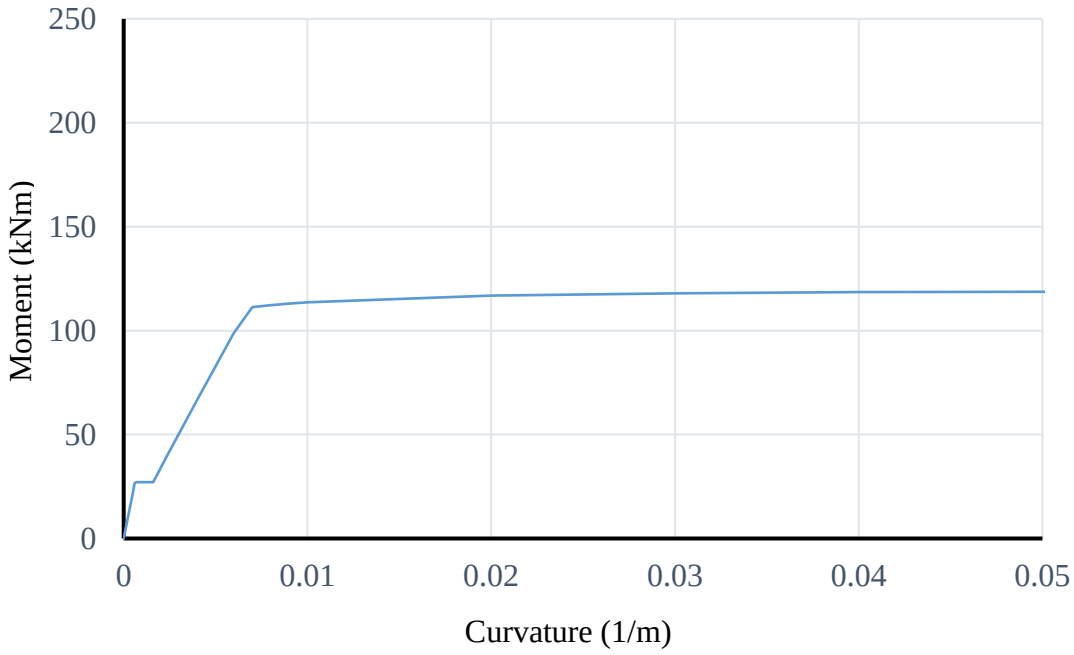

Figure G.7: Theoretical Moment Curvature Diagram for Specimen 25●-510↑

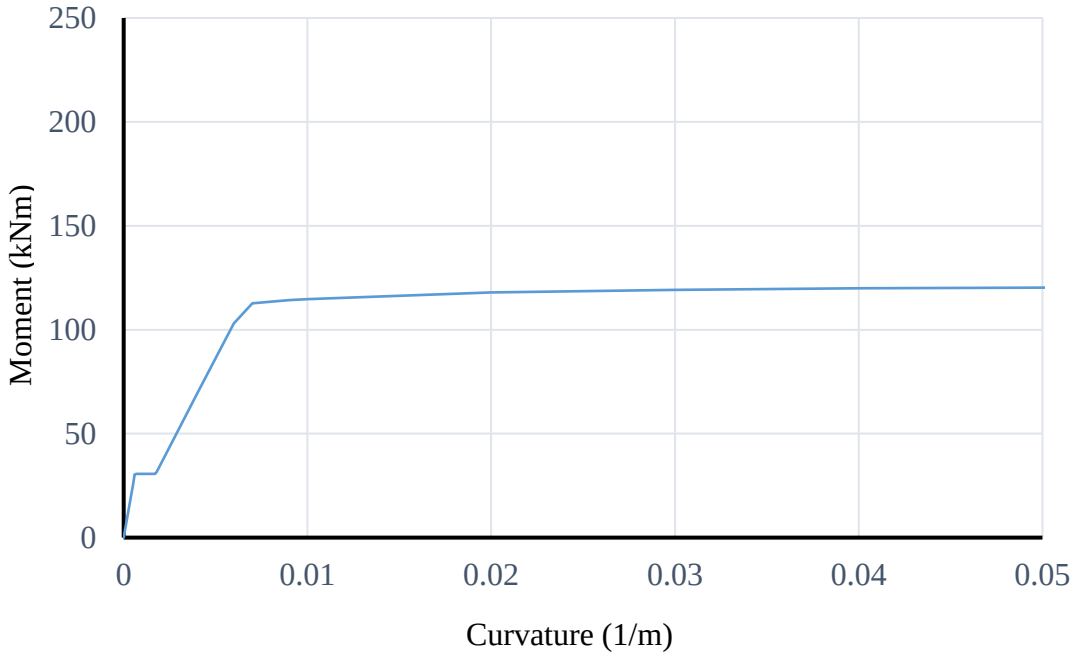

Figure G.8: Theoretical Moment Curvature Diagram for Specimen 25●-610↑

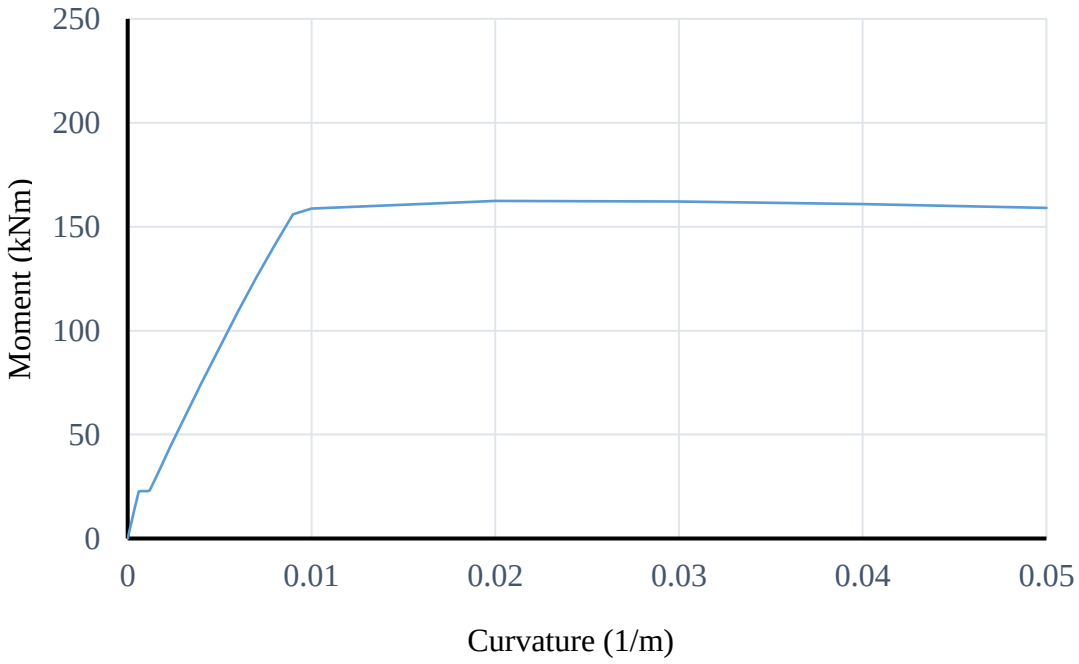

Figure G.9: Theoretical Moment Curvature Diagram for Specimen 32●-410↓ and 32●-610↓

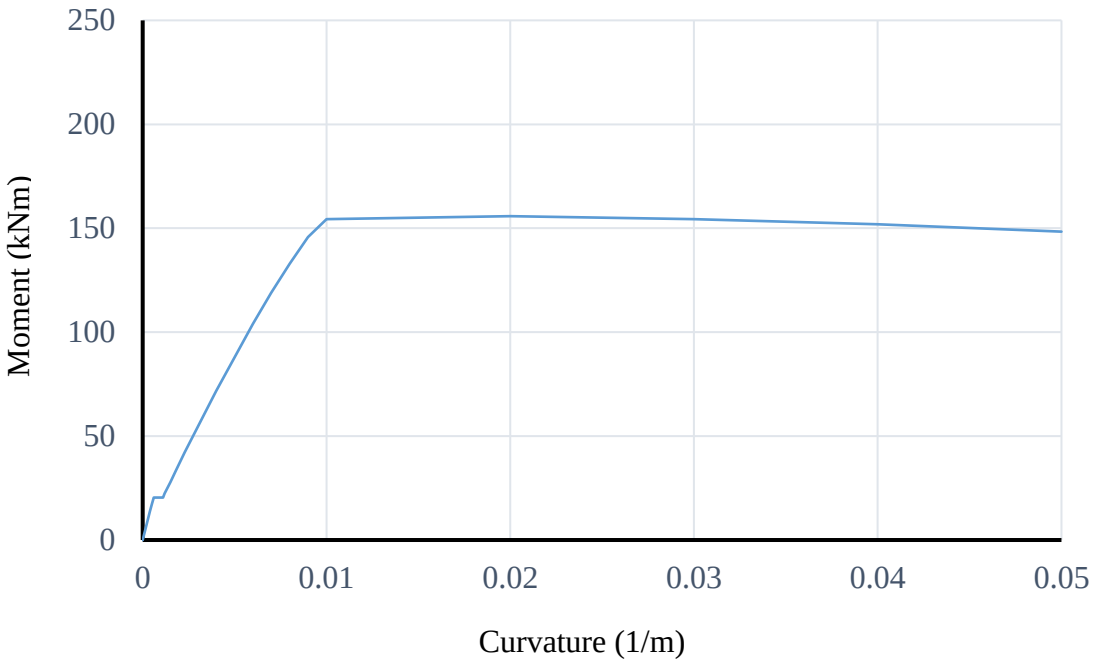

Figure G.10: Theoretical Moment Curvature Diagram for Specimen 32●-810↓

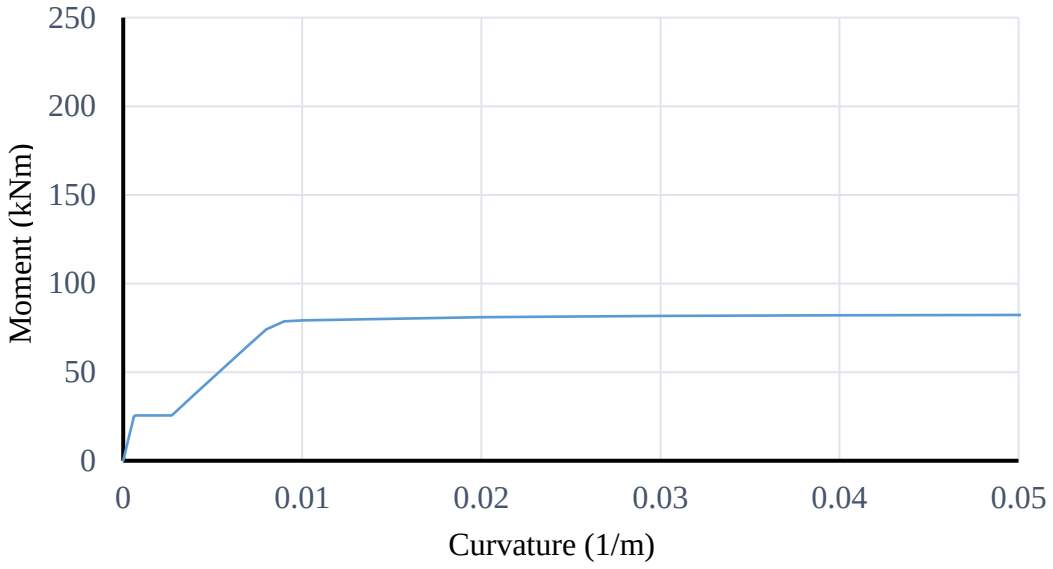

Figure G.11: Theoretical Moment Curvature Diagram for Specimen 19■-410↓

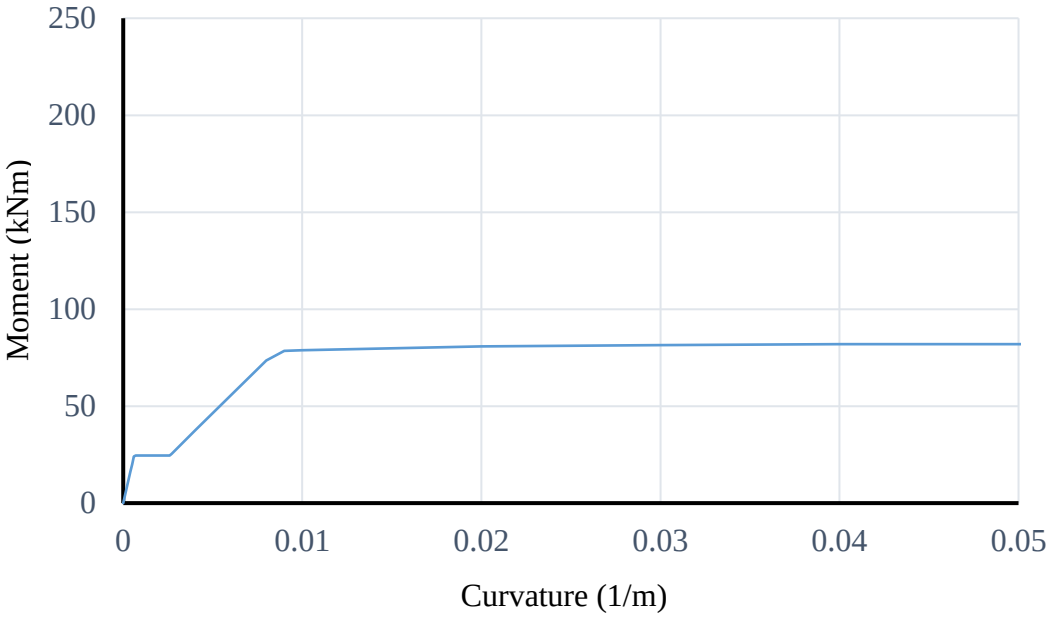

Figure G.12: Theoretical Moment Curvature Diagram for Specimen 19■-410↑

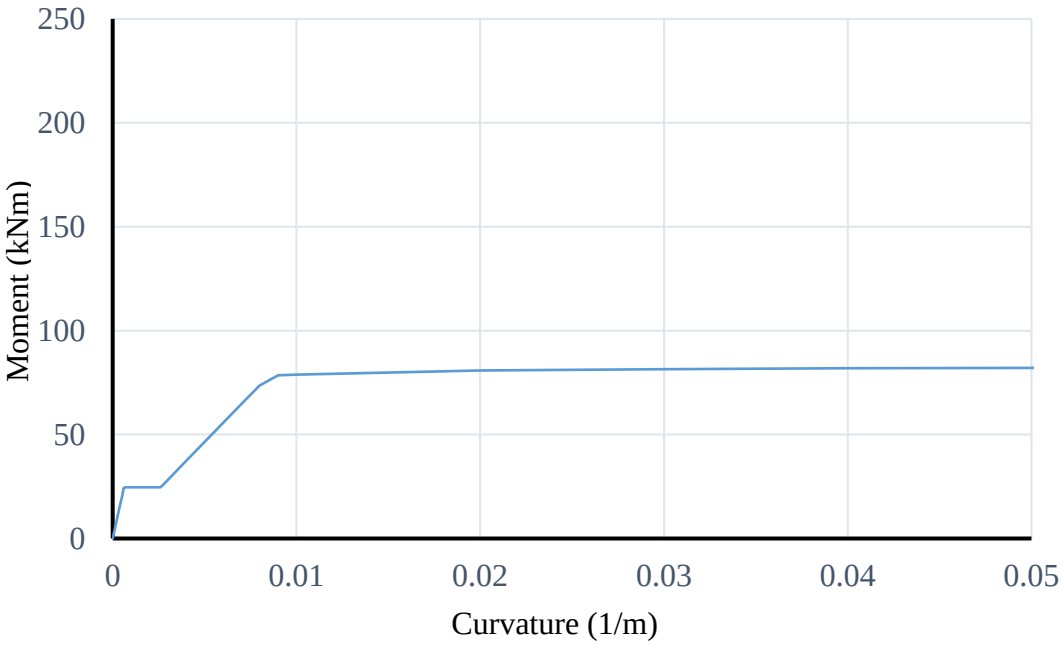

Figure G.13: Theoretical Moment Curvature Diagram for Specimen 19■-510↑

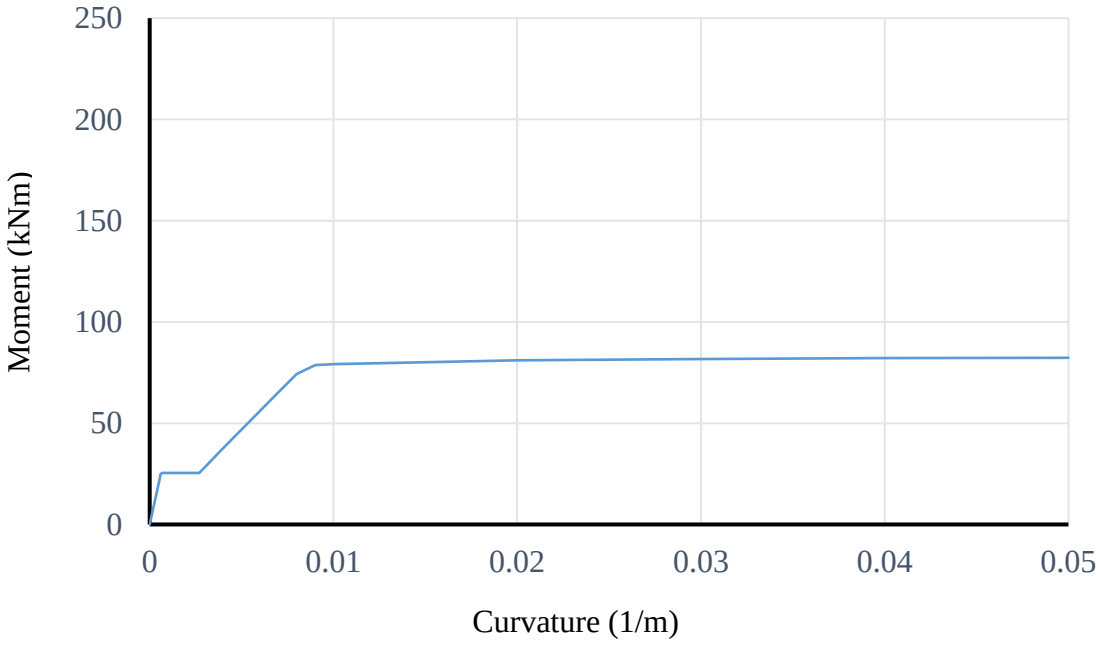

Figure G.14: Theoretical Moment Curvature Diagram for Specimen 19■-610↑

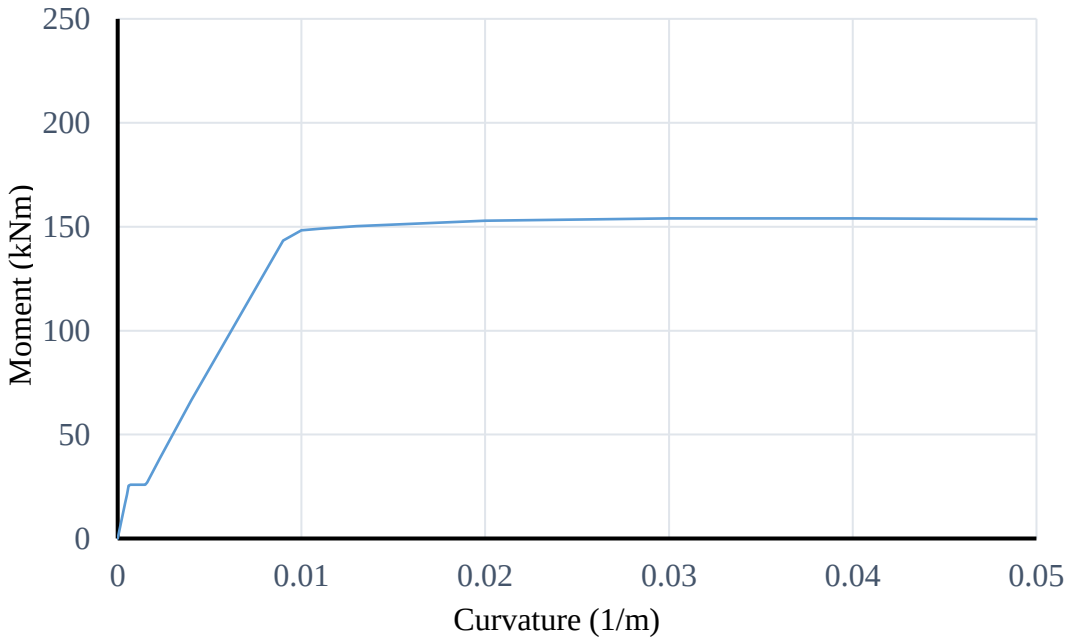

Figure G.15: Theoretical Moment Curvature Diagram for Specimen 25■-410↓

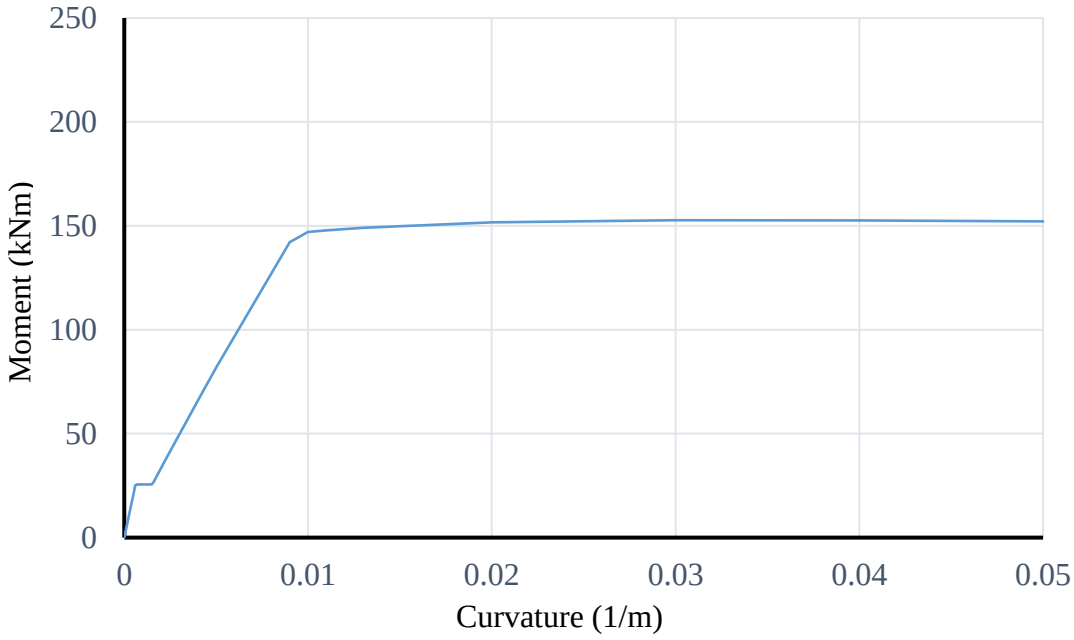

Figure G.16: Theoretical Moment Curvature Diagram for Specimen 25■-510↓

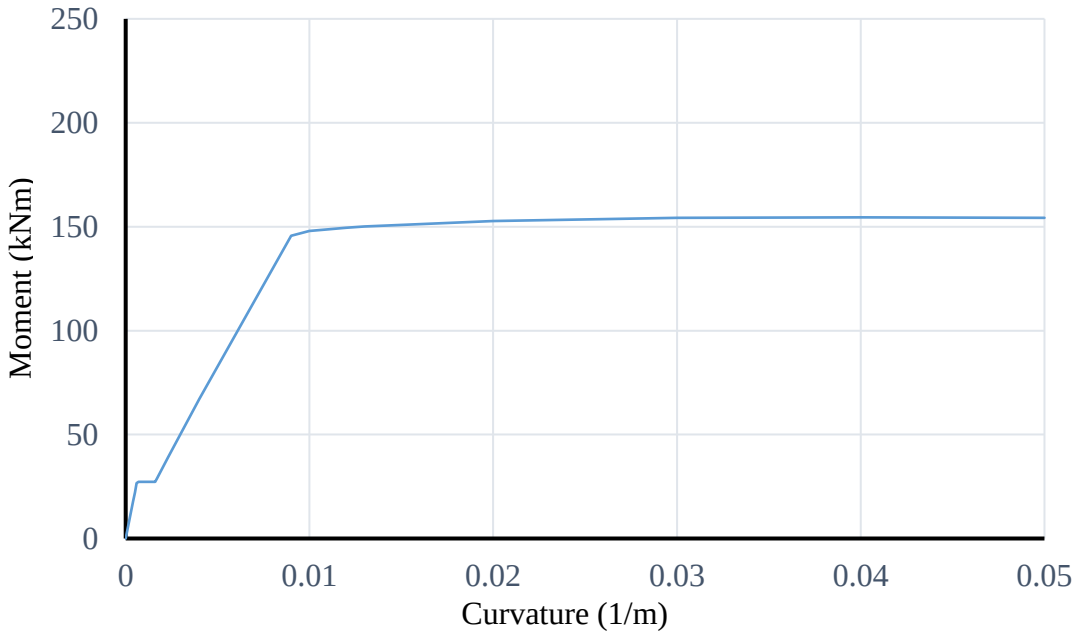

Figure G.17: Theoretical Moment Curvature Diagram for Specimen 25■-610↓

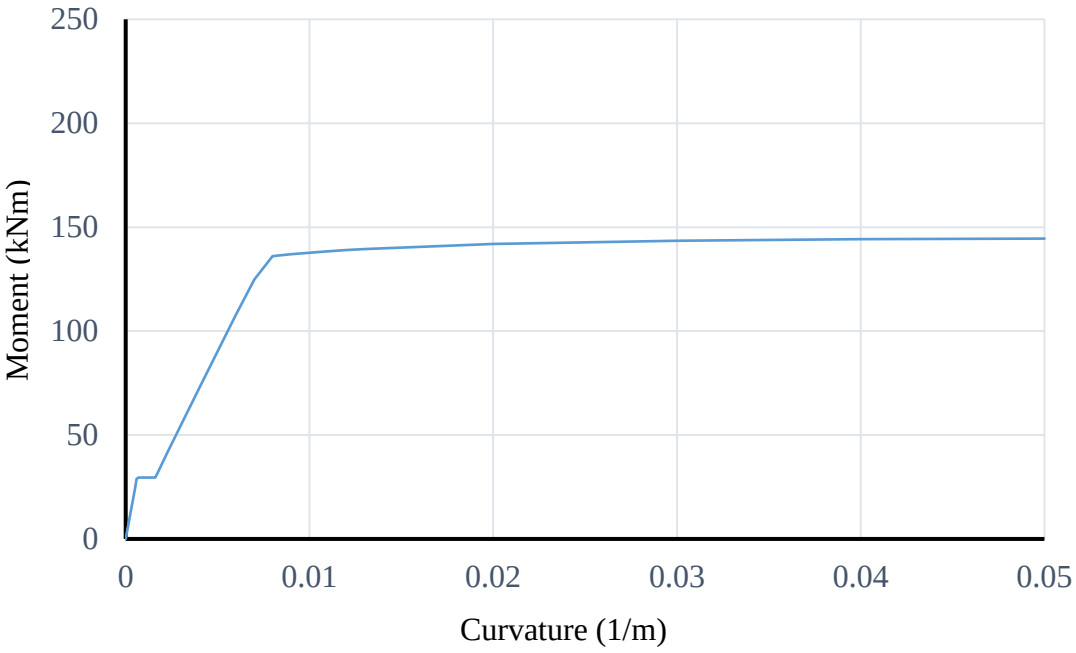

Figure G.18: Theoretical Moment Curvature Diagram for Specimen 25■-410↑ and 25■-610↑

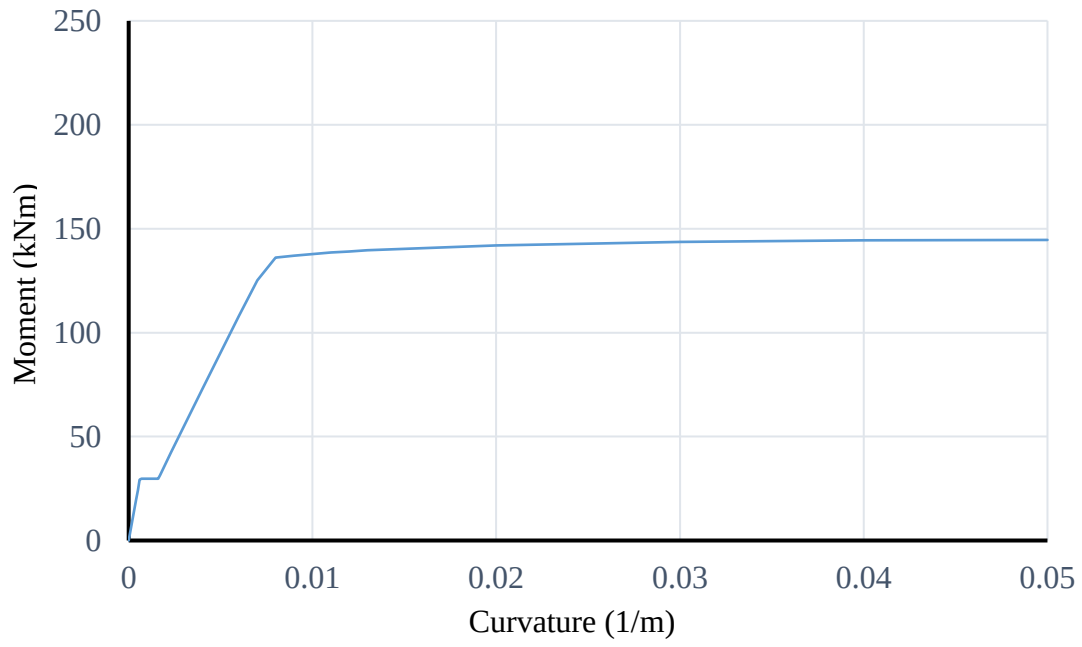

Figure G.19: Theoretical Moment Curvature Diagram for Specimen 25■-510↑

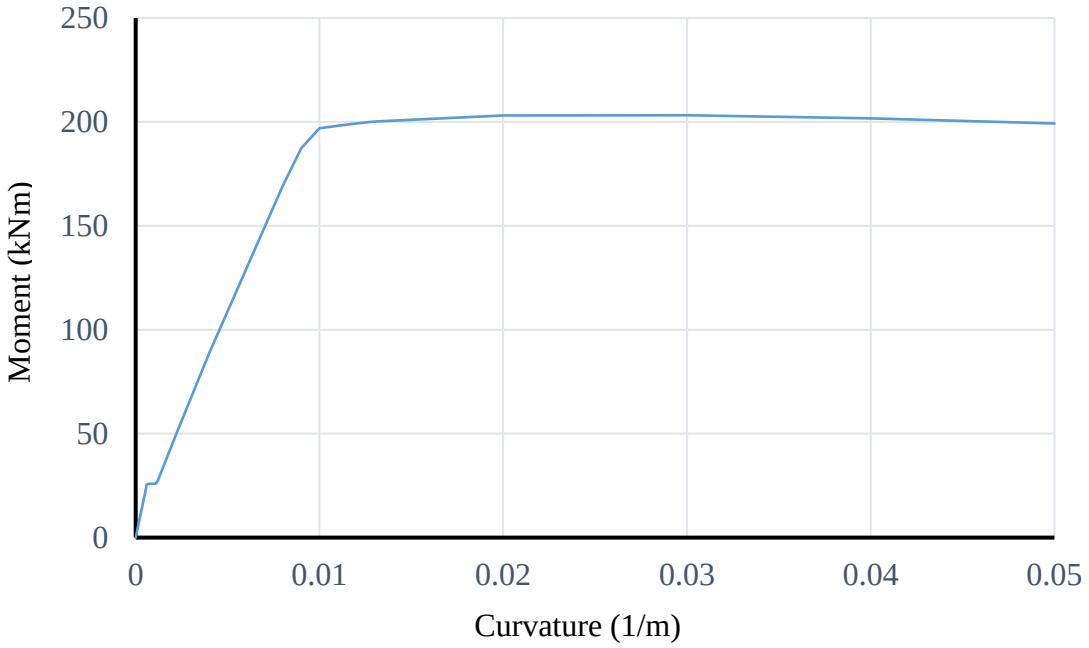

Figure G.20: Theoretical Moment Curvature Diagram for Specimen 32■-410↓

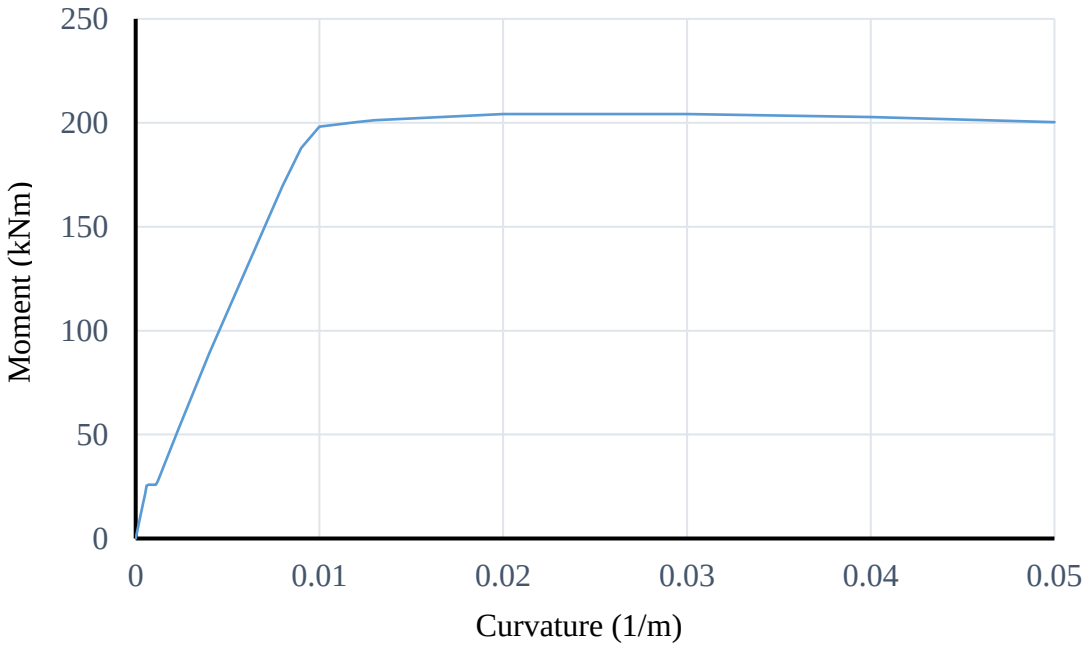

Figure G.21: Theoretical Moment Curvature Diagram for Specimen 32■-610↓

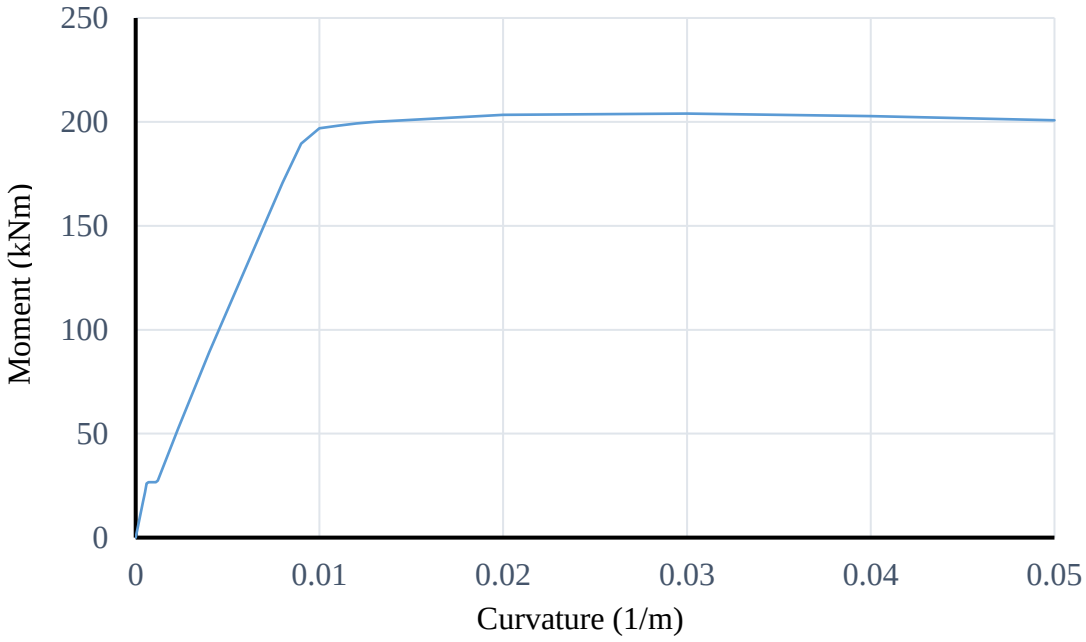

Figure G.22: Theoretical Moment Curvature Diagram for Specimen 32■-810↓

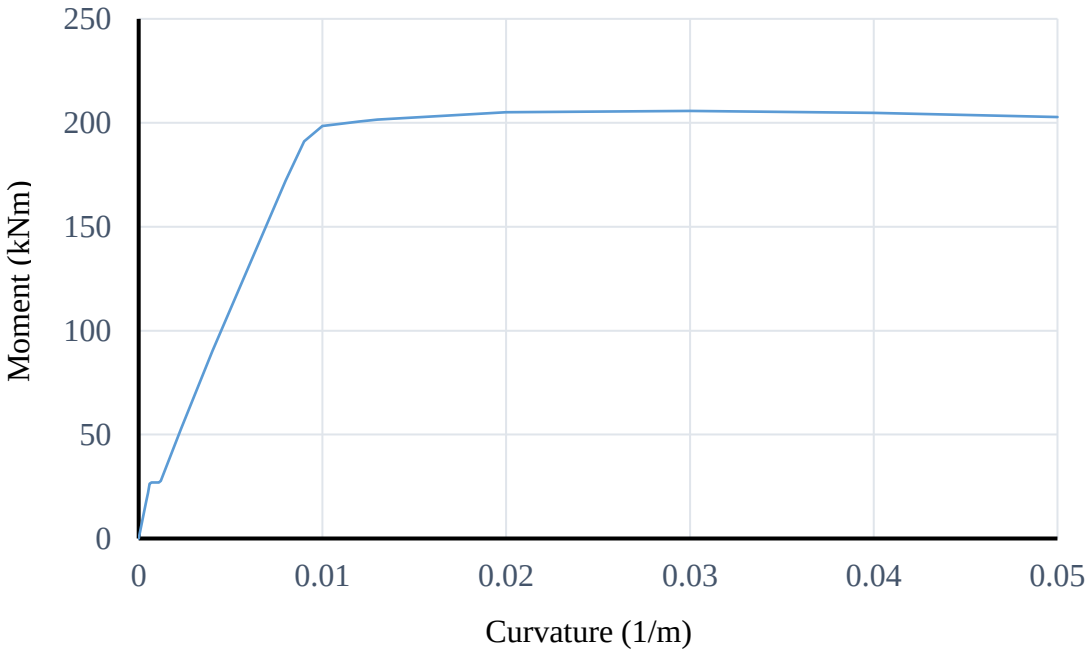

Figure G.23: Theoretical Moment Curvature Diagram for Specimen 32■-410↑

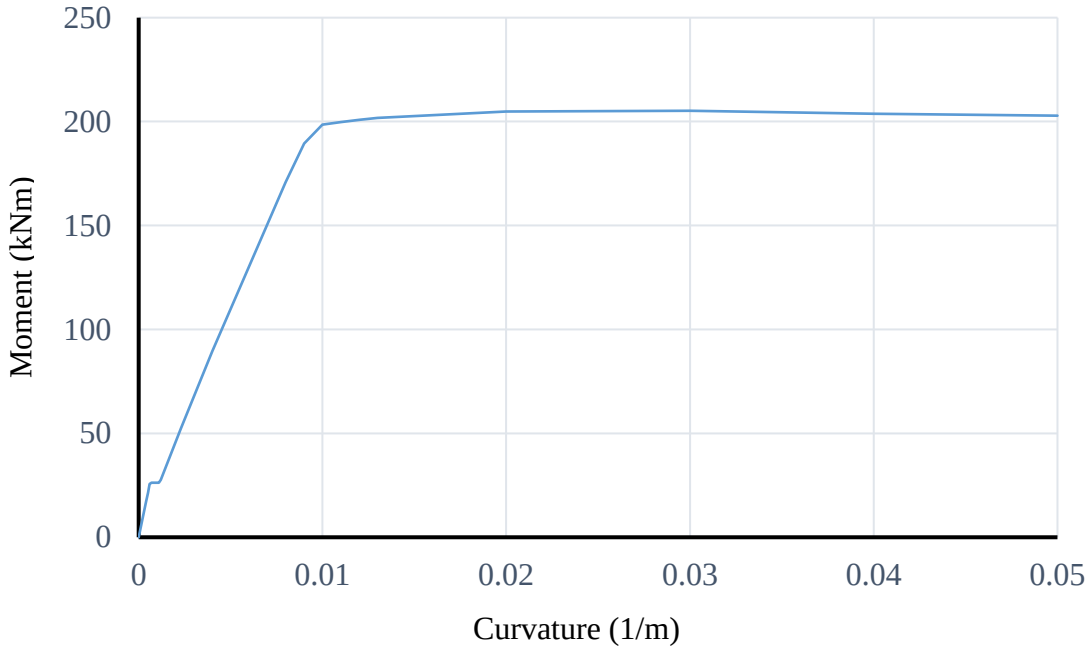

Figure G.24: Theoretical Moment Curvature Diagram for Specimens 32■-610↑ and 32■-810↑

Appendix H: Error Associated with Selection of 100 Segments in Moment Curvature Analysis

This appendix provides the error associated with the selection of the number of segments used to calculate resisting moment. Figure H.1 shows the moment corresponding to a fixed curvature of 0.0038 for specimen 19●-510↓ with 1, 2, 5, 10, 20, 50, 100, 200, 300, 400, and 500 segments. A curvature value of 0.0038 was selected such that curvature was located in a linear segment of the moment curvature diagram shortly before yielding of the reinforcement. The moment closely approached the value of 34.9488 kNm when the number of segments was greater than or equal to 300. Hence the approximate asymptote (Figure H.1) was reported as 34.9488 kNm. As the moment corresponding to 100 segments was 34.9486 kNm, the error associated with the selection of 100 segments was negligible (i.e. 0%).

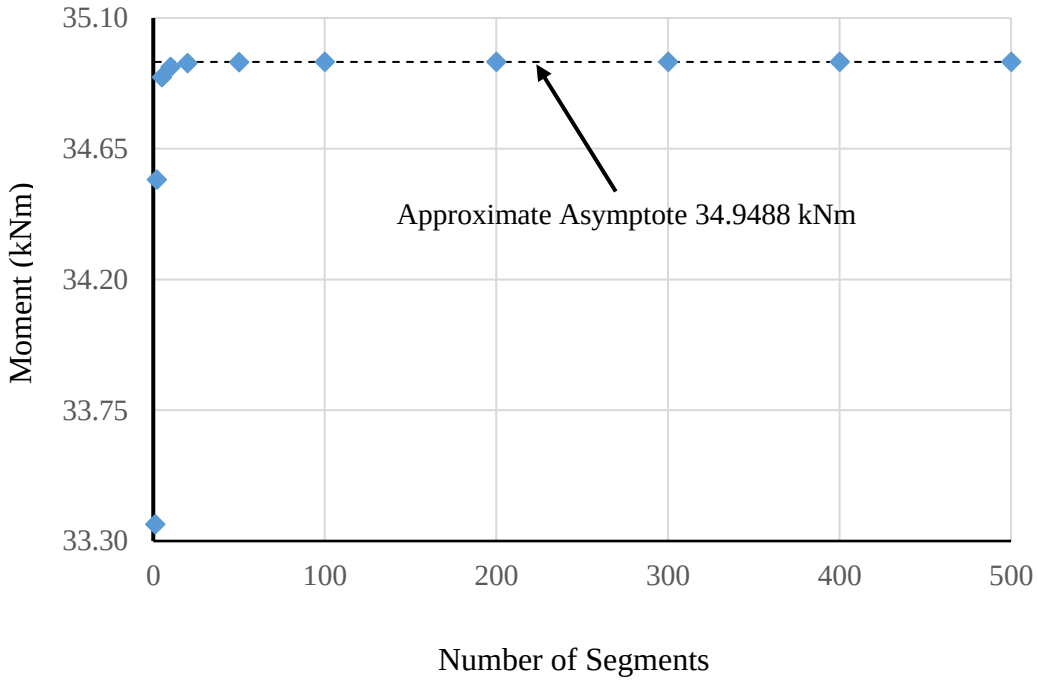

Figure H.1: Moment Corresponding to a Curvature of 0.0038/m as a Function of the Number of Segments Incorporated in the Analysis of Specimen 19●-510↓

Appendix I: Comparison of Two Different Methods for Calculating the Tensile Resistance of the Spliced Reinforcement

Figure I.1 shows the comparison of the two methods of the calculation of tensile resistance of the reinforcement at the maximum load level. In method 1, the moment resistance was calculated as a product of the tensile force in the longitudinal reinforcement and the lever arm (i.e. distance between the centroids of tension force and compression force), whereas in method 2, the moment resistance was calculated as a product of compressive force in the concrete and the same lever arm. The mean and standard deviation of the ratio of the tensile resistance as calculated from method 1 to method 2 are 0.98 and 0.003, respectively. As the neutral axis depth was calculated from a higher value to a lower value until the difference between compressive force and tensile force was within 0.5%, method 2 gave slightly greater value of tensile resistance than method 1. Method 1 was chosen as it yielded lower tensile resistance which would ultimately lead to longer, and so more conservative, lap splice length.

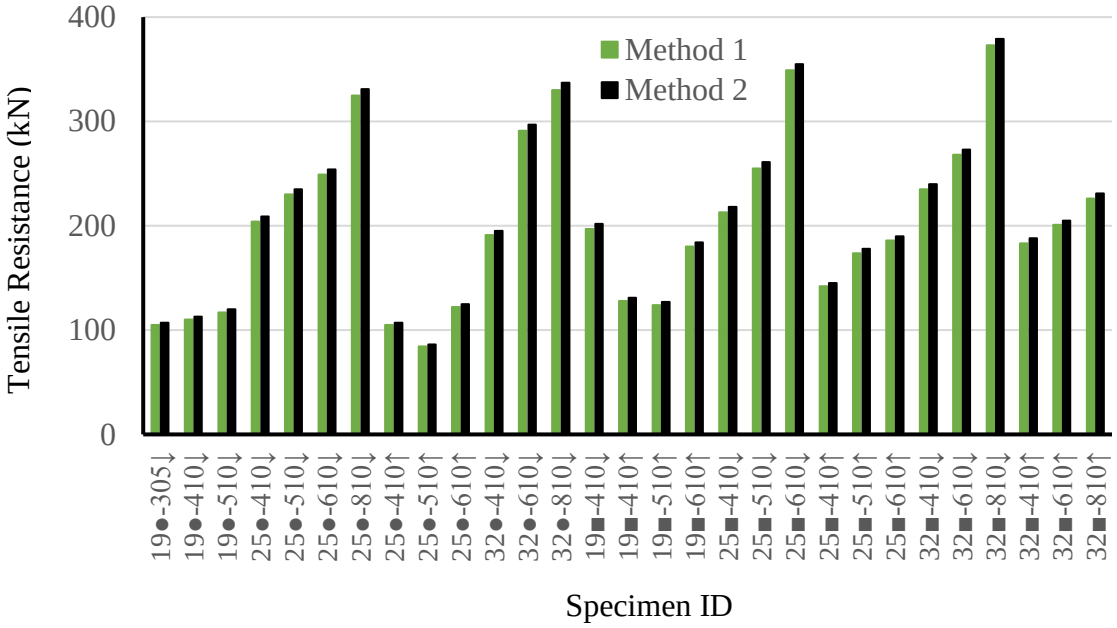

Figure I.1: Comparison of Two Different Methods for Calculating the Tensile Resistance of the Spliced Reinforcement at the Maximum Load

Appendix J: Results for Specimens Reinforced with Deformed Bars

Appendix J provides the results for specimens reinforced with deformed bars.

Table J.1: Concrete and Longitudinal Reinforcing Steel Material Properties for Specimens Reinforced with Deformed Bars

	Concrete				Longitudinal Reinforcing Steel				
Specimen ID	Age of Concrete at Test Date (days)	Slump (mm)	Compressive Strength f'_c MPa	Tensile Strength MPa	Measured Bar Size d_b (mm)	Dynamic Yield Strength f_{yd} MPa	Static Yield Strength f_{ys} MPa	Ultimate Strength fu MPa	Modulus of Elasticity Es MPa
20◙-410↓[a]	52	80	21.8	2.31	20.0	419	394	574	185
20◙-610↓[a]	55		21.2	2.51	20.0				

[a]The first number in specimen identification represents the nominal bar size of the longitudinal reinforcement. The symbol that follows represents that the bar is a deformed bar. The number following the hyphen represents the lap splice length of longitudinal bars in mm and the final symbol (↓) represents that lap spliced bars were cast in bottom position.

Table J.2: Test Results of the Lap Splice Specimens Reinforced with Deformed Bars

Specimen ID	Splice Length as a Function of Bar Size L_s/d_b	Maximum Normalized Load $P_{max}/\sqrt{f'_c}$ (kN/√MPa)	Predicted Normalized Load $P_{max}/\sqrt{f'_c}$ (kN/√MPa)	Midspan Deflection at Maximum Load (mm)
20◙-410↓	20.5	24.6	22.6	16.7
20◙-610↓	30.5	29.5	22.8	50.7

Table J.3: Companion Concrete Cylinder Properties for Specimens Reinforced with Deformed Bars

Specimen ID	Concrete Cylinder ID[a]	Age at Test Date (days)	Compressive Strength f'_c(MPa)	Tensile Strength (MPa)
20■-410↓	C-1-21	52	23.8	
	C-1-22		19.7	
	C-1-23		21.8	
	C-1-24			2.39
	C-1-25			2.23
Coefficient of Variation			9.42%	4.90%
20■-610↓	C-1-26	55	24.2	
	C-1-27		23.3	
	C-1-28		16.2	
	C-1-29			2.32
	C-1-30			2.70
Coefficient of Variation			20.6%	10.7%

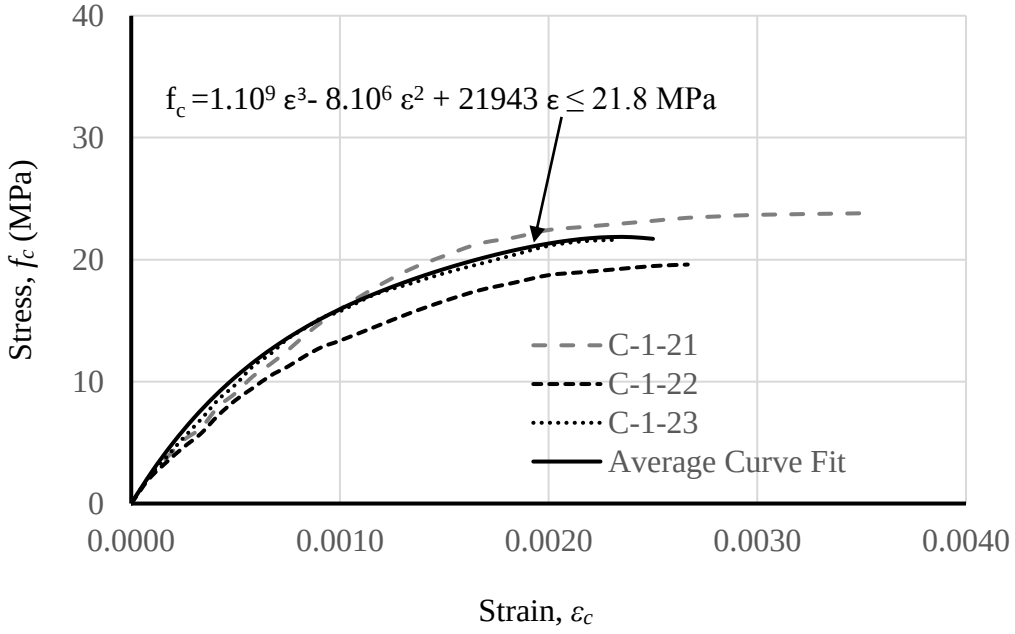

Figure J.1: Stress-Strain relationship of Concrete Companion Specimen associated with Specimen 20▣-410↓

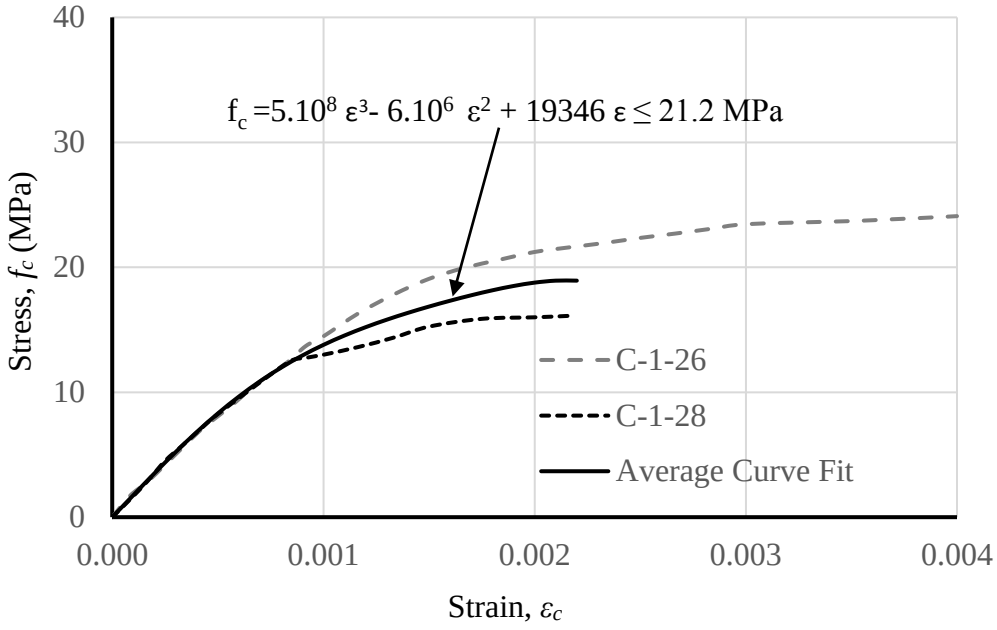

Figure J.2: Stress-Strain relationship of Concrete Companion Specimen associated with Specimen 20▣-610↓

Table J.4:Properties of Deformed Longitudinal Reinforcement

Associated Splice Specimen ID	Steel Specimen ID[a]	Dynamic Yield Strength f_{yd}(MPa)	Static Yield Strength f_{ys}(MPa)	Modulus of Elasticity, E_s (GPa)
20◙-410↓, and 20◙-610↓	S-20-◙-1-1	417	394	190
	S-20-◙-1-2	420	393	180
	S-20-◙-1-3	n/a*	n/a*	n/a*
Coefficient of Variation		0.51%	0.18%	3.82%

* No data due to error occurred while testing

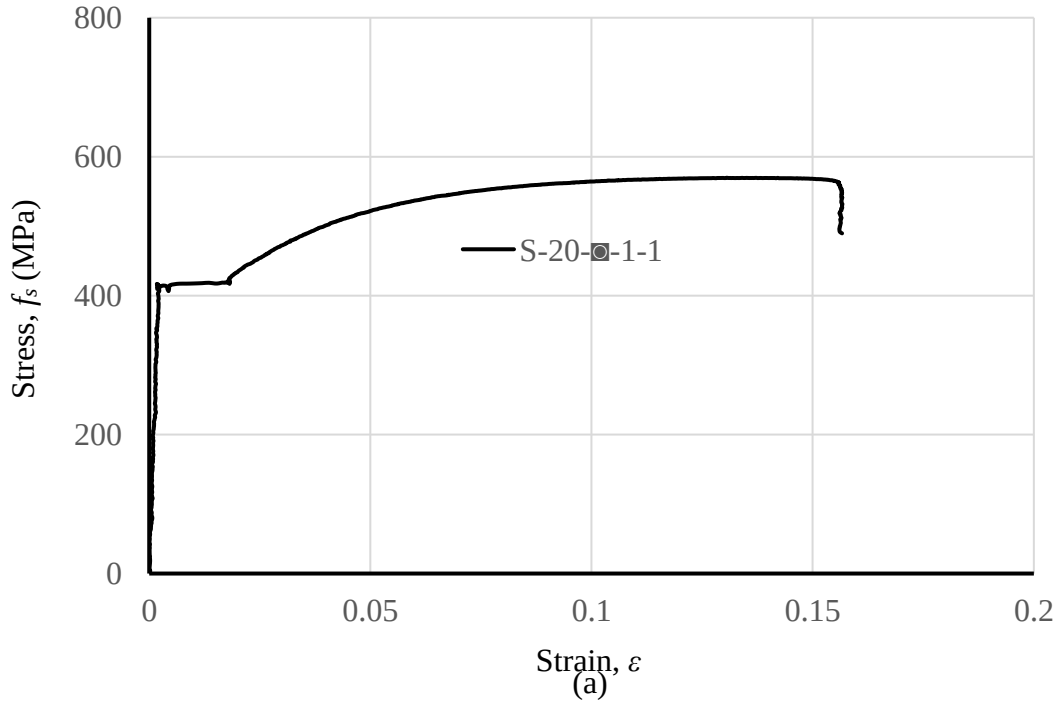

(a)

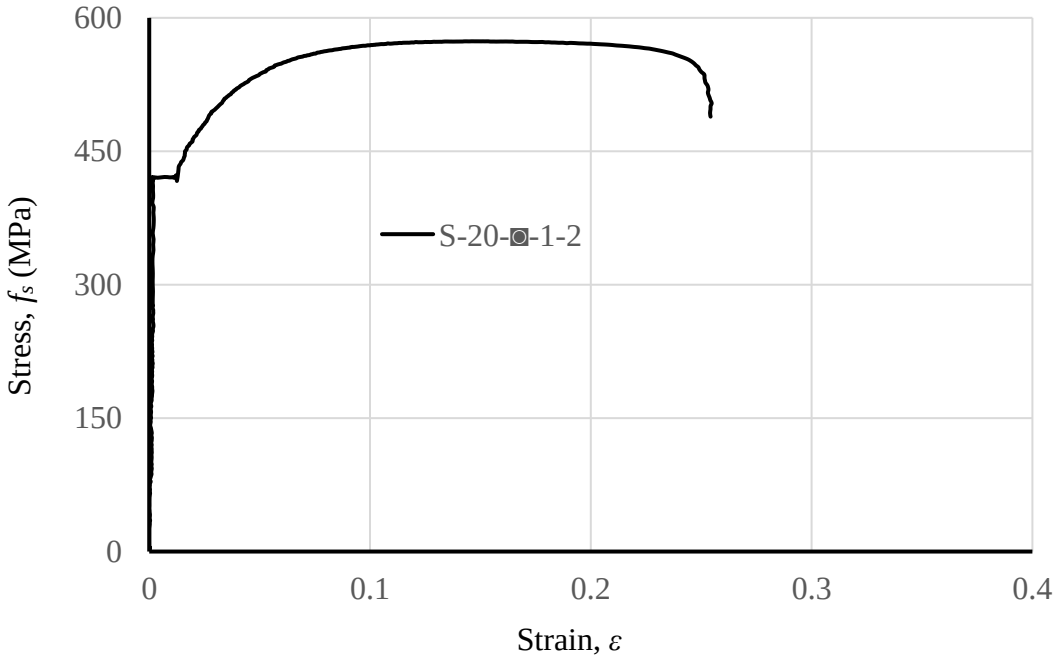

(b)

Figure J.3: Stress Versus Strain for 20mm Deformed Bar: (a) S-20-◙-1-1, and (b) S-20-◙--1-2,

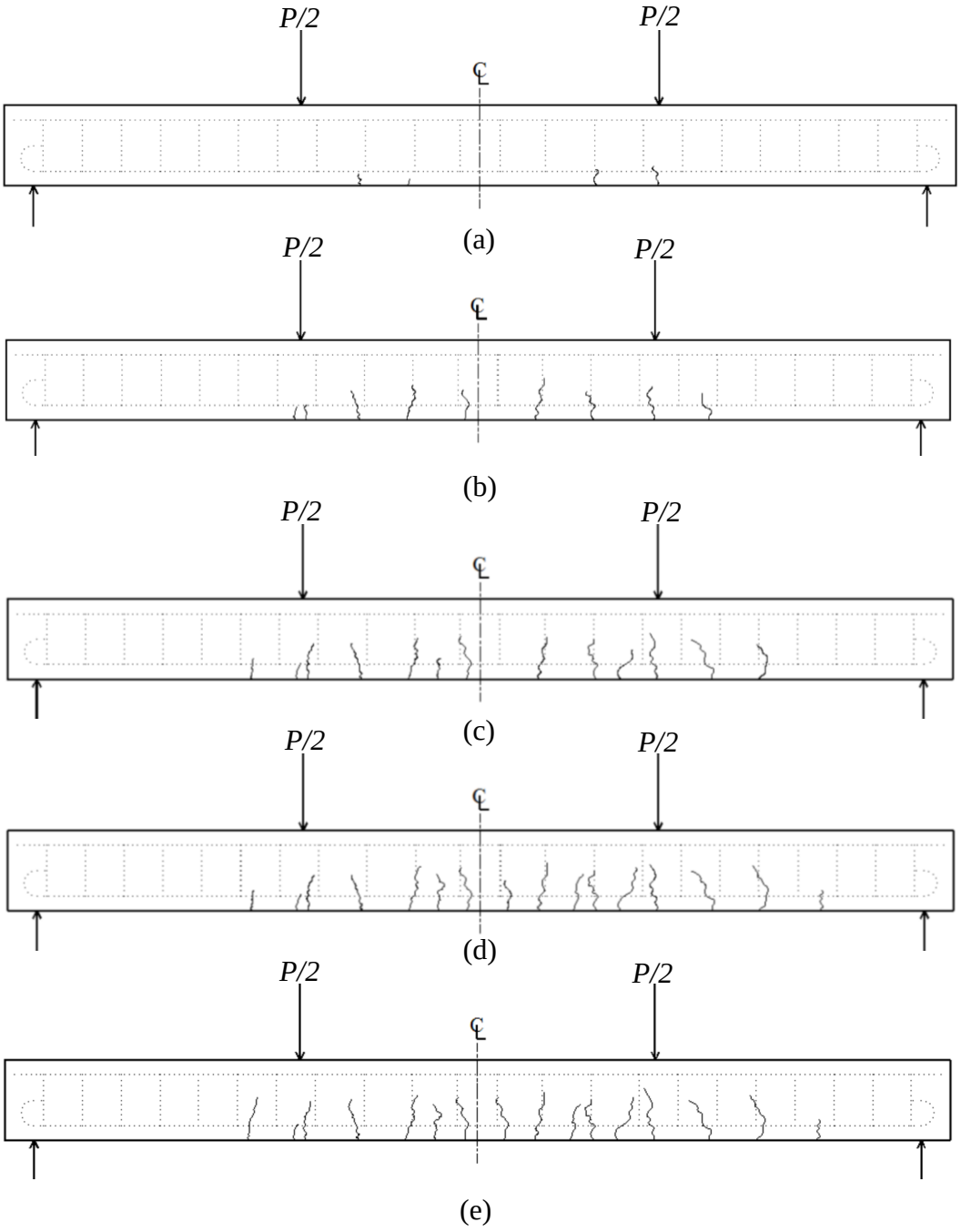

Figure J.4: Crack Pattern for Specimen 20■-410↓: (a) P=0.3 P_{max}, (b) P=0.5 P_{max}, (c) P=0.7 P_{max}, (d) P=0.9 P_{max}, and (d) P=P_{max}

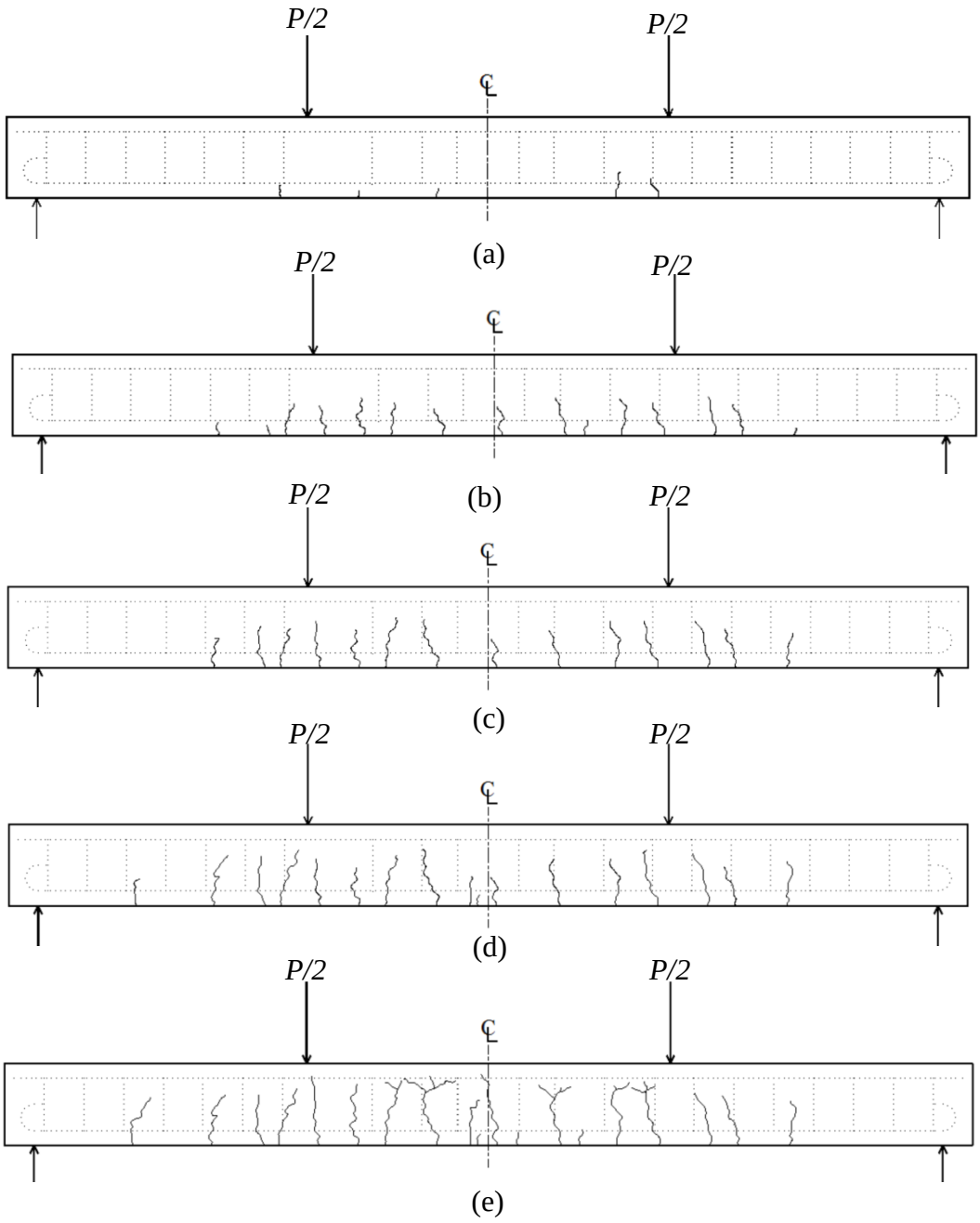

Figure J.5: Crack Pattern for Specimen 20◙-610↓: (a) P=0.25 P_{max}, (b) P=0.5 P_{max}, (c) P=0.7 P_{max}, (d) P=0.9 P_{max}, and (d) P=P_{max}

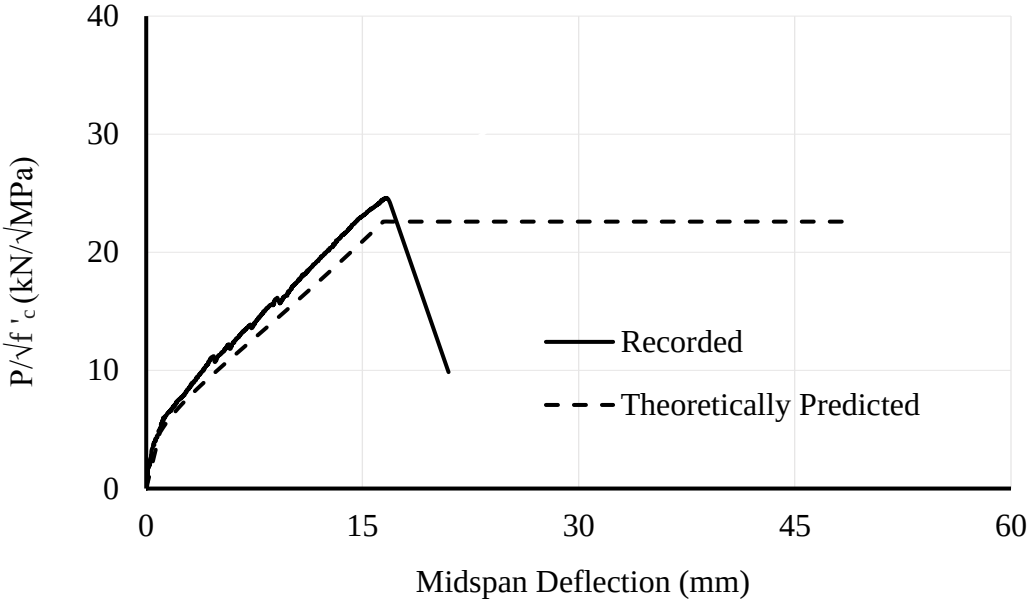

Figure J.6: Normalized Applied Load Versus Midspan Deflection for Specimen 20□-410↓

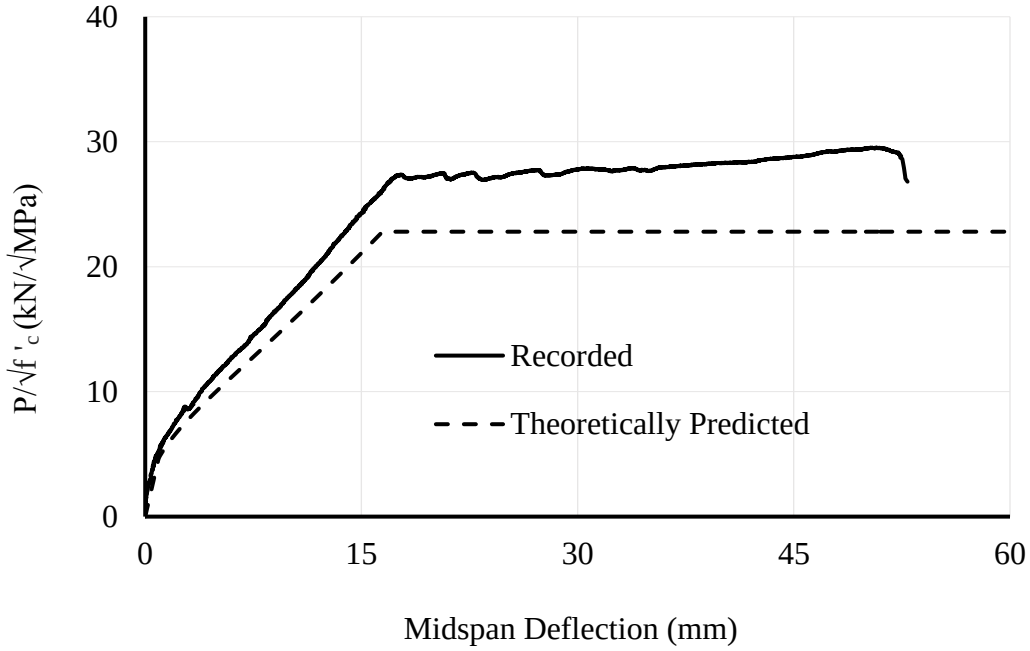

Figure J.7: Normalized Applied Load Versus Midspan Deflection for Specimen 20□-610↓

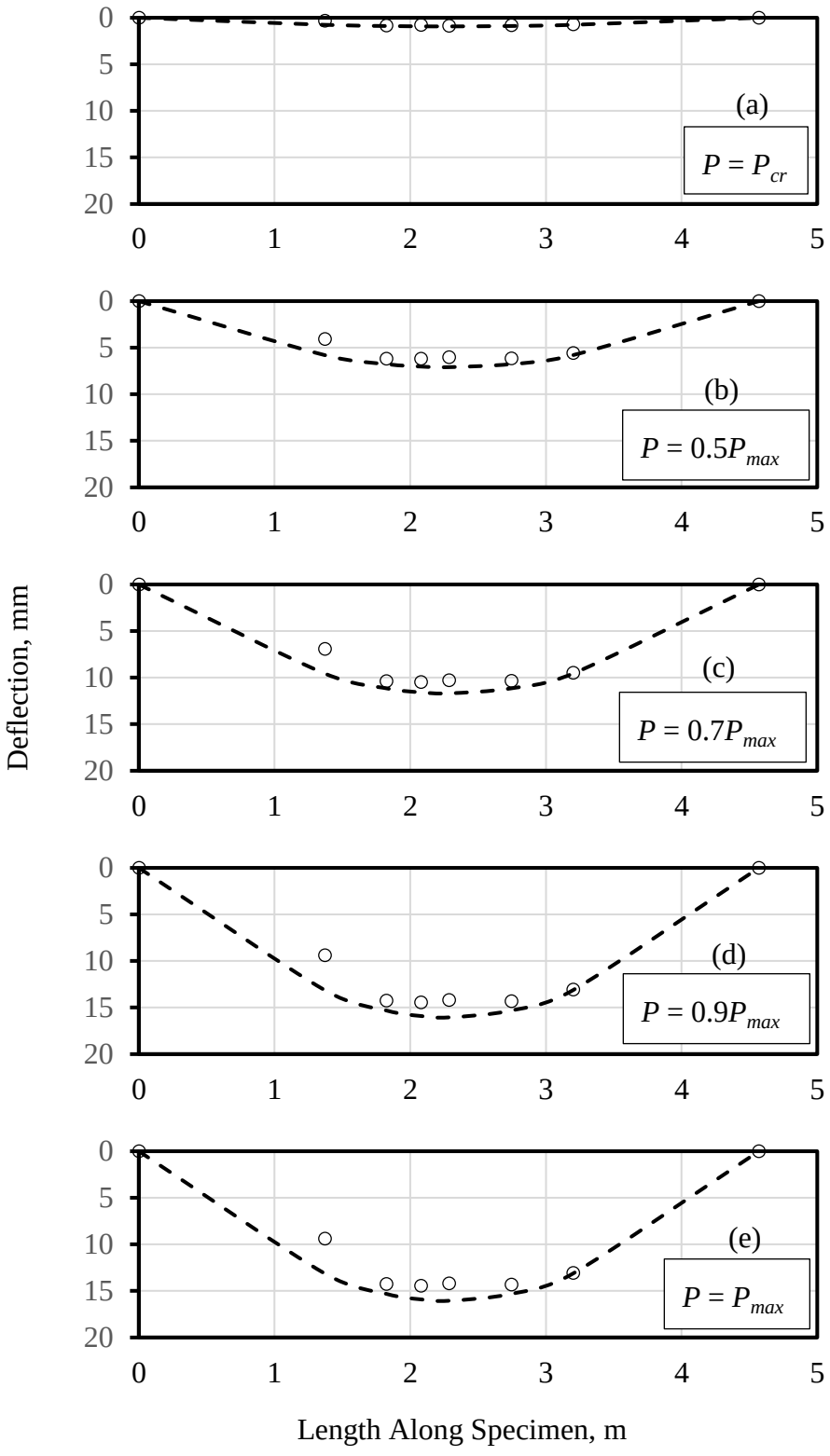

Figure J.8: Deflection Profile at Different Load Levels for Specimen 20■-410↓: (a) $P=P_{cr}$, (b) P=0.5 P_{max}, (c) P= 0.7 P_{max}, (d) P= 0.9 P_{max}, and (e) $P=P_{max}$

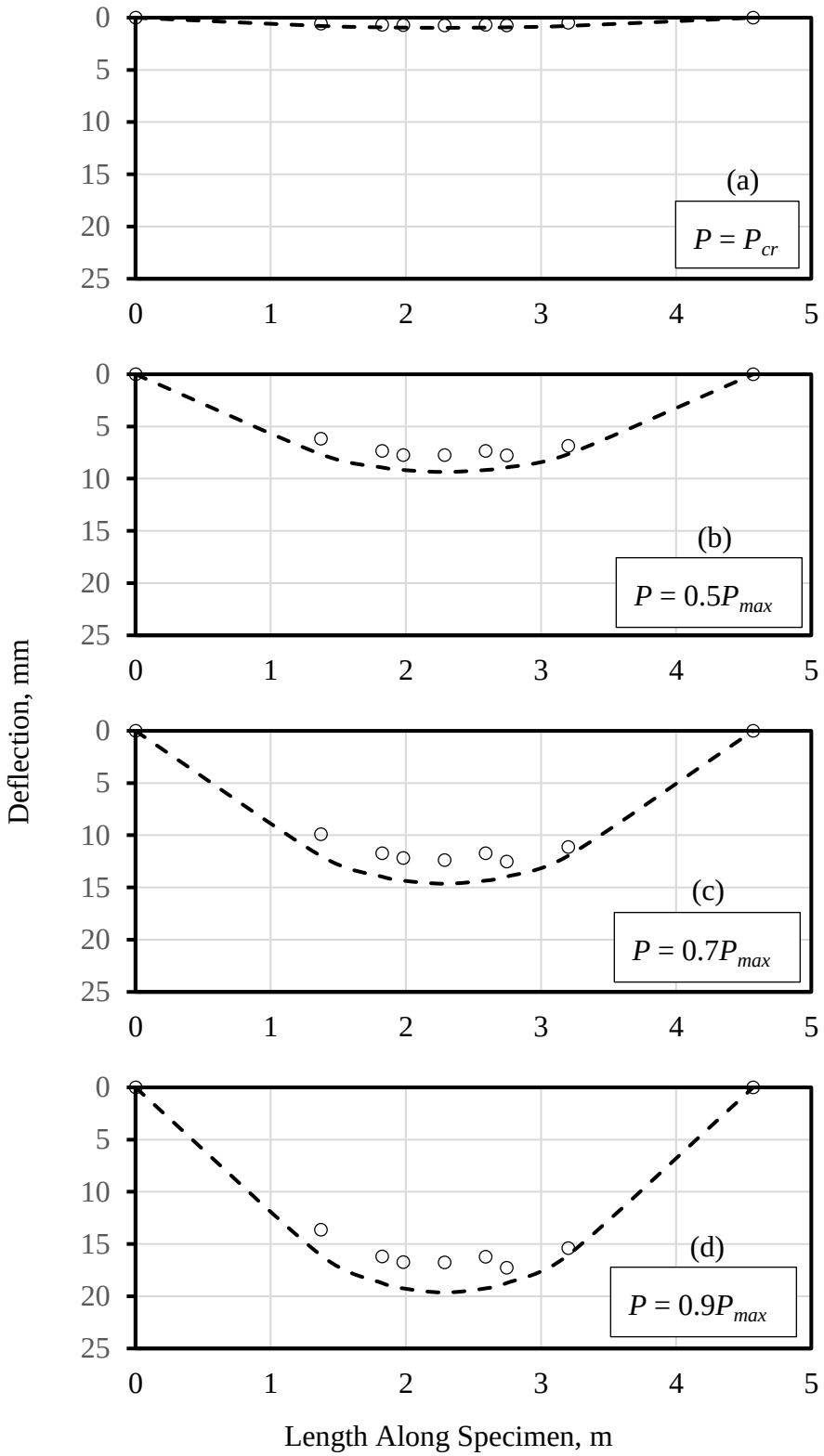

Figure J.9: Deflection Profile at Different Load Levels for Specimen 20■-610↓: (a) $P=P_{cr}$, (b) P=0.5 P_{max}, (c) P= 0.7 P_{max}, and (d) P= 0.9 P_{max}

Appendix K: Concrete Companion Specimens Associated with Splice Specimens Reinforced with Ransome Bars

Five concrete companion cylinders were tested on same day as each associated splice specimens, as explained in Section 3.7. Three of them were tested to measure the concrete compressive strength, whereas the remaining two were tested to measure the tensile strength. Table K.1 presents the compressive strength and tensile strength of cylinders tested in the current experimental program.

Figures K.1 to K.9 show the stress versus strain relationships for the cylinders that were tested in compression. These figures also show the average curve fit equation, obtained by fitting a polynomial regression line with zero intercept to the average stress versus strain curve. Stress versus strain relationships were not reported for the specimens tested by Knight and Feldman (2013).

Table K.1: Companion Concrete Cylinder Properties

Specimen ID	Concrete Cylinder ID[a]	Age at Test Date (days)	Compressive Strength f'_c (MPa)	Tensile Strength f_r (MPa)
19◆-305↓ 19◆-410↓	C-2-21	34	25.2	
	C-2-22		22.3	
	C-2-23		28.6	
	C-2-24			2.03
	C-2-25			2.21
Coefficient of Variation			12.4%	6.00%
19◆-510↓	C-3-1	35	25.2	
	C-3-2		23.7	
	C-3-3		26.2	
	C-3-4			2.40
	C-3-5			2.72
Coefficient of Variation			5.03%	8.84%
19◆-305↑	C-3-6	36	24.2	
	C-3-7		22.5	
	C-3-8		25.3	
	C-3-9			2.12
	C-3-10			2.03
Coefficient of Variation			5.88%	3.07%
19◆-410↑	C-3-11	38	27.1	
	C-3-12		24.8	
	C-3-13		23.8	
	C-3-14			2.47
	C-3-15			2.14
Coefficient of Variation			6.71%	10.1%
19◆-510↑	C-3-16	37	23.3	
	C-3-17		18.6	
	C-3-18		22.9	
	C-3-19			2.52
	C-3-20			1.92
Coefficient of Variation			12.1%	19.1%
32◆-410↓	C-3-21	29	22.6	
	C-3-22		25.6	
	C-3-23		23.4	
	C-3-24			2.61
	C-3-25			2.14
Coefficient of Variation			6.51%	14.0%

Table K.1 Cont'd: Companion Concrete Cylinder Properties

Specimen ID	Concrete Cylinder ID[a]	Age at Test Date (days)	Compressive Strength f'_c(MPa)	Tensile Strength (MPa)
32◆-610↓	C-3-26	28	23.8	
	C-3-27		24.1	
	C-3-28		22.3	
	C-3-29			2.63
	C-3-30			2.16
Coefficient of Variation			4.12%	13.9%
32◆-810↓ 32◆-810↑	C-4-1	30	22.9	
	C-4-2		19.6	
	C-4-3		22.2	2.28
	C-4-4			2.27
	C-4-5			
Coefficient of Variation			8.06%	0.31%
32◆-410↑ 32◆-610↑	C-4-6	31	21.3	
	C-4-7		22.4	
	C-4-8		23.0	
	C-4-9			2.40
	C-4-10			2.14
Coefficient of Variation			3.88%	8.10%

[a] "C" in the concrete cylinder ID refers to concrete, the first number refers to concrete batch number and final number following the second hyphen refers to cylinder serial number.

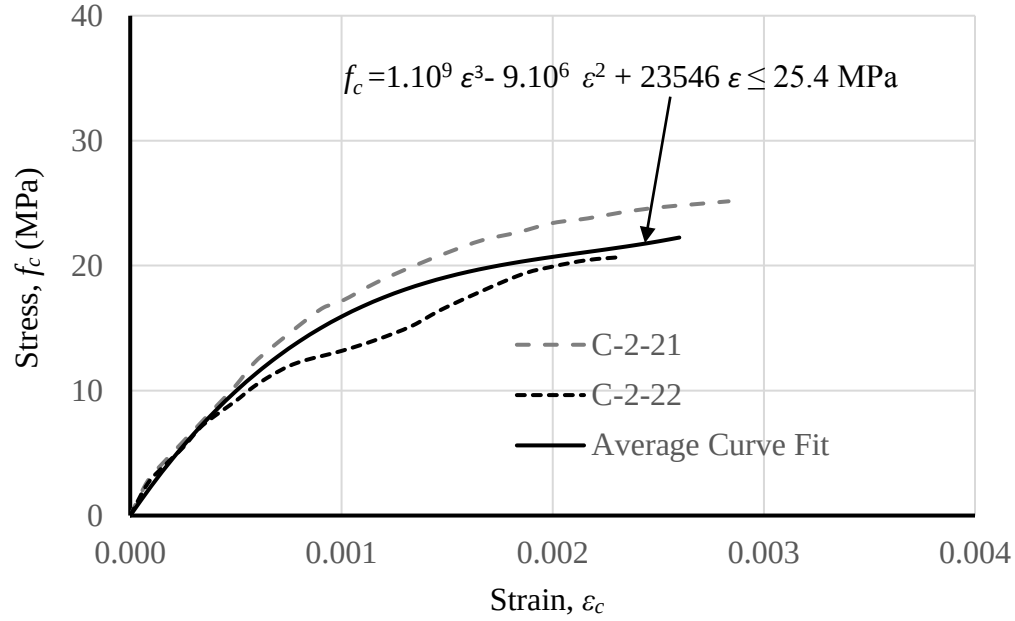

Figure K.1: Stress-Strain Relationship of Concrete Companion Specimen Associated with Specimen 19◆-305↓ and 19◆-410↓

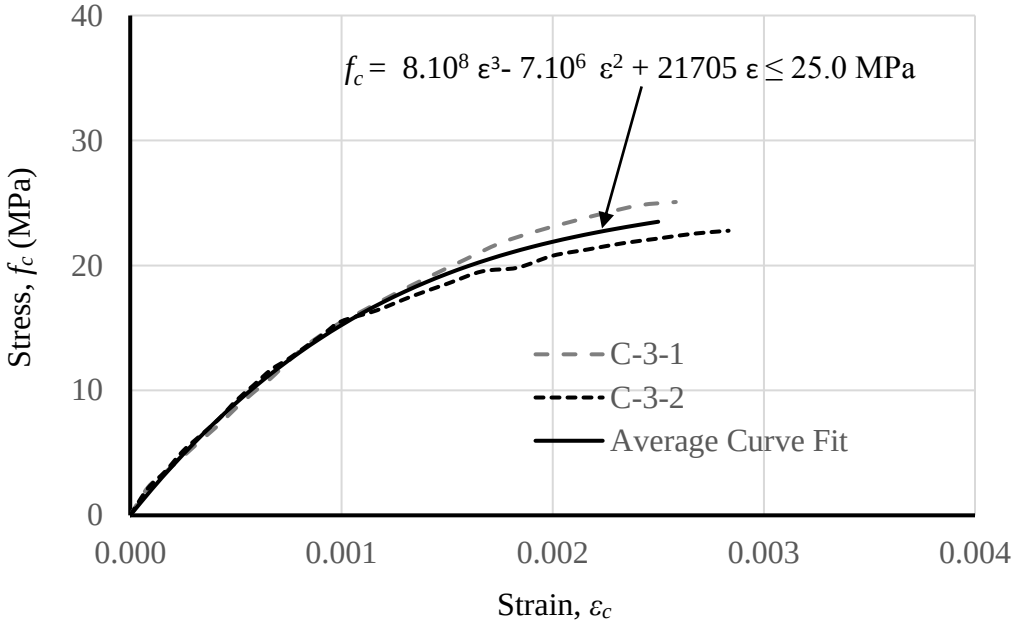

Figure K.2: Stress-Strain Relationship of Concrete Companion Specimen Associated with Specimen 19◆-510↓

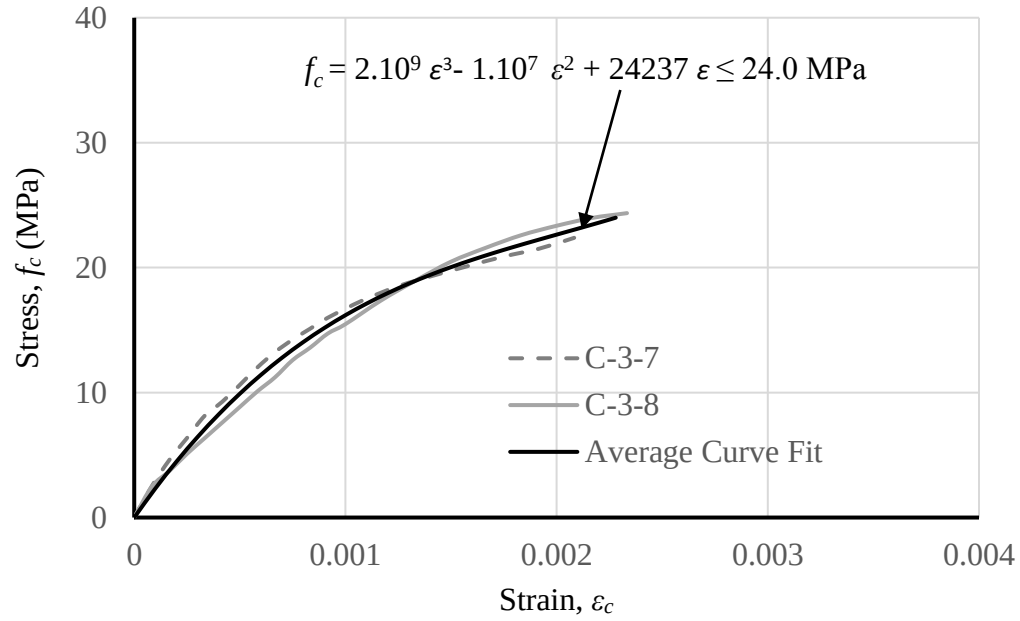

Figure K.3: Stress-Strain Relationship of Concrete Companion Specimen Associated with Specimen 19◆-305↑

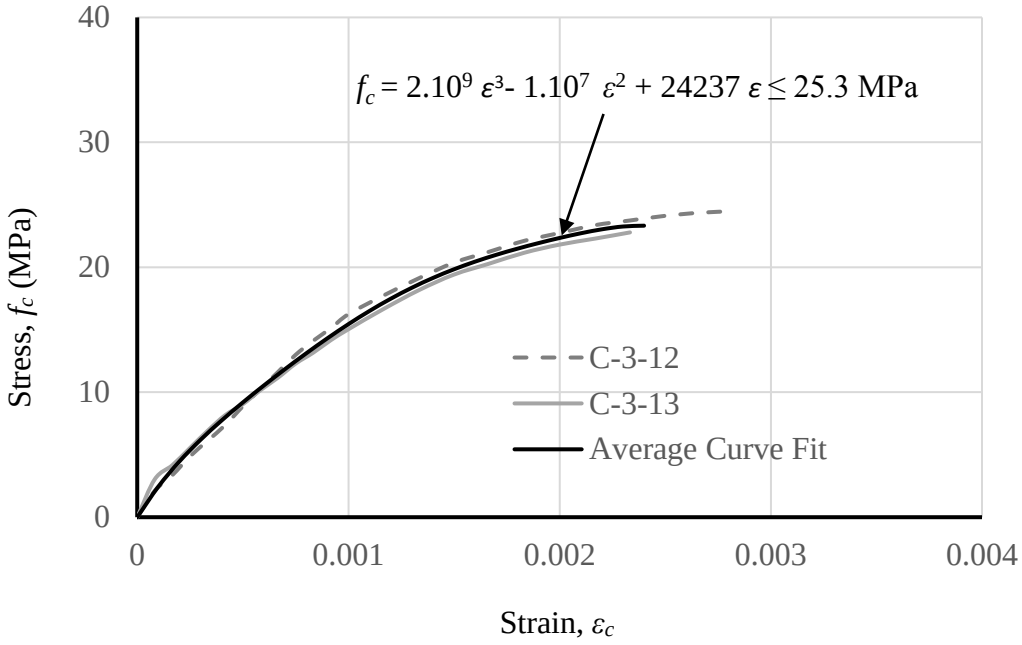

Figure K.4: Stress-Strain Relationship of Concrete Companion Specimen Associated with Specimen 19◆-410↑

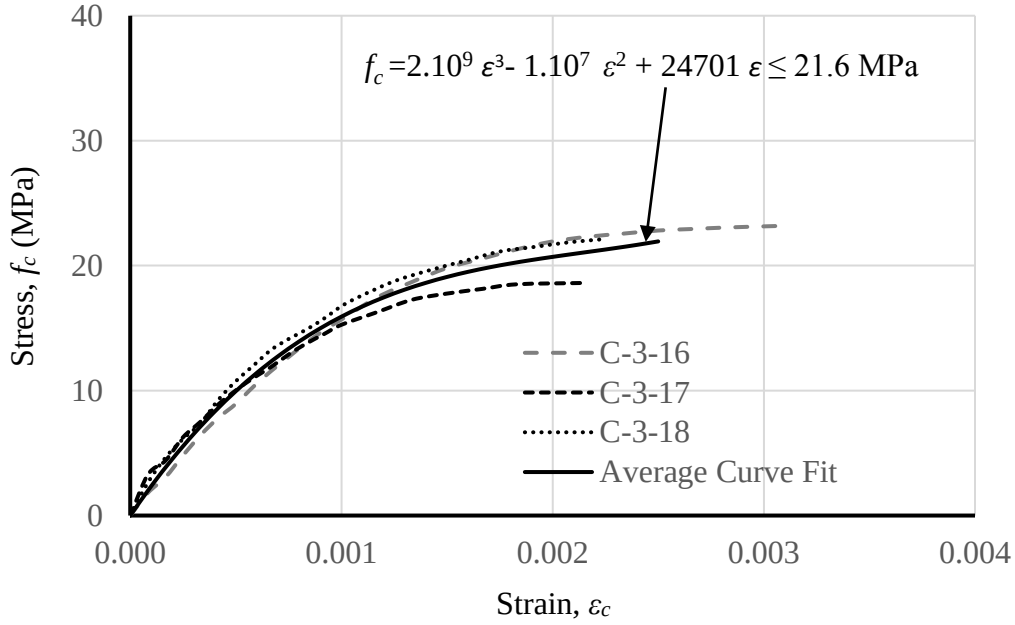

Figure K.5: Stress-Strain relationship of Concrete Companion Specimen associated with Specimen 19◆-510↑

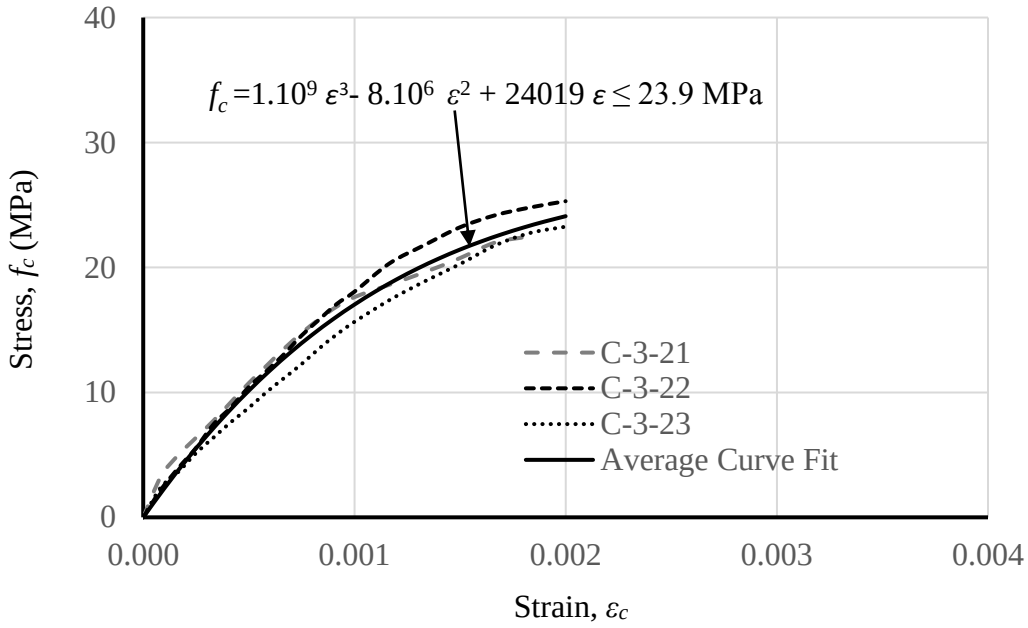

Figure K.6: Stress-Strain relationship of Concrete Companion Specimen associated with Specimen 32◆-410↓

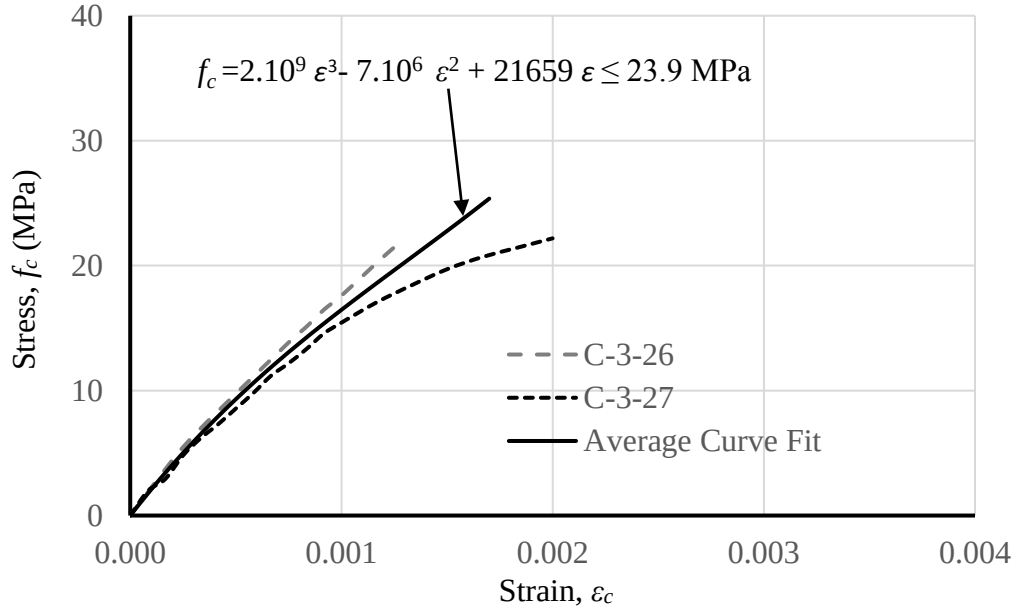

Figure K.7: Stress-Strain relationship of Concrete Companion Specimen associated with Specimen 32◆-610↓

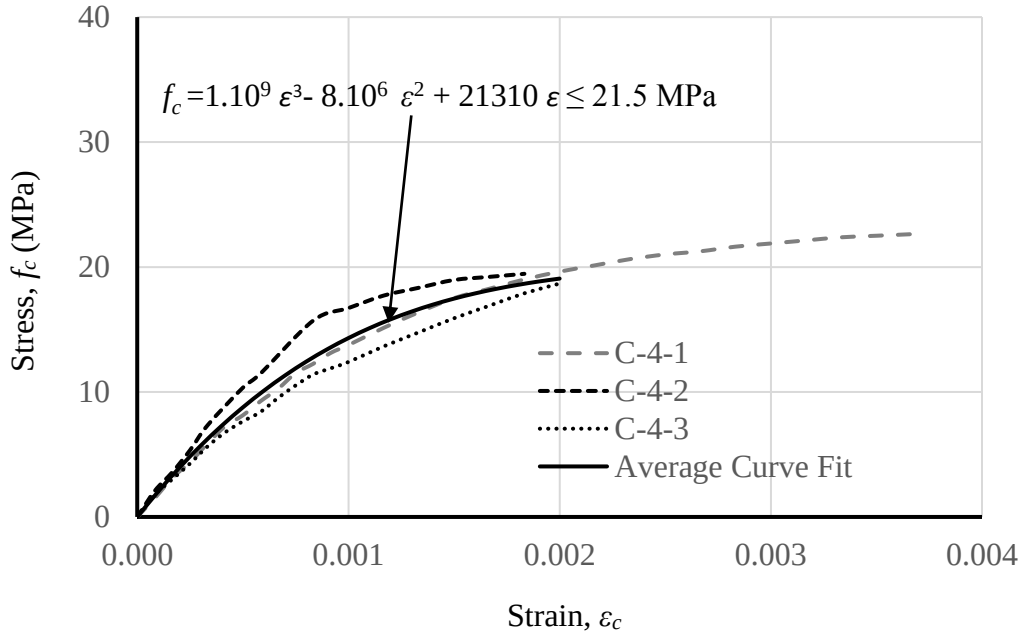

Figure K.8: Stress-Strain Relationship of Concrete Companion Specimen Associated with Specimen 32◆-810↓ and 32◆-810↑

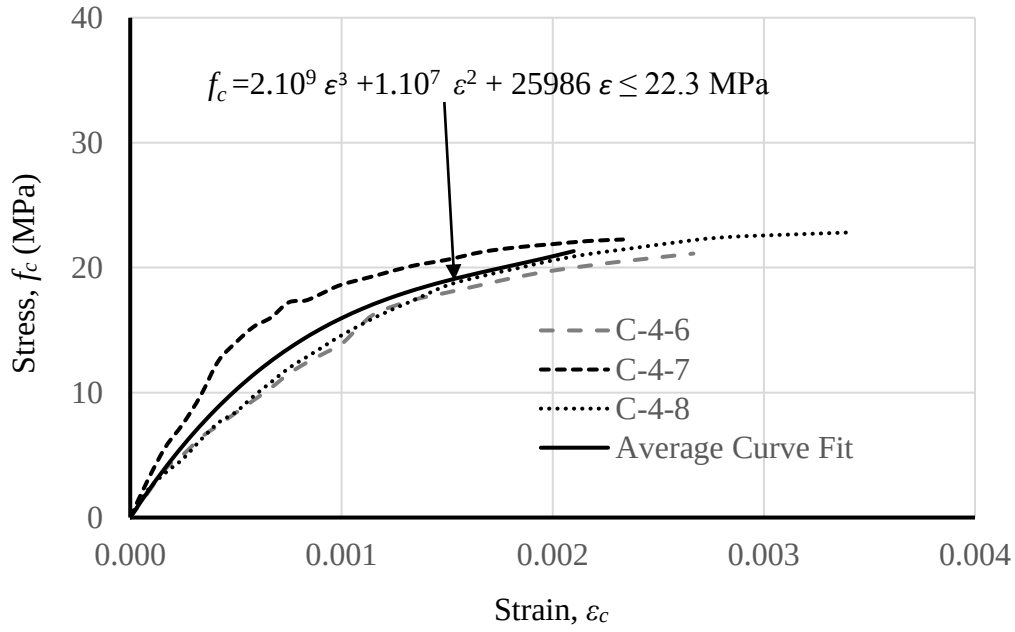

Figure K.9: Stress-Strain Relationship of Concrete Companion Specimen Associated with Specimen 32◆-410↑ and 32◆-610↑

Appendix L: Properties of the Longitudinal Ransome Bars

Three tensile test specimens for 32 mm bars for each heat batch were machined and tested, as explained in Section 3.7.3. Similarly, six tensile specimens were tested for each heat batch and each size of the reinforcement for 19 and 25 mm bars, where three of them were intact bar lengths, and the remaining three of them were machined coupon as explained in Section 3.7.3. Table L.1 shows the dynamic yield strength, static yield strength, and modulus of elasticity for each tensile specimen tested in the current investigation. Figures L.1 to L.4 present the stress versus strain relationships obtained from the tensile tests.

Table L.1: Properties of Plain Longitudinal Reinforcement

Associated Splice Specimen ID	Steel Specimen ID[a]	Dynamic Yield Strength f_{yd} (MPa)	Static Yield Strength f_{ys} (MPa)	Ultimate Strength f_u (MPa)	Modulus of Elasticity, E_s (GPa)
19◆-305↓, 19◆-410↓, 19◆-510↓, 19◆-305↑, 19◆-410↑, 19◆-510↑	S19◆I-1-1	514	477[c]	597	75.6
	S19◆I-1-2	503	466[c]	604	143
	S19◆I-1-3	490	460	605	103
	S19◆C-1-1	n/a[b]	n/a[b]	637	n/a
	S19◆C-1-2	n/a[b]	n/a[b]	636	n/a
	S19◆C-1-3	523	484[c]	629	196
Coefficient of Variation		2.81%	2.29%	2.91%	40.4%
25◆-410↓, 25◆-510↓, 25◆-610↓, 25◆-410↑, 25◆-510↑, 25◆-610↑	S25◆I-1-1	466	438	622	90.5
	S25◆I-1-2	488	460	619	119
	S25◆I-1-3	464	n/a	n/a	134
	S25◆C-1-1	n/a	n/a	621	n/a
	S25◆C-1-2	n/a	n/a	625	n/a
	S25◆C-1-3	477	448	637	208
Coefficient of Variation		2.34%	2.46%	1.15%	36.3%
32◆-410↓, 32◆-610↓, 32◆-810↓, 32◆-410↑	S32◆C-1-1	489	461	614	219
	S32◆C-1-2	488	457	607	206
	S32◆C-1-3	477	449	608	217
Coefficient of Variation		1.37%	1.34%	0.62%	3.27%
32◆-610↑, 32◆-810↑	S32◆C-2-1	512	484	637	233
	S32◆C-2-2	519	491	642	234
	S32◆C-2-3	521	493	640	277
Coefficient of Variation		0.91%	0.97%	0.39%	10.1%

[a] The first letter in the steel specimen ID, S, refers to steel, the first number refers to the size of the longitudinal reinforcing bars (i.e. side face dimension), and diamond shape (◆) refers to the fact that a Ransome bar was used. The letter I represents that tensile specimens were tested as intact bar lengths, whereas the letter C represents that machined coupons were tested. The second number represents the heat batch number, whereas the third number represents the replicate number within the test series.

[b] Strain response from the laser extensometer had a lot of noise

[c] Strain rate slightly exceeded the upper bound limit as discussed in Section 4.2.2

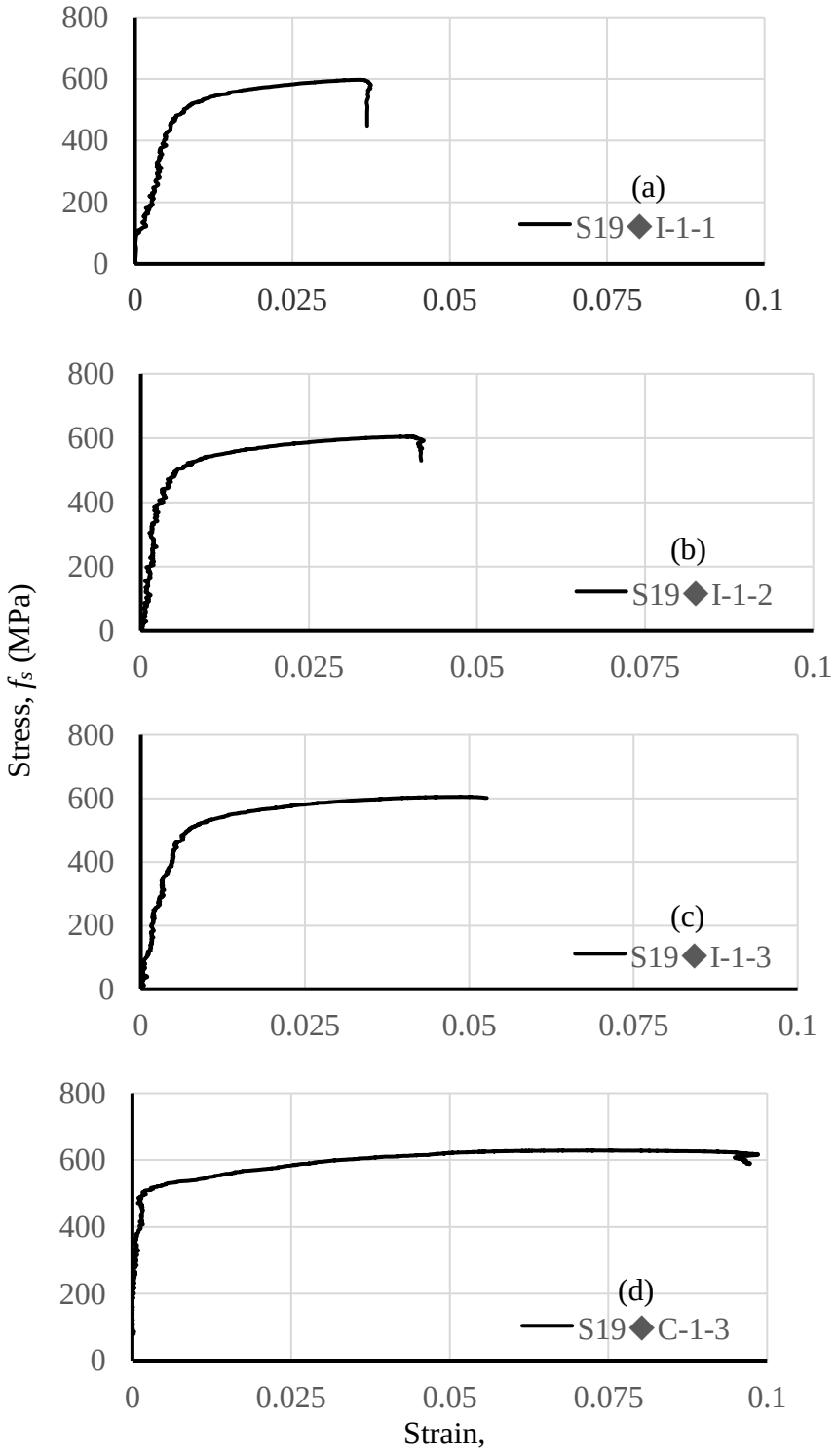

Figure L.1: Stress Versus Strain for 19mm Ransome Bar: (a) S19◆F1-1, (b) S19◆F1-2, (c) S19◆F1-3, and (d) S19◆C1-3

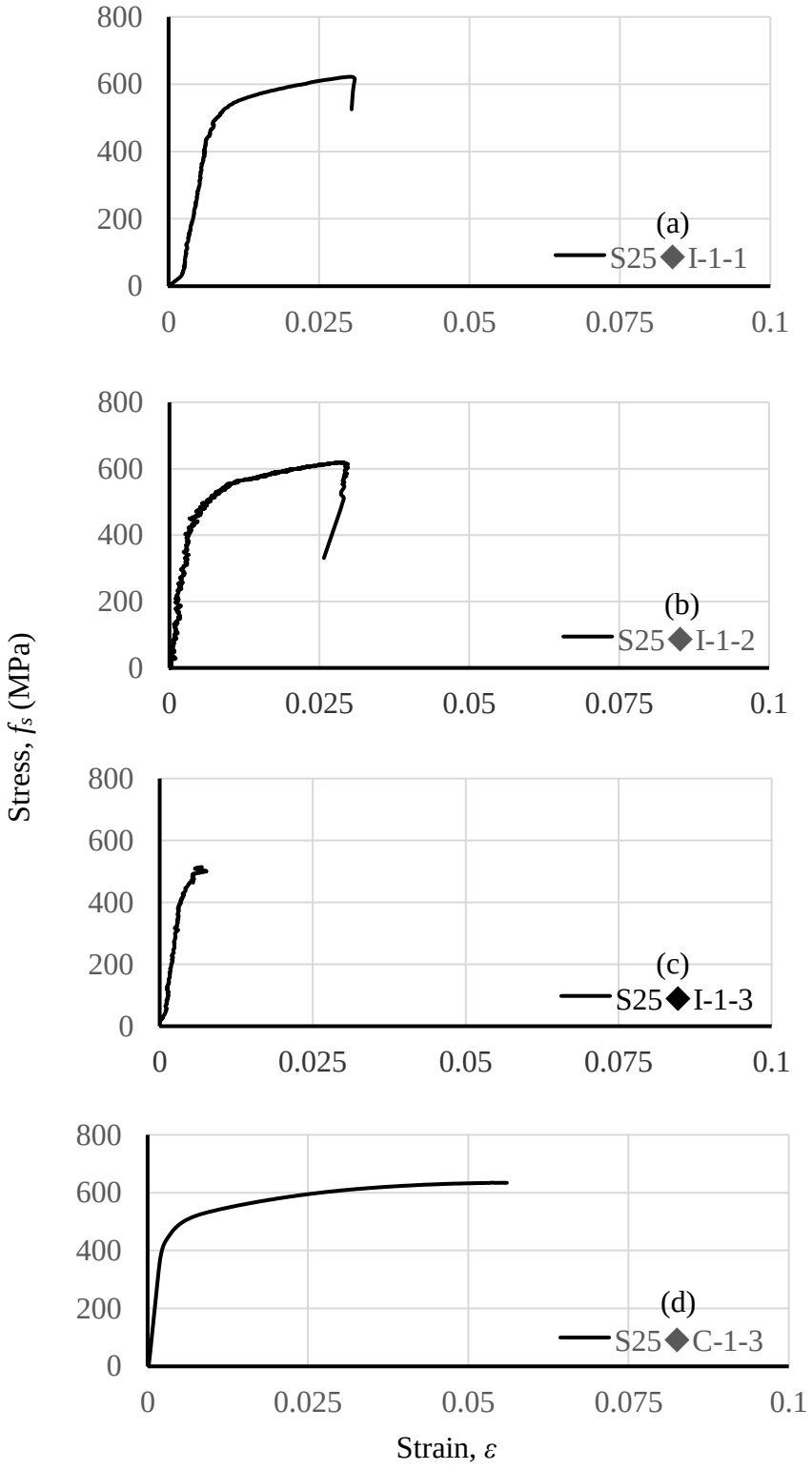

Figure L.2: Stress Versus Strain for 25mm Ransome Bar: (a) S25◆F1-1, (b) S25◆F1-2, (c) S25◆F1-3, and (e) S25◆C1-3

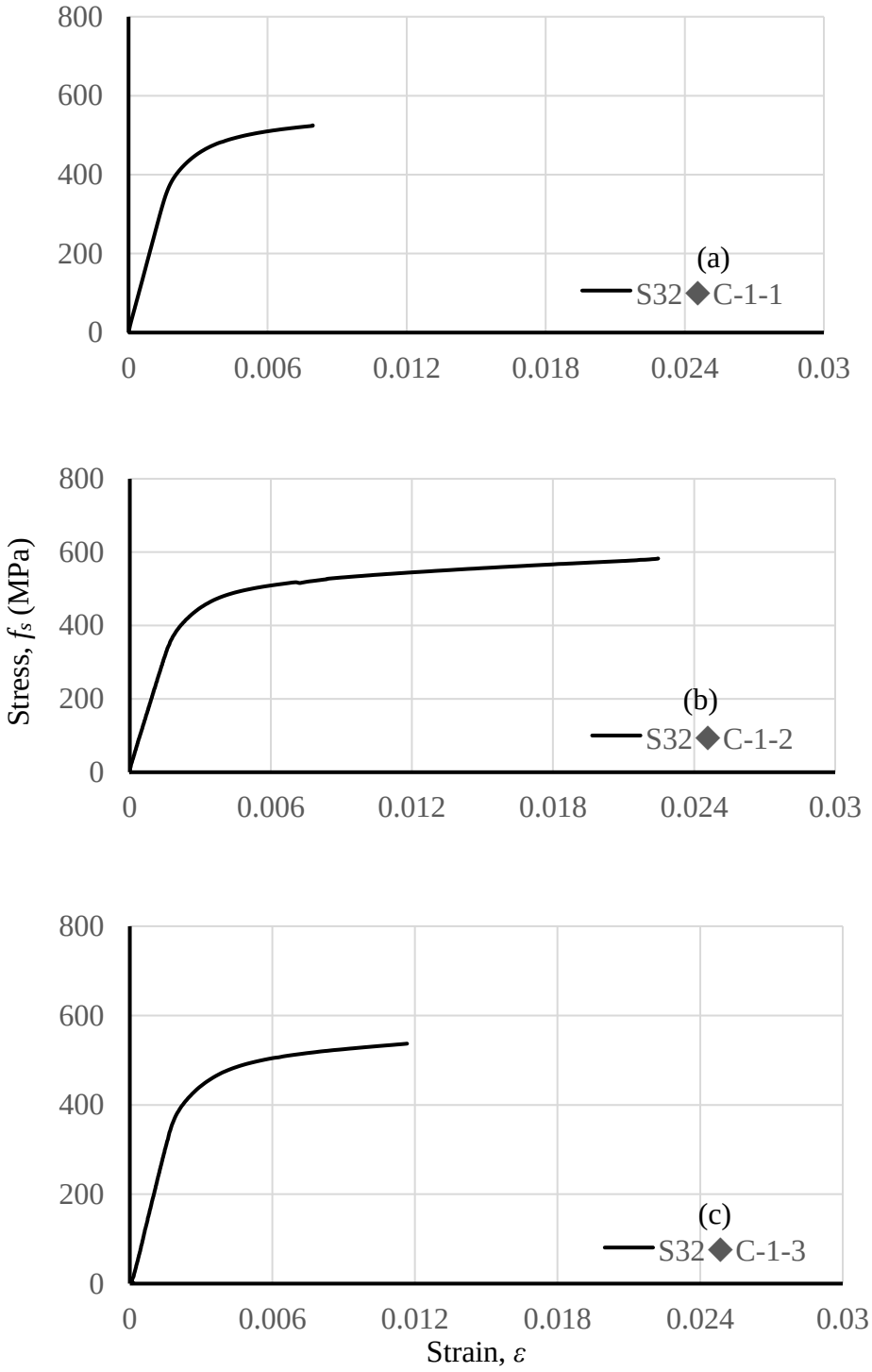

Figure L.3: Stress Versus Strain for 32mm Ransome Bar (Batch One): (a) S32◆C1-1, (b) S32◆C1-2, and (c) S32◆C1-3

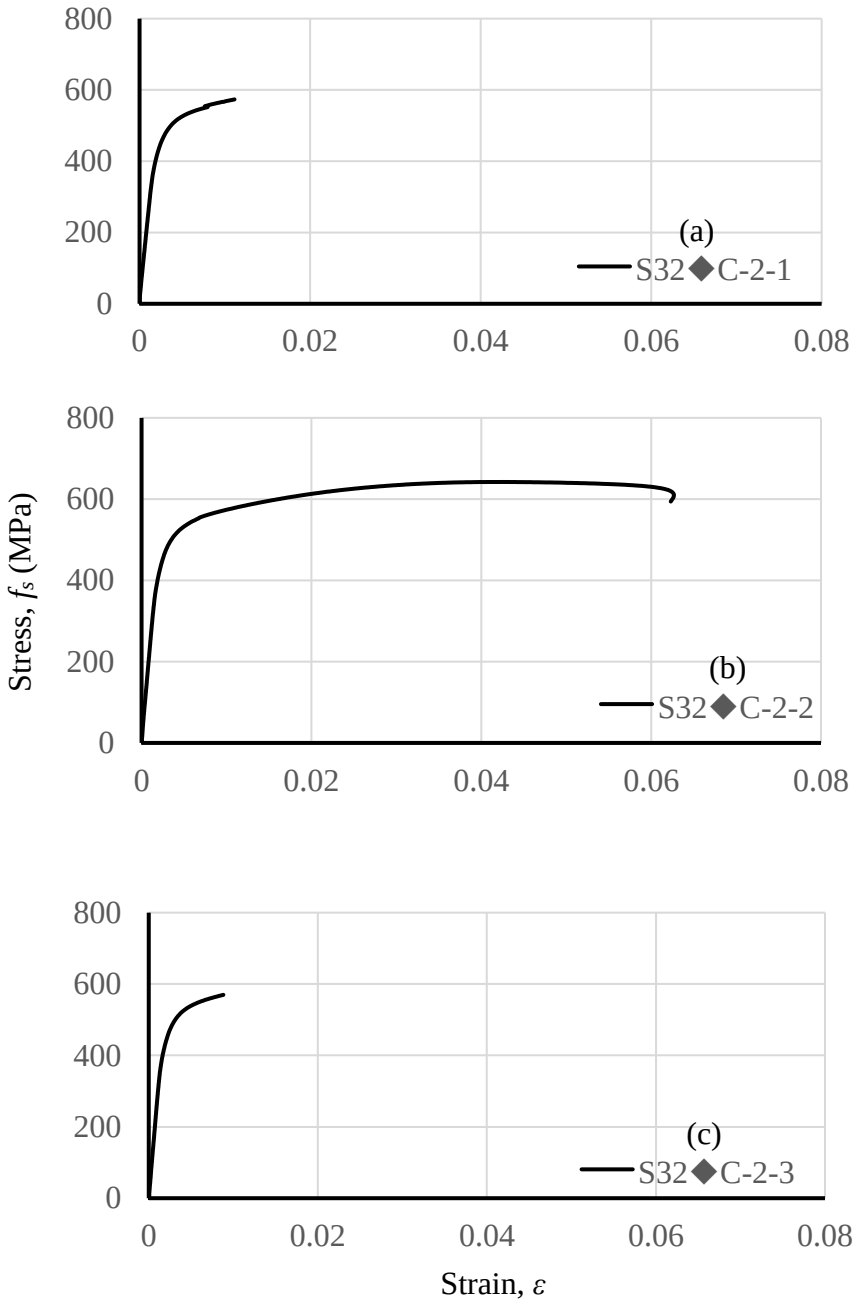

(c)

Figure L.4: Stress Versus Strain for 19mm Plain Round Bar: (a) S32◆C2-1, (b) S32◆C2-2, and (c) S32◆C2-3

Appendix M: Observed Crack Pattern of the Splice Specimens Reinforced with Ransome Bars

Cracks were marked as tests of the splice specimens progressed. Figures M.1 to M.8 show the observed crack patterns of the splice specimens reinforced with Ransome bars during testing. Crack patterns are shown from the lowest to highest load levels in which new cracks were evident. Crack patterns were not reported for the specimens tested by Knight and Feldman (2013).

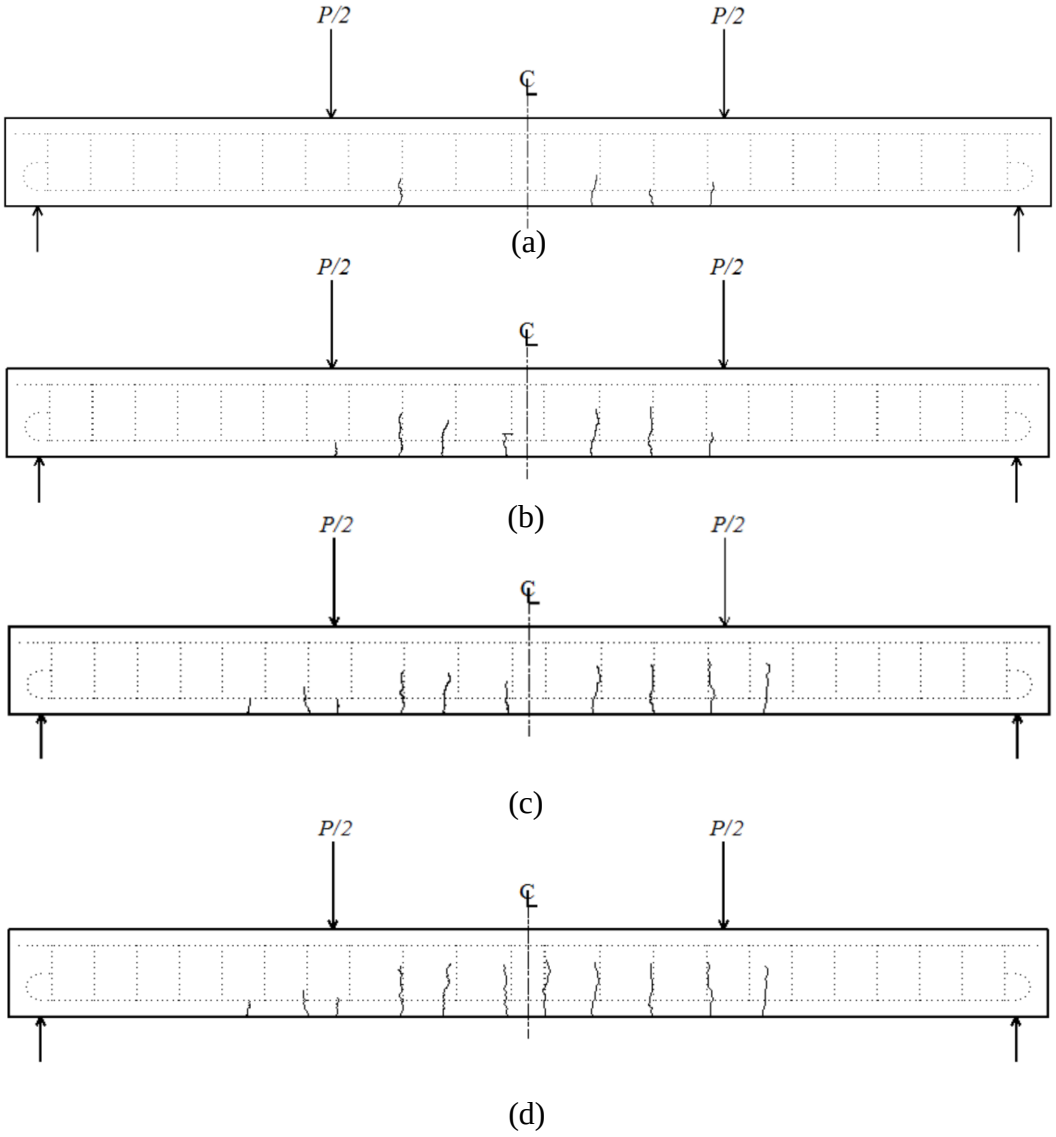

Figure M.1: Crack Pattern for Specimen 19◆-305↓: (a) P=0.5 P_{max}, (b) P=0.7 P_{max}, (c) P=0.9 P_{max}, and (d) P=P_{max}

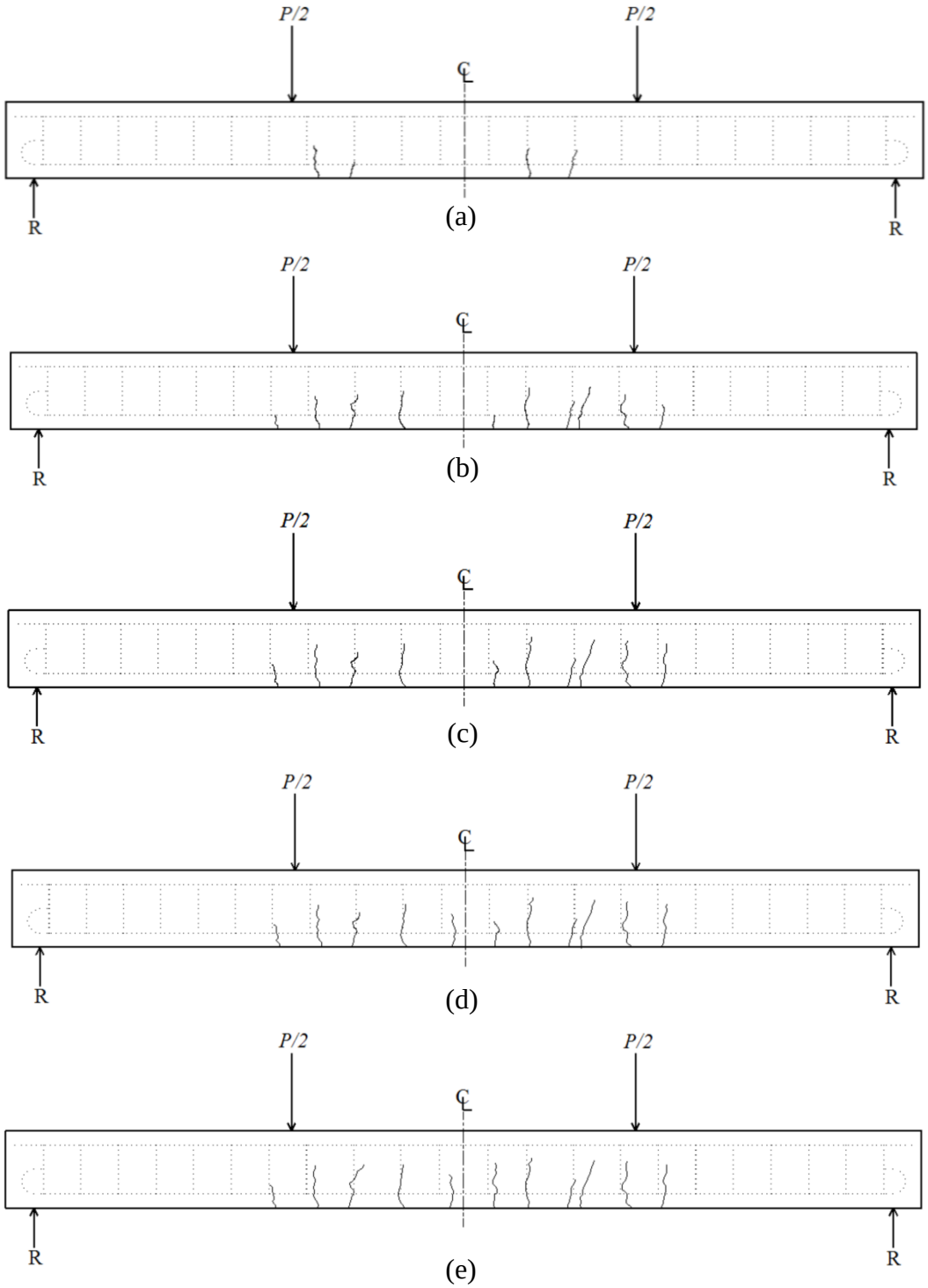

Figure M.2: Crack Pattern for Specimen 19◆-510↓: (a) P=0.4 P_{max}, (b) P=0.6 P_{max}, (c) P=0.8 P_{max}, (d) P= 0.9 P_{max}, and (d) P=P_{max}

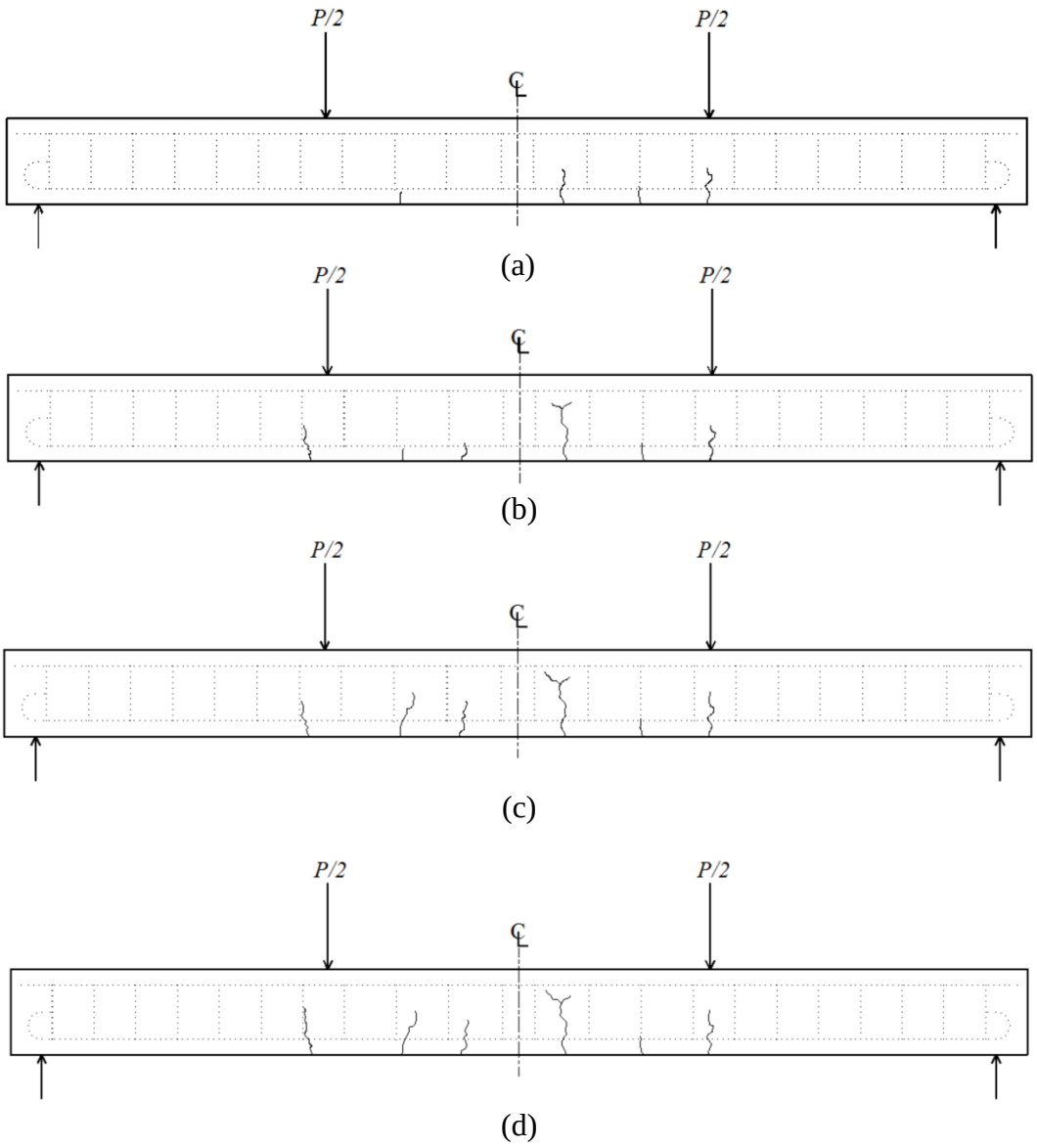

Figure M.3: Crack Pattern for Specimen 19◆-305↑: (a) P=0.65 P_{max}, (b) P=0.75 P_{max}, (c) P=0.9 P_{max}, and (d) P=P_{max}

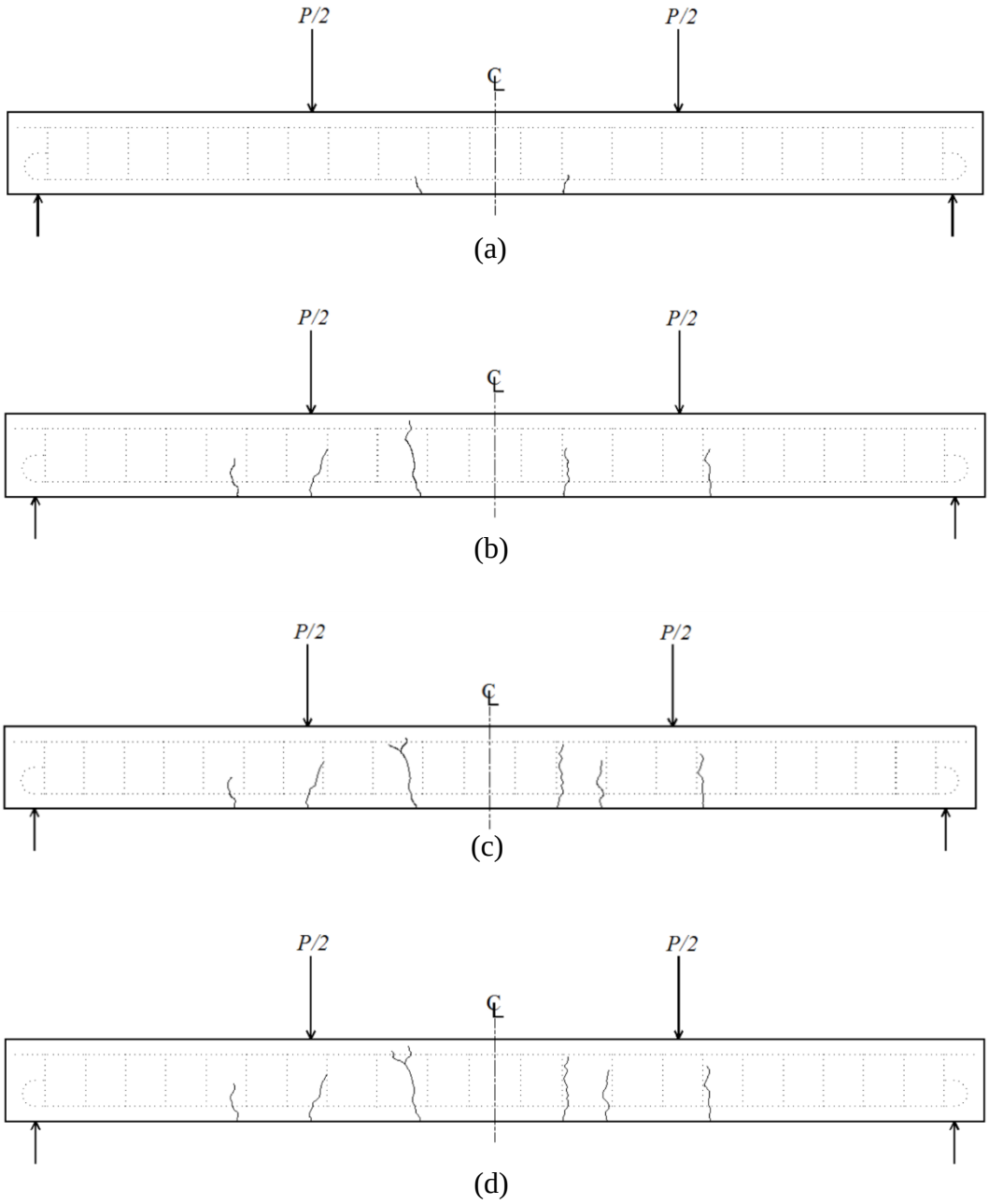

Figure M.4: Crack Pattern for Specimen 19◆-510↑: (a) P=0.4 P_{max}, (b) P=0.6 P_{max}, (c) P=0.8 P_{max}, and (d) P=P_{max}

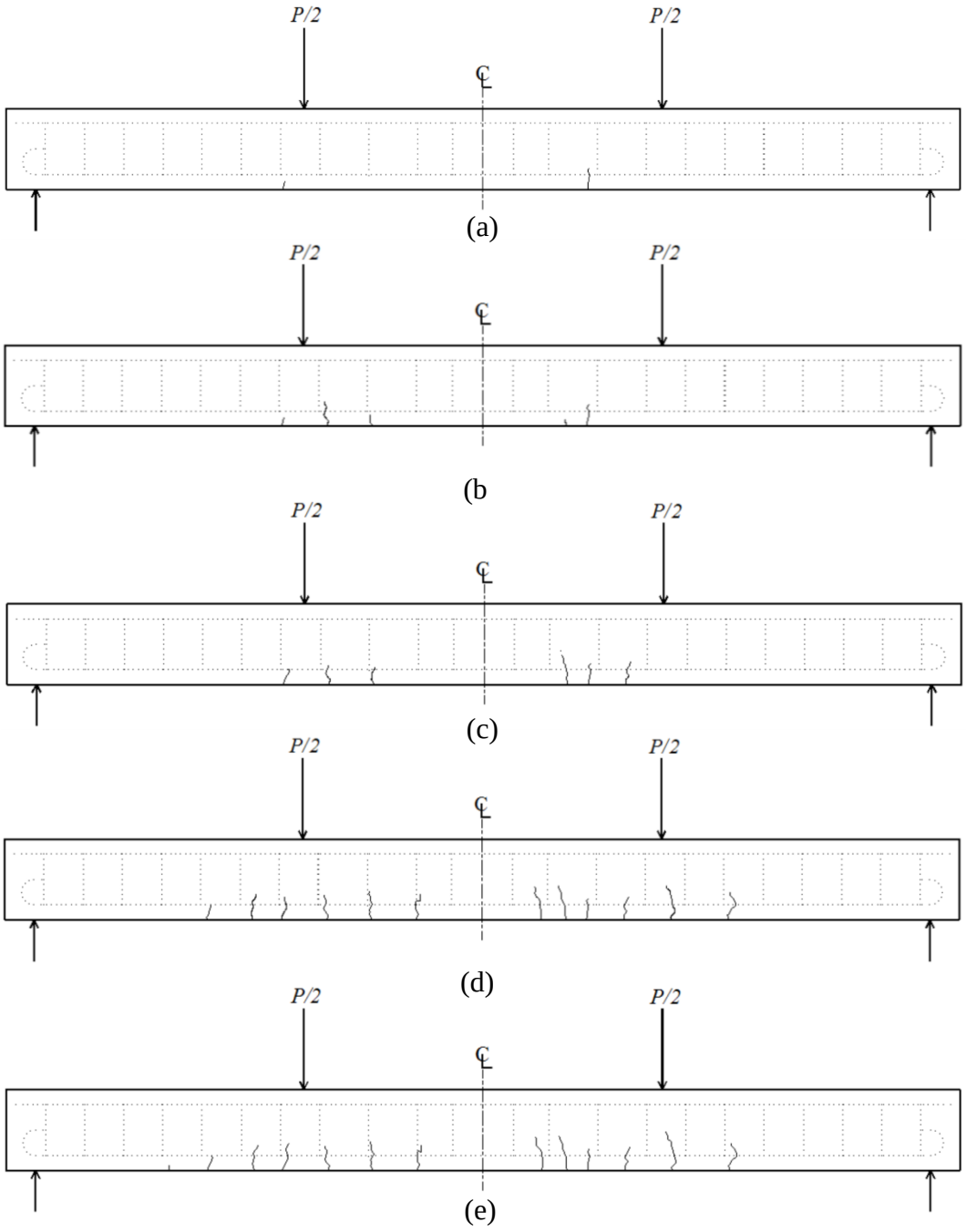

Figure M.5: Crack Pattern for Specimen 32◆-610↓: (a) P=0.35 P_{max}, (b) P=0.5 P_{max}, (c) P=0.7 P_{max}, (d) P= 0.9 P_{max}, and (e) P=P_{max}

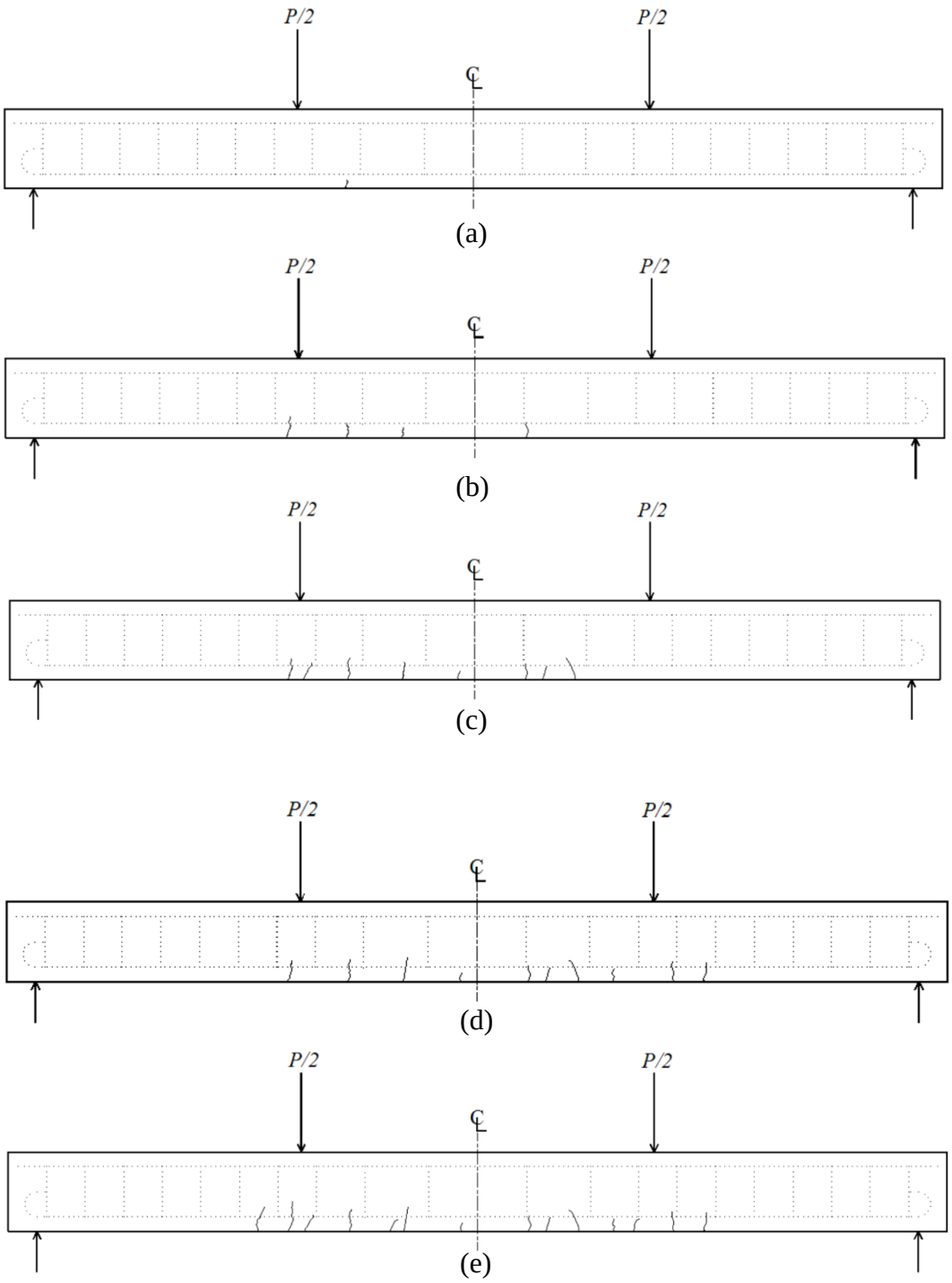

Figure M.6: Crack Pattern for Specimen 32◆-810↓: (a) P=0.4 P_{max}, (b) P=0.6 P_{max}, (c) P=0.8 P_{max}, (d) P= 0.9 P_{max}, and (e) P=P_{max}

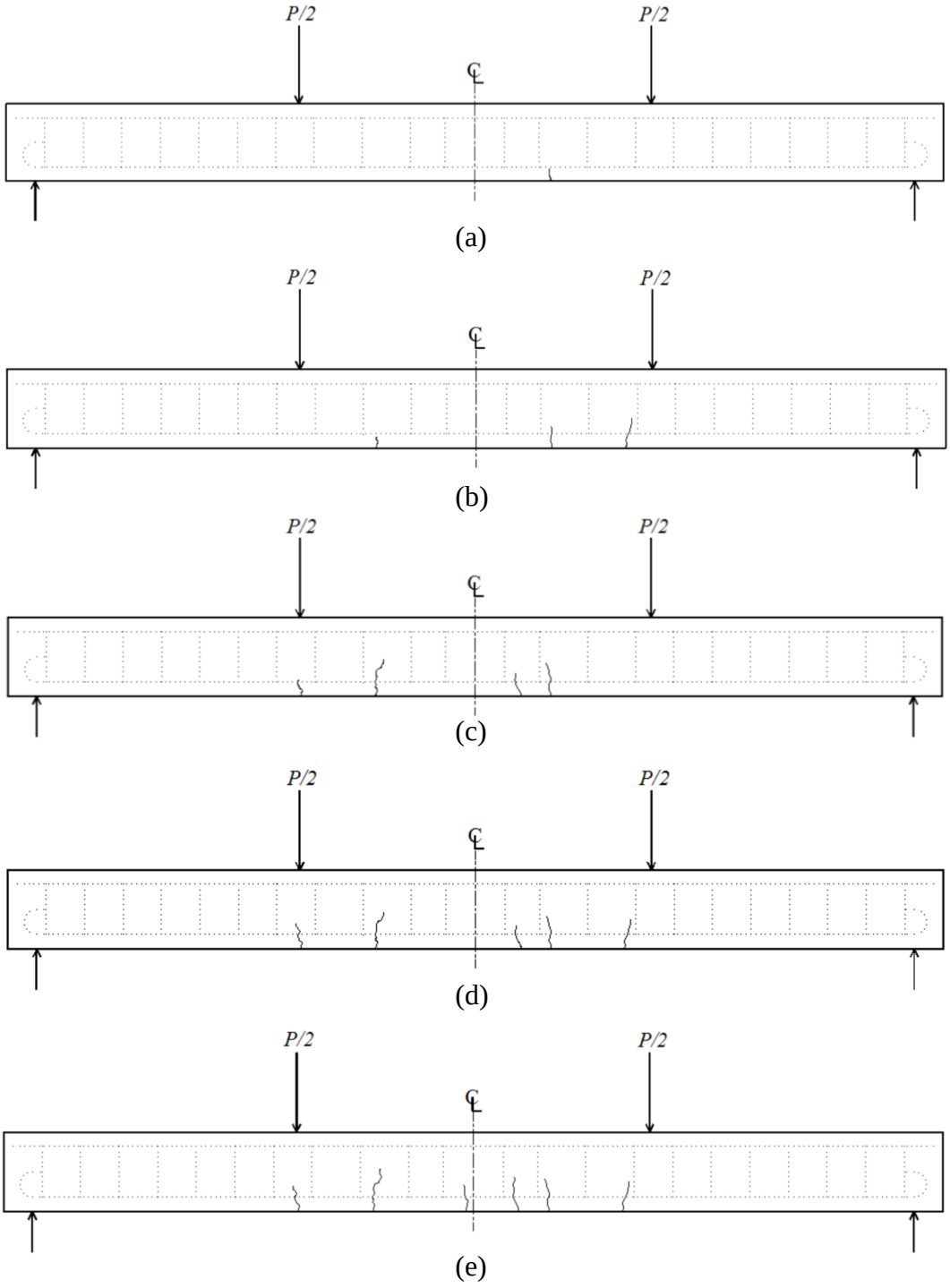

Figure M.7: Crack Pattern for Specimen 32◆-610↑: (a) P=0.45 P_{max}, (b) P=0.65 P_{max}, (c) P=0.8 P_{max}, (d) P=0.9 P_{max}, and (e) P=P_{max}

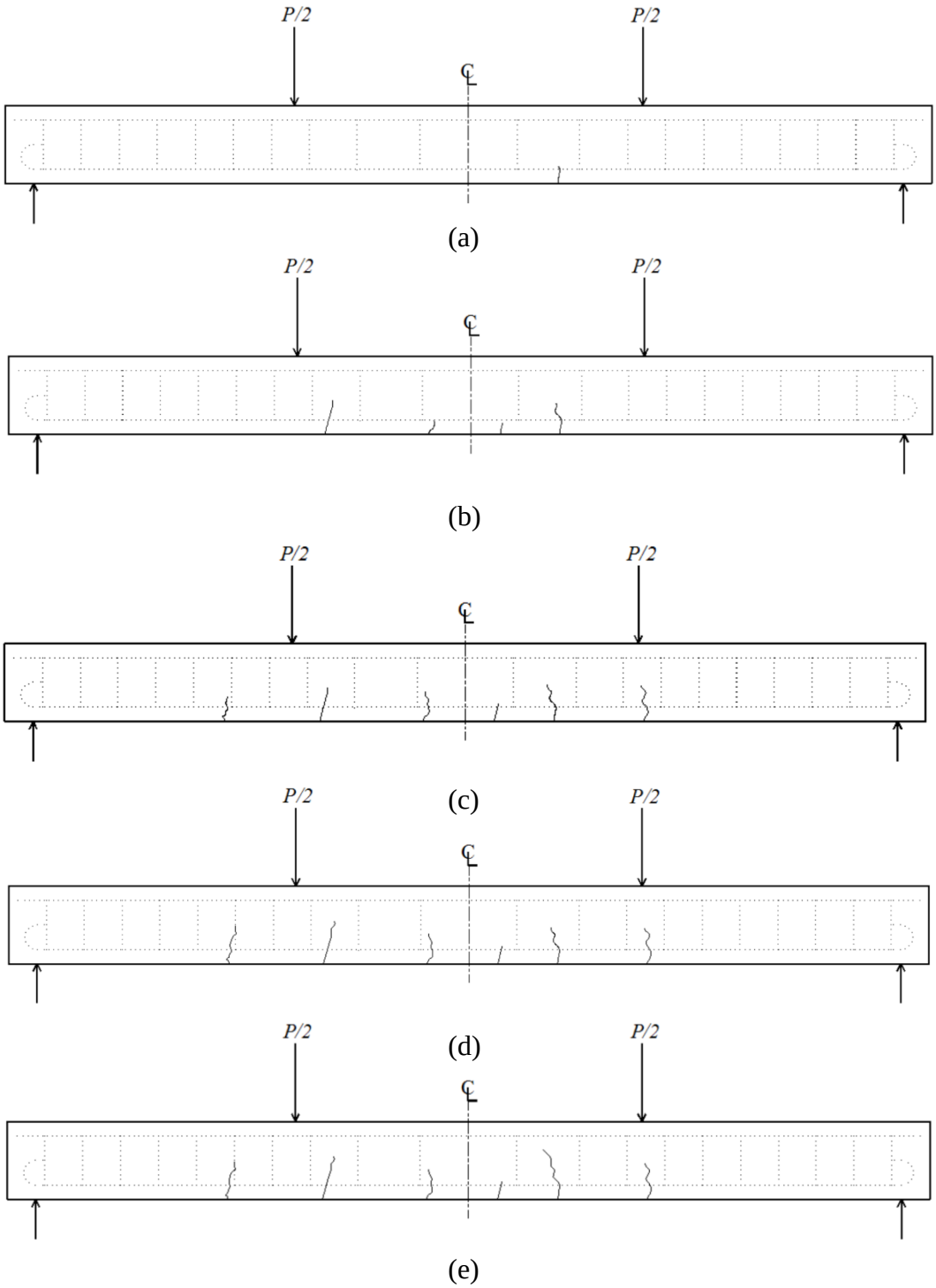

Figure M.8: Crack Pattern for Specimen 32◆-810↑: (a) P=0.35 P_{max}, (b) P=0.5 P_{max}, (c) P=0.7 P_{max}, (d) P=0.9 P_{max}, and (e) P=P_{max}

Appendix N: Observed End-Slip of the Longitudinal Reinforcement for Specimens Reinforced with Ransome Bars

The concrete surrounding the spliced longitudinal reinforcement was removed after testing to observe whether there was a slip of the longitudinal reinforcement or not, as explained in Section 5.3.2. Figures N.1 to N.6 show the observed end-slip of the reinforcement in the specimens tested by Knight and Feldman (2013).

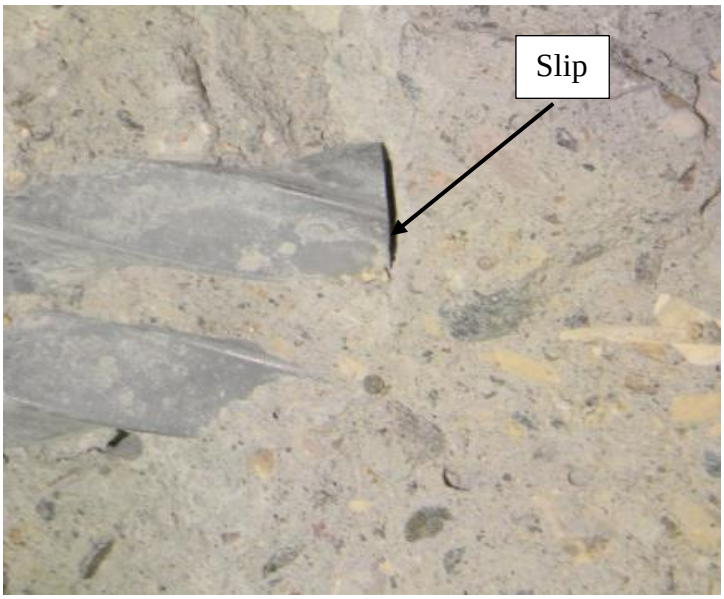

Figure N.1: End Slip of Longitudinal Reinforcement Following Concrete Removal for Specimen 25◆-410↓

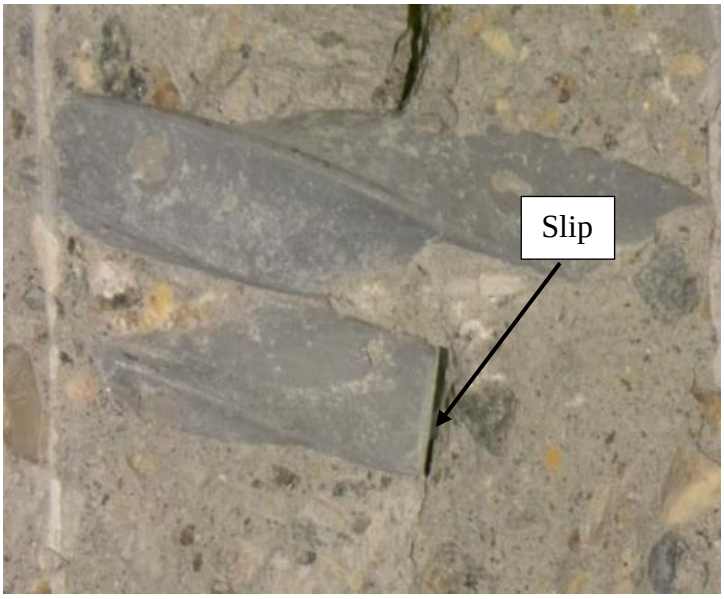

Figure N.2: End Slip of Longitudinal Reinforcement Following Concrete Removal for Specimen 25◆-510↓

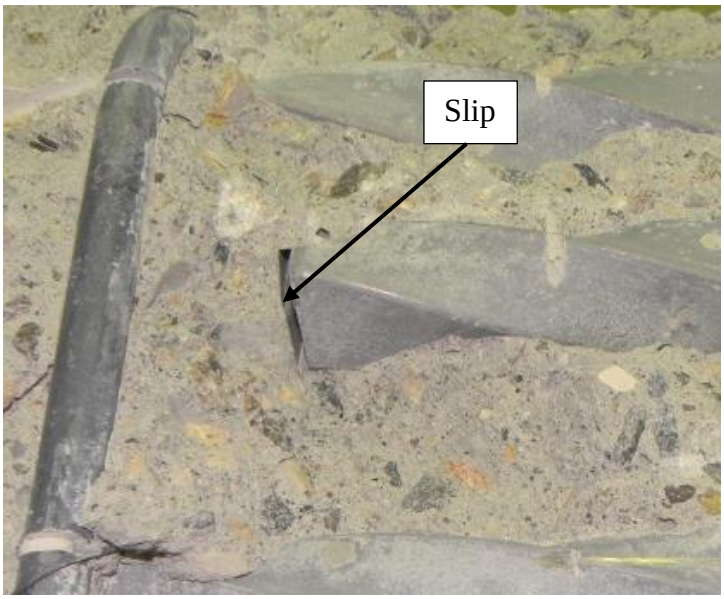

Figure N.3: End Slip of Longitudinal Reinforcement Following Concrete Removal for Specimen 25◆-610↓

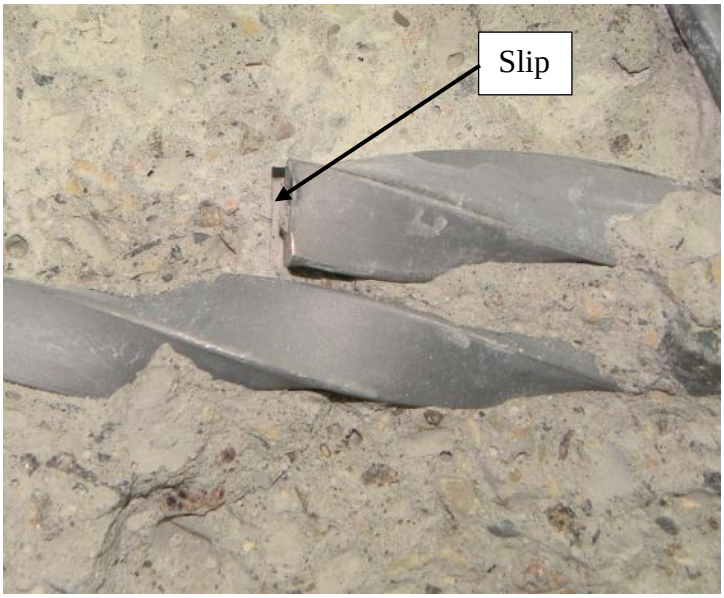

Figure N.4: End Slip of Longitudinal Reinforcement Following Concrete Removal for Specimen 25◆-410↑

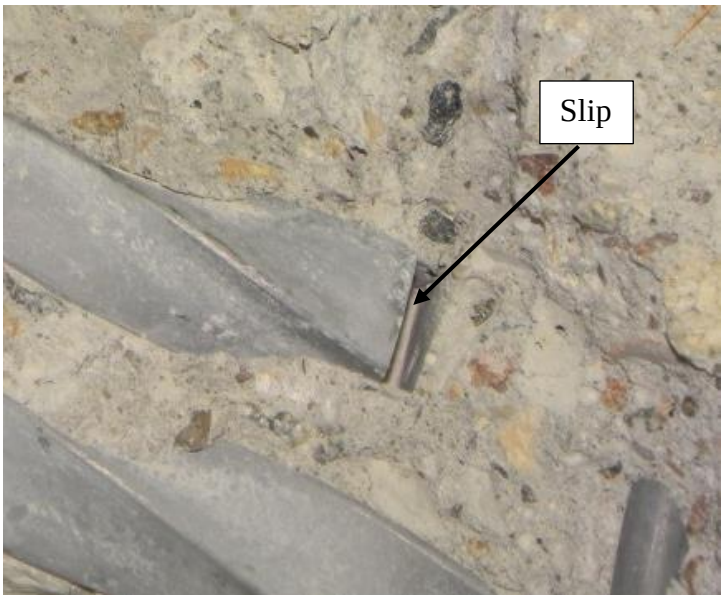

Figure N.5: End Slip of Longitudinal Reinforcement Following Concrete Removal for Specimen 25◆-510↑

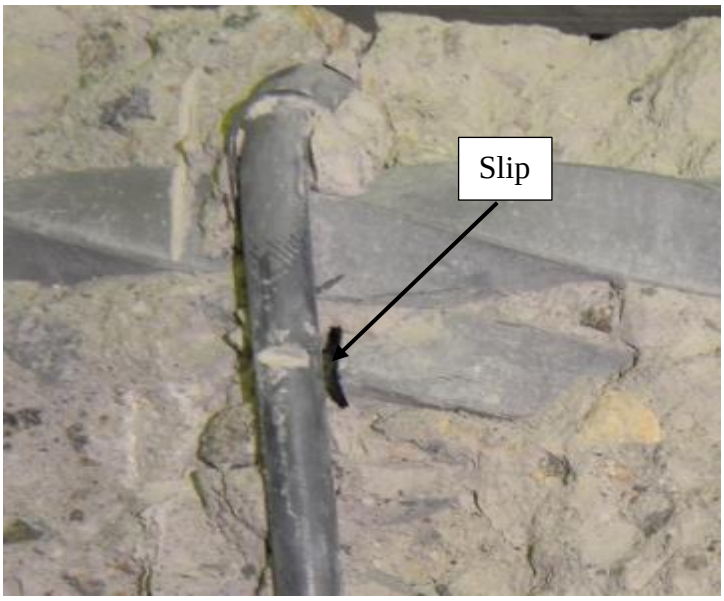

Figure N.6: End Slip of Longitudinal Reinforcement Following Concrete Removal for Specimen 25◆-610↑

Appendix O: Normalized Applied Load Versus Mid Span Deflection for the Splice Specimens Reinforced with Ransome Bars

Figures O.1 to O.14 show the normalized applied load versus midspan deflection for the splice specimens reinforced with Ransome bars. The theoretically predicted deflection is shown by a dashed line, whereas the actual recorded deflection is shown by a solid line.

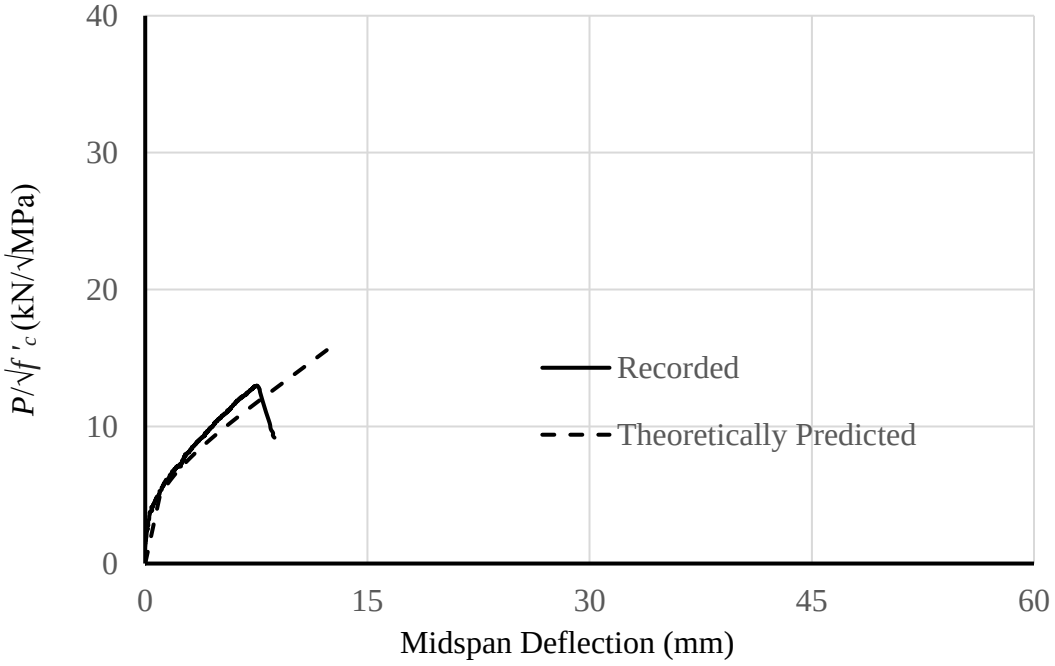

Figure O.1: Normalized Applied Load Versus Midspan Deflection for Specimen 19◆-305↓

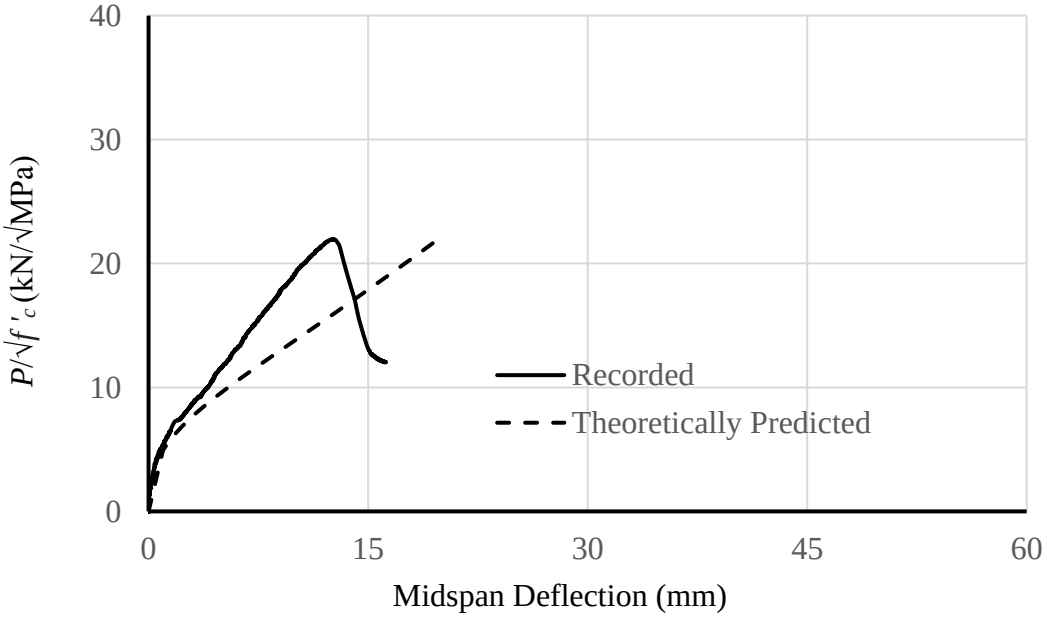

Figure O.2: Normalized Applied Load Versus Midspan Deflection for Specimen 19◆-510↓

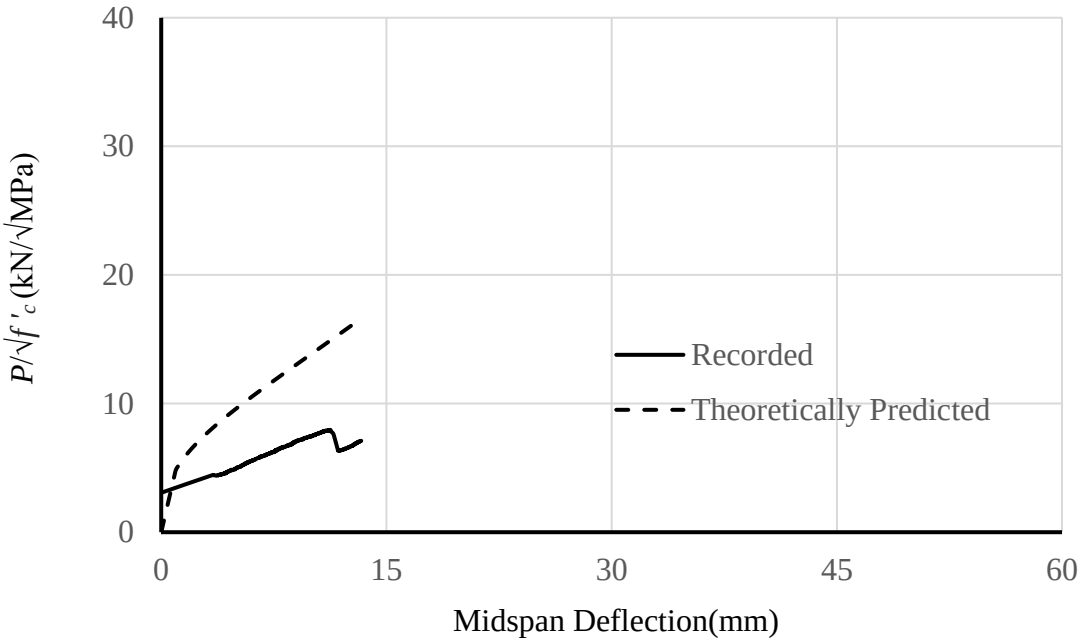

Figure O.3: Normalized Applied Load Versus Midspan Deflection for Specimen 19◆-305↑

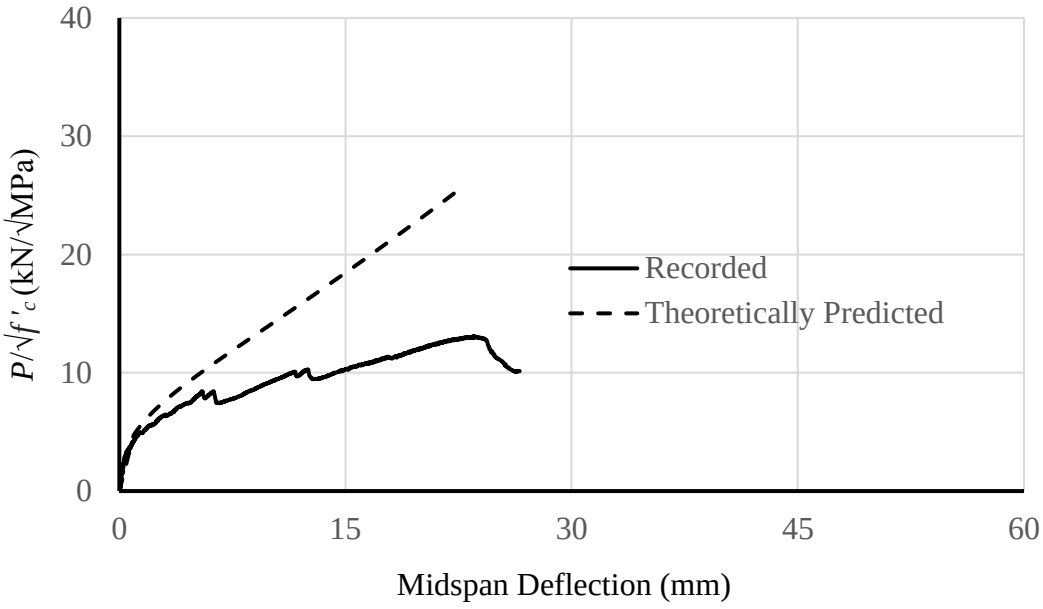

Figure O.4: Normalized Applied Load Versus Midspan Deflection for Specimen 19◆-510↑

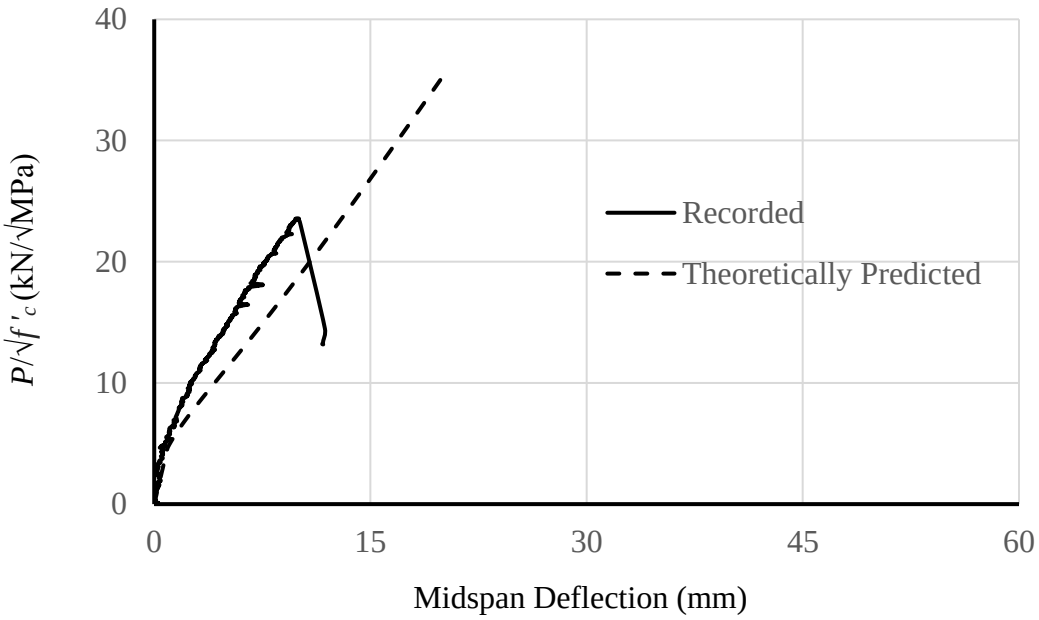

Figure O.5: Normalized Applied Load Versus Midspan Deflection for Specimen 25◆-410↓

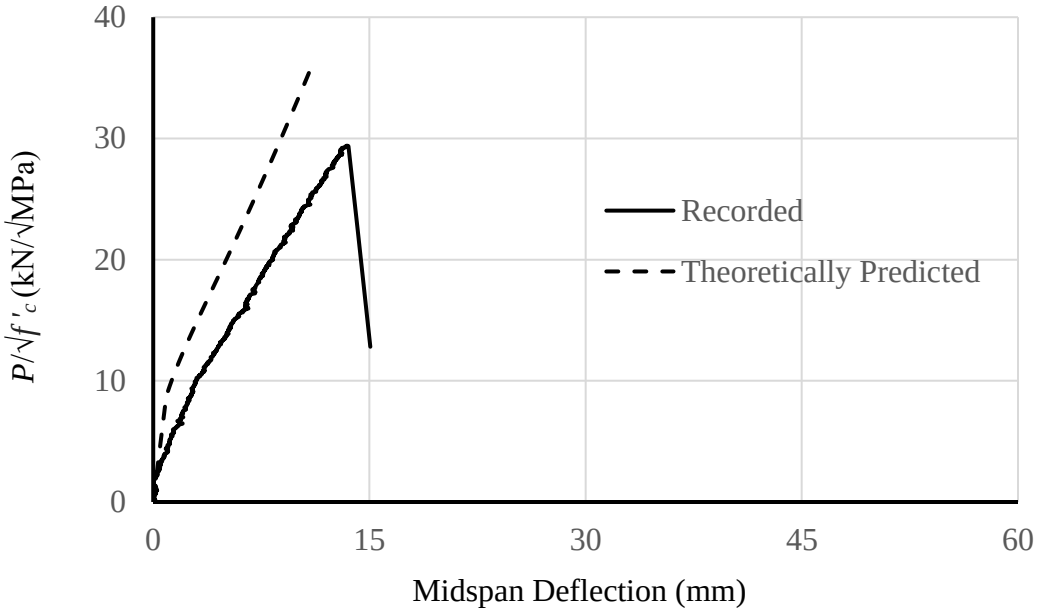

Figure O.6: Normalized Applied Load Versus Midspan Deflection for Specimen 25◆-510↓

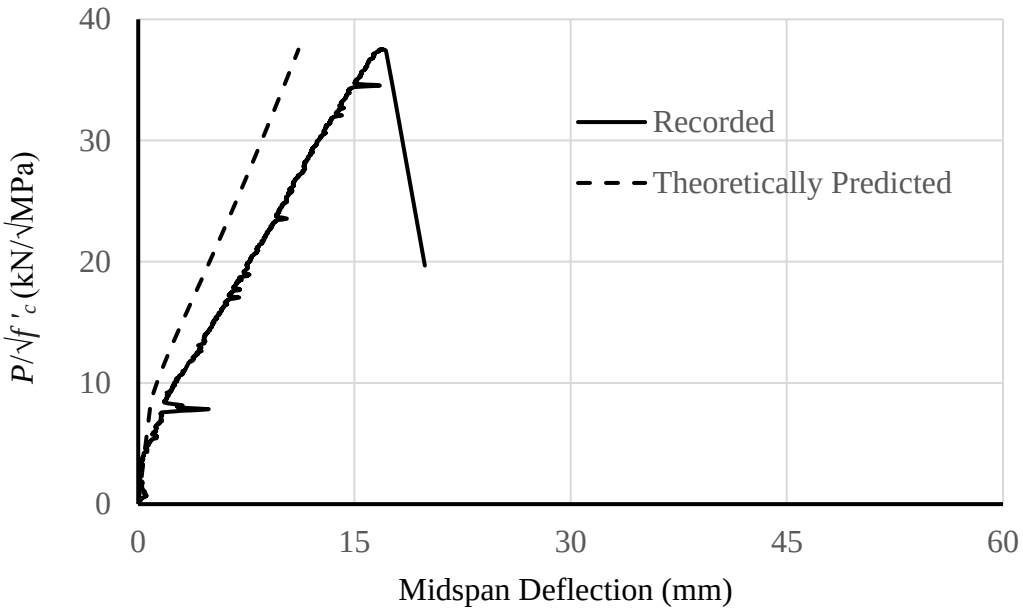

Figure O.7: Normalized Applied Load Versus Midspan Deflection for Specimen 25◆-610↓

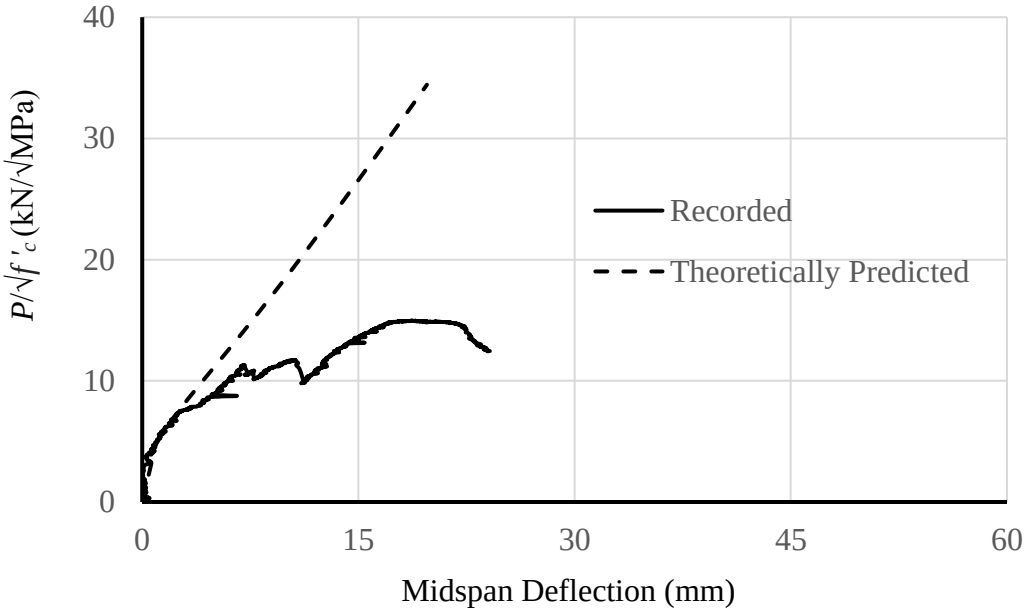

Figure O.8: Normalized Applied Load Versus Midspan Deflection for Specimen 25◆-410↑

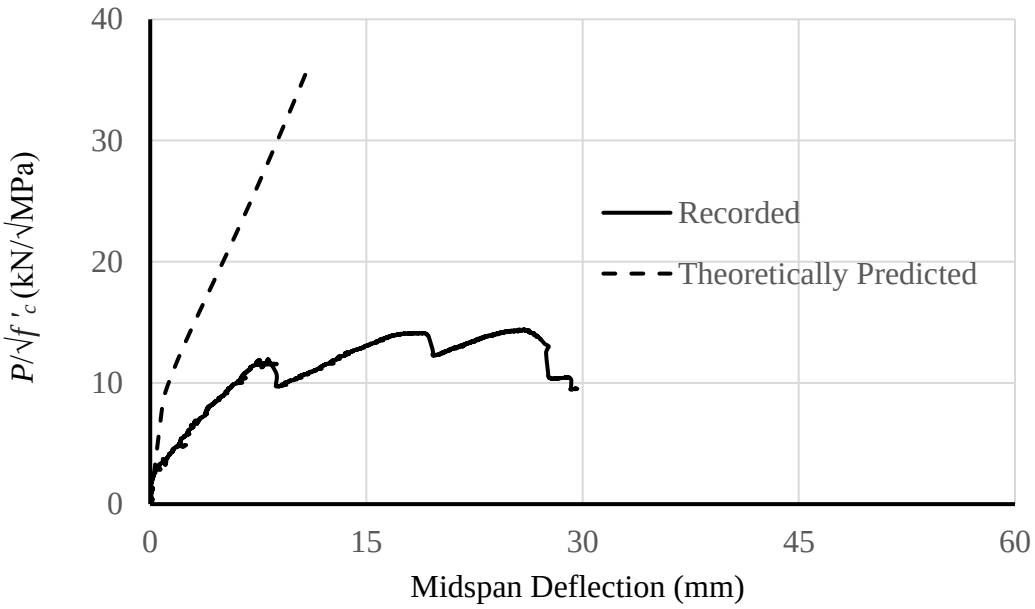

Figure O.9: Normalized Applied Load Versus Midspan Deflection for Specimen 25◆-510↑

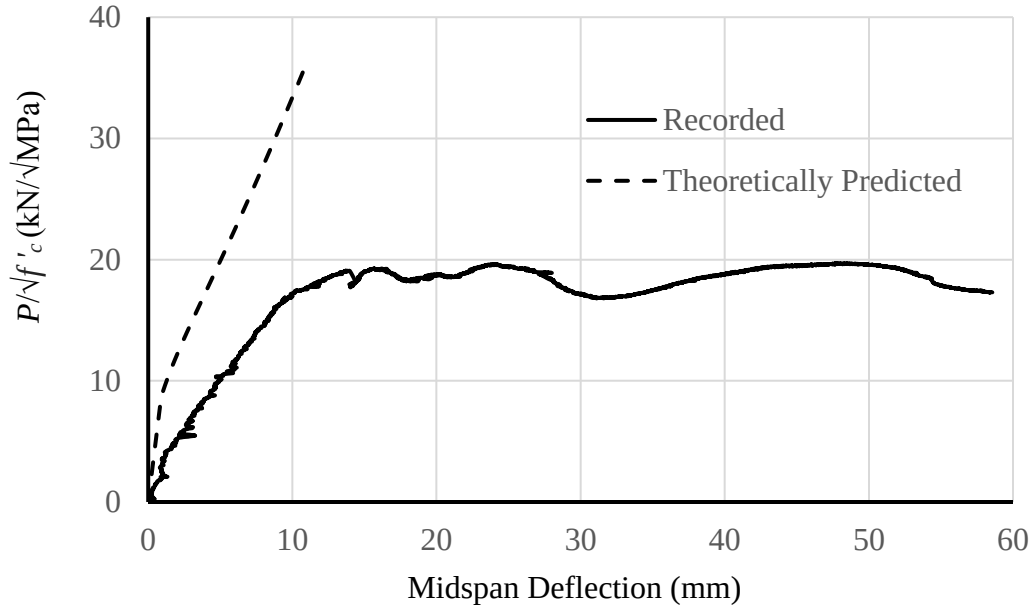

Figure O.10: Normalized Applied Load Versus Midspan Deflection for Specimen 25◆-610↑

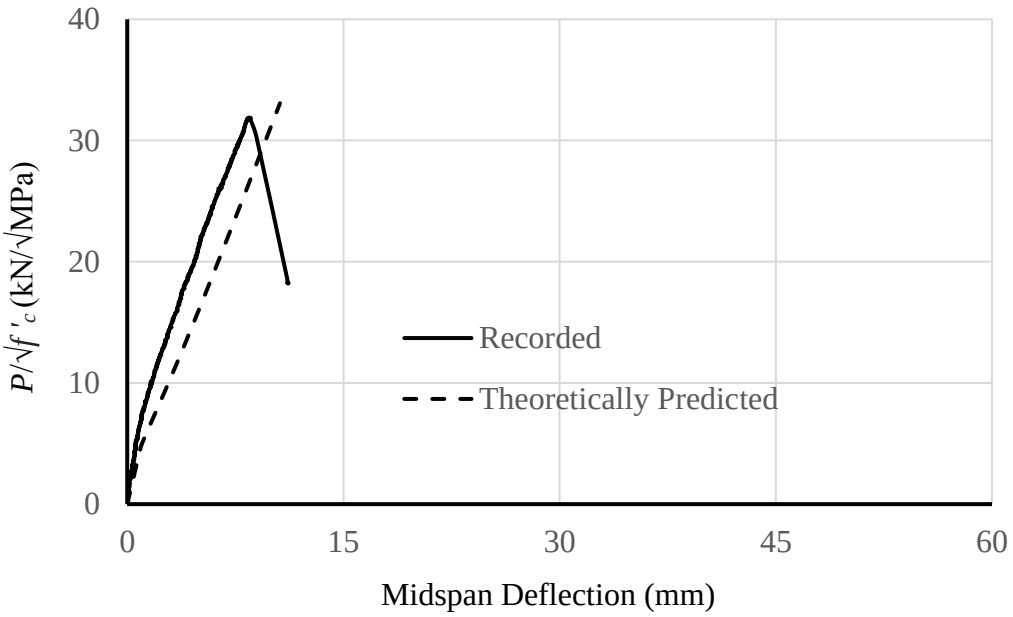

Figure O.11: Normalized Applied Load Versus Midspan Deflection for Specimen 32◆-610↓

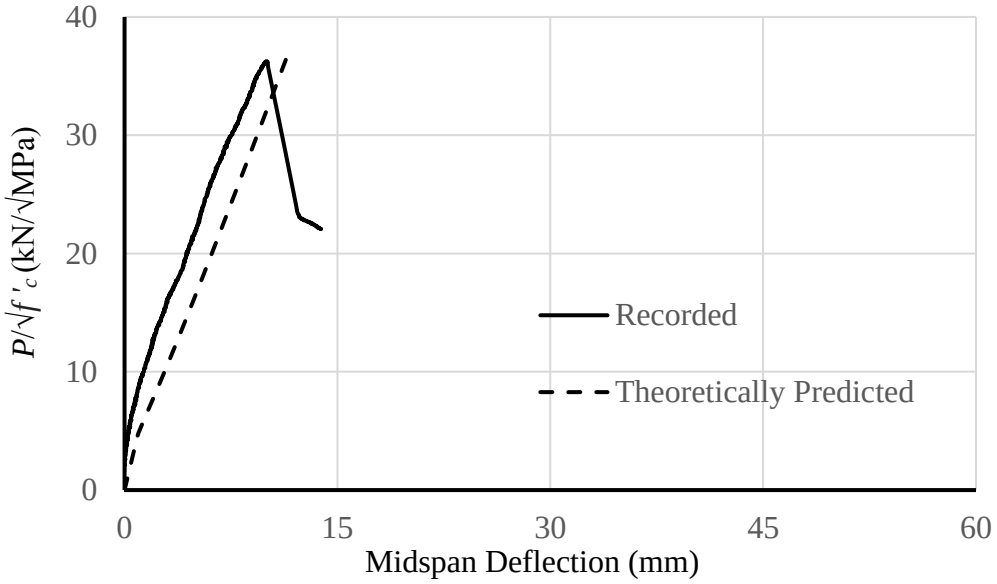

Figure O.12: Normalized Applied Load Versus Midspan Deflection for Specimen 32◆-810↓

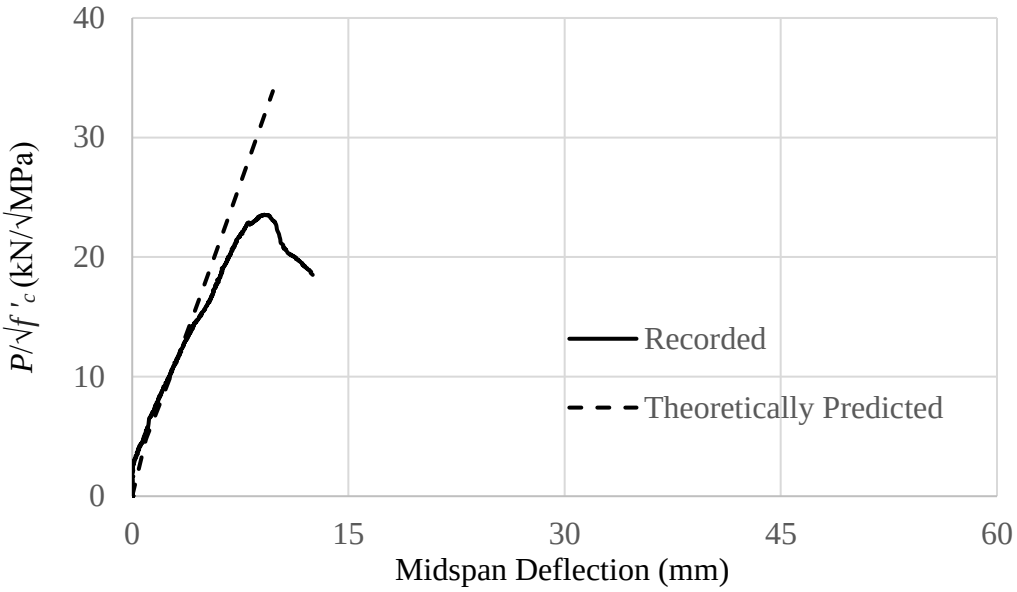

Figure O.13: Normalized Applied Load Versus Midspan Deflection for Specimen 32◆-610↑

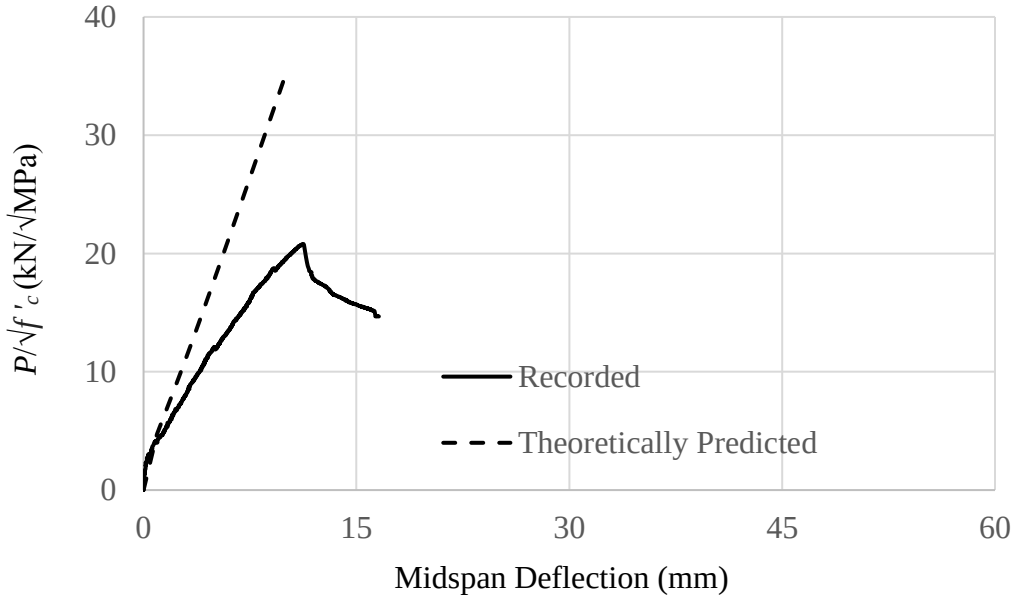

Figure O.14: Normalized Applied Load Versus Midspan Deflection for Specimen 32◆-810↑

Appendix P: Deflection Profiles of Splice Specimens Reinforced with Ransome Bars

Figures P.1 to P.14 show the deflection profiles of splice specimens reinforced with Ransome bars at different load levels. Markers shown in the figures indicate the recorded deflection obtained from LVDTs that were located along the length of the specimens. The dashed curves represent the theoretically calculated deflection.

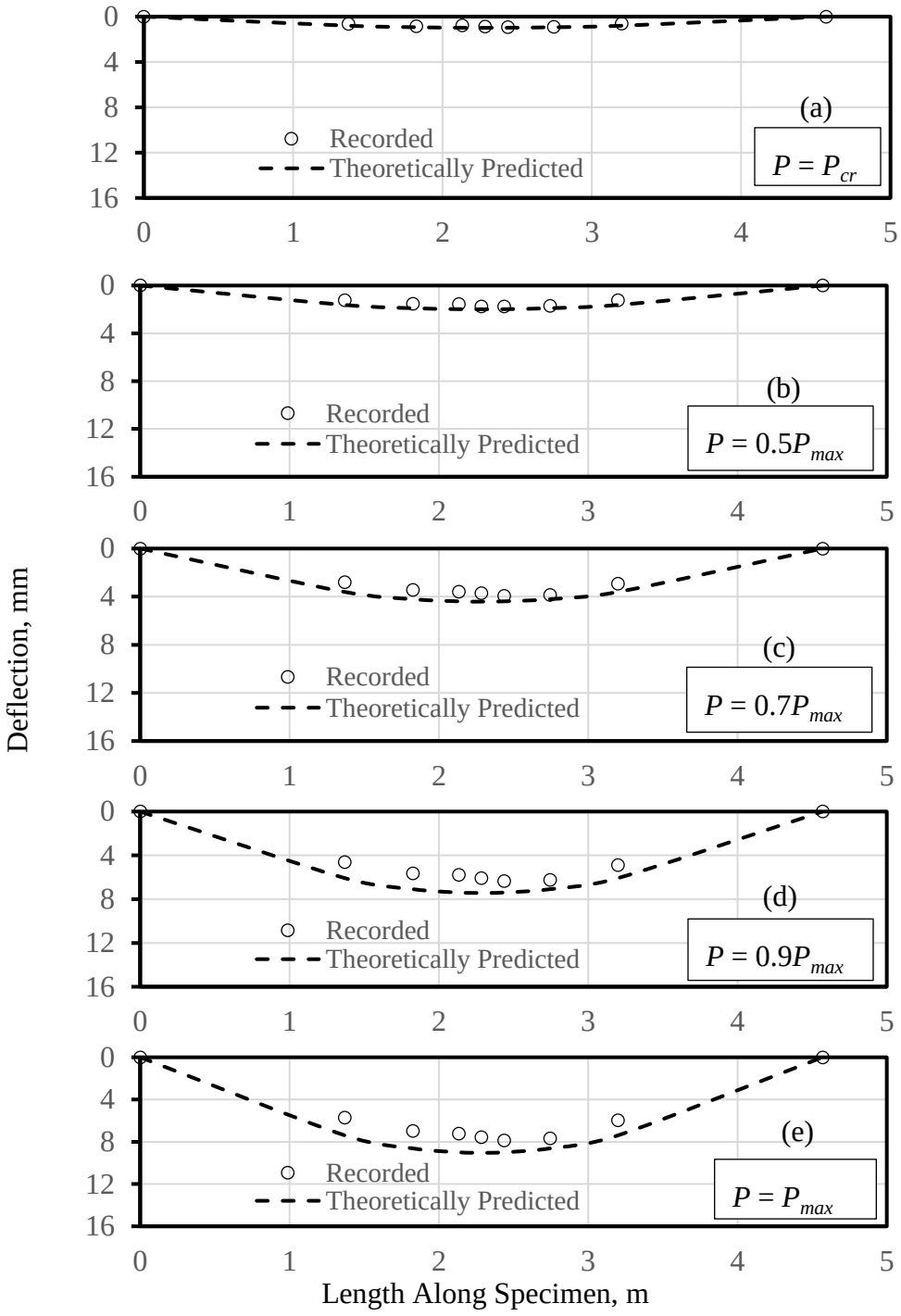

Figure P.1: Deflection Profile at Different Load Levels for Specimen 19◆-305↓: (a) $P=P_{cr}$, (b) P=0.5 P_{max}, (c) P= 0.7 P_{max}, (d) P= 0.9 P_{max}, and (e) $P=P_{max}$

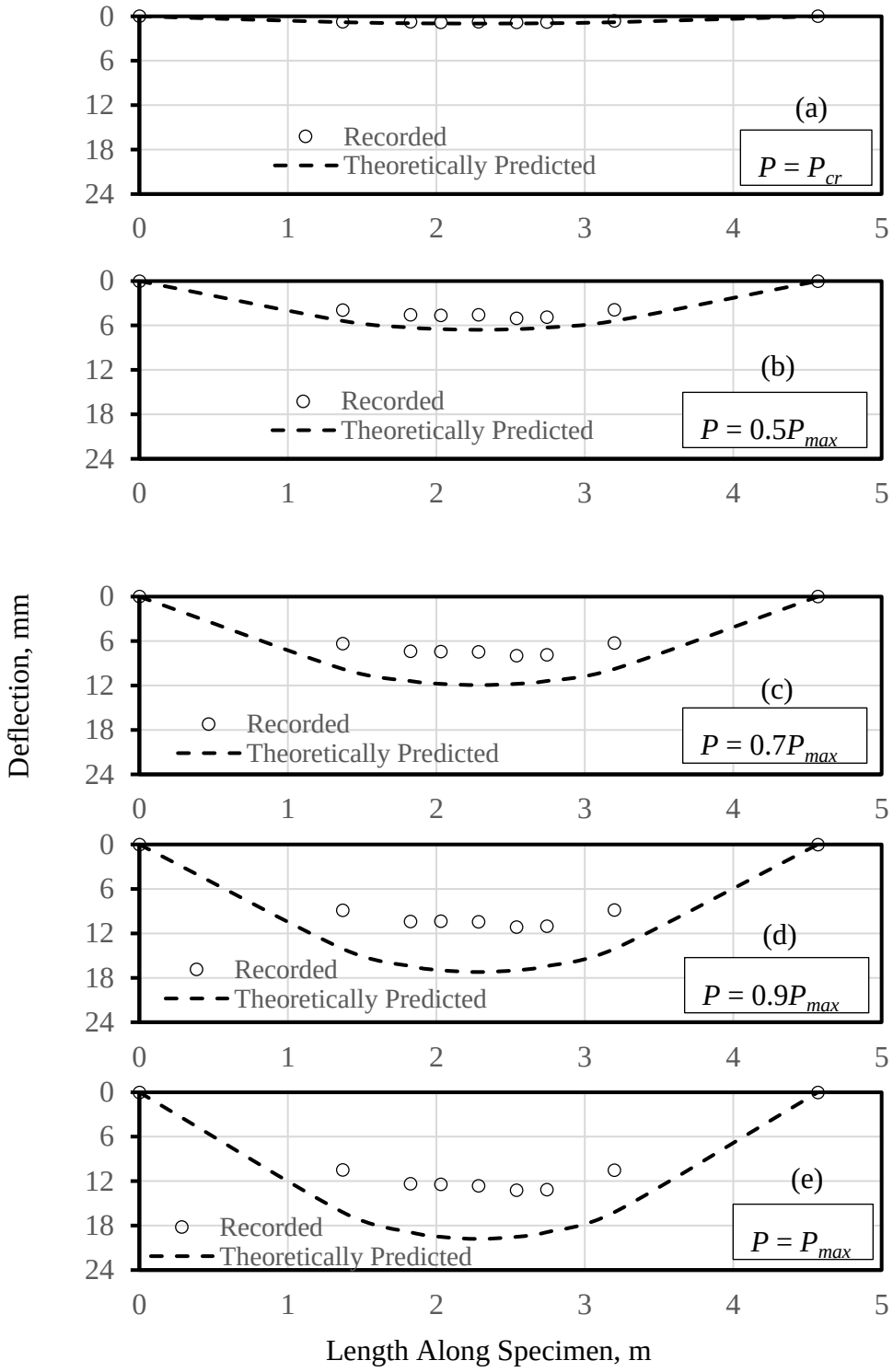

Figure P.2: Deflection Profile at Different Load Levels for Specimen 19◆-510↓: (a) $P=P_{cr}$, (b) P=0.5 P_{max}, (c) P= 0.7 P_{max}, (d) P= 0.9 P_{max}, and (e) $P=P_{max}$

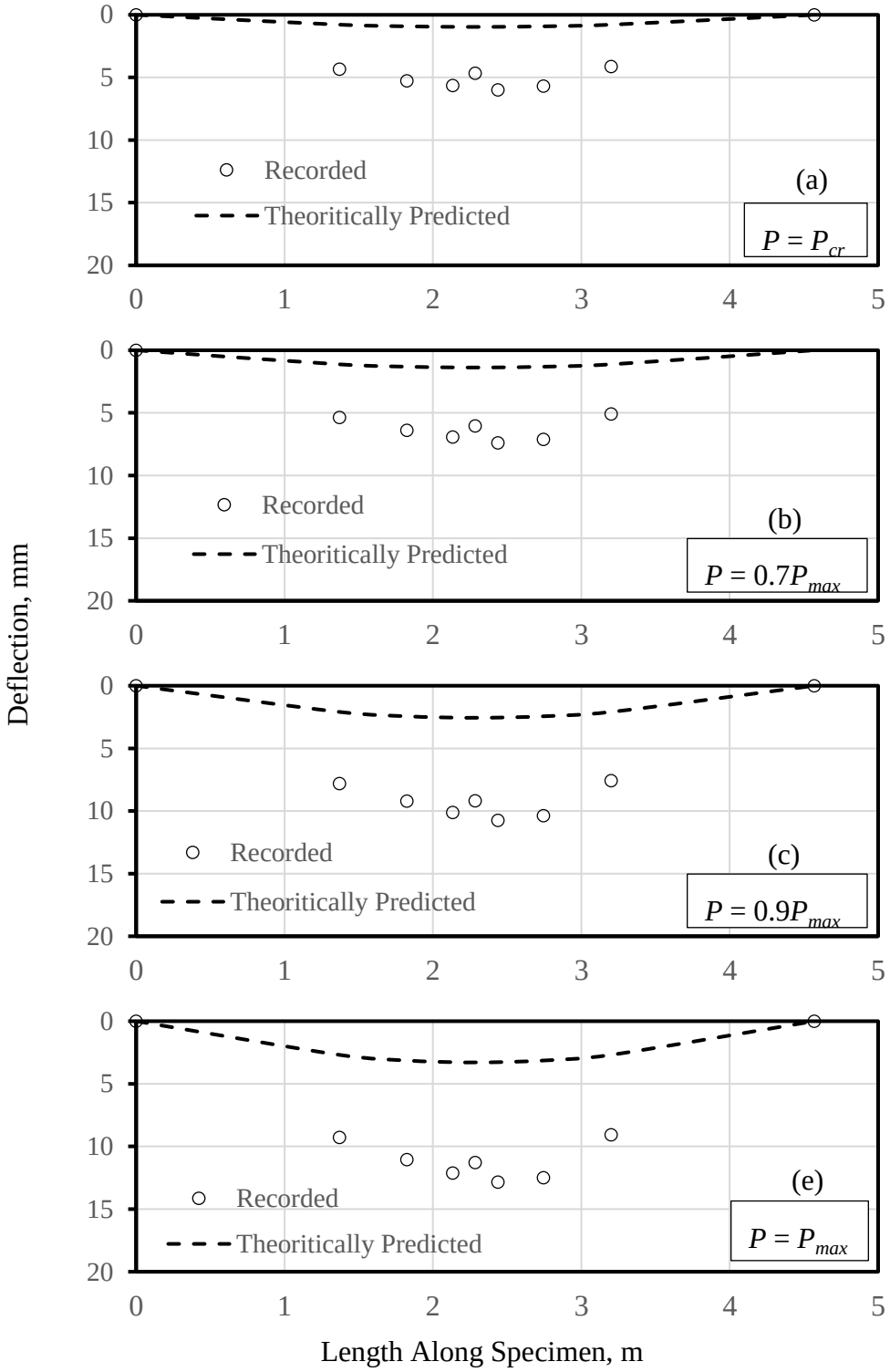

Figure P.3: Deflection Profile at Different Load Levels for Specimen 19◆-305↑: (a) $P=P_{cr}$, (b) $P= 0.7\ P_{max}$, (c) $P= 0.9\ P_{max}$, and (d) $P=P_{max}$

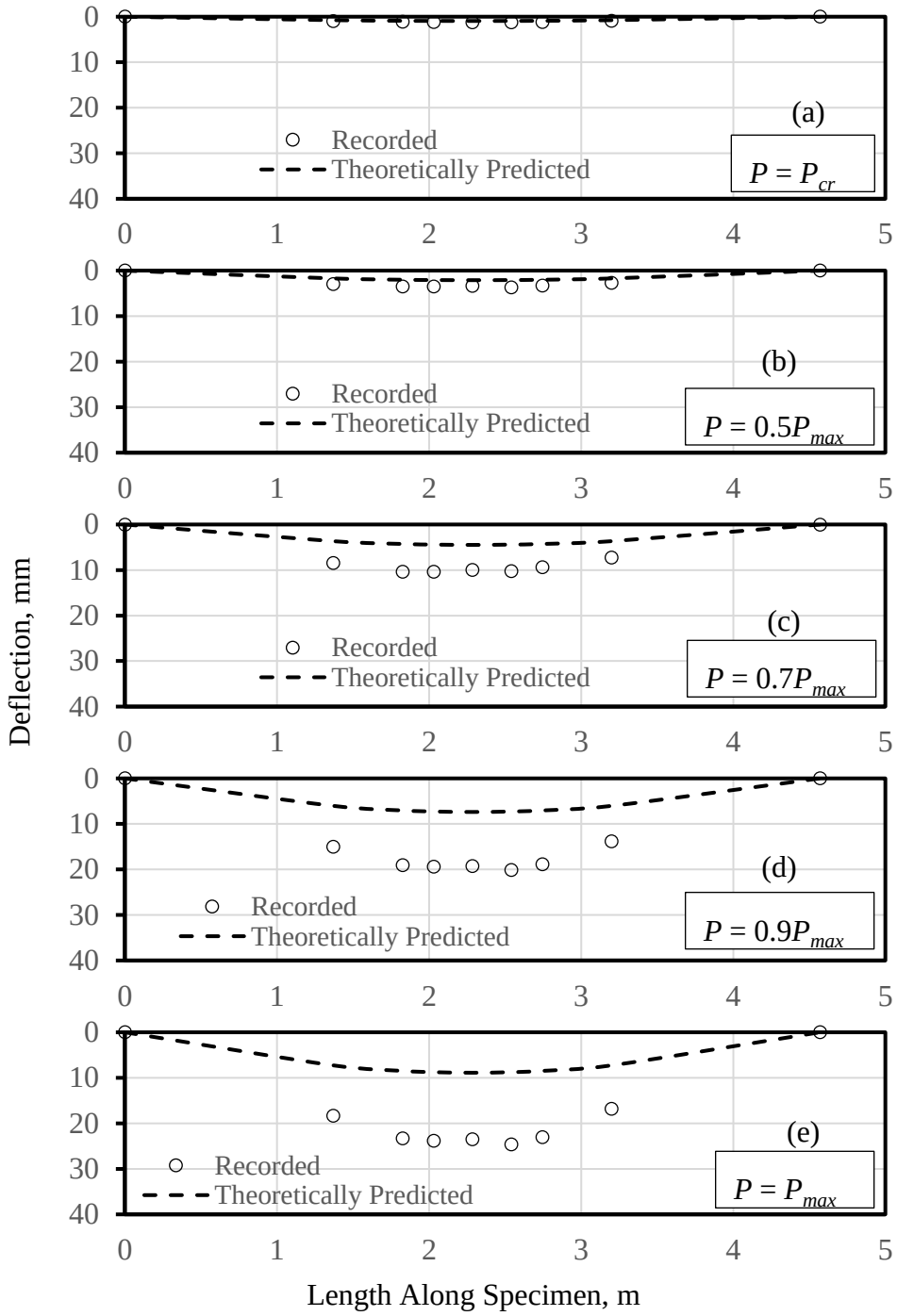

Figure P.4: Deflection Profile at Different Load Levels for Specimen 19◆-510↑: (a) $P=P_{cr}$, (b) P=0.5 P_{max}, (c) P= 0.7 P_{max}, (d) P= 0.9 P_{max}, and (e) $P=P_{max}$

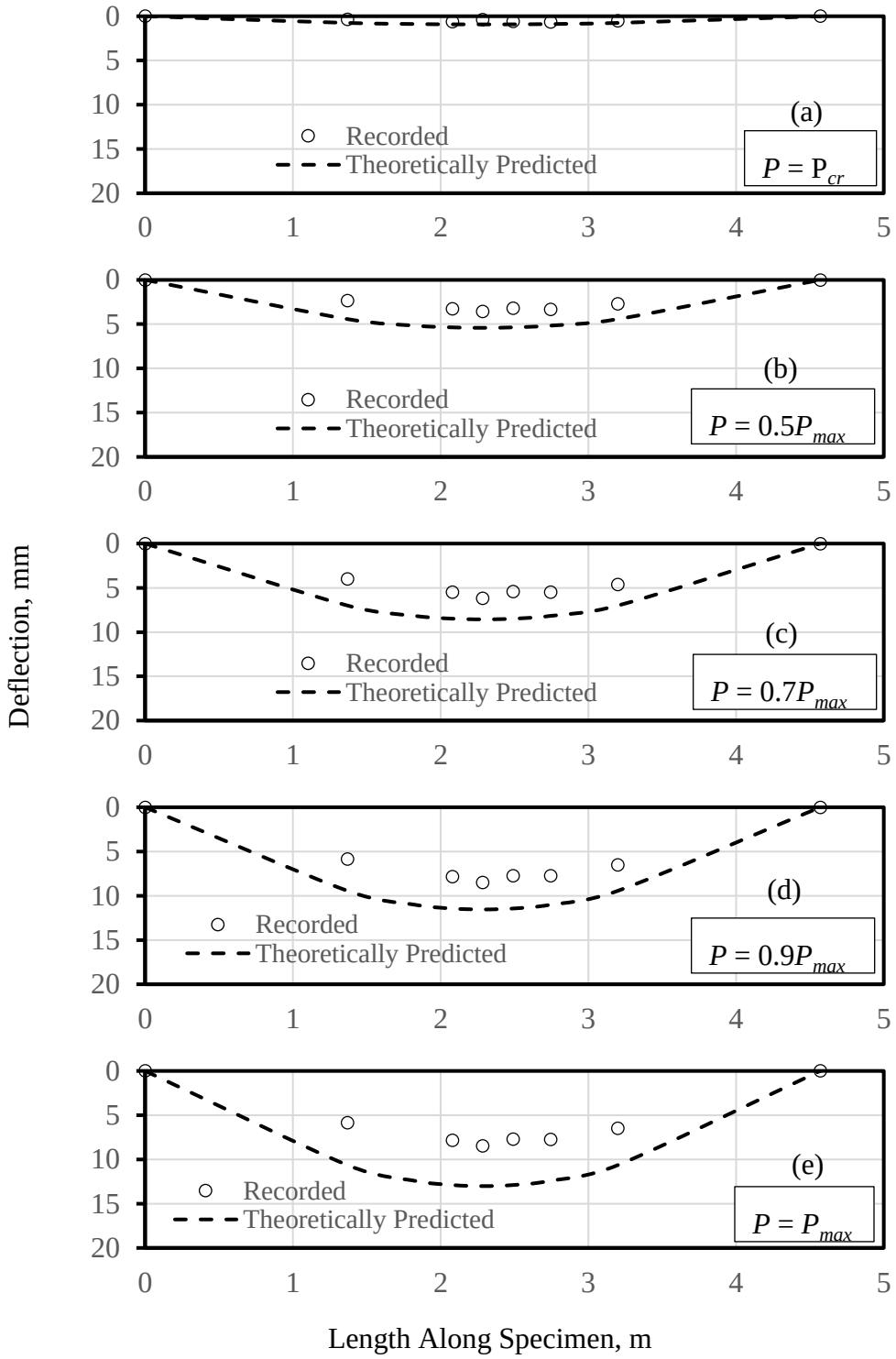

Figure P.5: Deflection Profile at Different Load Levels for Specimen 25◆-410↓: (a) $P=P_{cr}$, (b) P=0.5 P_{max}, (c) P= 0.7 P_{max}, (d) P= 0.9 P_{max}, and (e) $P=P_{max}$

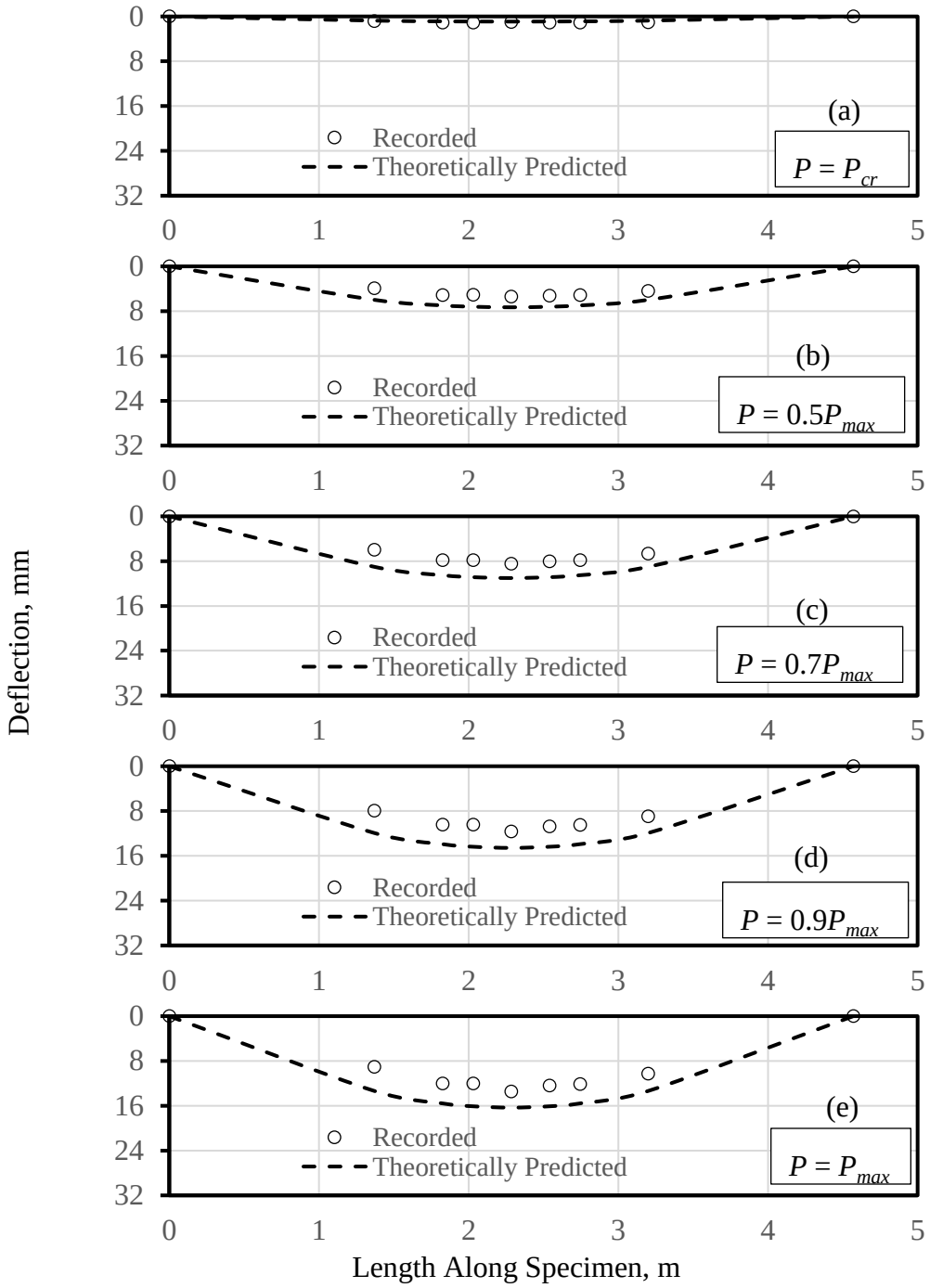

Figure P.6: Deflection Profile at Different Load Levels for Specimen 25◆-510↓: (a) $P=P_{cr}$, (b) P=0.5 P_{max}, (c) P= 0.7 P_{max}, (d) P= 0.9 P_{max}, and (e) $P=P_{max}$

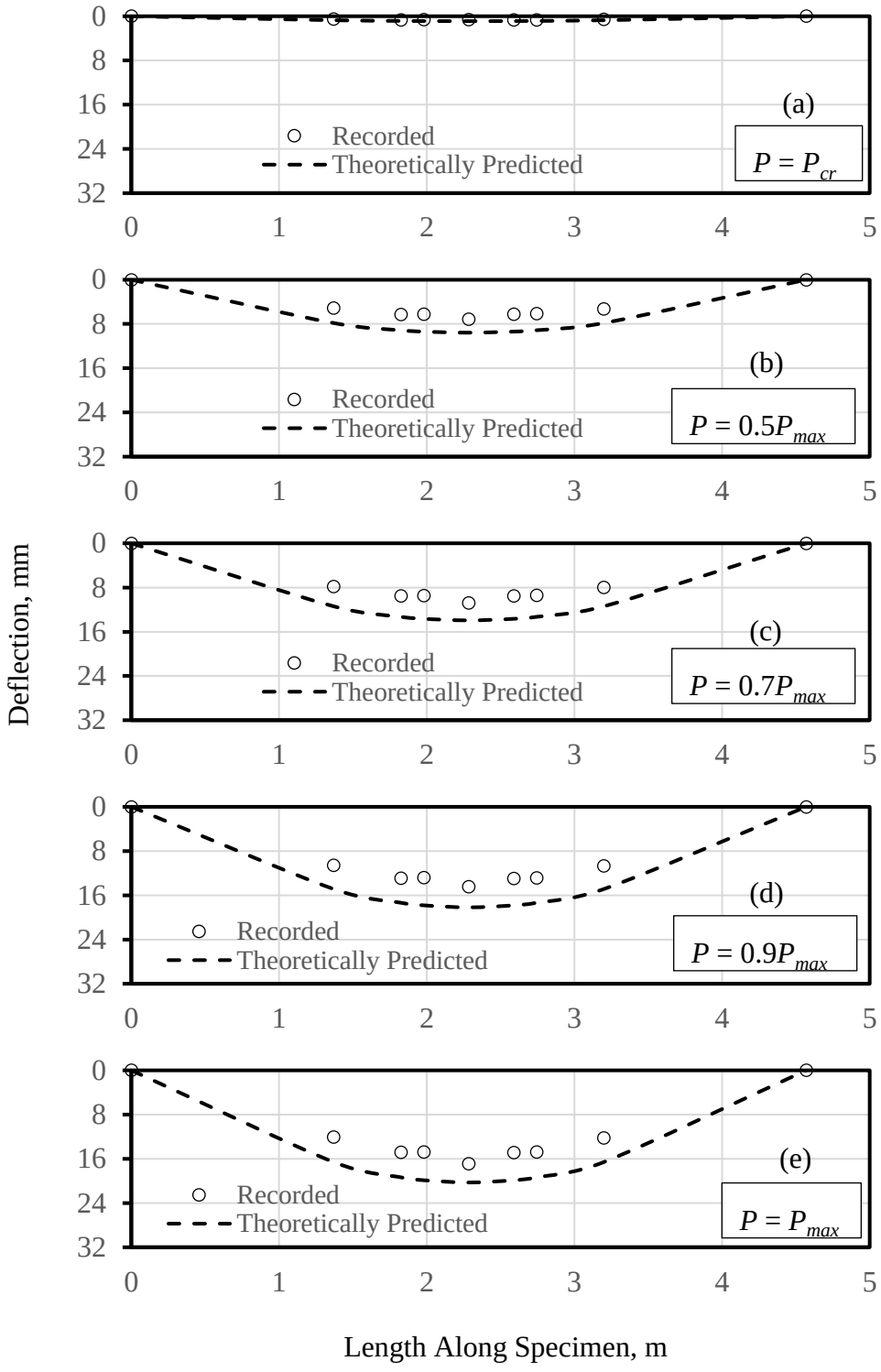

Figure P.7: Deflection Profile at Different Load Levels for Specimen 25◆-610↓: (a) $P=P_{cr}$, (b) P=0.5 P_{max}, (c) P= 0.7 P_{max}, (d) P= 0.9 P_{max}, and (e) $P=P_{max}$

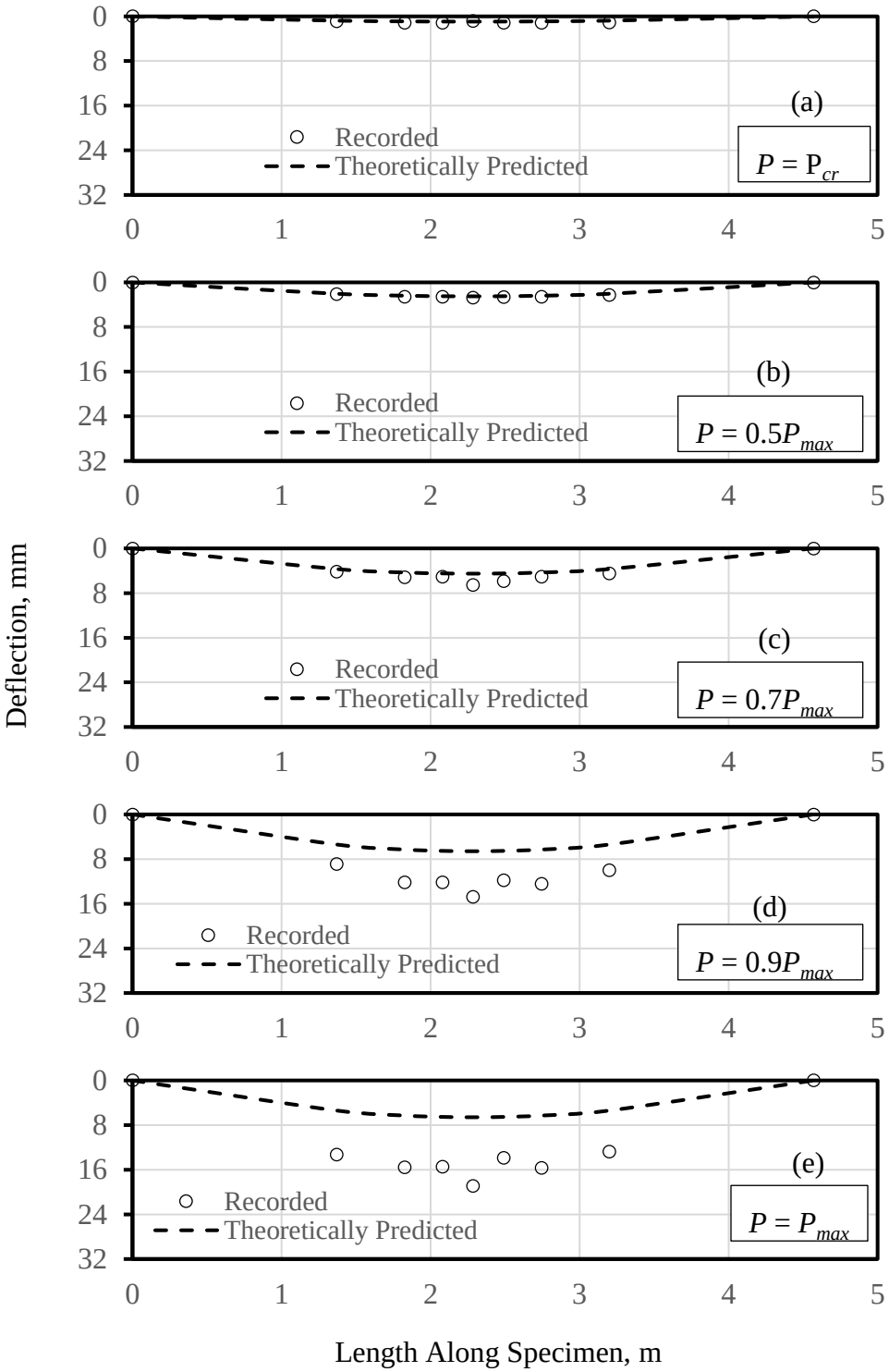

Figure P.8: Deflection Profile at Different Load Levels for Specimen 25◆-410↑: (a) $P=P_{cr}$, (b) P=0.5 P_{max}, (c) P= 0.7 P_{max}, (d) P= 0.9 P_{max}, and (e) $P=P_{max}$

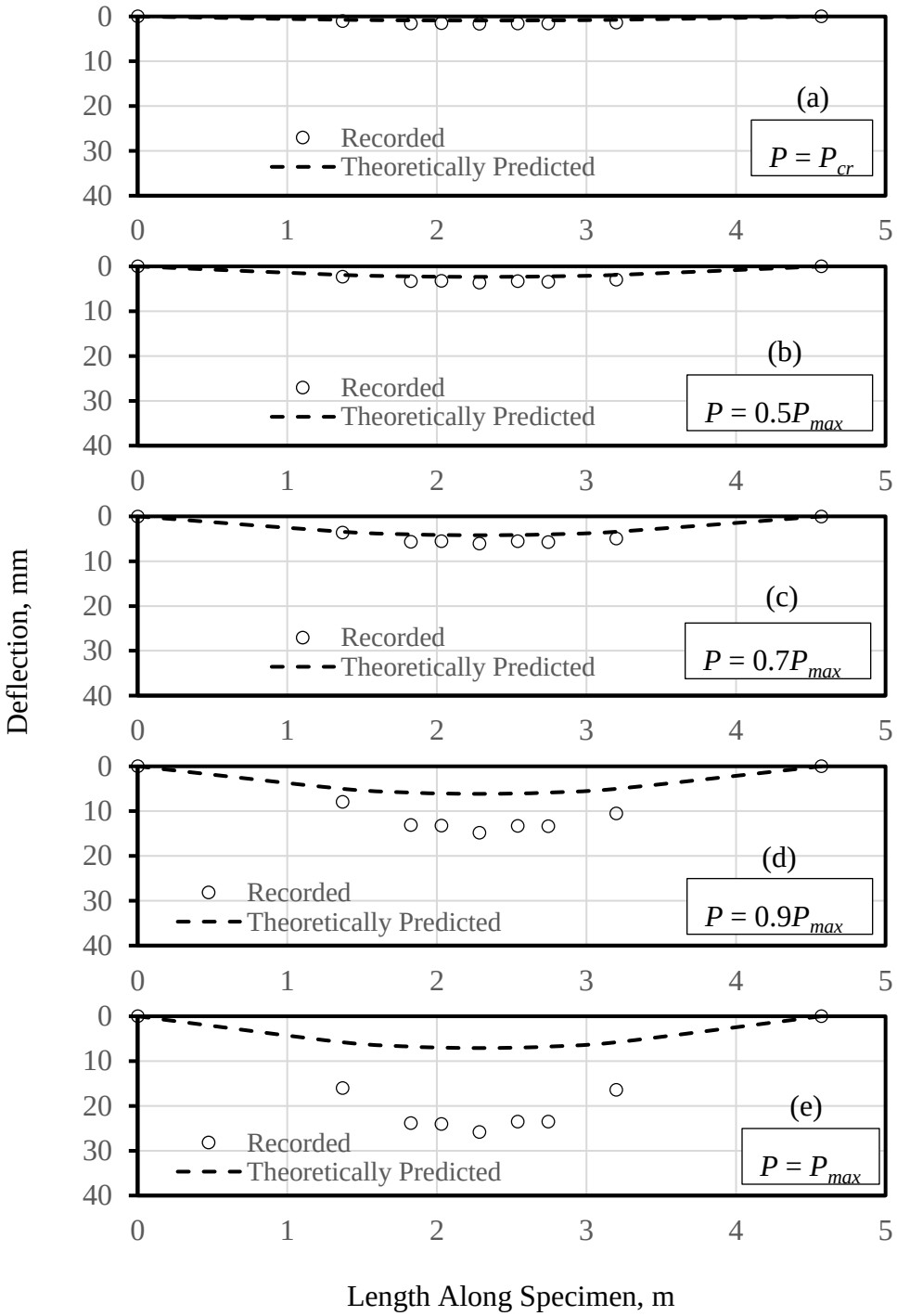

Figure P.9: Deflection Profile at Different Load Levels for Specimen 25◆-510↑: (a) $P=P_{cr}$, (b) P=0.5 P_{max}, (c) P= 0.7 P_{max}, (d) P= 0.9 P_{max}, and (e) $P=P_{max}$

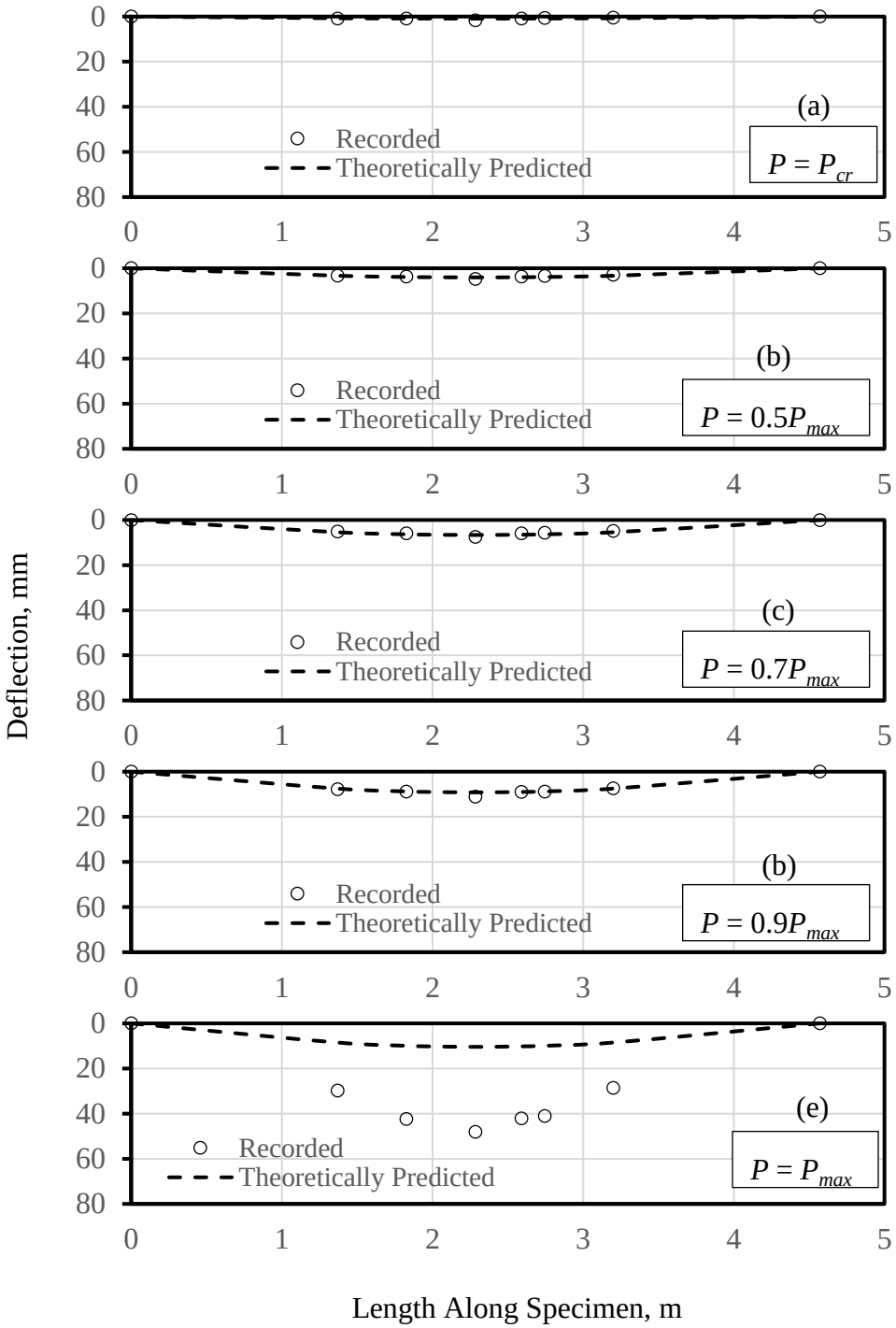

Figure P.10: Deflection Profile at Different Load Levels for Specimen 25◆-610↑: (a) $P=P_{cr}$, (b) P=0.5 P_{max}, (c) P= 0.7 P_{max}, (d) P= 0.9 P_{max}, and (e) $P=P_{max}$

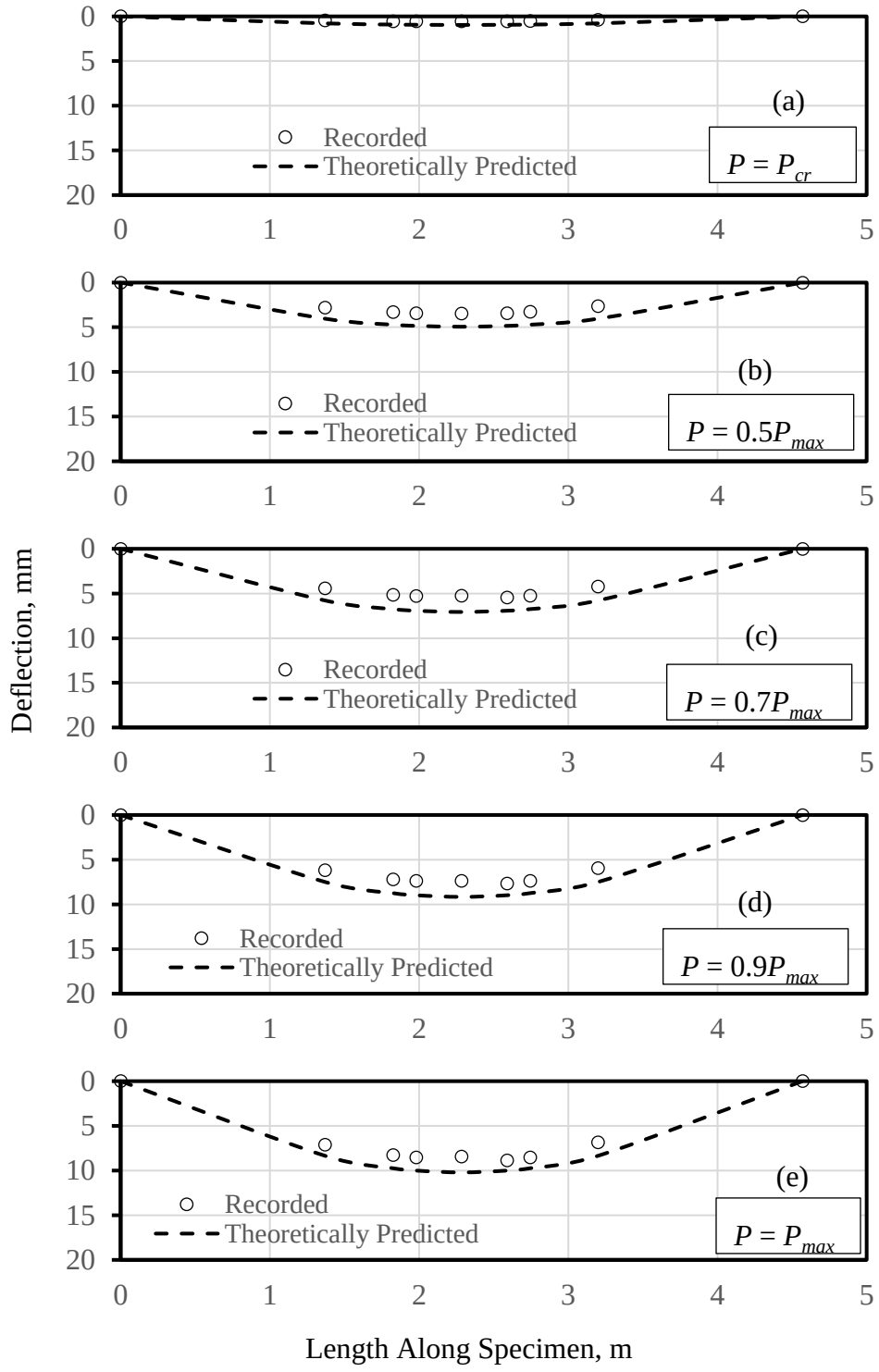

Figure P.11: Deflection Profile at Different Load Levels for Specimen 32◆-610↓: (a) $P=P_{cr}$, (b) P=0.5 P_{max}, (c) P= 0.7 P_{max}, (d) P= 0.9 P_{max}, and (e) $P=P_{max}$

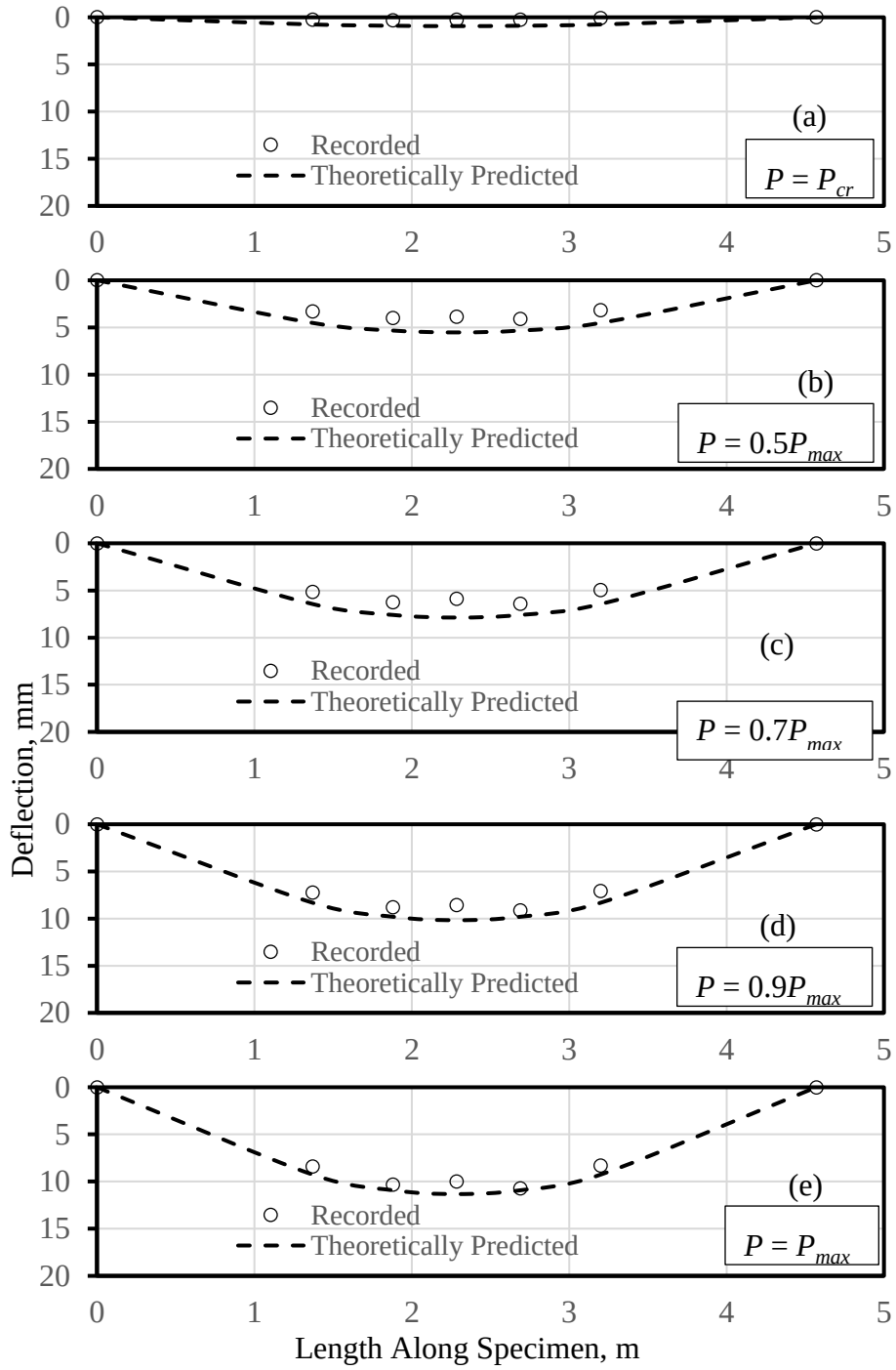

Figure P.12: Deflection Profile at Different Load Levels for Specimen 32◆-810↓: (a) $P=P_{cr}$, (b) P=0.5 P_{max}, (c) P= 0.7 P_{max}, (d) P= 0.9 P_{max}, and (e) $P=P_{max}$

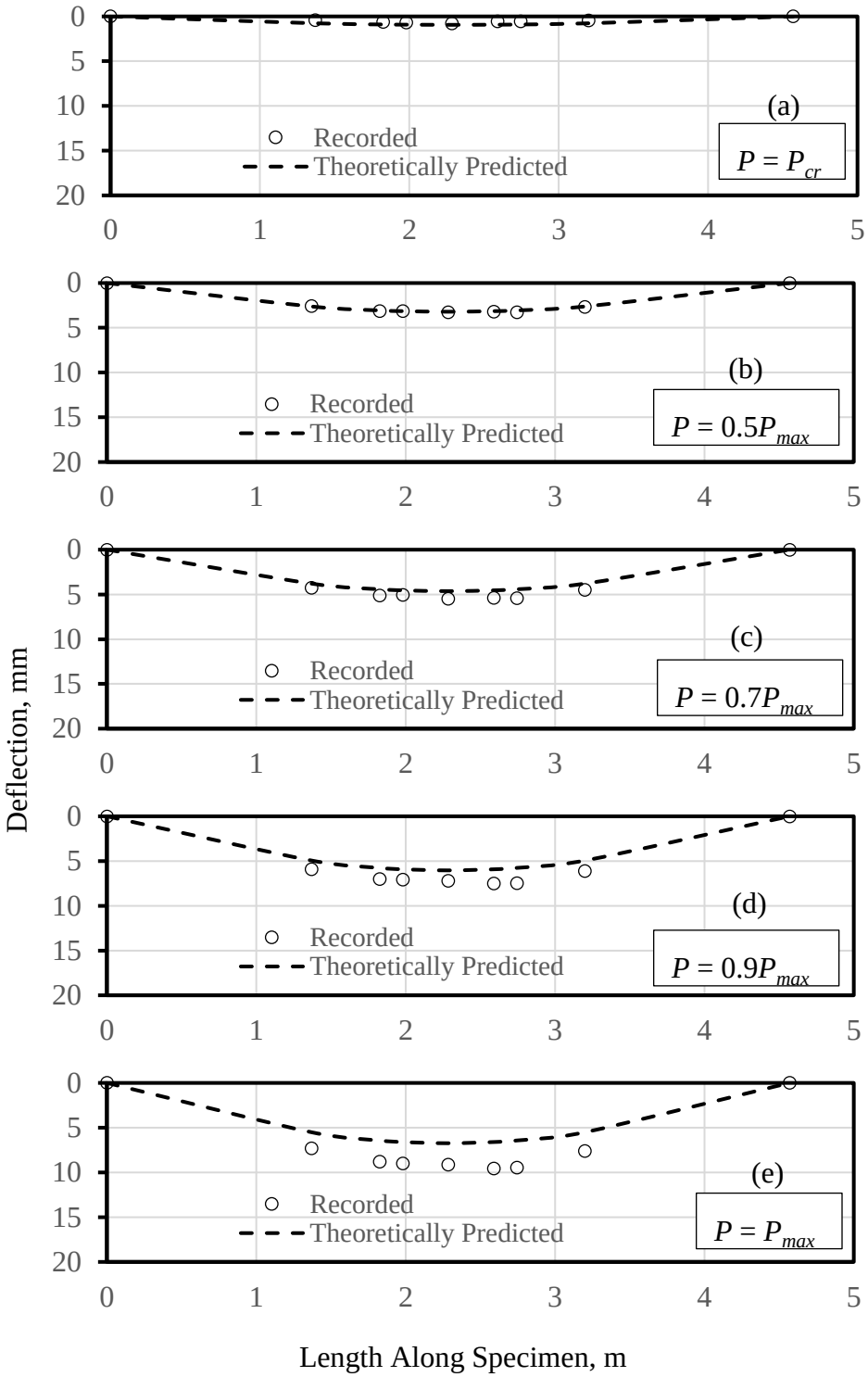

Figure P.13: Deflection Profile at Different Load Levels for Specimen 32◆-610↑: (a) $P=P_{cr}$, (b) P=0.5 P_{max}, (c) P= 0.7 P_{max}, (d) P= 0.9 P_{max}, and (e) $P=P_{max}$

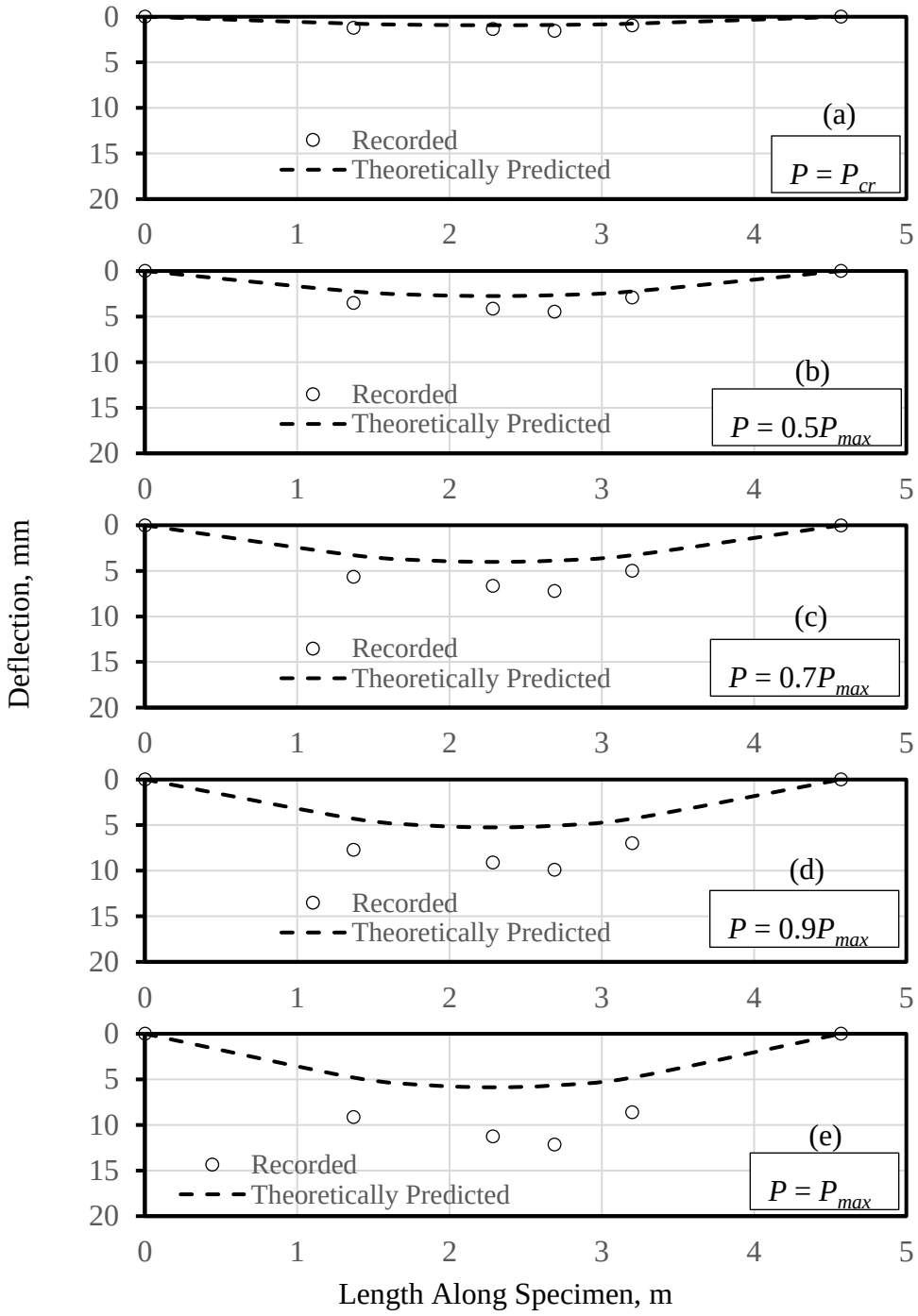

Figure P.14: Deflection Profile at Different Load Levels for Specimen 32◆-610↑: (a) $P=P_{cr}$, (b) P=0.5 P_{max}, (c) P= 0.7 P_{max}, (d) P= 0.9 P_{max}, and (e) $P=P_{max}$

Appendix Q: Moment Versus Curvature Plots of Splice Specimens Reinforced with Ransome Bars

Figures Q.1 to Q.16 show the theoretical moment versus curvature plots of splice specimens reinforced with Ransome bars.

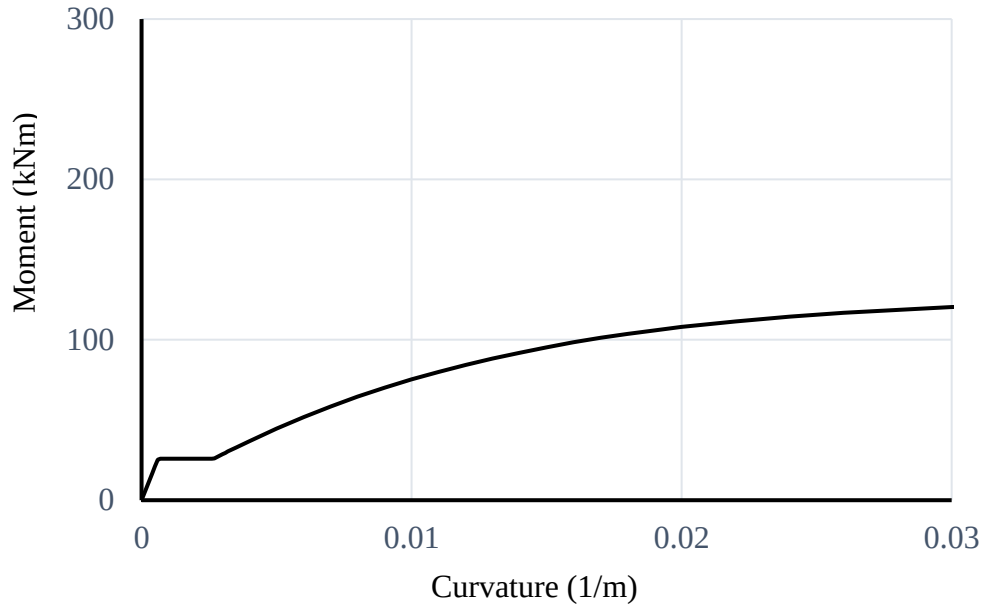

Figure Q.1: Theoretical Moment Curvature Diagram for Specimen 19◆-305↓ and 19◆-410↓

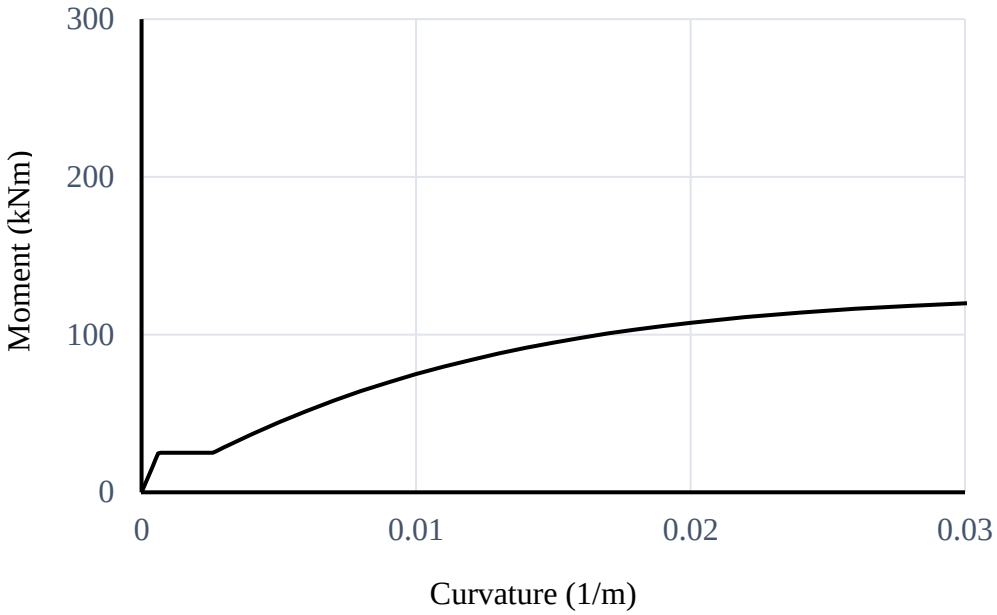

Figure Q.2: Theoretical Moment Curvature Diagram for Specimen 19◆-305↑

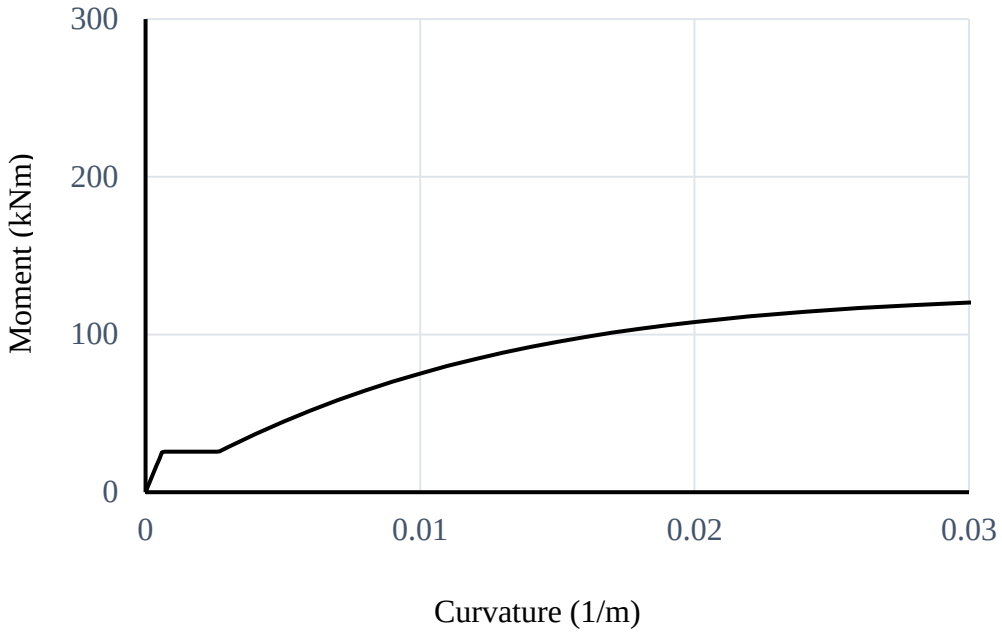

Figure Q.3: Theoretical Moment Curvature Diagram for Specimen 19◆-410↑

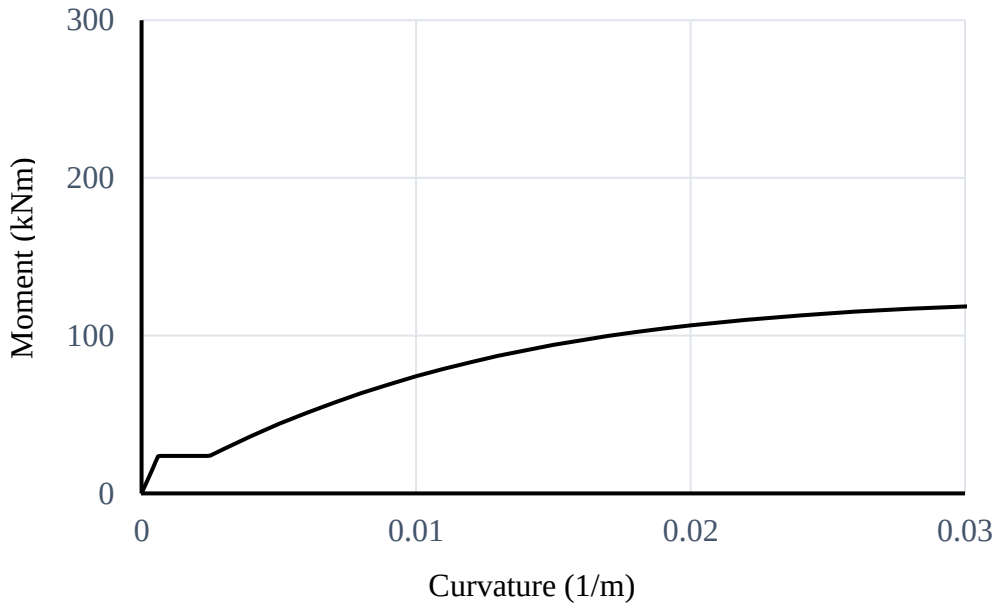

Figure Q.4: Theoretical Moment Curvature Diagram for Specimen 19◆-510↑

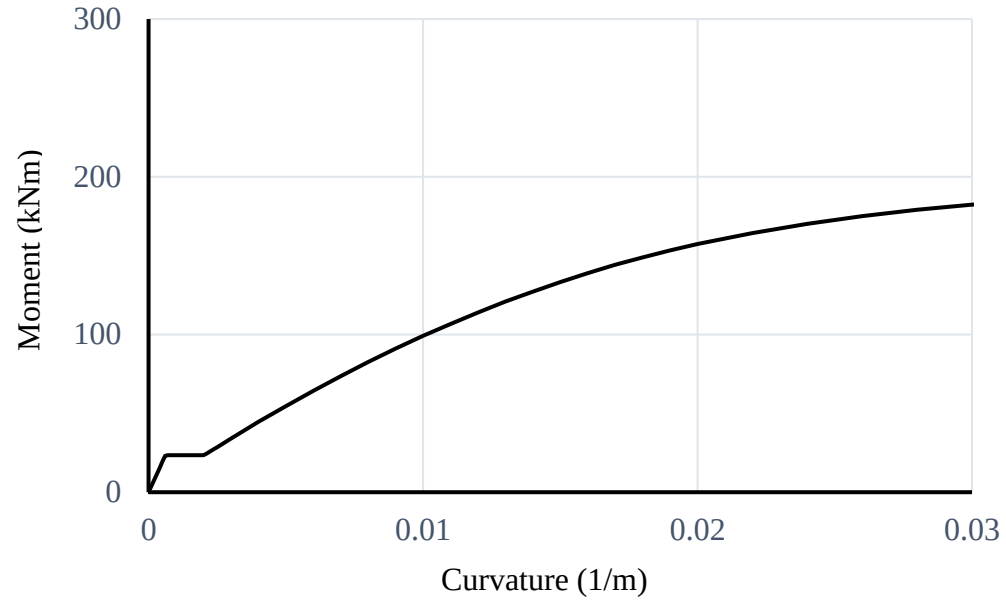

Figure Q.5: Theoretical Moment Curvature Diagram for Specimen 25◆-410↓

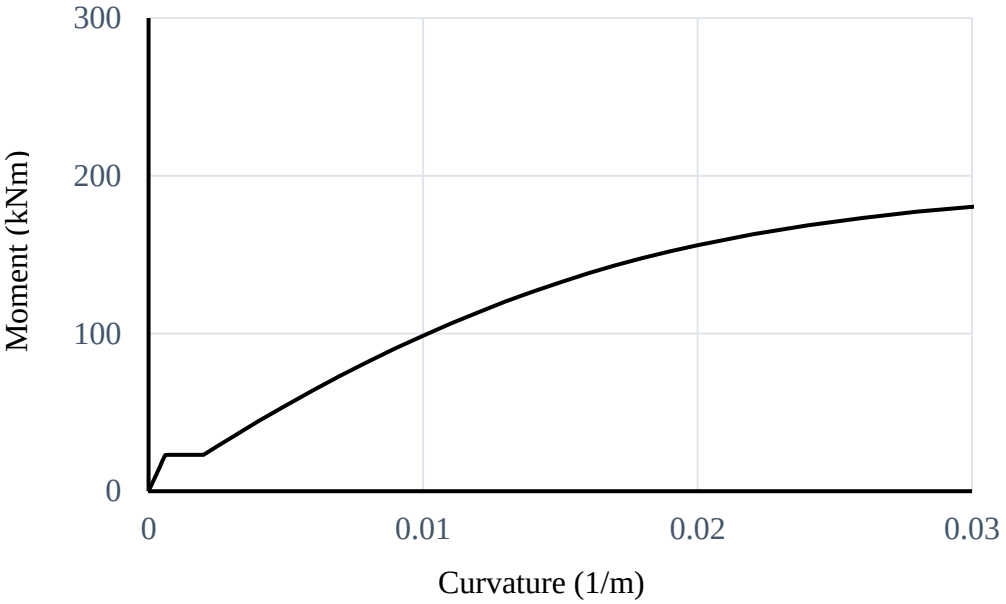

Figure Q.6: Theoretical Moment Curvature Diagram for Specimen 25◆-510↓

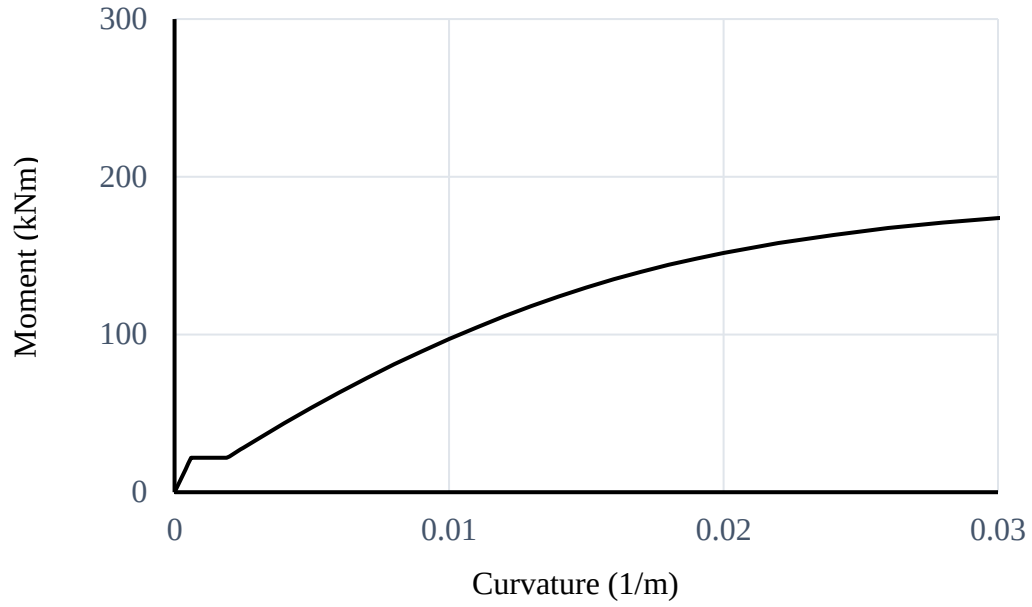

Figure Q.7: Theoretical Moment Curvature Diagram for Specimen 25◆-610↓

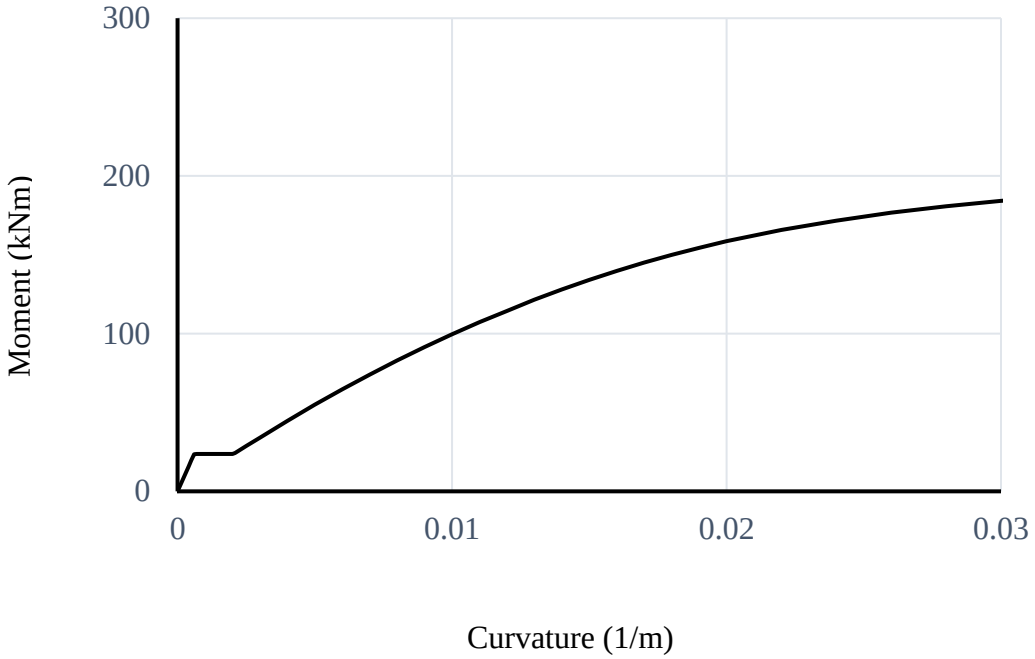

Figure Q.8: Theoretical Moment Curvature Diagram for Specimen 25◆-410↑

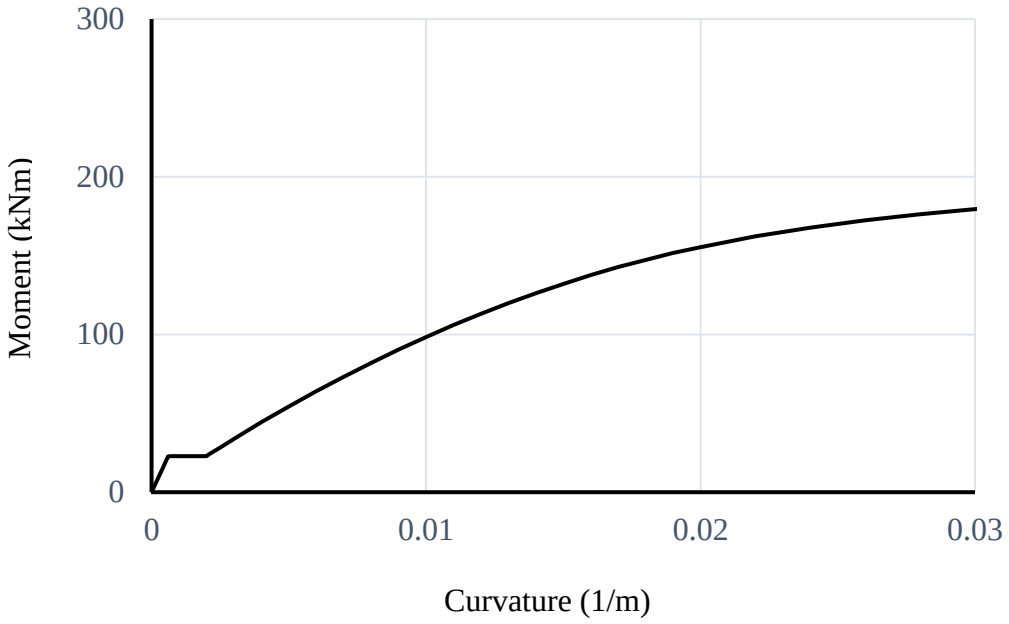

Figure Q.9: Theoretical Moment Curvature Diagram for Specimen 25◆-510↑

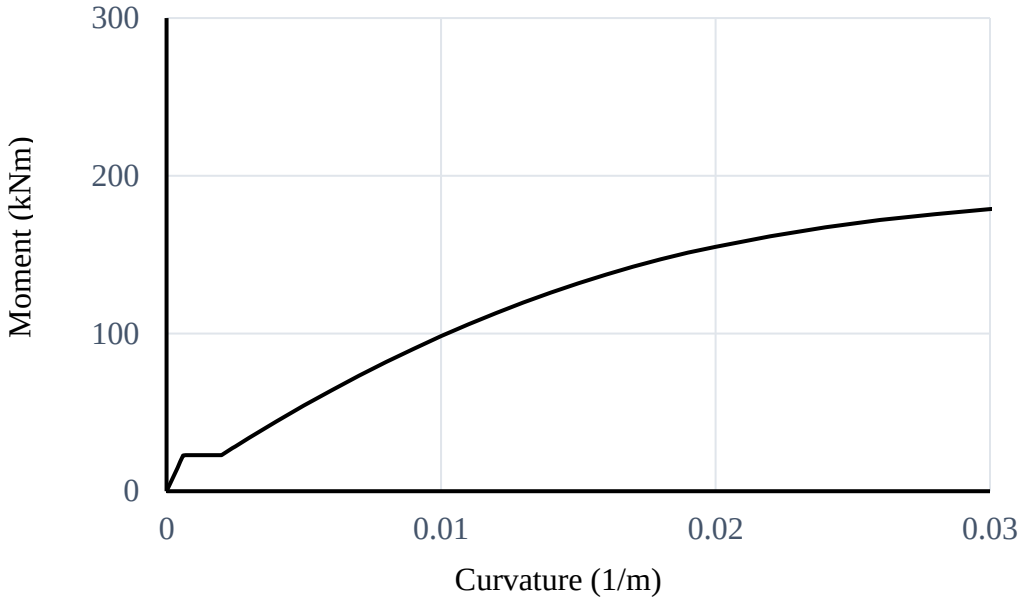

Figure Q.10: Theoretical Moment Curvature Diagram for Specimen 25◆-610↑

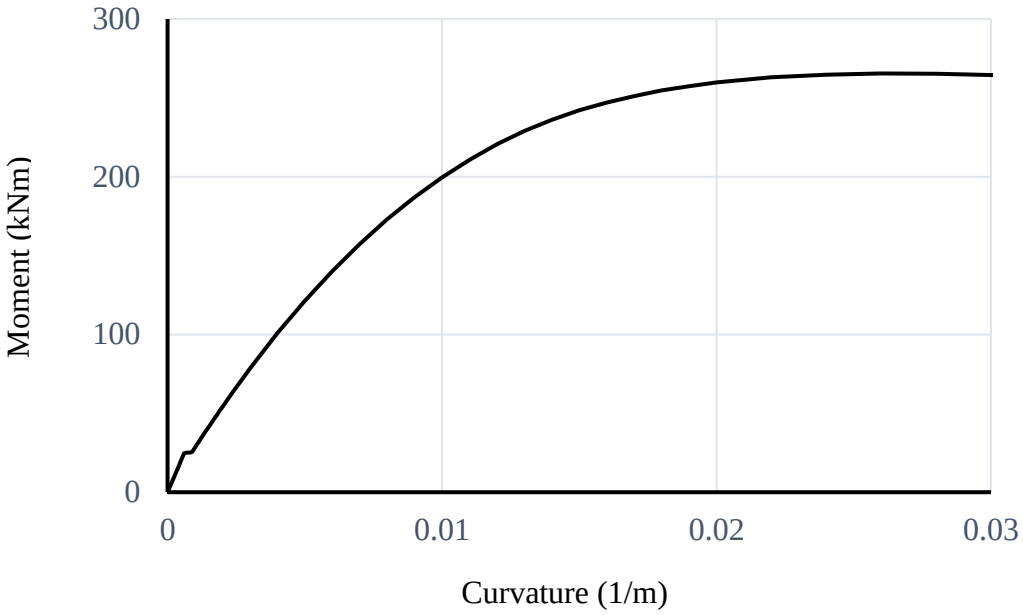

Figure Q.11: Theoretical Moment Curvature Diagram for Specimen 32◆-410↓

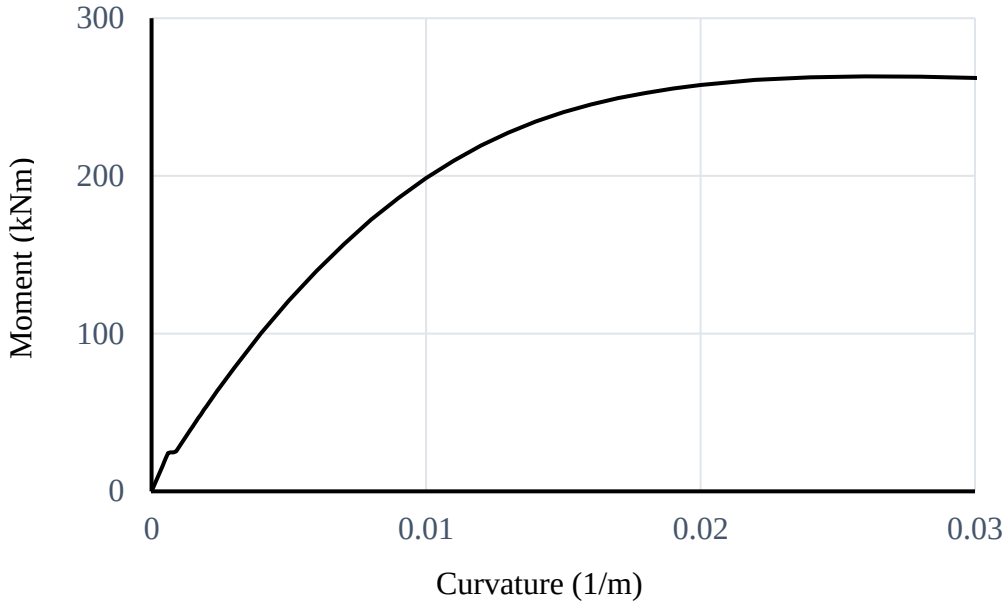

Figure Q.12: Theoretical Moment Curvature Diagram for Specimen 32◆-610↓

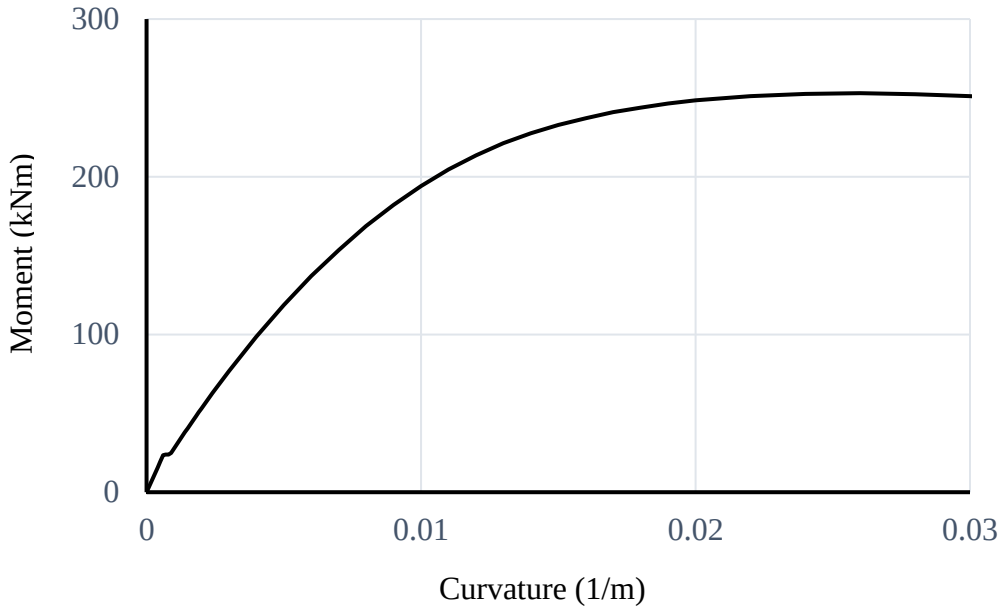

Figure Q.13: Theoretical Moment Curvature Diagram for Specimen 32◆-810↓

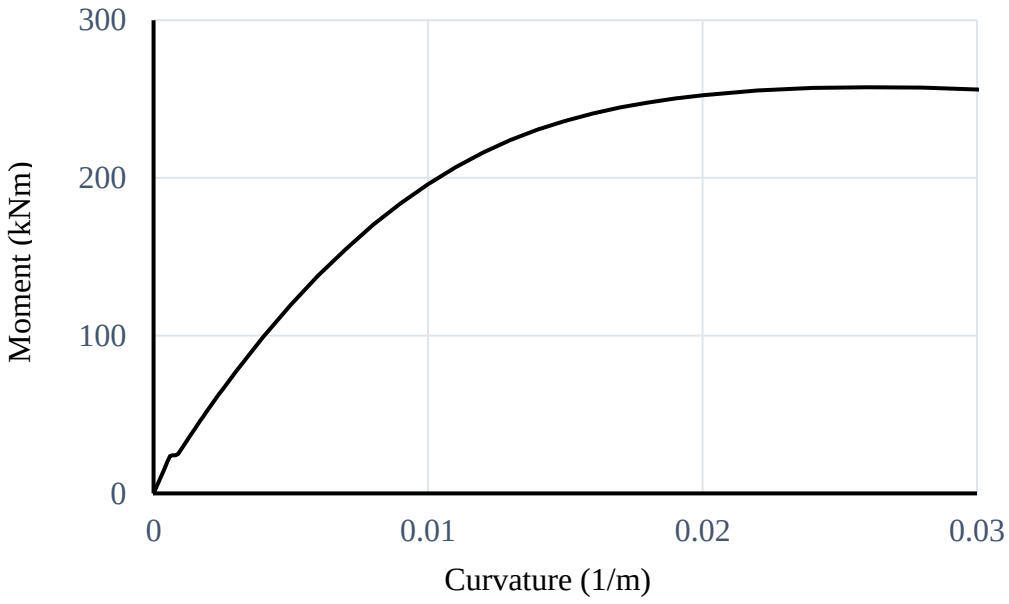

Figure Q.14: Theoretical Moment Curvature Diagram for Specimen 32◆-410↑

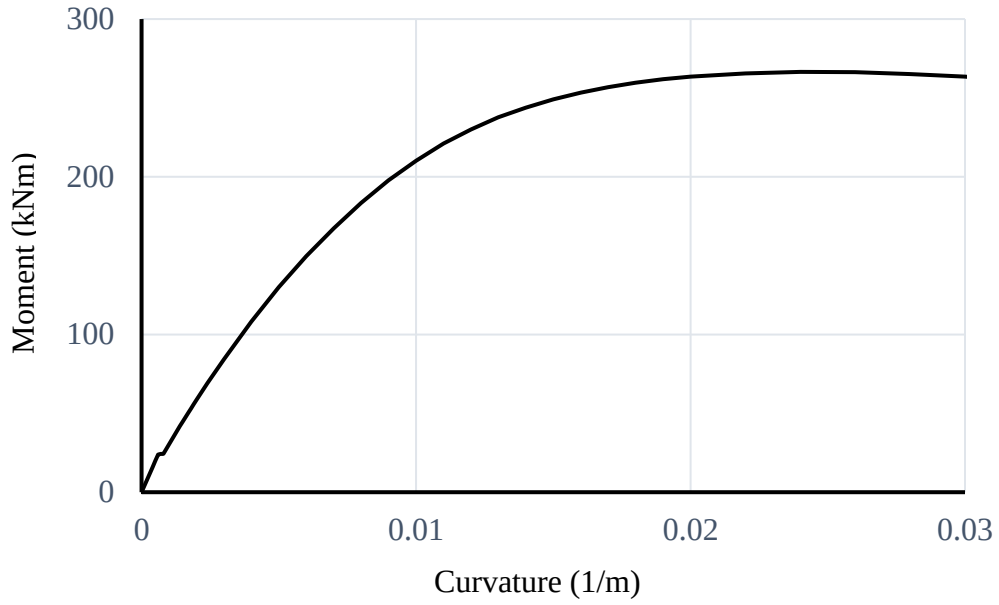

Figure Q.15: Theoretical Moment Curvature Diagram for Specimen 32◆-610↑

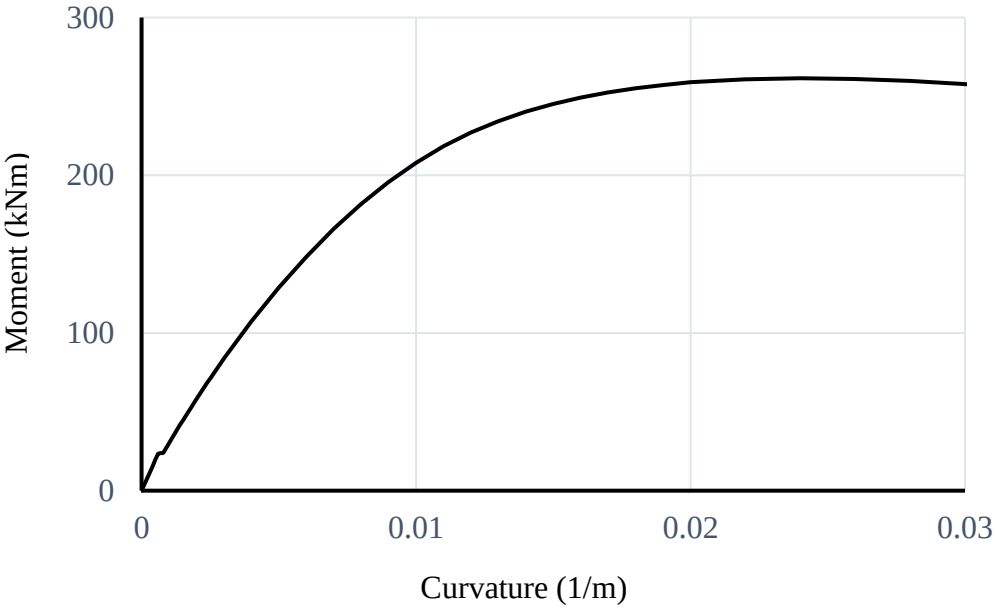

Figure Q.16: Theoretical Moment Curvature Diagram for Specimen 32◆-810↑

Appendix R: Error Associated with Selection of 100 Segments in Moment Curvature Analysis

This appendix provides the error associated with the selection of the number of segments used to calculate the resisting moment. Figure R.1 shows the moment corresponding to a fixed curvature of 0.0095 for specimen 19◆-510↓ with 1, 2, 5, 10, 20, 50, 100, 200, 300, 400, and 500 segments. A curvature value of 0.0095 was selected in such a way that it was located before yielding of the reinforcement in moment curvature diagram. The moment closely approached the value of 72.6395 kNm when the number of segments was greater than or equal to 200. Hence the approximate asymptote (Figure R.1) was reported as 72.6395 kNm. As the moment corresponding to 100 segments was 72.6392 kNm, the error associated with the selection of 100 segments was therefore negligible (i.e.0.00%).

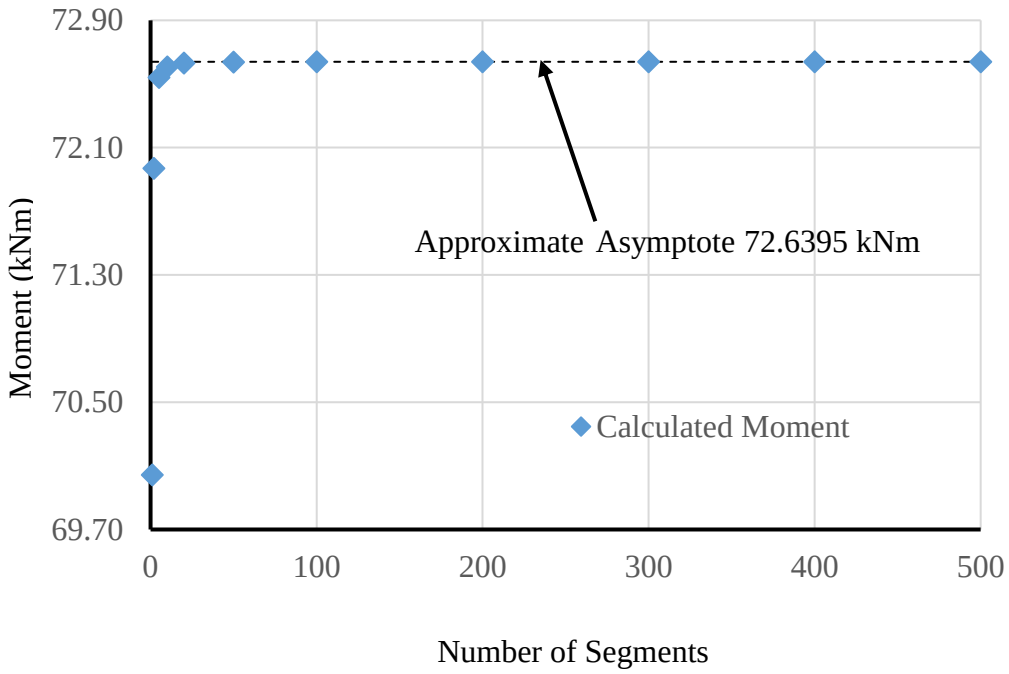

Figure R.1: Moment Corresponding to a Curvature of 0.0095/m as a Function of the Number of Segments Incorporated in the Analysis of Specimen 19◆-510↓

Appendix S: Comparison of Two Different Methods for Calculating the Tensile Resistance of the Spliced Reinforcement

Figure S.1 shows the comparison of two different methods for calculating the tensile resistance of the reinforcement at the maximum load level. In method 1, the moment resistance was calculated as a product of the tensile force in the longitudinal reinforcement and the lever arm (i.e. distance between the centroids of tension force and compression force), whereas in method 2, the moment resistance was calculated as a product of compressive force in the concrete and the same lever arm. The mean and standard deviation of the ratio of the tensile resistance as calculated from methods 1 and method 2 are 0.98 and 0.002, respectively. As the neutral axis depth was calculated from a higher value to a lower value until the difference between compressive force and tensile force was within 0.5%, method 2 gave slightly greater values of tensile resistance than method 1. Method 1 was chosen as it yielded a lower tensile resistance which would ultimately lead to longer and so more conservative lap splice lengths.

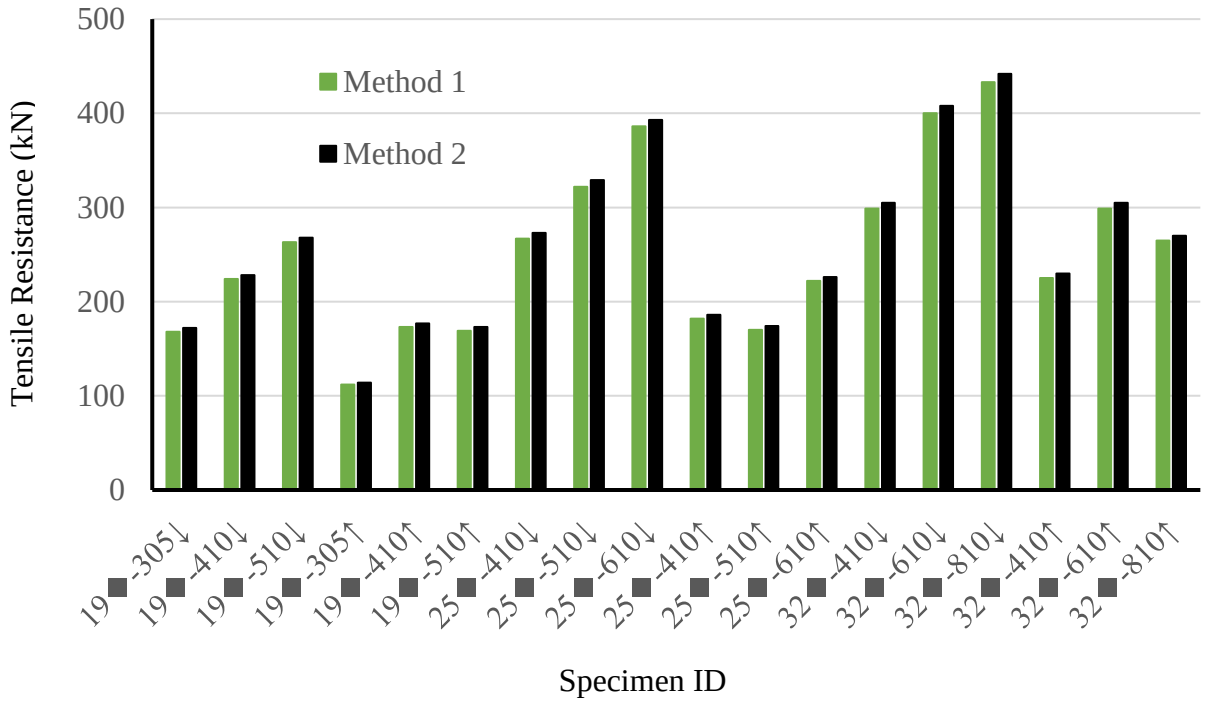

Figure S.1: Comparison of Two Different Methods for Calculating the Tensile Resistance of the Spliced Reinforcement at the Maximum Load